Michael Dreifke

# Cozy and Pleasant Surroundings –

# Coenzyme Regeneration in Mesoporous Silicas

**Dissertation**

zur Erlangung des Grades

Doktor der Naturwissenschaften (Dr. rer. nat.)

an der Fakultät für Mathematik, Informatik und Naturwissenschaften

im Fachbereich Chemie der Universität Hamburg

September 2017

Die Druckfreigabe für diese Arbeit wurde am 03.11.2017 durch das Studienbüro des Fachbereichs Chemie der Universität Hamburg erteilt.

Die vorliegende Arbeit wurde im Zeitraum von Januar 2013 bis September 2017 in der Arbeitsgruppe von Prof. Dr. Michael Fröba am Institut für Anorganische und Angewandte Chemie im Fachbereich Chemie der Universität Hamburg angefertigt.

1. Gutachter: Prof. Dr. Michael Fröba

2. Gutachter: JProf. Dr. Simone Mascotto

Tag der Disputation: 03.11.2017

**Eidesstattliche Erklärung**

Hiermit versichere ich an Eides statt, die vorliegende Dissertation selbst verfasst und keine anderen als die angegebenen Hilfsmittel benutzt zu haben. Die eingereichte schriftliche Fassung entspricht der auf dem elektronischen Speichermedium. Ich versichere, dass diese Dissertation nicht in einem früheren Promotionsverfahren eingereicht wurde.

Hamburg, den 27.09.2017

Michael Dreifke

# Danksagung

Herrn Prof. Dr. Michael Fröba danke ich für das sehr interessante Thema meiner Doktorarbeit, welches mich nach wie vor in seinen Bann zieht und sehr fasziniert. Vielen Dank für Ihr Vertrauen und die wissenschaftliche Freiheit, die ich im Rahmen meiner Arbeit hatte, immer mit dem Wissen, dass Sie hinter mir stehen.

Herrn JProf. Simone Mascotto danke ich für die freundliche Übernahme des Zweitgutachtens sowie Herrn Prof. Dr. Ralph Holl und Herrn Prof. Dr. Dr. h.c. mult. Wittko Francke für das Beiwohnen der Prüfungskommission.

Ein großes Dankeschön gebührt Dr. Felix J. Brieler für den spannenden fachlichen Austausch in den Untergruppentreffen sowie den zahlreichen persönlichen und konstruktiven wissenschaftlichen Gesprächen und das Korrekturlesen meiner Arbeit.

Mit Dr. Dorothee I. Fried und Dr. Katharina Peikert hatte ich über einen langen Zeitraum meiner Doktorarbeit zwei perfekte Laborpartnerinnen, die einem netten Pläuschchen neben der Arbeit immer aufgeschlossen gegenüber standen.

Ich danke den Kollegen aus AC 213 – Natascha Speil, Timo Stein, Ruben Heimböckel und Dr. Sebastian Kraas – für die lustige Zeit und die vielen gemeinsamen Aktivitäten. Unvergessen bleibt ganz besonders die zauberhafte Runde des perfekten Bürodinners mit vielen kulinarischen Highlights; ganz gleich ob eine kalorienfreie, locker, leichte Sauce Hollandaise oder Ananas und/oder Erdbeeren. Unsere geselligen Abende waren einzigartig und haben uns zu Freunden gemacht.

Jakob Benedikt Mietner danke ich für eine wunderbare Zeit. *You know what I mean, girl.*

Uta Sazama und Sandra König danke ich für die Durchführung zahlreicher Thermoanalysen und Physisorptionsmessungen. Vielen Dank für gesellige und entspannte Mittagspausen mit Gesprächsthemen jenseits der Chemie.

Dem gesamten Arbeitskreis Fröba danke ich für den stets freundschaftlichen Umgang miteinander und die Hilfsbereitschaft in allen Lebenslagen – in und außerhalb der Uni.

Zum Schluss danke ich den wichtigsten Menschen in meinem Leben – meiner Familie. Vielen Dank für Eure jahrelange Unterstützung und Euren Rückhalt, nicht nur über die Zeit des Studiums, sondern bei allem, was ich angehe. Ihr haltet immer zu mir und wir halten immer zusammen. Dafür danke ich Euch von Herzen.

*„In der Wissenschaft brauchen wir vor allem Vorstellungskraft. Es ist nicht alles Mathematik oder Logik, sondern auch Schönheit und Poesie.“*

Maria Mitchell
(1818-1889)

# TABLE OF CONTENTS

# 0 LIST OF ABBREVIATIONS

| | |
|---|---|
| 3D | 3-Dimensional |
| 3K6P | 3-Keto-6-phosphate |
| 5-HMF | 5-Hydroxymethylfurfural |
| 6PG | 6-Phosphogluconate |
| 6PGL | 6-Phophogluconolactonase |
| 6PGDL | 6-Phosphogluconate-δ-lactone |
| 6PGDH | 6-Phosphogluconic dehydrogenase |
| abs. | Absolute |
| ADH | Alcohol dehydrogenase |
| ADP | Adenosine diphosphate |
| ATP | Adenosine triphosphate |
| AIE | Amount of immobilized enzyme |
| APTES | (3-Aminopropyl)-triethoxysilane |
| BCA | Bicinchoninic acid |
| BET | *Brunauer-Emmett-Teller* |
| BRENDA | Braunschweig Enzyme Database |
| BSA | Bovine serum albumin |
| CAT | Catalase |
| CBBG | Coomassie brilliant blue |
| $c_i$ | Initial concentration |
| CMC | Critical micelle concentration |
| *C.p.*CR | Carbonyl reductase from *Candida parapsilosis* |
| CPO | Chloroperoxidase |
| CTAB | Cetyltrimethylammonium bromide |

| | |
|---|---|
| d | Day(s) |
| DCM | Dichloromethane |
| dist. | Distilled |
| DMF | Dimethylformamide |
| DMSO | Dimethylsulfoxide |
| $D_p$ | Pore width |
| DSC | Differential scanning calorimetry |
| DTA | Differential thermal analysis |
| $E_a$ | Activation energy |
| E.C. | Enzyme commission |
| *E.c.* | *Escherichia coli* |
| *E.c.*ADH | Alcohol dehydrogenase from *Escherichia coli* |
| EE | Enzyme efficiency |
| EI | Electron ionization |
| EO | Ethylene oxide |
| F6P | Fructose-6-phosphate |
| FDH | Formate dehydrogenase |
| FDU | *Fundan University* |
| FWHM | Full width at half maximum |
| G6P | Glucose-6-phosphate |
| GAP | Glyceral-3-phosphate |
| G6PDH | Glucose-6-phosphate dehydrogenase |
| GHS | Global harmonized system |
| GOD | Glucose oxidase |
| *G.s.* | *Geobacillus stearothermophilus* |

| | |
|---|---|
| *G.s.*6PGDH | 6-Phosphogluconate dehydrogenase from *Geobacillus stearothermophilus* |
| η | Effectiveness factor |
| h | Hour(s) |
| H | Hazard statements |
| HEPES | 2-[4-(2-hydroxyethyl)piperazin-1-yl]ethanesulfonic acid |
| *H.l.*ADH | Alcohol dehydrogenase from *Horse liver* |
| HRP | Horseradish peroxidase |
| IR | Infrared |
| IUPAC | *International Union of Pure and Applied Chemistry* |
| $k_{cat}$ | Rate constant of the decay of the enzyme-substrate complex |
| $K_i$ | Inhibition constant |
| KIT | *Korea Advanced Institute of Science and Technology* |
| $K_m$ | Michaelis-Menten constant |
| KRD | Keto reductase |
| LDH | Lactate dehydrogenase |
| *L.m.* | *Leuconostoc mesenteroides* |
| *L.m.*G6PDH | Glucose-6-phosphate dehydrogenase from *Leuconostoc mesenteroides* |
| m | Multiplett |
| MCF | Mesocellular Siliceous Foams |
| MCM | Mobil Composition of Matter |
| min | Minute |
| MS | Mass spectrometry |
| MTBE | Methyl *tert*-butyl ether |
| $NAD^+$/H | Nicotinamide adenine dinucleotide |
| $NADP^+$/H | Nicotinamide adenine dinucleotide phosphate |

# 0 List of Abbreviations

| | |
|---|---|
| NBNR | Nitrobenzene nitroreductase |
| NLDFT | Non-local density functional theory |
| NMR | Nuclear magnetic resonance |
| o/w | Oil in water |
| P | Precautionary statements |
| PDB | Protein data bank |
| PEG | Polyethylene glycol |
| PEO | Polyethylene oxide |
| PFTE | Polytetrafluoroethylene |
| Phos. | Phosphate buffer solution (50 mM, pH 7.5) |
| pI | Isoelectric point |
| PK | Pyruvate kinase |
| PMO | Periodic mesoporous organosilica |
| PPM | Parts per million |
| PPO | Polypropylene oxide |
| PSD | Pore size distribution |
| PVDF | Polyvinylidene fluoride |
| $\rho_f$ | Functionalization density |
| rpm | Revolutions per minute |
| rt | Room temperature |
| Ru5P | Ribulose-5-phosphate |
| s | Singulett |
| SBA | *Santa Barbara Amorphous* |
| $S_{BET}$ | BET surface |
| *S.c.* | *Saccharomyces cerevisiae* |
| *S.c.*6PGDH | 6-Phosphogluconate dehydrogenase from *Saccharomyces cerevisiae* |

| | |
|---|---|
| SDA | Structure directing agent |
| SEM | Scanning electron microscopy |
| SOD | Superoxide dismutase |
| TA | Thermal analysis |
| *T.b.*ADH | Alcohol dehydrogenase from *Thermoanaerobium brockii* |
| TEOS | Tetraethylorthosilicate |
| TMOS | Tetramethylorthosilicate |
| TG | Thermogravimetry |
| TMB | 1,3,5-Trimethylbenzol (mesitylene) |
| TTN | Total turnover number |
| U | Unit |
| UV/Vis | Ultraviolet/visible |
| $v_0$ | Initial reaction rate |
| $v_{max}$ | Maximal reaction rate |
| $V_p$ | Pore volume |

# 1 INTRODUCTION

## 1.1 Enzymes – Mother nature's fascinating biocatalysts

Since the discovery of the first enzyme in 1833, enzymes have not lost any of its admiration.[1] In an almost fascinating manner, they catalyze innumerable reactions in all spheres of nature. These complex three-dimensional biocatalysts convert their substrate specifically with a pronounced chemo-, regio- and diastereoselectivity as well as enantionselectivity. The respective selectivity is far superior to synthetic catalysts. Furthermore, the absence of any side reactions and the mild reaction conditions has prematurely aroused the interest of preparative working chemists. Against the background of *green chemistry*, which is of course a controversially discussed issue, the application of enzymes in catalysis is very attractive and forward-looking. However, nowadays, a lot of prejudices against the application of enzymes in laboratory or industrial scale are still widespread. On one hand it is argued that enzymes are expensive. On the other hand, a certain sensitivity in terms of its structure is attributed to enzymes. The immobilization of an enzyme onto a suitable host material can lead to its stabilization. In particular, the immobilization of the favored enzyme onto the surface of nanoporous materials is known to be frequently accompanied by a stabilization of the enzyme. Furthermore, an immobilization ensures the reusability of the enzyme. Thus, the employment of an expensive enzyme in organic chemistry becomes more attractive and the cost factor relativizes.

Commonly, it is stated that enzymes are only active in the presence of its natural substrate and in their natural environment. At present it is a matter of common knowledge that most enzymes possess a broad substrate acceptance independent on its natural origin. Thus, likewise synthetic substrates can be converted when distinct requirements are fulfilled. Certainly, an enzyme gains its highest activity in aqueous media or rather in the medium corresponding to its natural environment. However, they can even be active in unconventional media or in biphasic systems, where the enzymatic reaction takes place on the interface. Frequently, this is enabled due to the immobilization of the respective enzyme, as the immobilization onto an appropriate hydrophilic support guarantees the presence of sufficient water molecules needed for an adequate enzymatic activity.

Some disadvantages make the utilization of enzymes very challenging. A lot of enzymes are dependent on a cofactor or coenzyme. In the case of a cofactor no

[1] A. Payen, J.-F. Persoz, *Annales de chimie et de physique* **1833**, *53*, 73–92.

difficulties arise, as it is tightly bound to the enzyme. This prosthetic group does not dissociate into the reaction medium. On the contrary, after chemical conversion, a coenzyme dissociates into the reaction medium. At best, it becomes recycled in a subsequent step in order to ensure its reuse. Here again, the immobilization of the needed enzyme contributes to higher efficiency, as beside the regeneration of the coenzyme, the enzyme employed for the recycling can be reutilized.

As mentioned above, enzymes react under mild conditions (temperature, pH). This can be disadvantageous when the reaction rate of the enzyme is quite low, as the variation of the temperature and/or pH value can lead to its denaturation. Moreover, according to its composition of natural D-amino acids, merely one enantiomer can be obtained, as mirror-image enzymes are non-existent. Enzyme engineering can circumvent these drawbacks given above and optimize the efficient application of enzymes in organic chemistry. Hence, enzymes are no *ready-to-use* catalysts but when their utilization is optimized they are far superior to synthetic catalysts.[2]

### 1.1.1 Enzymes in general

Enzymes are fascinating three-dimensional biocatalysts and omnipresent in all metabolic processes and pathways in nature. Live without enzymes is unimaginable. All the more, it is astonishing that they are merely composed of the 20 natural amino acids that are linked *via* peptide bonds to polypeptide chains forming the backbone of the enzyme. According to this, proteins and enzymes possess a C-terminus as well as a N-terminus (Figure 1). The polypeptide chain of an enzyme consists of several hundred amino acids. Amino acids can be differenced according to their side chains (Table 1). With regard to the chemical properties of the organic residues of the amino acids, hydrophilic, hydrophobic as well as electrostatically charged areas within the three-dimensional structure and primarily on the surface arise.[3]

[2] K. Faber, *Biotransformations in Organic Chemistry*, 6th Edition, Springer, Heidelberg, Dordrecht, London, New York, **2011**.
[3] E. Breitmaier, G. Jung, *Organische Chemie*, 5., überarbeitete Auflage, Georg Thieme Verlag, Stuttgart, New York, **2005**.

**Table 1.** Classification of the 20 natural amino acids according to its organic residue.[3]

| classification | amino acid |
|---|---|
| aliphatic amino acids | Gly, Ala, Val, Leu, Ile |
| hydroxyamino acids | Ser, Thr |
| amino dicarbonic acids | Asp, Asn, Glu, Gln |
| basic amino acids | Lys, Arg, His |
| sulfur containing amino acids | Cys, Met |
| cyclic amino acids | Pro |
| aromatic and heteroaromatic amino acids | Phe, Tyr, Try |

### 1.1.2 Enzyme structure

The overall structure of an enzyme can be subdivided into several spheres. The primary structure describes the amino acid sequence of the polypeptide chain (Figure 1).

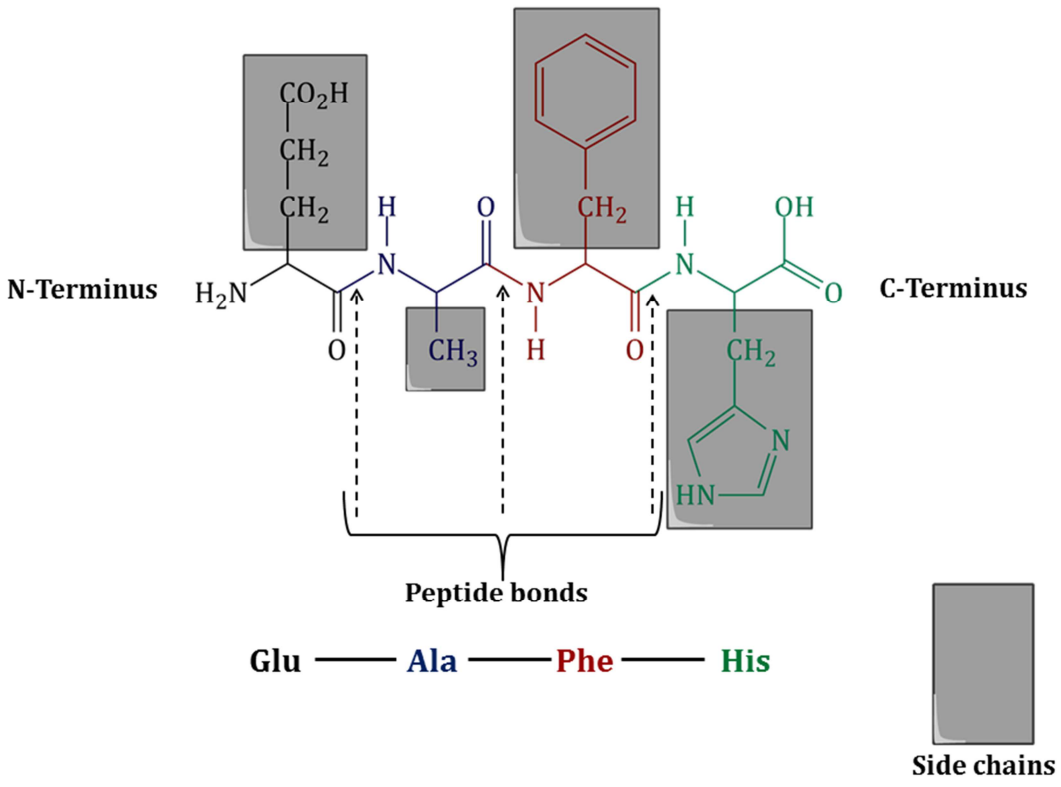


**Figure 1.** Schematic depiction of the primary structure of an oligopeptide. The amino acids are linked *via* peptide bonds. Correspondingly, the peptide chain possesses a N-terminus as well as a C-terminus. An enzyme is composed of several hundred amino acids that are linked *via* peptide bonds, whereat the side chains of the amino acids are responsible for the chemical characteristics of the protein.[3]

The spatial conformation of the amino acids within an enzyme is defined by the secondary structure. The most meaningful structural elements are the α-helix as well as the β-sheet (Figure 2). In an α-helix, all carbonyl residues of the polypeptide chain are oriented into one direction; whereas the N-H groups are positioned into the opposite direction. Hydrogen bonds between the protons of the N-H function of the peptide bonds and the oxygen atoms of the carbonyl groups of the respective amino acid 3.6 positions earlier in the amino acid sequence result in a right-hand-coiled α-helix. Hence, one turn consists of a 13-membered ring. This conformation leads to a reduction of the spatial distance between the amino acids incorporated into the hydrogen bonds as well as to a tensionless arrangement of the amino acids within the polypeptide chain. In this conformation the side chains of the amino acid are oriented outwardly (Figure 2a).[3]

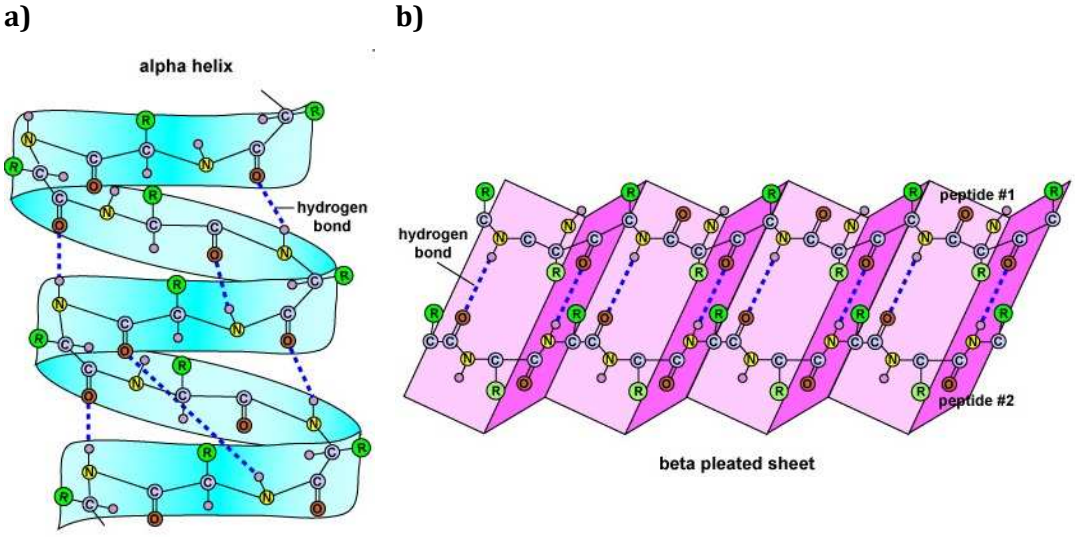


**Figure 2.** Graphical depiction of the most meaningful structural elements within the secondary structure of an enzyme or protein: **a)** α-helix and **b)** β-sheet (parallel sheet). The residue "R" designates the organic side chain of the amino acids. Figure adapted from [4]. Copyright by Dr. Gary Kaiser, COMMUNITY COLLEGE OF BALTIMORE COUNTY, CATONSVILLE CAMPUS.

A further structural element within the three-dimensional structure of proteins and enzymes is the β-sheet. In this conformation the peptide bonds as well as the carbon atoms adjacent to the carboxylic residues are arranged in a corrugated manner. Hence, the organic side chains of the amino acids are associated alternately below or above the corrugated plain. Stabilizing hydrogen bonds between the protons of the N-H groups of one polypeptide chain to the oxygen atoms of the

[4] LibreTexts Libraries: https://bio.libretexts.org/TextMaps/Map%3A_Microbiology_(Kaiser)/Unit_7%3A_Microbial´_Genetics_and_Microbial_Metabolism/19%3A_Review_of_Molecular_Genetics/19.1%3A_Polypeptides_and_Proteins, **09.2017**.

carbonyl groups of an adjacent polypeptide chain results in a parallel or anti-parallel β-sheet (Figure 2b).[3] A widespread motif in enzyme structures is the linkage of α-helices and β-sheets to a pairwise βαβαβ formation. The so called "Rossmann fold" is a supersecondary structure and the cleft formed between the βαβαβ pair is essential for the fixation of the coenzymes $NAD^+$ as well as $NADP^+$.[5, 6]

The tertiary structure of an enzyme or protein is defined by the overall arrangement of the structure elements of the secondary structure; whereas the aggregation of several folded polypeptide chains is defined as the quaternary structure of an enzyme.[3]

Basically, the outer shell of an enzyme is composed of hydrophilic amino acids and a hydrate shell consisting of strongly coordinated water molecules. The proportion of structural water ranges between 5 and 30 % with respect to the dry weight of the enzyme. As it is tightly bound to the enzyme surface, it possesses different physical properties in comparison to bulk water. For example, its freezing point is reported to be at -20 °C and its removal due to lyophilization is impossible. On one hand, the presence of hydrophilic amino acids on the surface of an enzyme can be referred to its natural environment, as the polar residues as well as the hydrate shell ascertain the water solubility of the enzyme. On the other hand, the hydrate shell contributes significantly to the spatial structure or rather to the conformation of the enzyme and consequently to its catalytic activity. The strong water-protein interactions within the outer hydration shell initiate the association of hydrophobic amino acid residues in the inner core of the enzyme. The driving force of these hydrophobic interactions is the increase of the entropy that comes along with a decrease of the free energy. Thus, the association of hydrophobic amino acid residues is accompanied by the replacement of water molecules on the contact area of the respective interacting hydrophobic side chains of the amino acids. The globular folding of the polypeptide chains minimizes the contact areas between hydrophobic residues and the aqueous medium. Hence, hydrophobic amino acids are preferably arranged in the inner core of an enzyme.[2, 3, 7, 8, 9, 10]

[5] M.G. Rossmann, D. Moras, K.W. Olsen, *Nature* **1974**, *250*, 194-199.
[6] H.R. Horton, L.A. Moran, K.G. Scrimgeour, M.D. Perry, J.D. Rawn, *Biochemie*, 4., aktualisierte Auflage, Pearson Education Deutschland, München, **2008**.
[7] R. Cooke, I.D. Kuntz, *Ann. Rev. Biophys. Bioeng.* **1974**, *3*, 95-126.
[8] W. Blokzijl, J.B.N.F. Engberts, *Angew. Chem.* **1993**, *105*, 1610-1648.
[9] V. Puddu, C.C. Perry, *ACS Nano* **2012**, *6*, 6356-6363.
[10] J.-L. Ochoa, *Biochimie* **1978**, *60*, 1-15.

Besides, various additional intermolecular interactions contribute to the conservation of the unique three-dimensional structure of an enzyme aiming at a high catalytic activity (Figure 3).

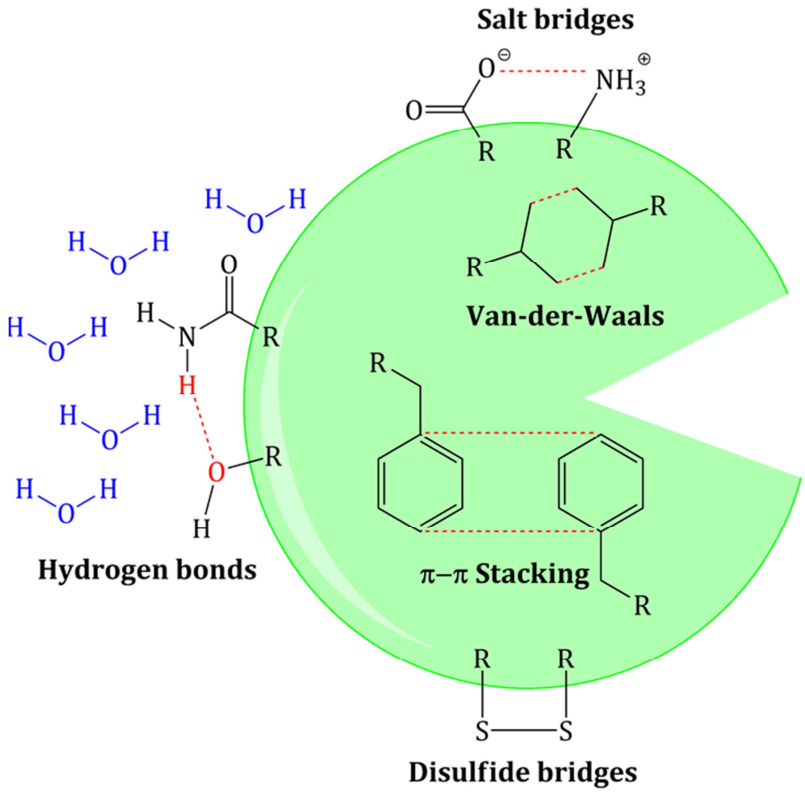


**Figure 3.** Schematic illustration of intermolecular interactions that are present within the three-dimensional structure of an enzyme or protein. Besides hydrophobic interactions, these interactions contribute to the spatial structure of an enzyme/protein. Copyright Springer-Verlag Berlin Heidelberg 2011. Reproduced with permission of Springer.[2]

As mentioned above, hydrogen bonds are the predominant interactions in the formation of α-helices as well as β-sheets. Moreover, hydrogen bonds likewise occur between further polar amino acid residues within the three-dimensional structure of an enzyme. The binding force of hydrogen bonds is known to be very weak. However, in the absence of water molecules in the hydrophobic core of an enzyme, their stabilizing effect is pronounced (Figure 3).[2, 3]

Van-der-Waals forces or rather London forces are attractive intermolecular forces and prevail in the inner hydrophobic core of an enzyme. They arise from spontaneous polarization accompanied by an induced dipole between non-polar amino acid residues that are not covalently bonded and occur mainly in the inner core of an enzyme. Additionally, weak π-π interactions between the aromatic

systems of phenylalanine, tryptophan and tyrosine in the hydrophobic core of an enzyme can arise (Figure 3).[2, 3, 11, 12, 13]

Electrostatic interactions between carboxylate, ammonium or guanidine residues on the hydrophilic surface of the enzyme form stable salt bridges. These ionic interactions are very strong. The thermal stability of an enzyme is directly dependent on the number of ionic interactions on its outer shell. Thermophilic enzymes possess a large number of salt bridges on the outer surface. Hence, they are stable up to 60 – 80°C and its temperature optimum can frequently be found at elevated temperature. Likewise, disulfide bridges contribute to the pronounced stability of a thermostable enzyme. Disulfide bridges are formed by a covalent bond between the thiol groups of two cysteine residues (Figure 3).[2, 3]

Generally, it can be stated that the optimal or preferred conformation of an enzyme possesses the lowest Gibbs energy.[14]

### 1.1.3 Enzyme catalysis

The intent and purpose of the application of a catalyst in a chemical reaction is the reduction of the activation energy ($E_a$). The reduction of $E_a$ is accompanied by an increase of the reaction rate. In the absence of a catalyst, $E_a$ of a given reaction is considerably higher. Correspondingly, the reaction rate is very low or even the reaction does not proceed under the given conditions.[15]

Enzymes are very efficient biocatalyst and enzyme-catalyzed reactions belong to the fastest reactions known.[16] The first reaction step of an enzyme-catalyzed reaction is marked by the formation of the enzyme-substrate complex. Within the enzyme-substrate complex, the functional groups of the binding site of the enzyme and the respective functional groups of the substrate are oriented and the chemical reaction occurs (Figure 4). After the release of the product, the enzyme remains unaltered and converts a further substrate molecule.[2]

[11] C.A. Hunter, J.K.M. Sanders, *J. Am. Chem. Soc.* **1990**, *112* (14), 5525-5534.
[12] C.R. Martinez, B.L. Iverson, *Chem. Sci.* **2012**, *3*, 2191-2201.
[13] C.E. Mortimer, U. Müller, *Chemie*, 8., komplett überarbeitete und erweiterte Auflage, Georg Thieme Verlag, Stuttgart 2003.
[14] C.B. Anfinsen, *Science* **1973**, *181*, 223-230.
[15] R. Hopp, *Grundlagen der Chemischen Technologie*, 4., vollständige überarbeitet und erweiterte Auflage, WILEY-VCH, Weinheim, **2001**.
[16] R. Wolfenden, M.J. Snider, *Acc. Chem. Res.* **2001**, *34*, 938-945.

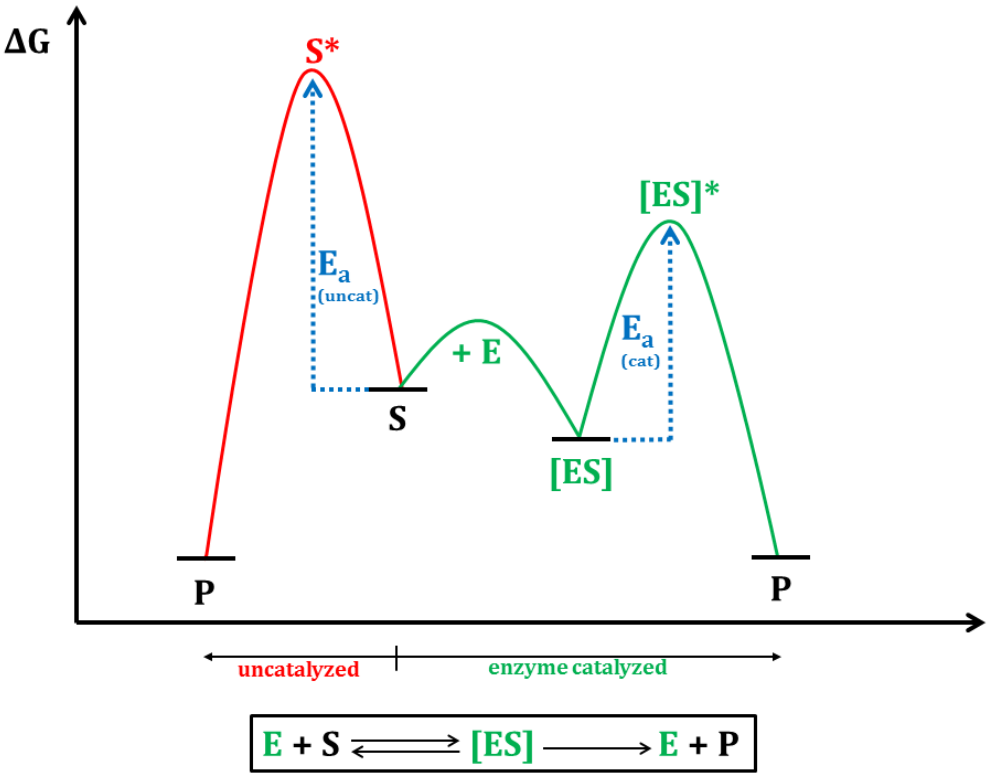


**Figure 4.** Energy diagram of an enzyme catalyzed reaction (green path) in comparison to an uncatalyzed reaction (red path). In terms of an enzyme catalyzed reaction, the activation energy ($E_a$) is significantly reduced (E: enzyme; S: substrate; ES: enzyme-substrate complex; P: product). Copyright Springer-Verlag Berlin Heidelberg 2011. Redrawn with permission of Springer.[2]

In previous times, an enzyme was assumed to be very rigid and it was assumed that the enzyme and its substrate match up as lock (enzyme) and key (substrate; Figure 5a).[17] However, this proposal is inconsistent, as it is in contradiction with the broad substrate acceptance of numerous enzymes. Moreover, enzymes are frequently capable to convert synthetic substrates. Hence, a more differentiated approach was required to explain the theoretical background concerning the binding of the substrate.

[17] E. Fischer, *Ber. dtsch. chem. Ges.* **1894**, *27*, 2985-2993.

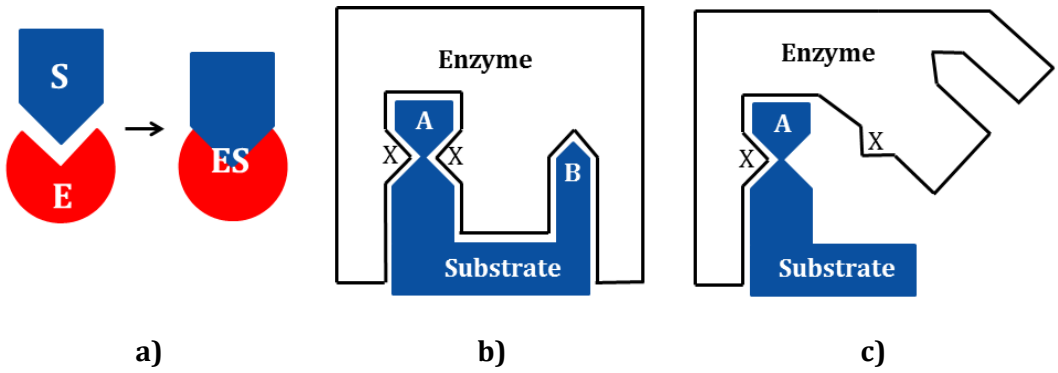


**Figure 5.** Proposed binding mechanisms of an enzyme and its substrate: **a)** The traditional lock-key mechanism implies a certain rigidity of the enzyme and its substrate indicating that they match like lock and key. **b)** Nowadays, it is known that the enzyme and its substrate possess a distinct flexibility. Thus, the coincidence of the enzyme and the substrate induces slight conformational changes of both in order to form the enzyme-substrate complex (induced-fit theory). **c)** In the absence of distinct structural elements, the substrate cannot be bound by the enzyme. Correspondingly, no conversion of the substrate takes place (no induced-fit). Figure 5b) and 5c): Copyright Springer-Verlag Berlin Heidelberg 2011. Reproduced with permission of Springer.[2]

A widely accepted theory is the induced-fit theory (Figure 5b, 5c). The induced-fit mechanism concedes a certain flexibility or rather mobility to the enzyme. Thus, the amino acid residues of the active center and surrounded areas are able to undergo necessary conformational changes to completely infold the substrate in order to form the enzyme-substrate complex. These conformational changes within the enzyme structure are induced by the specific structural properties of the substrate (Figure 5b). In the absence of these structural properties, the enzyme is unable to bind the substrate and a conversion of the substrate is impossible (Figure 5c). Frequently, the procedures of the induced-fit model are compared with the principle of a hand (substrate) and a glove (enzyme).[2, 18, 19]

[18] D.E. Koshland, *Proc. Natl. Acad. Sci. USA* **1958**, *44*, 98-104.
[19] D.E. Koshland, K.E. Neet, *Ann. Rev. Biochem.* **1968**, *37*, 359-410.

#### 1.1.3.1 Classification

As varied as enzymes are, as versatile are the reactions that are catalyzed by an enzyme. Hence, enzymes are formally organized according to the type of reaction they are catalyzing (Table 2).

**Table 2.** Categorization of enzymes according to the type of catalyzed reaction.[2, 3]

| enzyme class | catalyzed reactions / reaction types |
|---|---|
| 1. oxidoreductases | coenzyme-dependent redox reactions |
| 2. transferases | transfer of functional groups |
| 3. hydrolases | hydrolyses |
| 4. lyases | addition/elimination of molecules on double bonds |
| 5. isomerases | racemizations, epimerizations, rearrangements |
| 6. ligases | condensation-induced formation of CO-, CN-, CC-bonds assisted by adenosine-triphosphate (ATP) |

In addition, each enzyme class of this rough classification is subdivided in more detail with regard to the respective substrate class or transferred functional group as well as the required coenzyme.[2]

## 1.2 Pentose phosphate pathway

The pentose phosphate pathway is an enzymatic reaction sequence that proceeds in the cytosol of nearly all cells and belongs to the catabolic part of the metabolism. Its general purpose is the degradation of glucose and thus it fulfills important tasks, as the degradation of glucose aims at the provision of NADPH as well as ribose-5-phosphate. Within living cells, NADPH is an important reducing agent and prevents them against oxidative stress, whereas ribose-5-phosphate is mandatory for the nucleotide biosynthesis.[20, 21]

The pentose phosphate pathway can be subdivided into an irreversible oxidative as well as a reversible non-oxidative section. The irreversible and oxidative path involves the oxidation of glucose-6-phosphate (G6P) to ribulose-5-phosphate (Ru5P; Scheme 1).

[20] F. Horn, *Biochemie des Menschen*, 4. Auflage, Thieme-Verlag, Stuttgart, **2009**.
[21] A. Kremer, *Crashkurs Biochemie*, 1. Auflage, Elsevier, München, **2005**.

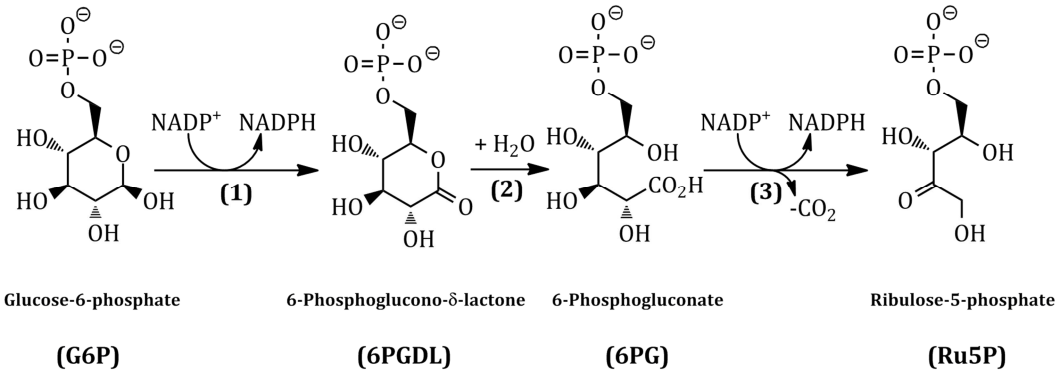


**Scheme 1.** Irreversible and oxidative part of the pentose phosphate pathway: Stepwise oxidation of glucose-6-phosphate to ribulose-5-phosphate. (1) Glucose-6-phosphate dehydrogenase (G6PDH); (2) 6-Phosphogluconolactonase (6PGL); (3) 6-Phosphogluconate dehydrogenase (6PGDH).[20, 21] A detailed discussion of the respective reaction mechanisms can be found in the chapters 1.2.1 (G6PDH) as well as 1.2.2 (6PGDH).

In the first reaction step, glucose-6-phosphate dehydrogenase (G6PDH) oxidizes G6P to 6-phosphoglucono-δ-lactone (6PGDL) with concomitant reduction of $NADP^+$ to NADPH. Subsequently, the 6-phosphogluconolactonase (6PGL) hydrolyzes 6PGDL to 6-phosphogluconate (6PG) that is oxidized further by the 6-phosphogluconate dehydrogenase (6PGDH) to Ru5P and $CO_2$ along with the reduction of one equivalent $NADP^+$ to NADPH. To that effect, the oxidative sequence of the pentose phosphate pathway supplies two equivalents NADPH per equivalent G6P. Hence, the amount of G6P that is introduced into the pentose phosphate pathway is dependent on the cellular demand for NADPH.[20, 21]

The reversible and non-oxidative part of the pentose phosphate pathway establishes a connection to the glycolysis. After an epimerase- or isomerase-catalyzed rearrangement of Ru5P to xylulose-5-phosphate or ribose-5-phosphate, a transketolase as well as a transaldolase catalyze the ensuing reactions to fructose-6-phosphate (F6P) or glyceral-3-phosphate (GAP). F6P and GAC are intermediates of the glycolysis.[20, 21]

### 1.2.1 Gucose-6-phosphate (G6PDH) from *Leuconostoc mesenteroides*

G6PDH is the first enzyme of the irreversible and oxidative sequence of the pentose phosphate pathway. It catalyzes the oxidation of G6P to 6PGDL. In the further course of the pentose phosphate pathway, the ring opening hydrolysis of 6PGDL to 6PG is required.[20, 21] Within living cells, the hydrolysis of 6PGDL occurs spontaneously even in the absence of the 6PGL (Scheme 2). However, the electrophilic 6PGDL possesses a considerably life-time. Thus, it can accumulate

within the cell and react with cellular nucleophiles or even rearrange to the dead-end species 6-phosphoglucono-γ-lactone. To circumvent this fact, the hydrolysis of 6PGDL to 6PG is accelerated by the 6PGL (Scheme 1).[22] On the contrary, extracellular, in the absence of nucleophiles and in the presence of a buffered, ultrapure, aqueous medium, there is no need for the utilization of the 6PGL. The hydrolysis of 6PGDL to 6PG occurs spontaneously and rapid, which may potentially be supported by the high water content of the buffer solution in comparison to the water content of the cytoplasm (Scheme 2).

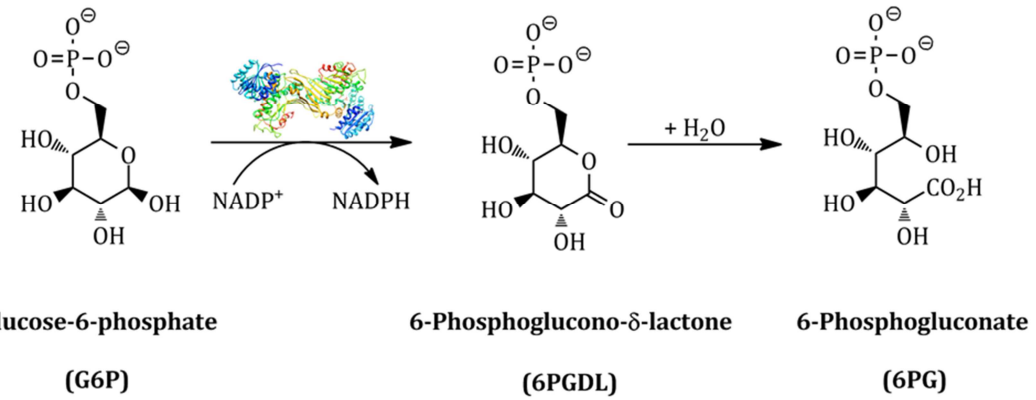


**Scheme 2.** The $NADP^+$ dependent G6PDH catalyzes the oxidation of G6P to 6PGDL. Extracellular, in aqueous media, the ring opening hydrolysis does not necessarily need to be catalyzed by a 6PGL. 6PGDL hydrolyzes spontaneously to give 6PG.[20]

G6PDH from *Leuconostoc mesenteroides* (*L.m.*G6PDH) is a homodimeric oxidoreductase (Figure 6a). Each monomeric subunit consists of 485 amino acids and possesses a molecular weight of 54.5 kDa.[23, 24, 25] The largest diameter of the enzyme was measured to be 11.2 nm.[26] Foremost hydrophilic amino acid residues are arranged on the surface of the enzyme (Figure 6b). As the isoelectric point (pI) of the *L.m.*G6PDH was detected to be at pH 4.6, the surface amino acids are mostly negatively charged at pH 7.0 (Figure 6c).

[22] E. Miclet, V. Stoven, P.A.M. Michels, F.R. Opperdoes, J.-Y. Lallemand, F. Duffieux, *J. Biol. Chem.* **2001**, *276*(37) 34840-34846.
[23] P. Rowland, A.K. Basak, S. Gover, H.R. Levy, M.J. Adams, *Structure* **1994**, *2*(11), 1073-1087.
[24] M.S. Cosgrove, C. Naylor, S. Paludan, M.J. Adams, H.R. Levy, *Biochemistry* **1998**, *37*, 2759-2767.
[25] M.S. Cosgrove, S.N. Loh, J.-H. Ha, H.R. Levy, *Biochemistry* **2002**, *41*, 6939-6945.
[26] D.I. Fried, Designed Enzyme-Inorganic Hybrid Materials for Application in Biocatalysis, Dissertation, Universität Hamburg, **2014**.

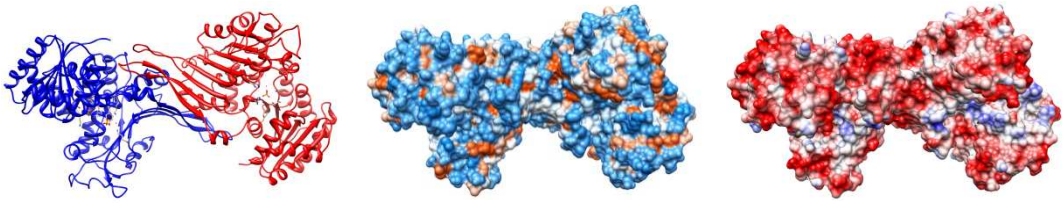


**Figure 6.** G6PDH with bound substrate (PDB ID: 1dpg): a) Ribbon model: Monomer A (red) and monomer B (blue); Surface mapping: b) Hydrophilic areas (blue) and hydrophobic areas (red); c) Coulomb surface: Positively charged areas (blue), negatively charged areas (red), neutral (white) at pH 7.[27]

The secondary structure of *L.m.*G6PDH is determined by 15 β-sheet strands as well as 17 α-helices. Each subunit of the enzyme consists of two domains. The smaller domain (amino acids 1 - 177) harbors the coenzyme binding site, which is composed of a typical Rossmann fold. This domain is separated by a cleft from the larger β+α domain (amino acids 178 - 485). The cleft between the domains was identified to be the active site; whereas the β+α domain is mainly incorporated into the formation of the dimeric structure. The attractive interactions between the monomers resulting in the formation of the dimer are mainly hydrophobic. Beside two main chain hydrogen bonds, salt bridges were found to contribute to the construction of the dimer. Within the homodimeric structure, the monomers are rotated by 178.6°. Moreover, Pro149 in one subunit is *cis* configured, whereas it is in *trans* configuration in the second subunit leading to significant structural changes within this region (amino acids 147 - 176).[25]

*L.m.*G6PDH accepts $NADP^+$ as well as $NAD^+$ as a coenzyme. In the presence of $NADP^+$, the coenzyme is bound firstly prior to the binding of G6P; whereas in the presence of $NAD^+$ binding of the coenzyme and the substrate is performed in a random order.[24] The proposed catalytic mechanism of *L.m.*G6PDH is depicted in Scheme 3.

[27] E.F. Pettersen, T.D. Goddard, C.C. Huang, G.S. Couch, D.M. Greenblatt, E.C. Meng, T.E. Ferrin, *J. Comput. Chem.* **2004**, *25*, 1605–1612.

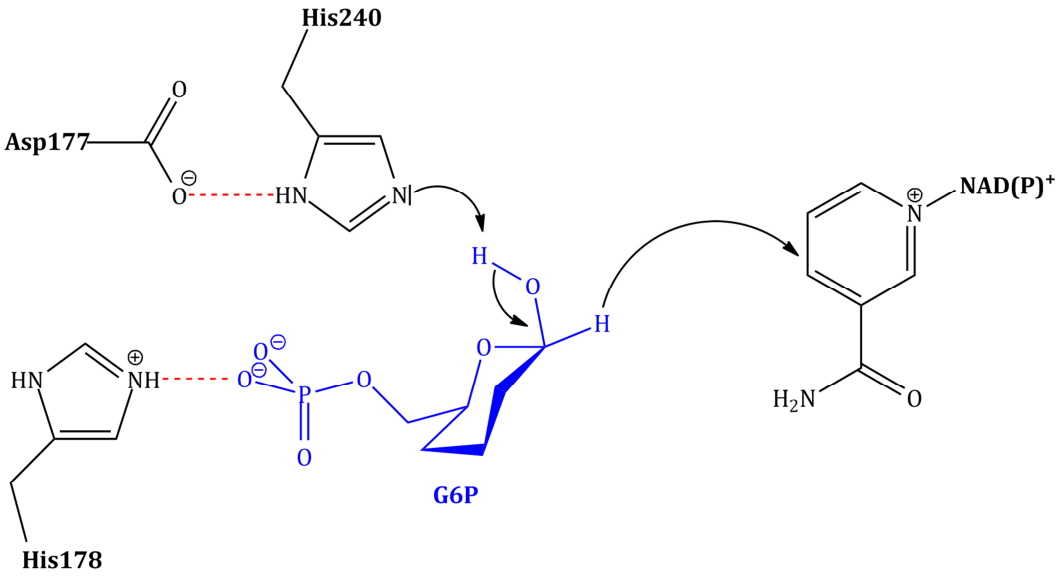


**Scheme 3.** Mechanism of the G6PDH-catalyzed oxidation of G6P as well as the simultaneous reduction of NAD(P)$^+$ under consideration of the incorporated amino acids of the active site of G6PDH. Reprinted with permission from [24]. Copyright 1998 American Chemical Society.

His240 abstracts the proton of the hydroxyl group in C1 position (C1-OH) of G6P. The arising negative charge of His240 is stabilized by Asp177 that is hydrogen bonded to the imidazole residue of His240. However, Asp177 is likewise supposed to increase the basicity of His240. The deprotonation of the C1-OH group is followed by a hydride transfer from C1 of the G6P to NADP$^+$. The imidazole residue of His178 contributes to the substrate fixation by means of a hydrogen bond to a negatively charged oxygen atom of the phosphate moiety of G6P accompanied by charge-charged interactions.[24, 25]

### 1.2.2 6-Phosphogluconate dehydrogenase (6PGDH)

6PGDH is the third enzyme of the oxidative path of the pentose phosphate pathway. It catalyzes the oxidation of 6PG to Ru5P accompanied by the reduction of $NADP^+$ to NADPH (Scheme 4).[20]

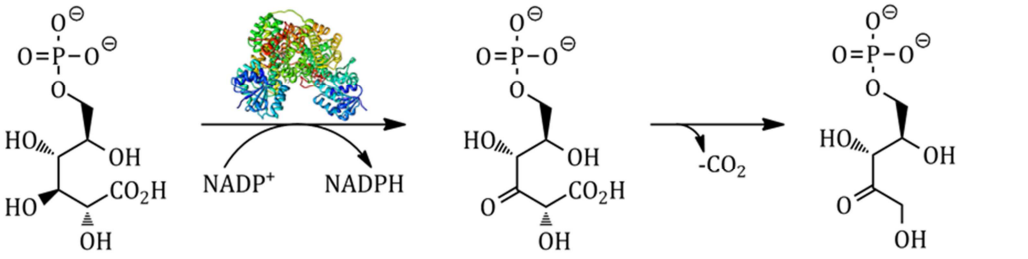


**6-Phosphogluconate (6PG)** | **3-Keto-6-phosphogluconate (3K6P)** | **Ribulose-5-phosphate (Ru5P)**

**Scheme 4.** The $NADP^+$ dependent 6PGDH catalyzes the oxidation of 6PG to Ru5P. The first reaction step is characterized by the formation of the intermediate 3-keto-6-phosphogluconate (3K6P). The subsequent spontaneous decarboxylation provides Ru5P.[20]

6PGDH from *Geobacillus stearothermophilus* (*G.s.*6PGDH) is a $NADP^+$ dependent, homodimeric oxidoreductase (Figure 7a). Each monomeric unit is composed of 469 amino acids and possesses a molecular weight of 57 kDa.[28] The largest diameter of the enzyme was measured to amount 8.5 -9.0 nm.[29] The *G.s.*6PGDH shows thermophilic behavior. Thus, enzymatic activity can even be detected at elevated temperatures (< 80 °C). The enzyme retains its full activity up to 60 °C, which corresponds to the optimal growth temperature of *Geobacillus stearothermophilus*. However, denaturation sets in when exceeding a temperature of 60 °C. The half-time of the denaturation increases significantly from 70 °C (80 min) to 80 °C (3 min). The optimal enzymatic activity is obtained at pH 8.0 and 43 °C.[30, 31, 32, 33]

The surface of *G.s.*6PGDH is mainly covered by polar and thus hydrophilic amino acids ensuring a good water solubility (Figure 7b). As surface mapping of the Coulomb surface disclosed, broad areas of the protein surface are uncharged at pH 7.0 (Figure 7c). The pI of the *G.s.*6PGDH is reached at pH 6.5.

[28] S.C. Cameron, V.P. Martini, J. Iulek, W.N. Hunter, *Acta Cryst.* **2009**, *F65*, 450-454.
[29] PDBsum: 2w8z: http://www.ebi.ac.uk/pdbsum/2w8z, **2016**.
[30] B.M.F. Pearse, J.I. Harris, *FEBS letters* **1973**, *38*(1), 49-52.
[31] F.M. Veronese, E. Boccù, A. Fontana, C.A. Benassi, E. Scoffone, *Biochim. Biophys. Act.* **1974**, *334*, 31-44.
[32] F.M. Veronese, E. Boccù, A. Fontana, *Biochemistry* **1976**, *15*(18), 4026-4033.
[33] H.J. Lubberding, P.V.M. Bot, *Arch. Microbiol.* **1984**, *137*, 115-120.

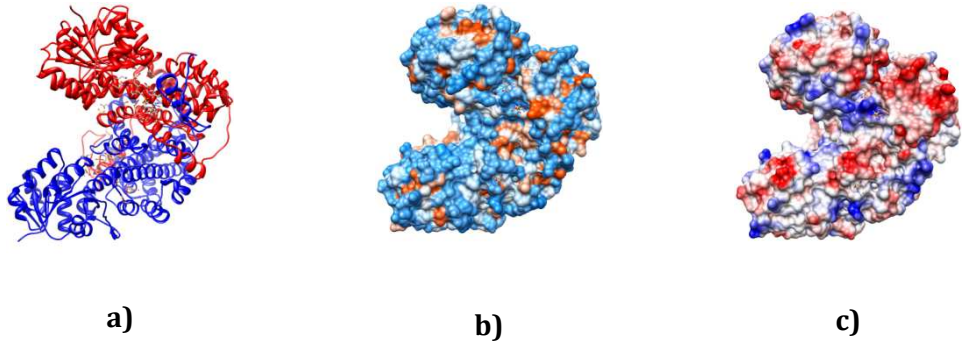

a) b) c)

**Figure 7.** 6PGDH with bound substrate (PDB ID: 2w8z): a) Ribbon model: Monomer A (red) and monomer B (blue); Surface mapping: b) Hydrophilic areas (blue) and hydrophobic areas (red); c) Coulomb surface: Positively charged areas (blue), negatively charged areas (red), neutral (white) at pH 7.0.[27]

The $NADP^+$ binding site of the *G.s.*6PGDH is composed of the amino acid residues 1 - 174 of the N-terminal domain due to a common Rossmann fold; whereas the residues 175 – 433 are arranged in ten α-helices. These are essential for the formation of the homodimeric structure. The substrate binding site of the 6PGDH is constructed by amino acid residues of the N-terminus of one monomer and the residues Arg446 as well as His452 of the partner monomer (Figure 8). The fixation of 6PG is carried out by means of hydrogen bonds and water mediated hydrogen between the respective amino acid residues of the active site and oxygen atoms of 6PG.[28]

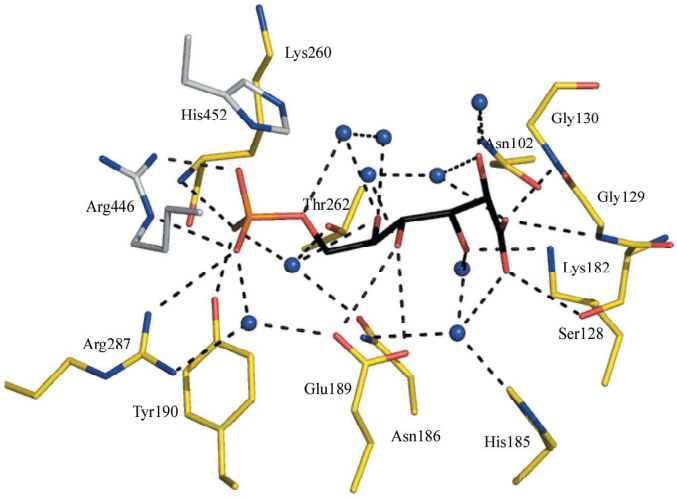


**Figure 8.** Active site *G.s.*6PGDH with bound 6PG. Both monomeric units of the dimer contribute to the fixation of the substrate. Monomer A: C-atoms yellow; monomer B C-atoms grey (Arg446, His452). Reproduced with permission of the International Union of Crystallography (http://journals.iucr.org/).[28]

Within the last 20 years, an acid-base mechanism turned out to be responsible for the enzymatic conversion of 6PG to Ru5P. With respect to this mechanism, Lys182 was identified to acts as a base; whereas Glu189 figured out to serve as the acid. Moreover, Lys182 (Lys183) and Glu189 (Lys190) are incorporated in the sequences of all determined 6PGDH species. Hence, the reaction mechanism of 6PGDH is equal independent on the organism of its expression. The enzymatic conversion of 6PG proceeds in three steps (Scheme 5).[34, 35, 36, 37]

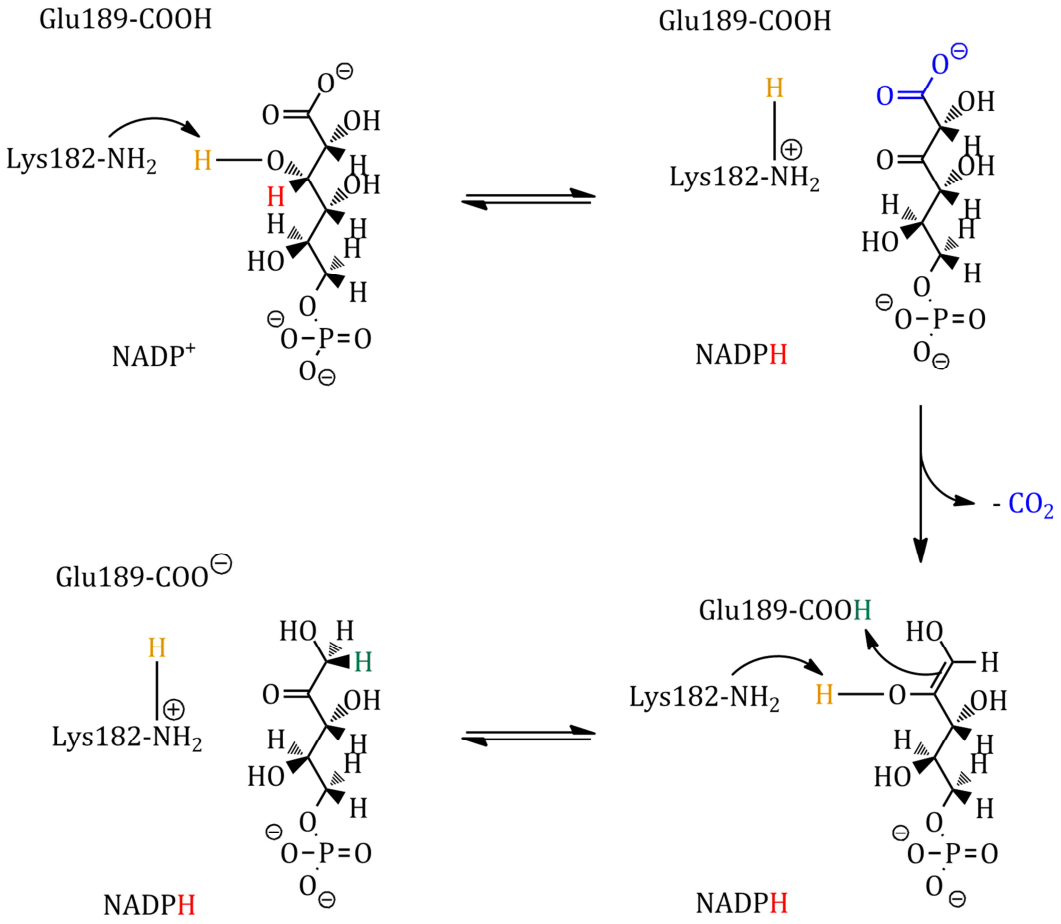


**Scheme 5.** Reaction mechanism of the 6PGDH-catalyzed oxidation of 6PG with reference to the most important amino acid residues of the active site incorporated into the conversion.[34, 35, 36, 37] Figure redrawn with permission of the *Journal of Biological Chemistry*.[37]

The initial step of the oxidation of 6PG is the deprotonation of the hydroxyl group on C3 by the basic amino residue of Lys182 resulting in the intermediate 3-keto-6-phosphogluconate. This reaction step is accompanied by a hydride transfer

[34] M.J. Adams, G.H.Ellis, S. Gover, C.E. Naylor, C. Phillips, *Structure* **1994**, *2*(7), 651-668.
[35] W.E. Karsten, L. Chooback, P.F. Cook, *Biochemistry* **1998**, *37*, 15691-15697.
[36] L. Zhang, L. Chooback, P.F. Cook, *Biochemistry* **1999**, *38*, 11231-11238.
[37] S. Hanau, K. Montin, C. Cervellati, M. Magnani, F. Dallocchio, *J. Biol. Chem.* **2010**, *285*(28), 21366-21371.

from C3 to $NADP^+$. After the release of $CO_2$ from 3K6P associated with the protonation of the oxygen atom on C2 (former C3) by Lys182, an 1,2-enediol intermediate is formed. The final step of the conversion of 6PG is characterized by the tautomerization of the intermediate, involving the deprotonation of the carboxyl group of Glu189 as well as the re-protonation of the amino group of Lys182.[34, 35, 36, 37]

### 1.3 Cofactors and coenzymes

Numerous enzymes are dependent on a coenzyme or cofactor. Within the enzymatic conversion of a substrate, coenzymes and cofactors supply or gain electrons, protons, hydrogen or oxygen atoms or molecule fragments. This is indispensable for a reliable and complete conversion of the respective substrate. Thus, in its absence, no substrate conversion is observed. Cofactors are covalently (prosthetic group) or coordinately (metal ions) bound to the enzyme. Conversely, coenzymes are merely temporarily bound to the coenzyme binding site of an enzyme *via* hydrogen bonds and it dissociates into the reaction medium after the conversion of the substrate.[2, 20, 21]

Most oxidoreductases are dependent on the coenzymes nicotinamide adenine dinucleotide phosphate ($NADP^+$) or nicotinamide adenine dinucleotide ($NAD^+$, Scheme 6).

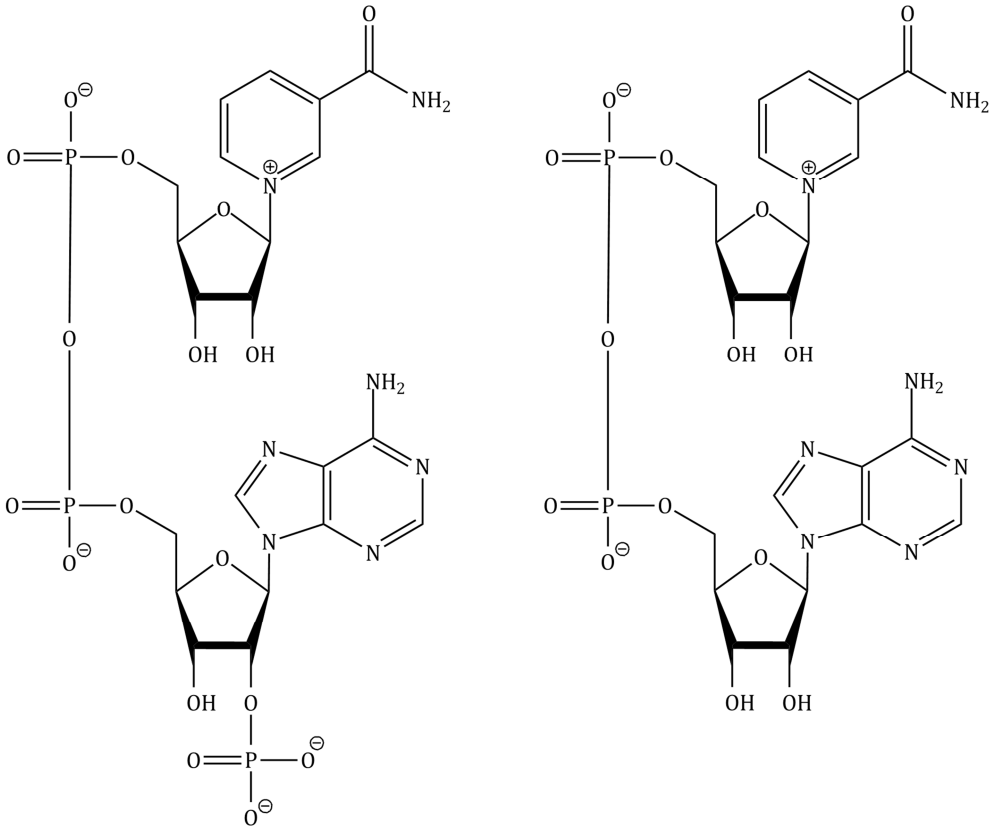


**Scheme 6.** Graphical depiction of nicotinamide adenine dinucleotide phosphate $NADP^+$ and nicotinamide adenine dinucleotide ($NAD^+$).

$NADP^+$ as well as $NAD^+$ originate from niacin (vitamin $B_3$).[20] As oxidoreductases catalyze redox reactions, the coenzyme is responsible for the donation or acceptance of a proton and two electrons (Scheme 7).

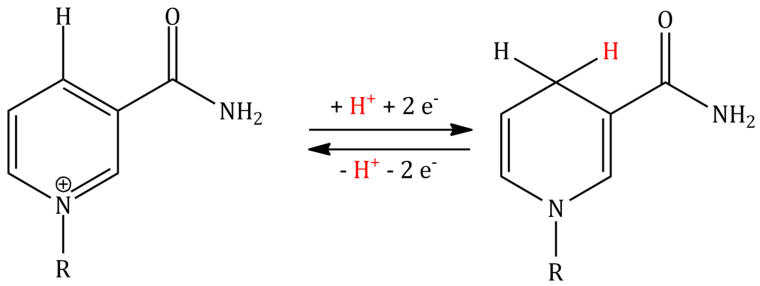


**Scheme 7.** Reduction (forward reaction) and oxidation (back reaction) of the nicotinamide residue of $NAD(P)^+/H$. The protonation/deportation is carried out in C4 position.

Within living cells, the demand on $NAD(P)^+/H$ is regulated very sensitively by various metabolic pathways. However, the dependency of enzymes on

$NAD(P)^+/H$ limits its application in organic synthesis, as these coenzymes in their reduced as well as oxidized form are very cost-intensive and a stoichiometric provision is necessary. Hence, recycling of the coenzyme is required in order to increase the efficiency of an enzyme catalytic approach in laboratory scale.

### 1.3.1 Coenzyme recycling

The efficient employment of coenzyme-dependent enzymes in cell free systems requires a reliable and high-performance regeneration method of the coenzyme. Within the last decades, different coenzyme recycling principles were established. However, solely the substrate-coupled as well as the enzyme-coupled recycling are of importance, nowadays.

The quality of a coenzyme recycling system is quantified on basis of the total turnover number (TTN). The dimensionless TTN is defined by the ratio of the molar amount of product ($n_p$) and the molar amount of the consumed coenzyme ($n_{NAD(P)^+/H}$; Eq. 1).[38]

$$TTN = \frac{n_p}{n_{NAD(P)^+/H}} \qquad \textbf{Eq. 1}$$

The TTN describes the number of reaction cycles that are performed until the coenzyme molecule is degraded. In laboratory scale TTN values of 1000 – 10,000 are adequate, whereas TTN values of ≥100,000 are required with respect to industrial applications.[2]

In the following section the above mentioned fundamental principles of the regeneration of $NAD(P)^+$ or NAD(P)H are introduced, whereas, at this point, the focus was placed onto non-immobilized enzymes.

**Substrate-coupled recycling.** The substrate-coupled approach of the coenzyme recycling is characterized by the provision of a second type of substrate initiating the opposite enzymatic reaction (Scheme 8). After the conversion of the main substrate accompanied by the oxidation/reduction of the coenzyme, the second substrate is converted by the same enzyme with concomitant re-oxidation/re-reduction of the coenzyme. Thus, the reconverted coenzyme can be introduced into the main reaction again.[2, 38] To avoid lack of the essential form of the coenzyme, the main reaction is required to be rate-determining. Conversely, the

[38] R. Wichmann, D. Vasic-Racki, *Adv. Biochem. Engin./Biotechnol.* **2005**, *92*, 225-260.

reaction rate of the coenzyme recycling step needs to be considerable higher than the reaction rate of the main reaction.[39]

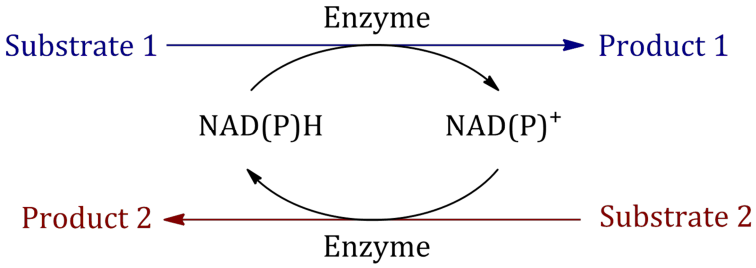


**Scheme 8.** Schematic illustration of the substrate-coupled coenzyme recycling. NAD(P)H is regenerated by the addition of a second substrate (substrate 2). Its enzymatic conversion requires the oxidized form of the coenzyme ($NAD(P)^+$). Copyright Springer-Verlag Berlin Heidelberg 2011. Reproduced with permission of Springer.[2]

The reduction of 6-methyl-5-heptene-2-one (sulcatone; 25 mM) to 6-methyl-5-heptene-2-ol (sulcatol) by the alcohol dehydrogenase from *Thermoanaerobium brockii* (*T.b.*ADH, 2.9 U) is accompanied by the oxidation of NADPH (0.2 mM) to $NADP^+$. $NADP^+$ was re-oxidized due to the likewise *T.b.*ADH-catalyzed oxidation of 2-propanol (3 M) to acetone (Scheme 9).[39]

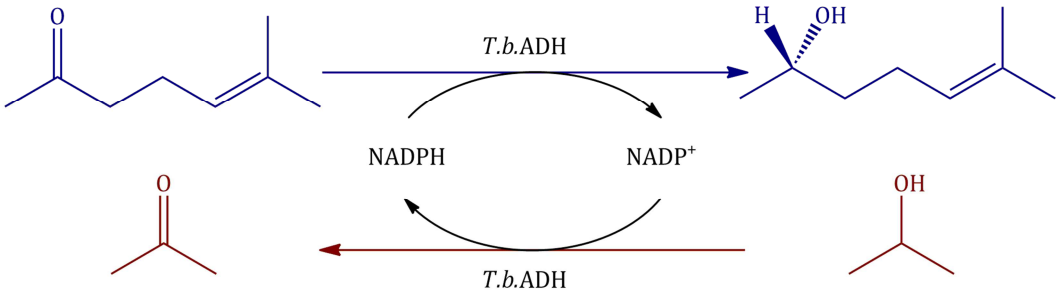


**Scheme 9.** The reduction of sulcatone to sulcatole by the *T.b.*ADH is accompanied by the oxidation of NADPH to $NADP^+$ (blue path). The presence of 2-propanol in the reaction mixture introduces the *T.b.*ADH-catalyzed re-reduction of $NADP^+$ to NADPH (red path). Copyright 1999 Kluwer Academics Publisher. Redrawn with permission of Springer.[39]

The main reaction and the recycling reaction were carried out in a biphasic system as sulcatone as well as sulcatole are non-miscible with water. Hence, the enzymatic reactions take place at the phase interface. Since $NADP^+$ in the main reaction was enzymatically re-reduced to NADPH immediately, the conversion of sulcatone was irreversible. After 72 h, 100 % of the sulcatone amount applied was

[39] F. de M. Bastos, A.G. dos Santos, J. Jones Jr, E.G. Oestreicher, G.F. Pinto, L.M.C. Paiva, *Biotechnol. Tech.* **1999**, *13*, 661-664.

reduced. This corresponds to a TTN of 125. The recycling reaction was determined to be faster than the main reaction and the inhibition of the *T.b.*ADH due to sulcatole was negligible. This was referenced to the large excess of the recycling substrate 2-propanol.[39, 40]

In a further approach the ADH from *Horse liver* (*H.l.*ADH) was utilized in a substrate-coupled NADH regenerating system. Moreover, the *H.l.*ADH was exposed to toluene as an unconventional media. The enzyme was deposited in a buffered solution containing methyl cellulose or polyvinyl butyral as well as $NAD^+$. Subsequent, the mixture was freeze-dried over 8 h. Prior to the addition of the enzyme preparation to the substrate solution, containing cyclohexanone and Cyclohexanol in toluene, the former was incubated in buffer solution overnight (Scheme 10).[41]

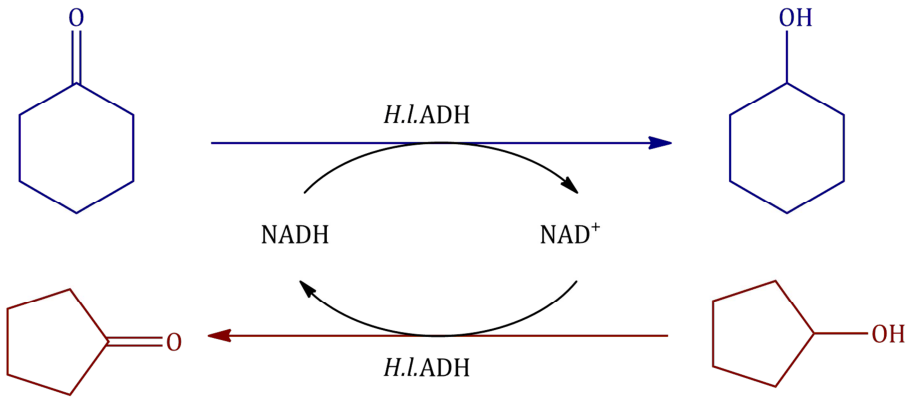


**Scheme 10.** The reduction of cyclohexanone to cyclohexanol by the *H.l.*ADH is accompanied by the oxidation of NADH to $NAD^+$ (blue path). The presence of cyclopentanol in the reaction mixture introduces the *H.l.*ADH-catalyzed re-reduction of $NAD^+$ to NADH (red path). Reproduced with permission of Springer.[41]

In the catalytic cycle, the *H.l.*ADH catalyzes the reduction of cyclohexanone to cyclohexanol with concomitant oxidation of NADH. The reconversion of $NAD^+$ to NADH was initiated due to cyclopentanol that was enzymatically oxidized to cyclopentanone. More than 75 % of the deployed cyclohexanone amount was enzymatically reduced and a TTN of about 100000 was detected for the coenzyme.[41] Hence, this approach is very promising as TTNs of >10000 are required with respect to an efficient reuse of the coenzyme.[2]

[40] F. de M. Bastos, T.K. Franca, G.D.C. Machato, G.F. Pinto, E.G. Oestreicher, L.M.C. Paiva, *J. Mol. Catal. B.: Enzym.* **2002**, *19-20*, 459-465.
[41] C. Virto, I. Svensson, P. Adlercreutz, B. Mattiasson, *Biotechnol. Lett.* **1995**, *17*(8), 877-882.

**Enzyme-coupled recycling.** In the case of an enzyme-coupled coenzyme recycling, a second enzyme and its substrate coexist, besides the actual enzyme and its substrate (Scheme 11). After the conversion of the main substrate, which comes along with the oxidation/reduction of the coenzyme, the second enzyme converts its substrate with re-conversion of the coenzyme. Hence, the recycled coenzyme can be introduced into the main reaction path again. Special attention has to be paid concerning the reaction rates of the coexisting enzymes. To avoid lack of one form of the coenzyme the reaction rates of both enzymes are required to be almost equal.[2, 38]

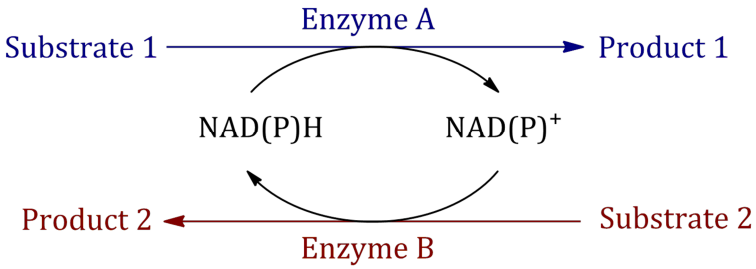


**Scheme 11.** Schematic depiction of the enzyme-coupled coenzyme recycling. NAD(P)H is regenerated by the addition of a second substrate (substrate 2) and a further enzyme (enzyme B) that requires the reduced coenzyme ($NAD(P)^+$). Copyright Springer-Verlag Berlin Heidelberg 2011. Reprinted with permission of Springer.[2]

A widespread method for the recovery of NADH is the utilization of formate dehydrogenase (FDH). The $NAD^+$-dependent FDH catalyzes the conversion of formic acid/$NAD^+$ to $CO_2$/NADH. TTN values of 600000 are reported. The application of FDH is attractive as inexpensive formic acid serves as the substrate.[2]

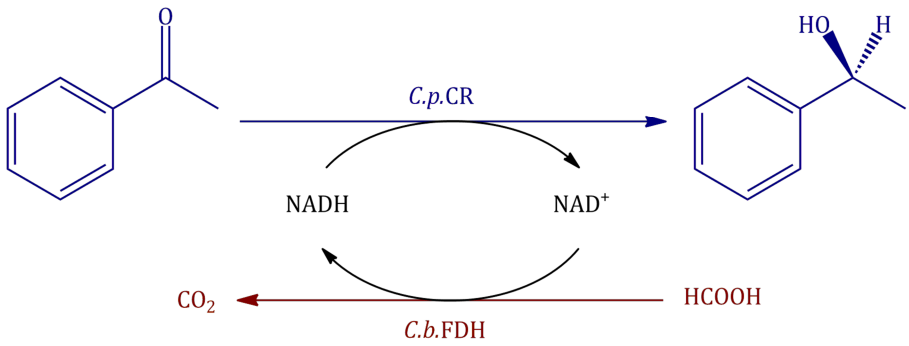


**Scheme 12.** The reduction of acetophenone to (*S*)-phenylalcohol by the *C.p.*CR is accompanied by the oxidation of NADH to $NAD^+$ (blue path). The presence of formic acid in the reaction mixture introduces the *C.b.*FDH-catalyzed re-reduction of $NAD^+$ to NADH (red path). Reprinted from [42]. Copyright 1999, with permission from Elsevier.

[42] S. Rissom, J. Beliczey, G. Giffels, U. Kragl, C. Wandrey, *Tetrahedron: Asymmetry* **1999**, *10*, 923-928.

The carbonyl reductase from *Candida parapsilosis* (*C.p.*CR) was used for the enzymatic reduction of acetophenone to (*S*)-phenylalcohol in a bi-membrane reactor. The simultaneously oxidized NADH was re-reduced due to a coupled FDH recycling system (Scheme 12). The TTN of the cofactor regeneration amounted to 1600 for this recycling approach.[42]

Likewise hydrogenases can be deployed for the generation of NADH. The reduction of cyclohexanone to cyclohexanol by the $NAD^+$/H dependent *H.l.*ADH was coupled to a hydrogenase-catalyzed re-reduction of $NAD^+$ (Scheme 13).[43]

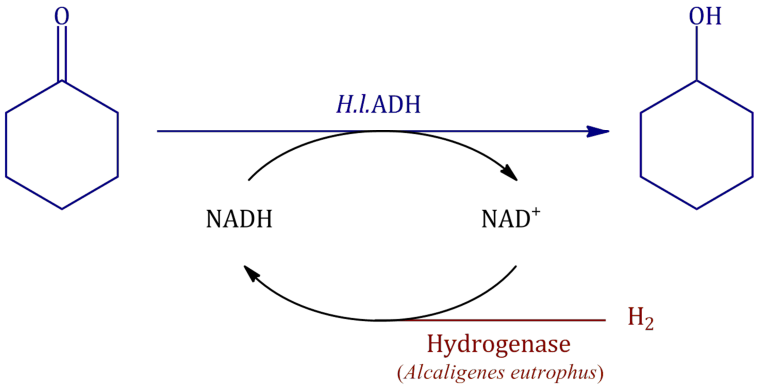


**Scheme 13.** The reduction of cyclohexanone to cyclohexanol by the *H.l.*ADH is accompanied by the oxidation of NADH to $NAD^+$ (blue path). The reaction medium is hydrogen-saturated. Thus, NADH can be recovered by a hydrogenase (red path). Reprinted with permission from Wiley-VCH.[43]

The reaction cycle was carried out in a biphasic system, whereupon the reduction of cyclohexanone was performed in various hydrogen-saturated organic solvents and the regeneration of NADH was operated in the buffered aqueous phase. In this approach, permeabilized cells of *Alcaligenes eutrophus* containing a hydrogenase in its cytosol were applied (0.6 – 6.1 mg). By reason of the minor stability of the hydrogenase, the efficiency of the coenzyme recycling step turned out to be highly dependent on the amount of the cells deployed. Under the given conditions (1 µmol $NAD^+$, 200 µmol cyclohexanone in heptane/ Tris-HCl buffer), a complete substrate conversion was achieved after approximately 90 h when a cell amount of 6.1 mg was provided.[43]

Beyond the introduced approaches regarding the regeneration of NAD(P)$^+$/H, several further but negligible approaches can be found in literature. The presence of sodium dithionite provides an opportunity for the *in-situ* re-reduction of

[43] M. Andersson, H. Holmberg, P. Adlercreutz, *Biotechnol. Bioeng.* **1998**, *57*, 79-86.

$NAD^+$ to NADH. Under certain conditions, NADH was regenerated 105-fold.[44] However, a turnover number of 105 is comparatively low and in many cases the presence of co-reagents such as sodium dithionite in enzymatic reactions is undesired. However, $NADP^+$ can even be simply reduced by hydrogen gas in the presence of a Ru(II) as well as a Rh(III) catalysts. This approach was discussed by means of the *T.b.*ADH-catalyzed reduction of 2-heptanone to (*S*)-2-heptanol with incorporated oxidation of NADPH. The reaction was carried out under a hydrogen atmosphere. Under the given conditions, the re-reduction of $NADP^+$ to NADPH was successful, whereas the enantiomeric excess of (*S*)-2-heptanol decreased from 99 % ee to 40 % ee. This was addressed to the additional reduction of amino acid side chains of the *T.b.*ADH affecting its enantioselectivity as well as to direct reduction of 2-heptanone by the hydrogen gas. Furthermore, the TTN amounted merely 10.[45]

The reduction of $NAD^+$ to NADH can also be accomplished due to electrochemical regeneration. With a TTN of 9 $NAD^+$ was reduced on the surface of a silver electrode covalently modified with L-histidine residues.[46]

The coexistence of NAD(P)H and methylene blue or N-methyl phenazonium methyl sulfate in an enzymatic reaction allows a photochemical regeneration of $NAD(P)^+$. After the irradiation of the dye using visible light accompanied by the transition into its excited state, it is able to oxidize NAD(P)H. When adding methylene blue to the *Yeast* ADH-catalyzed conversion of ethanol/$NAD^+$ to acetaldehyde/NADH a TTN of 1125 regarding the re-oxidation of NADH was achieved.[47]

[44] J.B. Jones, D.W. Sneddon, W. Higgins, A.J. Lewis, *J. Chem. Soc., Chem. Commun.* **1972**, 856-857.
[45] P.S. Wagenknecht, J.M. Penney, R.T. Hembre, *Organometallics* **2003**, *22*, 1180-1182.
[46] Y.-T. Long, H.-Y. Chen, *J. Electroanal. Chem.* **1997**, *440*, 239-242.
[47] M. Julliard, J. Le Petit, *Photochem. Photobiol.* **1982**, *36*, 283-290.

### 1.3.2 Alcohol dehydrogenase (ADH) from *Escherichia coli* (*E. coli*)

ADH from *E. coli* (*E.c.*ADH) is a $NADP^+$ dependent oxidoreductase. It catalyzes the oxidation of alcohols to the respective ketones (forward reaction) but also the reduction of ketones to the respective alcohols (back reaction; Scheme 14).

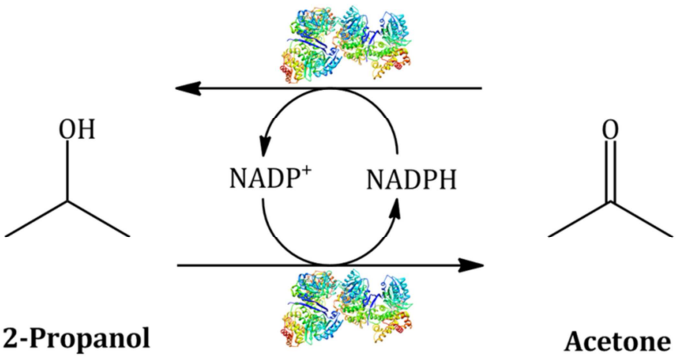


**Scheme 14.** Reaction scheme of ADH: Among others, ADH catalyzes the oxidation of 2-propanol to acetone with concomitant reduction of $NADP^+$ to NADPH. In the presence of a sufficient concentration of NADPH, ADH is additionally able to catalyze the back reaction of acetone to 2-propanol accompanied by the oxidation of the coenzyme to $NADP^+$.

*E.c.*ADH possesses a broad substrate acceptance. Besides the introduced conversion of 2-propanol/acetone, it is likewise able to convert various alcohols as well as aldehydes but also amino acids and sugars. A preference for alcohols with a carbon chain longer than $C_3$ was reported.[48, 49]

*E.c.*ADH is a homodimeric oxidoreductase with a molecular weight of 96 kDa and a maximum diameter of 12.3 nm (Figure 9a).[50, 51] The pH optimum was detected to be at pH 7.0 and the temperature optimum is at 37 °C.[49] The surface of the enzyme is mainly covered by hydrophilic amino acids, whereas hydrophobic amino acids are arranged in the core of the three dimensional structure (Figure 9b). Dependent on the pH value of the reaction medium, the ADH possesses a certain surface charge (Figure 9c). The isoelectric point (pI) was calculated to be at 6.1.[52, 53]

[48] G. Sulzenbacher, K. Alvarez, R.H.H. van den Heuvel, C. Versluis, S. Spinelli, V. Campanacci, C. Valencia, C. Cambillau, H. Eklund, M. Tegoni, *J. Mol. Biol.* **2004**, *342*, 489-502.
[49] J.M. Perez, F.A. Arenas, G.A. Pradenas, J.M. Sandoval, C.C. Vasquez, *J. Biol. Chem.* **2008**, *283*, 7346-7353.
[50] D. Burdette, J.G. Zeikus, *Biochem. J.* **1994**, 302, 163-170.
[51] PDBsum: 1OJ7: http://www.ebi.ac.uk/pdbsum/1OJ7, **2016**.
[52] ecoliwiki: http://ecoliwiki.net/colipedia/index.php/yqhD:Gene_Product(s), **2017**.
[53] RegulonDB: http://regulondb.ccg.unam.mx/gene?term=ECK120004123&organism=ECK12&format=jsp&type=gene, **2017**.

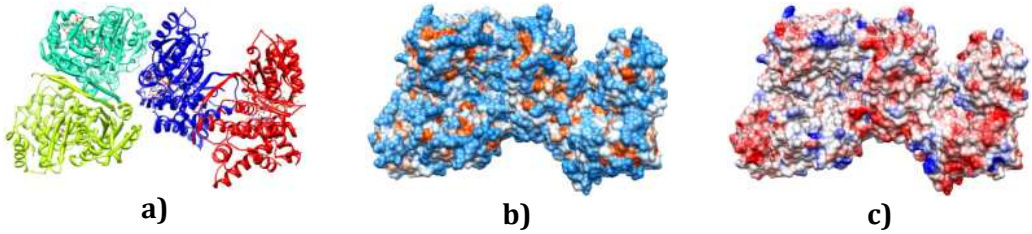


**Figure 9.** ADH from *E.coli* with bound $NADP^+$ (PDB ID: 1OJ7): a) Ribbon model depicting the 4 subunits of the enzyme; b) Hydrophilic (blue) and hydrophobic (red) surface areas; c) Coulomb surface: Positively charged surface areas (blue), negatively charged areas (red), neutral areas (white) at pH 7.[27]

Each of the four subunits of the homodimeric enzyme is composed of two subunits consisting of 387 amino acids and one zinc ion within the active site, respectively. The homodimeric structure of *E.c.*ADH is mainly realized due to attractive interactions between the α-helices of the amino acid residues 221-219 as well as 242-255. Within each subunit, one domain is responsible for the fixation of $NADP^+$/H and the other domain is involved in the coordination of the zinc ion (Figure 10). The diphosphate residue of $NADP^+$/H interacts with the Gly93-Gly94-Gly95-Ser96 motif, whereas the 2'-phosphate residue interacts with Gly37, Gly38, Gly39 and Ser40. Against this background, hydrogens bonds are formed to Gly38 and Ser40 as well as Gly95 and Ser96. Hence, *E.c.*ADH is dependent on $NADP^+$/H, as a 2'-phosphate group is absent in $NAD^+$/H. In particular, binding of the coenzyme is exclusively executed due to hydrogen bonds. Besides the mentioned amino acids, hydrogen bonds are formed between the residues of Asp99, Thr138, Asn147, Gly149, Lys160, Tyr179 as well as Thr179 and nitrogen or oxygen atoms of $NADP^+$/H contributing to its fixation (Figure 10).[48]

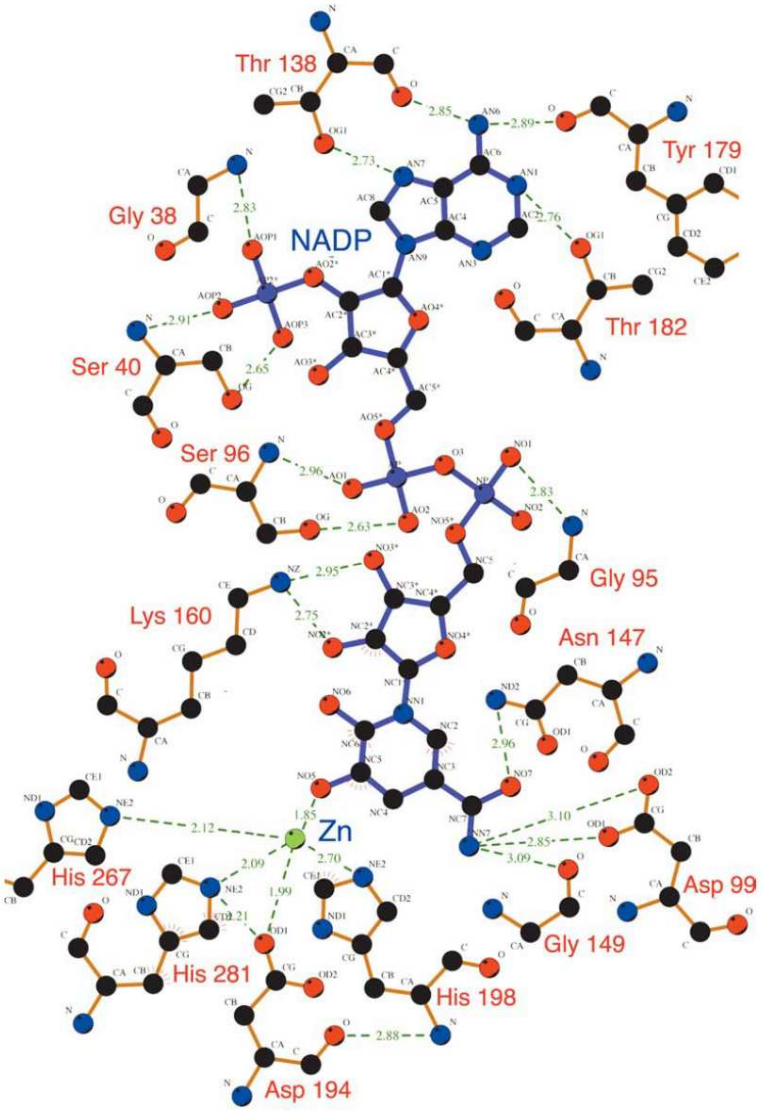


**Figure 10.** Subunit of *E.c.*ADH with modified and bound coenzyme ($NADPH(OH)_2$) as well as a coordinated Zn ion that is mandatory for catalysis. Reprinted from [48]. Copyright 2004, with permission from Elsevier.

The fixation of $NADP^+/H$ is accompanied by conformational changes within the active center. In relation to the coenzyme binding site, the active center rotates by 15°, whereas Thr182 serves as the linchpin.[48]

Investigations concerning the crystal structure of the ADH with bound coenzyme (holoenzyme) disclosed two covalently bound hydroxyl groups on C5 and C6 of the nicotinamide moiety of NADPH (Scheme 15).

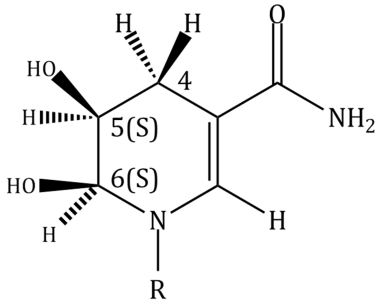


**Scheme 15.** Modification of the nicotinamide moiety ($NADPH(OH)_2$) of NADPH found after crystallization of the holoenzyme of *E.c.*ADH. Reprinted from [48]. Copyright 2004, with permission from Elsevier.

A hydroxylation in the C5 and C6 position of NADPH is unusual. However, a hydroxylation of C6 of the adenine residue of NADPH was described for ADH from *horse liver*. The formed hydroxyl group interacts with the Zn ion and contributes to its coordination.[54] However, in *E.c.*ADH the distance between the hydroxyl group on C6 of the adenine residue and the zinc ion is too long (3.8 Å) for the formation of a coordinative bond. Additionally, the hydroxyl group is directed away from the zinc ion. Furthermore, a contribution of the hydroxyl group on C6 on the hydride transfer can be excluded. However, the hydroxyl group on C5 forms a coordinative bond (1.85 Å) to the zinc ion of the active center. It was proposed that the hydroxylation of C5 and C6 can be addressed to the aerobic conditions and thus to oxygen stress to the *E.c.*ADH within the experiments.[48]

As previously mentioned, the active site of each of the four subunits contains a zinc ion. In the crystalized holoenzyme, the zinc atom is complexed due to distorted trigonal bipyramidal coordination by Asp194, His267 as well as a borate ion originating from the crystallization medium (Figure 10). The tips of the bipyramide are formed by coordinative bonds to the hydroxyl group in C5 position of the nicotinamide residue of NADPH and His281.[48] It can be assumed that the hydride transfer between the substrate and C4 of $NADP^+/H$ within the catalysis is implanted due to the coordination of the substrate molecule by the zinc ion and assisted by nicotinamide residue of the coenzyme in immediate vicinity.

## 1.4 Immobilization of enzymes onto solid carriers

Owing to its high substrate affinity the utilization of enzymes in synthetic chemistry and industry is widespread. However, enzymes cannot easily be separated from the reaction batch. Furthermore, an enzyme is usually denatured

[54] H. Eklund, J.P. Samma, L. Wallen, C.I. Branden, A. Akeson, T.A. Jones, *J. Mol. Biol.* **1981**, *146*, 561-587.

after removal from the reaction mixture. Thus, the employment of enzymes in chemical syntheses can rapidly become a cost factor. The immobilization of the desired enzyme onto a suited host material can bypass these difficulties. Besides an improved stability, the decisive advantage of an immobilized enzyme is its recyclability. The immobilisate can easily be separated by filtration or centrifugation and thus it can be reused. This benefits the employment of enzymes in chemical syntheses and industrial applications and contributes to an efficient application of enzymes in organic syntheses.[55, 56, 57, 58, 59]

Within the last two decades, an exorbitant quantity of possible carriers for enzymes and immobilization techniques has been established. Besides non-porous solids, primarily porous materials have attracted attention as a host material for enzymes.[55, 56, 60, 61] To date numerous strategies regarding the immobilization of an enzyme were developed. These procedures can be traced back to only a couple of main methods that will be discussed later on in the following chapters. Sometimes the immobilization of an enzyme is accompanied by an enhanced enzymatic activity. However, mostly a reduced activity of the immobilized enzyme is found in comparison to the native enzyme. L. Cao unbiasedly stated that the stabilization of an enzyme due to its immobilization can always be realized. Merely a suited host material need to be found, respectively.[62] Within this doctoral thesis it will turn out that this is easier said than done.

[55] M. Hartmann, *Chem. Mater.* **2005**, *17*, 4577-4593.
[56] D.I. Fried, F.J. Brieler, M. Fröba, *ChemCatChem* **2013**, *5*, 862-884.
[57] W. Tischer, F. Wedekind, *Top. Curr. Chem.* **1999**, *200*, 95-125.
[58] C.-H. Lee, T.-S. Lin, C.-Y. Mou, *Nano Today* **2009**, *4*, 165-179.
[59] U. Bornscheuer, *Angew. Chemie Int. Ed.* **2003**, *42*, 3336-3337.
[60] S. Datta, L.R. Christena, Y.R.S. Rajaram, *Biotech* **2013**, *3*, 1-9.
[61] S. Hudson, J. Cooney, E. Magner, *Angew. Chem. Int. Ed.* **2008**, *47*, 8582-8594.
[62] L. Cao, *Carrier-bound immobilized Enzymes*, Wiley-VCH, Weinheim, **2005**.

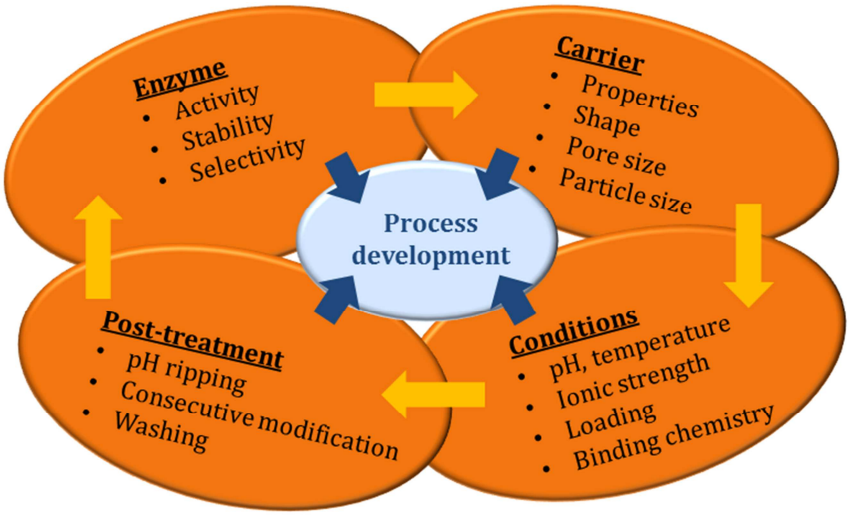


**Figure 11.** The efficient immobilization of an enzyme rests upon four pillars that mesh like cogwheels and need to be individually optimized. Figure redrawn with permission of Wiley-VCH.[62]

Once the immobilization of an enzyme is taken into account the four essential pillars of an immobilization need to be individually but carefully optimized in order to ascertain an efficient performance of the immobilized enzyme (Figure 11). The solid foundation of the development of an enzyme immobilization procedure is the optimization of the enzyme itself, as highly-purified and active enzymes are required. The selection of the host material is adjusted to the needs of the enzyme and it is closely coupled to the conditions of the immobilization procedure. The post-treatment of the immobilisate needs to be precisely inter-coordinated to the immobilization method and the requirements of the enzyme. The practicability of an immobilization method is assessed by means of the stability and accordingly the long-term activity of the immobilized enzyme.[62]

### 1.4.1 The stability of an immobilized enzyme

Before going into the insights of the enzyme immobilizations, it is indispensable to lose some general comments on the stability of an immobilized enzyme. This aspect is of paramount importance, as it is directly coupled to the catalytic activity of the immobilized enzyme. The stability and thus the quality of a carrier-bound enzyme (*immobilisate*) is considerably dependent on various factors.

In first instance, it is obvious that the stability of an immobilized enzyme is affected by the texture of the solid carrier.[63, 64] Porous carriers have been identified to stabilize the overall structure of the enzyme, as the pore wall shields the enzyme from external forces (shear forces e.g.). Whereas enzymes immobilized onto a non-

[63] J. Aparicio, J.V. Sinisterra, *J. Mol. Catal.* **1993**, *80*, 269-276.
[64] L. Bayne, R.U. Ulijn, P.J. Halling, *Chem. Soc. Rev.* **2013**, *42*, 9000-9010.

porous support material are directly exposed to these external forces leading to its rapid denaturation and thus to its inactivation.[65] However, enzymes that are immobilized onto a porous support are frequently affected by diffusion limitations of the substrate as well as the coenzyme from the bulk phase into the pore system.[66] Moreover, the relation between the enzyme size and the pore size of the carrier was identified to have a crucial impact on the stability of the immobilized enzyme (*pore-size matching*). It is evident that the main pore diameter of the host is required to be larger than the enzyme size in order to allow the enzyme to enter the porous network. However, a stabilization of the immobilized enzyme merely sets in when the pore size is only slightly larger than the maximum diameter of the enzyme (Figure 12). Otherwise the enzyme is affected from pronounced leaching, as the interactions between the surface of the enzyme as well as the pore walls are minimized.[67,68]

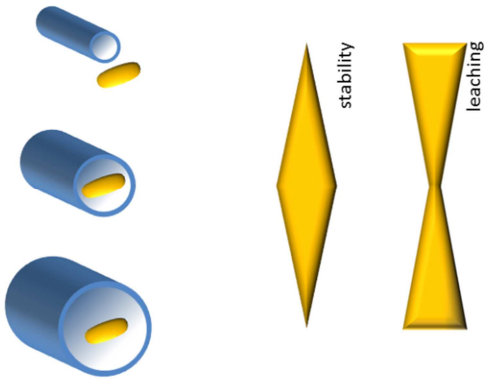


**Figure 12.** *Pore-size matching*: The stability of an enzyme that is immobilized onto a mesoporous carrier is dependent on the pore size of the host. An optimal stabilization of the enzyme can be achieved when the pore size is slightly larger than the enzyme size. Considerably larger pores in comparison to the enzyme size encourage leaching, which can be referenced to minimized interactions between the enzyme and the pore walls. Figure reprinted with permission from Wiley-VCH.[67]

Likewise, the chemical as well as the physical properties of the host material have an influence on the stability of an immobilized enzyme, too. These effects pertain to the microenvironment of the enzyme. The microenvironment represents the environment in close proximity to the bound enzyme. By reason of the chemical and physical characteristics, the surface of the carrier can exhibit hydrophobic (nonpolar) or hydrophilic (polar) properties as well as an electrostatic charge.[69]

[65] A.K. Singh, A.W. Flounders, J.V. Volponi, C.S. Ashley, K. Wally, J.S. Schoeniger, *Biosens. Bioelectron.* **1999**, *14*, 703-713.
[66] K. Buchholz, *Chem. Ing. Tech.* **1989**, *61*(8), 611-620.
[67] D.I. Fried, F.J. Brieler, M. Fröba, *ChemCatChem* **2013**, *5*, 862-884.
[68] H. Takahashi, B. Li, T. Sasaki, C. Miyazaki, T. Kajino, S. Inagaki, *Chem. Mater.* **2000**, *12*, 3301-3305.
[69] K.C. Dee, D.A. Puleo, R. Bizios, *An Introduction To Tissue-Biomaterials Interactions*, Wiley-Liss, Hoboken, **2002**.

Hence, buffer ions but also substrate or coenzyme molecules can potentially enrich and generate an alteration of the pH value and correspondingly a different ionic strength in the direct environment of the immobilized enzyme in comparison to the bulk buffer. This phenomenon is also known as *partition effect*. The accumulation of substrate/coenzyme molecules in direct proximity to the enzyme can induce an enhanced enzymatic activity, whereas the alteration of the pH value might negatively affect the enzymatic performance. Thus, the microenvironment of a carrier-bound enzyme obviously plays a decisive role with respect to the enzyme stability.[62, 70, 71, 72]

Furthermore, the immobilization of an enzyme is frequently performed *via* an organic linker (spacer) on the surface of the chosen support material.[73] The types of interactions between the surface of the enzyme and the spacers on the surface of the host as well as the number of attractive bonds formed likewise impair the activity of the immobilized enzyme. These interactions arise from covalent or adsorptive bonds.[62] The covalent immobilization of an enzyme prevents it from undesired leaching from the host, whereas the detachment of the immobilized enzyme is frequently pronounced in the case of an adsorptive immobilization. Moreover, a covalent immobilization is carried out by distinct amino acid residues on the surface of the enzyme. Correspondingly, the respective amino acid residues on the surface of the enzyme incorporated into the immobilization can be predicted and thus an immobilization *via* amino acid residues of the active site can be ruled out. Hence, the accessibility and function of the active sites is preserved. In contrast, an adsorptive immobilization rests upon electrostatic, polar or hydrophobic interactions. These interactions are required to be very strong in order to avoid leaching of the enzyme. Adsorptive interactions occur between broad areas of the enzyme surface and the surface of the carrier.[69, 74] Thus, it is hardly possible to verify defined amino acid residues that are involved in the immobilization. Nevertheless, with respect to a preferable high retention of enzymatic activity, an immobilization via amino acid residues contributing to the fixation of the substrate or coenzymes or rather participating in the actual catalysis should be excluded. This connection demonstrates the dependency of the enzyme stability on the method of its immobilization.

[70] J.N. Talbert, J.M. Goddard, *Colloids Surf., B* **2012**, *93*, 8-19.
[71] D.G. Castner, B.D. Ratner, *Surf. Sci.* **2002**, *200*, 28-60.
[72] L. Ferreira, M.A. Ramos, J.S. Dordick, M.H. Gil, *J. Mol. Catal. B: Enzym.* **2003**, *21*, 189-199.
[73] M. Shakeri, K. Kawakami, *Microporous Mesoporous Mater.* **2009**, *118*, 115-120.
[74] N.R. Mohamad, N.H.C. Marzuki, N.A. Buang, F. Huyop, R.A. Wahab, *Biotechnol. Biotechnol. Equip.* **2015**, *29*(2), 205-220.

Independent on the strategy of the immobilization, the size as well as the length and the composition of the organic spacer affects the retained activity of an immobilized enzyme, as the freedom to undergo necessary conformational changes within catalysis can be restricted. The constricted mobility of an enzyme immobilized via a linker can point out to be beneficial or unbeneficial concerning its retained activity and thus its stability.[75, 76, 77]

In general, in the run-up to an immobilization no universal predictions relating to the stability or activity retention of an enzyme can be derived. Thus, the best conditions concerning the immobilization of a distinct enzyme need to be individually as well as extensively investigated.

### 1.4.2 Immobilization techniques

Although, to date there have been numberless immobilization procedures published, most of these methods rest upon merely a couple of basic principles. The main immobilization techniques involve the binding of the enzyme onto a (non)porous support, cross-linking of enzyme molecules or the encapsulation of the enzyme into a suited host (Figure 13).[78, 79, 80]

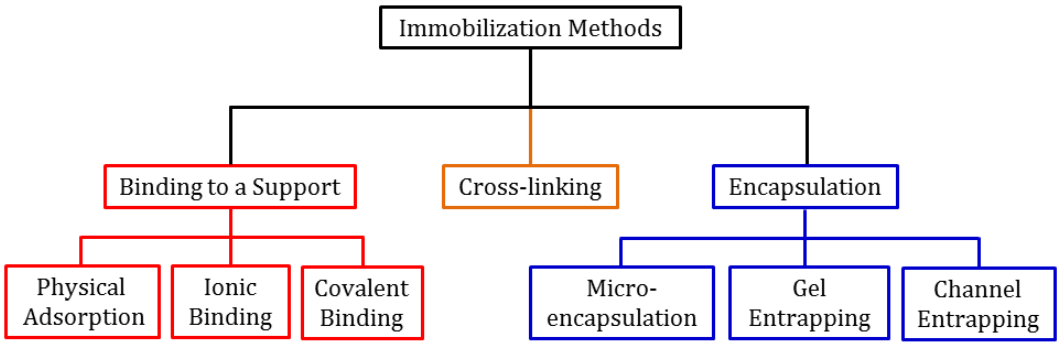


**Figure 13.** The general procedures employed for the immobilization of an enzyme can be subdivided into three main groups. These subgroups are starting bases for the development of new immobilization strategies. Figure reproduced from [79] with permission of The Royal Society of Chemistry.

[75] K. Itoyama, H. Tanibe, T. Hayashi, Y. Ikada, *Biomaterials* **1994**, *15*, 107-112.
[76] S. Yodoya, T. Takagi, M. Kurotani, Ta. Hayashi, M. Furuta, M. Oka, To. Hayashi, *Eur. Polym. J.* **2003**, *39*, 173-180.
[77] T. Hayashi, Y. Ikada, *Polym. Mater. Sci. Eng.* **1990**, *62*, 512-516.
[78] U. Hanefeld, L. Gardossi, E. Magner, *Chem. Soc. Rev.* **2009**, *38*, 453-468.
[79] M. Hartmann, D. Jung, *J. Mater. Chem.* **2010**, *20*, 844-857.
[80] R. Sheldon, *Adv. Synth. Catal.* **2007**, *349*, 1289-1307.

### 1.4.2.1 Enzyme immobilization *via* encapsulation

The immobilization procedures summarized under the main issue *encapsulation* primarily require a stable enzyme, as the synthesis of the host as well as the entrapment of the enzyme take place simultaneously. By employing these methods, the enzyme is either entrapped in a matrix (gel entrapping) or surrounded by a porous membrane (micro encapsulation, channel entrapping). Above all, gel entrapping gained of importance for biocatalytic applications since the early 1950s.[81] In particular, polymeric membrane basing on organic monomers and especially silica sol-gels, such as xerogels, ambigels or aerogels, have established for the inclusion of enzymes corresponding to the gel entrapping approach (Figure 14a). Micro-encapsulation, gel entrapping and channel entrapping resemble each other but the differences lies in the detail of its syntheses. These methods have in common that leaching is markedly decreased as the enzymes are spatially trapped in the support. However, the diffusion of substrate molecules and, if necessary, coenzyme molecules can be restricted.[62, 78, 80, 82, 83, 84]

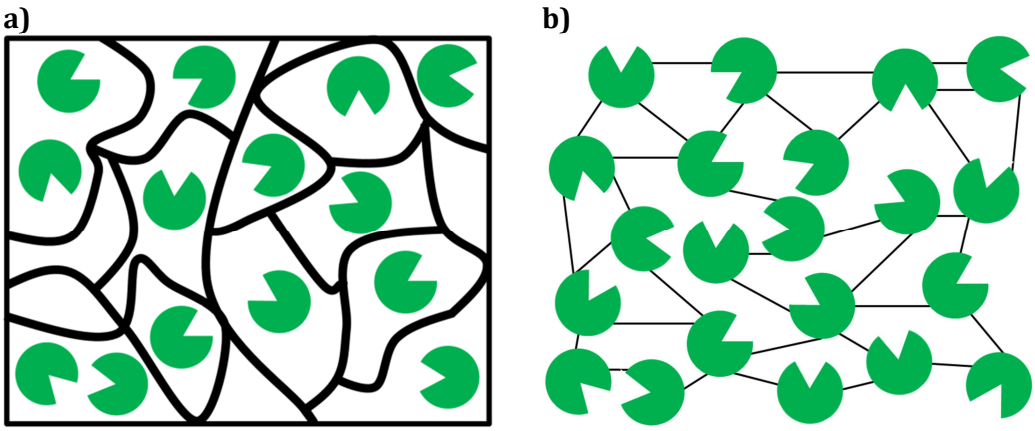


**Figure 14. a)** Enzymes entrapped in a porous matrix. Copyright Springer-Verlag 2017. With permission from Springer.[85] **b)** Cross-linked enzymes. Reproduced from [78] with permission of The Royal Society of Chemistry.

### 1.4.2.2 Enzyme immobilization *via* cross-linking

The immobilization of an enzyme can be operated even in the absence of a solid carrier. The addition of glutardialdehyde as a bifunctional reagent to an enzyme solution initiates the formation of cross-linkages of the protein molecules

[81] F.H. Dickey, *J. Phys. Chem.* **1995**, *59*, 695-707.
[82] S. Braun, S. Rappoport, R. Zusmann, D. Avnir, M. Ottolenghi, *Matter. Lett.* **1990**, *10*(1, 2), 1-5.
[83] A.C. Pierre, *Biocatal. Biotransform.* **2004**, *22*(3), 145-177.
[84] D. Avnir, T. Coradin, O. Lev, J. Livage, *J. Mater. Chem.* **2006**, *16*, 1013-1030.
[85] M. Dreifke, M. Fröba, *BIOspektrum* **2017**, *23*, 95-97.

*via* surface amino groups (CLE; Figure 14b). The cross-linking of enzymes leads to its amorphous precipitation, which can be attributed to hydrophobic effects. However, the enzymatic activity and the enzyme stability in general were detected to be poor after the cross-linking step.[86] Further development improved this approach. Cross-linking of enzyme crystals (CLEC) resulted in more stable preparations. Thus, CLECS are able to withstand higher temperatures, harsh pH values as well as even the presence of organic solvents.[87, 88, 89, 90] The final optimization of the cross-linking approaches led to the development of cross-linked enzyme aggregates (CLEA®). The preparation of CLEA is introduced by the formation of enzyme aggregate due to salting-out. This is followed by cross-linking of the aggregates in the presence of glutardialdehyde.[91, 92, 93] The advantage of CLEA over CLE and CLEC is the perpetuation of the pre-organized superstructure.[94] Hence, the activity retention after cross-linking is ensured to be comparable with the native enzyme.

The immobilization methods introduced in the previous chapters can be found from time to time in literature. However, the immobilization strategies that are related to the binding of an enzyme onto the surface of a solid carrier by means of covalent bonds as well as attractive interactions are by far most prevalent. Correspondingly, the discussion on enzyme immobilizations is focused on these methods in the following chapter.

#### 1.4.2.3 Enzyme immobilization *via* binding to a support

**Adsorptive immobilization of enzymes onto solid supports.** The immobilization due to physical attraction is classified according to the predominant enzyme-surface interactions resulting in the adsorption of the enzyme onto the surface of the host. Thus, the prevailing interactions are highly dependent on the texture of the carrier and the nature of the enzyme surface. Hydrophobic as well as ionic interactions are most prominent. This illustrates that no single amino acid residues are incorporated into the immobilization procedure but rather broad regions of the enzyme surface contribute to the formation of adsorptive bonds to the

[86] F.A. Quiocho, F.M. Richards, *Biochemistry* **1966**, *5*, 4062-4076.
[87] F.A. Quiocho, F.M. Richards, *Proc. Natl. Acad. Sci.* **1964**, *52*, 833-839.
[88] N.L.St. Clair, M.A. Navia, *J. Am. Chem. Soc.* **1992**, *114*, 7314-7316.
[89] M. Ayala, E. Horjales, M.A. Pickard, R. Vazquez-Duhalt, *Biochem. Biophys. Res. Commun.* **2002**, *295*, 828-831.
[90] L. Lalonde, *ChemTech* **1997**, *15*, 38-45.
[91] L. Cao, F. van Rantwijk, R. A. Sheldon, *Org. Lett.* **2000**, *2*, 1361-1364
[92] L.M. van Langen, N.H.P. Oosthoek, F. van Rantwijk, R.A. Sheldon, *Adv. Synth. Catal.* **2003**, *345*, 797-801.
[93] A. Illanes, L. Wilson, E. Caballero, R. Fernandez-Lafuenta, J.M. Guisan, *Appl. Biochem. Biotechnol.* **2006**, *133*, 189-202
[94] R.A. Sheldon, *Adv. Synth. Catal.* **2007**, *349*, 1289-1307.

surface of the host material. The adsorptive immobilization approaches are far away from being site-specific. Exactly for these reasons, the accessibility to the substrate/coenzyme binding sites has to be ensured. Basically, the number of bonds formed to the surface is considerably high in comparison to a site-specific immobilization (e.g. *via* covalent bonds) and a higher enzyme uptake is expected.[69, 78, 95]

Against the background of a high enzyme loading, an immobilization is commonly carried out at the respective pI of the enzyme. This circumvents the electrostatic repulsion of enzyme molecules among each other within the immobilization procedure (*lateral interactions*).[56, 69, 96] In the case of a neutral net charge of the enzyme surface, the driving forces of the immobilization are hydrophobic and minor extent polar interactions (van-der-Waals forces). Hydrophobic interactions arise between a hydrophobic host or merely hydrophobic areas on the surface of the host and hydrophobic regions on the enzyme surface. Frequently, these interactions are favored, as they are associated with an increase of the entropy of the system. Therefore, hydrophobic carriers are reported to generally possess a higher loading capacity in comparison to rather hydrophilic supports.[8, 9, 69]

In the event of an electrostatic charged surface of the carrier and an oppositely charged enzyme surface, electrostatic or rather ionic interactions are the driving force of the immobilization. In particular, these interactions appear when the immobilization is performed beyond the pIs of the enzyme as well as the host material.[69, 78]

Besides hydrophobic and electrostatic interactions, van-der-Waals interactions between polar surface areas of the enzyme and the support material emerge and contribute to an immobilization. These interactions can be referred to van-der-Waals interactions and they are known to be very weak. To that effect, they are commonly not the exclusive driving force of an immobilization but they rather accompany electrostatic or hydrophobic interactions.[56, 78] Furthermore, an immobilization via hydrogen bonds can be excluded. As immobilizations are commonly performed in aqueous buffer solution, formation of hydrogen bonds between water molecules and the surface of the host is more likely.[69]

Generally, the introduced adsorptive interactions are characterized by a certain reversibility. Hence, leakage of the immobilized enzyme is conceivable to

[95] H.H.P. Yiu, P.A. Wright, *J. Mater. Chem.* **2005**, *15*, 3690-3700.
[96] A. Vinu, M. Miyahara, K. Ariga, *J. Phys. Chem. B* **2005**, *109*, 6436-6441.

occur, even though the desorption of a carrier bound enzyme requires the simultaneous breakage of all bonds to the surface of the host.[69, 78, 97] In some extend, these interactions can be reinforced. In the case of an electrostatic immobilization the pH value of the immobilization can be varied aiming a stronger electrostatic attraction between the host material and the enzyme. Accordingly, the hydrophobicity of the surface on the carrier can be increased due to chemical modifications and thus stronger hydrophobic interaction between the enzyme and the host can be generated. However, stronger adsorptive interactions initiate a pronounced unfolding of the enzyme's tertiary structure (*time-spreading*) aiming in the reduction of the free energy of the immobilized enzyme. This comes along with a time-dependent inactivation of the enzyme (Figure 15).[69] Hence, the balance between sufficient strong enzyme-surface interactions and negligible unfolding of the enzyme structure has to be identified, respectively.

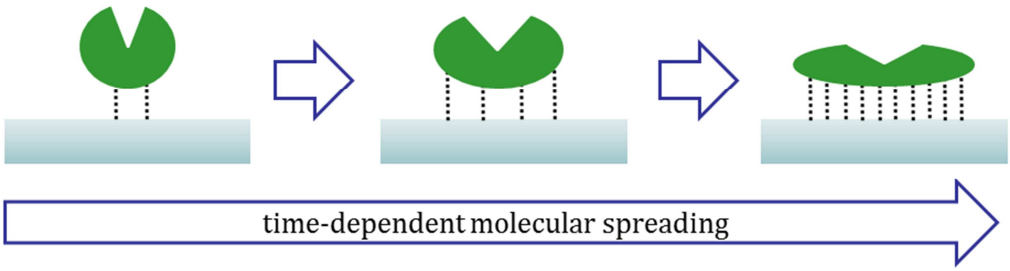


**Figure 15.** Schematic depiction of time-dependent molecular spreading. Strong adsorptive interactions between the enzyme and the surface of the host induce an unfolding of the enzyme's tertiary structure, which is accompanied by a denaturation of the enzyme over time**.** The reduction of the free energy of the enzyme was identified to be the driving force of the time-spreading. Reproduced with permission from Wiley-VCH.[69]

The immobilization of the cellulases from *Trichoderma reesei* as well as *Aspergillus niger* onto the surface of pristine fumed silica (non-porous) and Davisil® chromatographic silica (pore size: 6 nm) was precisely investigated by Bressler and coworkers. The adsorption onto the silicas was supposed to be performed due to the formation of initial hydrogen bonds between the oxygen atoms of the silanol groups on the surface of the silicas and hydrogen atoms of amino residues on the surface of the cellulases. These initial interactions were assumed to subsequent essentially change over to hydrophilic, electrostatic as well as van-der-Waals interactions.[98]

However, in some extend the author's discussion is incomprehensible. The variation of the ionic strength of the immobilization medium was reported not to be

[97] D. Gaffney, J. Cooney, E. Magner, *Top. Catal.* **2012**, *55*, 1101-1106.
[98] Y. Ikeda, A. Parashar, D.C. Bressler, *Biotechnol. Bioprocess. Eng.* **2014**, *19*, 621-628.

accompanied by a decrease of the cellulose uptake. Hence, actually electrostatic interactions as the driving force have to be excluded and hydrophobic interactions need to be taken into account; in particular against the background of the hydrophobicity of siloxane bridges (-Si-O-Si-).[9]

Independent on the prevailing interaction, solely minor leakage was observed and hence the adsorptive interactions were identified to be strong. The activity retention after immobilization was >90 % for the cellulase immobilized onto fumed silica and ~60 % for the enzyme immobilized onto Davisil® silica. The divergence in the enzymatic activities were addressed to the different textures of the silica carrier.[98]

**Covalent immobilization of enzymes onto solid supports.** The covalent immobilization of an enzyme relies on the formation of covalent bonds between the host material and certain amino acid residues on the surface of the enzyme. Thus, the surface of the support material needs to be organically modified with distinct functional groups. A frequently used method is the covalent immobilization onto carbonyl or oxiran functionalized host. Basic amino acid residues on the surface of an enzyme (lysine, arginine) are able to attack these residues nucleophily aiming at the formation of a covalent bond (Figure 16).[99, 100, 101]

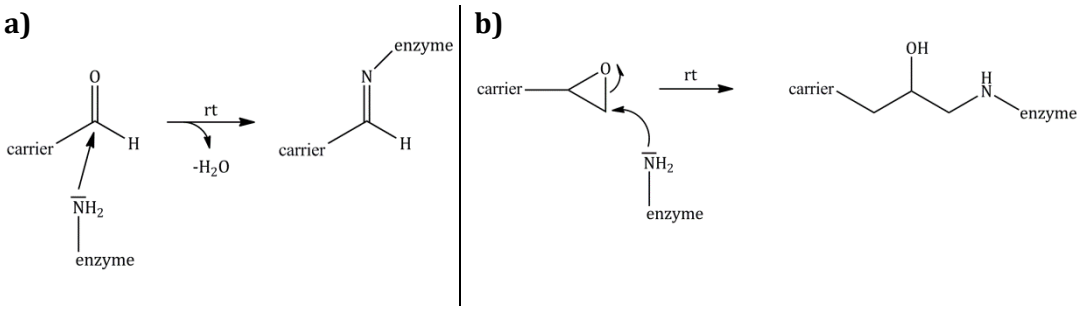


**Figure 16.** General principle of a covalent immobilization: **a)** The amino group of a lysine or arginine residue on the surface of an enzyme attacks the carbonyl group of a carbonyl modified host nucleophily. The formation of a Schiff base is accompanied by the covalent immobilization of the enzyme. **b)** Besides carbonyl functionalized carriers, oxiran modified host can be employed for the covalent immobilization of an enzyme, too.[78]

When the number and positions of basic residues on the enzyme surface has been identified the probable orientation of the enzyme on the host material can be specified. Hence, the generation of bonds between amino acids that are incorporated

[99] P. Xue, F. Xang, L. Xu, *Appl. Surf. Sci.* **2005**, *255*, 1625-1630.
[100] B. Berger, K. Faber, *J. Chem. Soc., Chem. Commun.* **1991**, 1198-1200.
[101] A. Pal, F. Khanum, *Process Biochem.* **2011**, *46,* 1315-1322.

in the enzymatic catalysis and the carrier can be avoided and a high retention of enzymatic activity is ensured. However, also the length of the organic spacer controls the performance of an immobilized enzyme due to the limitation of the flexibility. On one hand, this prevents the enzyme from unfolding and thus deactivation.[62, 78] On the other hand, necessary conformational changes of the enzyme within the catalysis can be hindered.[102, 103] As previously mentioned, a covalent immobilized enzyme is not affected from leaching. However, additional adsorptive as well as electrostatic interaction between the covalently immobilized enzyme and the organic residues bearing the carbonyl or oxiran function or rather the organic spacer in general are possible to arise. These additional interactions can result in pronounced loss of the enzymatic activity, as it is accompanied by unfolding of the enzyme's tertiary structure and thus the capability to bind the substrate or coenzyme is impeded or restricted.

The covalent immobilization of lipase from *Candida rugosa* onto the surface of carbon coated $Fe_3O_4$ nanoparticles combines two significant advantages (Figure 17). Besides the prevention of leaching, the magnetic particles can easily be separated from the substrate solution by using an external magnet.[104]

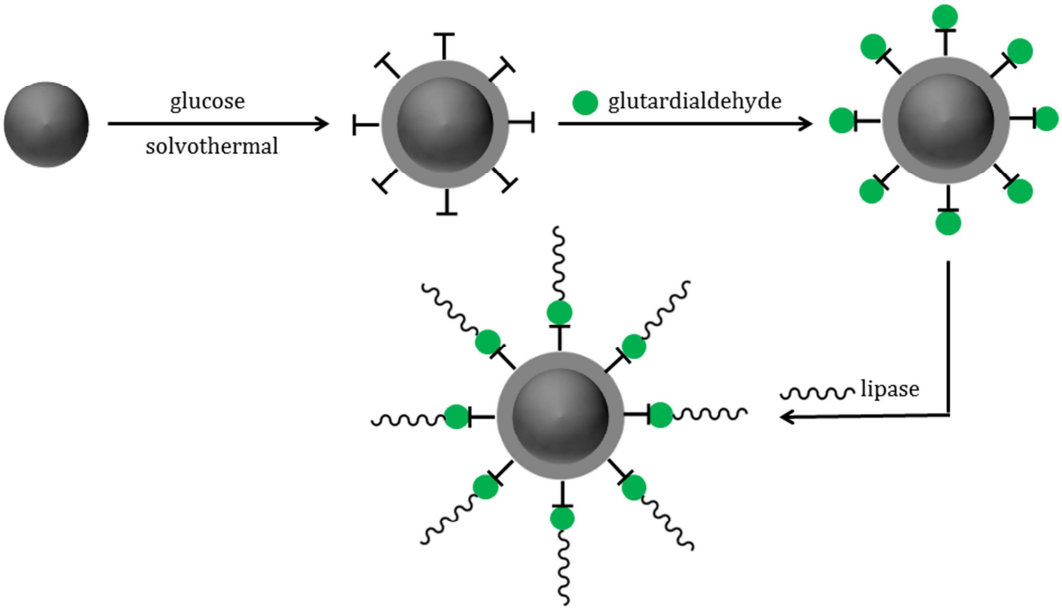


**Figure 17.** Schematic illustration of the synthesis of carbonyl modified carbon coated magnetic $Fe_3O_4$ particles that were used for the covalent immobilization of lipase. Adapted from [104] with permission of The Royal Society of Chemistry.

[102] A.S.M. Chong, X.S. Thao, *Catal. Today* **2004**, *93-95*, 293-299.
[103] C. Lei, Y. Shin, J. Liu, E.J. Ackerman, *Nanoletters*, *7*, 1050-1053.
[104] Z. Chen, W. Xu, L. Jin, J. Zha, T. Tao, Y. Lin, Z. Wang, *J. Mater. Chem. A* **2014**, *2*, 18339-18344.

After 2 h of immobilization the lipase retained 93 % of its origin activity that was determined by the hydrolysis of olive oil. A special focus was placed on the thermal stability of the immobilized enzyme, as elevated temperatures are required for different applications of this enzyme. The incubation of the native as well as the immobilized lipase at 50 °C for 10 h resulted in a loss of 68 % of the origin activity of the free enzyme, whereas the immobilized enzyme has lost merely 29 % of its enzymatic activity. Hence, the thermal stability of the carried-bound lipase has been improved due to the immobilization. Furthermore, cycle stability tests revealed a loss of approximately 32 % over 10 reaction cycles. With respect to these results, the immobilization of this lipase led to an increased stability in comparison to the native enzyme.[104]

## 1.5 Immobilization of enzymes onto nanoporous carriers

Within the last 25 years a lot of research has been done on the field of mesoporous silicas. Various silica materials with pore sizes spanning the whole mesoporous range from 2 – 50 nm have been developed. This was a major progress, since mesoporous silicas own a lot of advantages, as they are easy to produce and offer a high reproducibility. Additionally, they are mechanically and chemically stable and possess a good biocompatibility. The surface of mesoporous silicas can easily become modified due to a grafting step. Hence, various functional groups and thus different polarities can be introduced to the silica surface.[56, 61] Correspondingly, mesoporous silicas quickly aroused the interest of biotechnologist as a possible host material for the immobilization of biomolecules, especially proteins, enzymes and nowadays even whole cells.[56, 61, 105]

The synthesis of the first ordered and completely characterized mesoporous silica phase was succeeded by researchers of the MOBIL OIL CORPORATION in 1992. The utilization of cationic surfactants (quaternary ammonium surfactants) as structure directing agents (SDA) and the addition of auxiliaries in compliance with certain reaction conditions led to an ordered hexagonal array of cylindrical pores with diameters ranging from 1.6 – 10 nm. Tetramethylammonium silicate was used as a silica precursor. The removal of the SDA was operated due to calcination at 540 °C and the obtained material was designated as MCM-41. This was the first synthesis of mesoporous silicas exceeding a pore size of 1.5 nm of until then known molecular sieves. The pore size of MCM-41 can be tailored by means of the carbon

[105] Z. Zhao, X. Xie, Z. Wang, Y. Tao, X. Niu, X. Huang, L. Liu, Z. Li, *J. Biosci. Bioeng.* **2016**, *121*, 645-651.

chain lengths of the cationic surfactant.[106] Moreover, the employment of cationic surfactants in basic media paved the way for further MCM silica phases that were summarized as M41S phases (Figure 18).[106, 107, 108, 109]

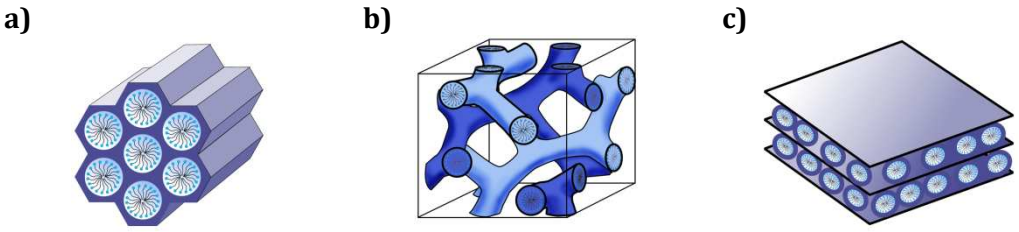


**Figure 18.** M41S silica phases: **a)** MCM-41: hexagonal structure; **b)** MCM-48: cubic structure; c) MCM-50: lamellar structure (unstable). Not shown: instable cubic octamer structure of [(CTMA)$SiO_2$]. Figure reprinted with permission from Wiley-VCH.[110]

In first instance, the formation of the mesopores in MCM-41 was referenced to a liquid-crystal template mechanism.[106] The true liquid-crystalline templating mechanism exists in the presence of high concentrations of the surfactant and is independent on the presence of the silica precursor (Figure 19, path a).[111]

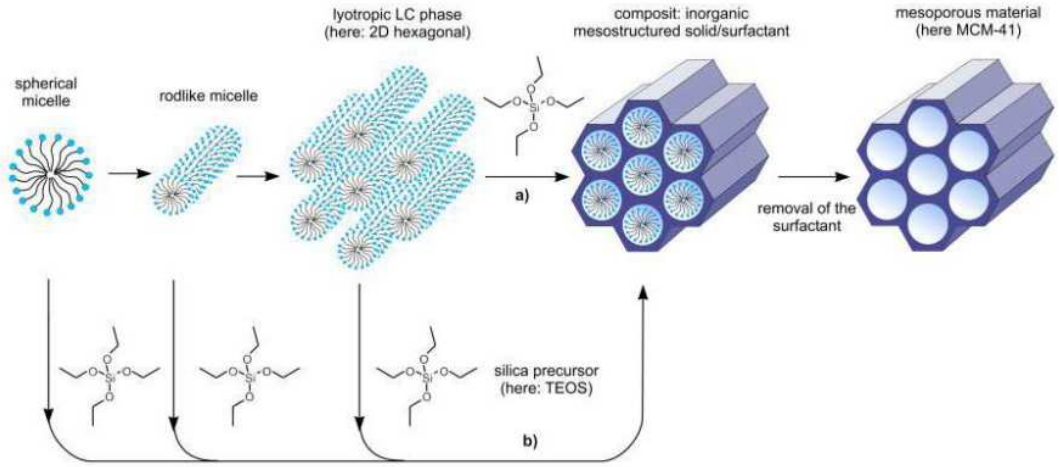


**Figure 19.** Postulated principles of the synthesis of mesoporous silicas: **a)** True liquid-crystalline templating mechanism; **b)** Cooperative liquid-crystal mechanism. Figure reprinted with permission from Wiley-VCH.[110]

[106] C.T. Kresge, M.E. Leonowicz, W.J. Roth, J.C. Vartuli, J.S. Beck, *Nature* **1992**, *359*, 710-712.
[107] J.S. Beck, J.C. Vartuli, W.J. Roth, M.E. Leonowicz, C.T. Kresge, K.D. Schmitt, C.T.-W. Chu, D.H. Olson, E.W. Sheppard, S.B. McCullen, J.B. Higgins, J.L. Schlenkert, *J. Am. Chem. Soc.* **1992**, 10834-10843.
[108] J.C. Vartuli, K.D. Schmitt, C.T. Kresge, W.J. Roth, M.E. Leonowicz, S.B. McCullen, S.D. Hellring, J.S. Beck, J.L. Schlenker, D.H. Olson, E.W. Sheppard, *Chem. Mater.* **1994**, *6*, 2317-2326.
[109] M. Dubois, Th. Gulik-Krzywicki, B. Cabane, *Langmuir* **1993**, *9*, 673-680.
[110] F. Hoffmann, M. Cornelius, J. Morell, M. Fröba, *Angew. Chem. Int. Ed.* **2006**, *45*, 3216-3251.
[111] G.S. Attard, J.C. Glyde, C.G. Göltner, *Nature* **1995**, *378*, 366-368.

Later on, it figured out that in the coexistence of a silica precursor and minor concentrations of the surfactant a cooperative liquid-crystal mechanism predominates. This mechanism is characterized by attractive interactions and thus self-organization between the silica precursor as well as the SDA (Figure 19, path b).[112] Usually, tetraethyl orthosilicate (TEOS) as well as tetramethyl orthosilicate (TMOS) act as a silica precursor in the syntheses of mesoporous silicas.

In general, a surfactant consists of a polar head group and a non-polar tail group. When exceeding a certain surfactant concentration in a solution micelles are formed. The concentration at which micelles are composed is designated as critical micelle concentration (CMC). Dependent on several factors, e.g. the size of the hydrophilic and hydrophobic residues, miscellaneous micelle structures due to aggregation are possible to arise (Figure 20).[113]

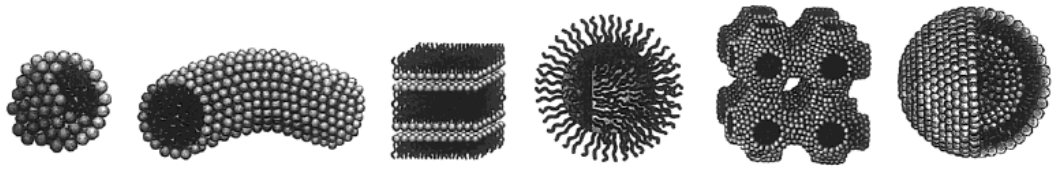

**Figure 20.** The exceedance of a certain surfactant concentration (CMC) in solution results in the formation of micelles. Dependent on environmental conditions, the micelles aggregate to generate typical micelle structures.[113, 114] Reprinted with permission from [113]. Copyright 2002 American Chemical Society.

The structure of a micelle is dependent on the geometrical molecular structure of the surfactant and intermolecular as well as entropic interactions. Most prominent intermolecular interactions are solvophilic, solvophobic and Coulomb interactions as well as hydrogen bonds.[113] The association of the silica precursor around the micelles is carried out either by electrostatic interactions, hydrogen bonds or van-der-Waals forces. Figure 21 contrasts the possible interactions between the silica precursor and the SDA schematically, whereas methods a) and f) are most important with respect to the synthesis of mesoporous silicas.

[112] A. Monnier, F. Schüth, Q. Huo, D. Kumar, D. Margolese, R.S. Maxwell, G.D. Stucky, M. Krishnamurty, P. Petroff, A. Firouzi, M. Janicke, B.F. Chmelka, *Science* **1993**, *261*, 1299-1303.
[113] G.J.D.A.A. Soler-Illia, C. Sanchez, B. Lebeau, J. Patarin, *Chem. Rev.* **2002**, *102*, 4093-4138.
[114] H. Evans, D.F. Wennerström, The Colloidal Domain Where Physics, Chemistry, Biology and Technology Meet, Wiley-VCH, Weinheim, **1994**.

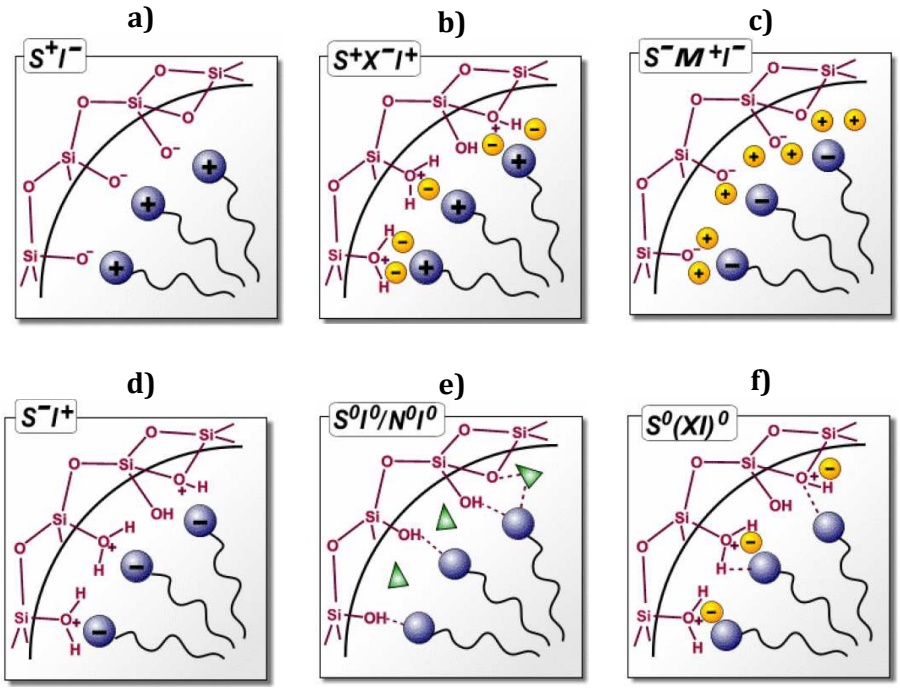


**Figure 21.** Interactions between the silica precursor (I) and the SDA (S) in basic (**a)**, **c)**), acidic (**b)**, **d)**, **f)**) as well as in neutral media (**e)**). $M^+/X^-$ mediator ions; $S^0$ or $N^0$ = nonionic SDA. Figure reprinted with permission from Wiley-VCH.[110]

In basic media the silanol groups of the silica precursor are deprotonated and thus negatively charged. Electrostatic interactions with the oppositely charged hydrophilic head group of a quaternary ammonium surfactant as the SDA result in the arrangement of the precursor around the micelles (Figure 21a). The synthesis of the M41S phases rests upon this mechanism. In acidic media, below the pI of the silica precursor, the silanol groups are protonated and thus positively charged. The initiation of attractive interactions between the positively charged silanol groups and the likewise positively charged head groups of the cationic SDA requires the addition of a mediator anion (Figure 21b). Conversely, in basic media, the silanol residues of the silica precursor are deprotonated and accordingly negatively charged. In order to promote attractive interactions between these negatively charged residues and a SDA that likewise possesses negatively charged head groups (e.g. alkyl phosphate) the addition of a cationic mediator ion is indispensable (Figure 21c). However, in this case, in acidic media a mediator ion is redundant, as the protonated and thus positively charged silanol residues of the silica precursor interact electrostatically with the oppositely charged head groups of the SDA (Figure 21d). On the contrary, regarding the utilization of a nonionic SDA in neutral as well as acidic media, attractive interactions between the SDA and the silica precursor are mediated *via* hydrogen bonds (Figure 21e, 21f). These methods play

an important role in terms of the syntheses of distinct mesoporous silicas that will be introduced in the following.[110, 115, 116]

In 1998, Zhao *et al.* published the successful incorporation of triblock copolymers as SDAs into the synthesis of a new mesoporous silica phase. The obtained material was designated as SBA-15 and possesses an ordered hexagonal pore structure according to MCM-41. However, in SBA-15 the hexagonally ordered cylindrical pores are interconnected by microporous channels (Figure 22). The pore size of SBA-15 is tailorable in the range of 4.6 – 30 nm, whereas the thickness of the pore walls was detected to amount 3.1 – 6.4 nm. Hence, in comparison to MCM-41, SBA-15 owns thicker pore walls, which is accompanied by an increased mechanical stability.[117, 118] In general, the development of SBA-15 or rather the employment of triblock copolymers as a SDA smoothed the way towards mesoporous silicas with pore sizes in the upper mesoporous range.

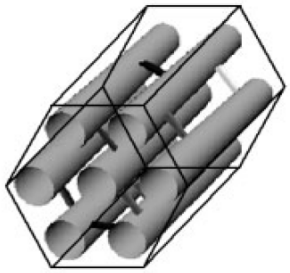

**Figure 22.** SBA-15 is constructed of hexagonal ordered cylindrical pores that are interconnected by microporous channels.[119]

Meanwhile the triblock copolymer PLURONIC® P123 ($EO_{20}$-$PO_{70}$-$EO_{20}$) has established as a SDA in the synthesis of SBA-15.[117, 118] The utilization of *Pluronic*® P123 under acidic conditions opens the possibility to additionally tailor the pore size of SBA-15 *via* the temperature of the hydrothermal treatment within the synthesis.[120, 121, 122] Additionally, the pore size of SBA-15 and even of the M41S silica phases can be controlled by the addition of so-called *swelling agents*. These auxiliaries are hydrophobic organic solvents (hexane, mesitylene (TMB),…) that

[115] Q. Huo, D.I. Margolese, U. Ciesla, P. Feng, T.E. Gier, P. Sieger, R. Leon, P.M. Petroff, F. Schüth, G.D. Stucky, *Nature* **1994**, *368*, 317-321.
[116] Q. Huo, D.I. Margolese, U. Ciesla, D.G. Demuth, P. Feng, T.E. Gier, P. Sieger, A. Firouzi, B.F. Chmelka, F. Schüth, G.D. Stucky, *Chem. Mater.* **1994**, *6*, 1176-1191.
[117] D. Zhao, J. Feng, Q. Huo, N. Melosh, G.H. Fredrickson, B.F. Chmelka, G.D. Stucky, *Science* **1998**, *279*, 548-552.
[118] D. Zhao, Q. Huo, J. Feng, B.F. Chmelka, G.D. Stucky, *J. Am. Chem. Soc.* **1998**, *120*, 6024-6036.
[119] G. Ertl, H. Knözinger, F. Schüth, J. Weitkamp, (F. Kleitz), Handbook of Heterogeneous Catalysis, 2nd, completely revised and enlarged edition, Wiley-VCH, Weinheim, **2008**.
[120] G. Karlström, *J. Phys. Chem.* **1985**, *89*, 4962-4964.
[121] P. Alexandridis, T.A. Hatton, *Colloids Surf., A* **1994**, *96*, 1-46.
[122] M. Kruk, L. Cao, *Langmuir* **2007**, *23*, 7247-7254.

intercalate into the hydrophobic core of the micelle leading to its expansion.[122, 123] When exceeding a distinct ratio of swelling agent to triblock copolymer in the synthesis of SBA-15 a transition of the pore morphology from cylindrical pores to spherical pores has been observed.[124]

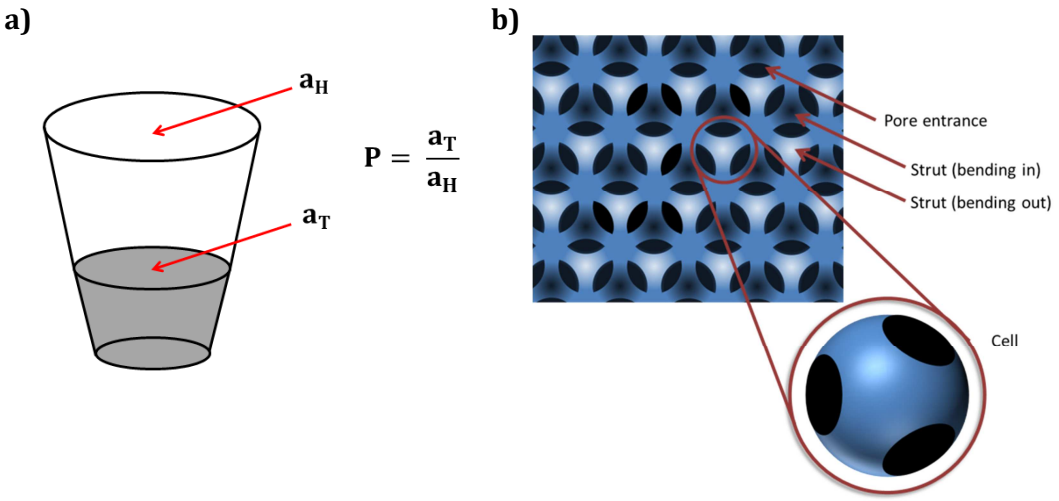


**Figure 23. a)** The packing factor P describes the ratio of the cross-sectional areas of the hydrophilic head group ($a_H$) as well as the hydrophobic tail group ($a_T$) of a block-copolymer in solution. Reprinted with permission from [124]. Copyright 2000 American Chemical Society. **b)** Illustration of the 3D network of mesoporous cellular siliceous foams (MCF). MCF is composed of spherical cells that are interconnected by smaller windows.[26]

In aqueous medium PLURONIC® P123 forms spherical micelles consisting of a hydrophobic PPO core as well as a hydrophilic PEO shell. Three water molecules are hydrogen bonded to each EO unit and further 16-22 water molecules hydrate these chains. Hence, the hydrophilic head group exhibits a large cross-sectional area ($a_H$) in comparison with the hydrophobic PPO core ($a_T$) and the packing factor (P) is small ($P < 1/3$), which comes along with a high surface curvature, whereas the amount of water within the hydrophobic core is rather low (Figure 23a). The addition of hydrochloric acid (HCl) initiates the dehydration of the PEO units and thus its water solubility is reduced. This is accompanied by a reduction of $a_H$ of the hydrophilic head group and thence an increase of P ($1/3 < P > 1/2$). In consequence the micelles arrange cylindrically with a reduced surface curvature. These findings are exploited in the synthesis of SBA-15. The addition of the hydrophobic swelling agent TMB leads to the expansion of the hydrophobic PPO core. When exceeding a certain saturation concentration of TMB (TMB:P123 ~ 0.2 (wt./wt.)), the further addition of the swelling agent initiates the transformation of the micelle morphology

[123] A. Katiyar, S. Yadav, P.G. Smirniotis, N.G. Pinto, *J. Chromatograph., A* **2006**, *1122*, 13-20.
[124] J.S. Lettow, Y.J. Han, P. Schmidt-Winkel, P. Yang, D. Zhao, G.D. Stucky, J.Y. Jing, *Langmuir* **2000**, *16*, 8291-8295.

from cylindrical to spherical. This observation is referred to the effort of the SDA macromolecules to encase the TMB molecules with a preferably minor amount of SDA molecules. TMB to PLURONIC® P123 ratios up to 0.2 (wt./wt.) results in the formation of cylindrical micelles and SBA-15 is obtained. With an increasing amount of TMB the spherical character of the micelles gains in importance. In the case of a TMB to PLURONIC® P123 rate of >0.3, merely spherical micelles are formed. This circumstance is exploited in the synthesis of *Mesoporous Cellular Siliceous Foams* (MCF). MCF is composed of a disordered three-dimensional network of spherical pores that are interconnected by smaller windows (Figure 23b). The size of the spherical cells can be tailored in range from 24 – 42 nm due to the employed amount of TMB (0.3 < TMB:PLURONIC® P123 ≤ 2.5 (wt./wt.)), whereas the size of the interconnecting windows is tailorable in the range from 9 – 22 nm. The windows arise at the contact points of the spherical micelles. To a certain extent, the addition of ammonium fluoride ($NH_4F$) to the synthesis of MCF enables the variation of the size of the cross-linking windows. TEOS is employed as a precursor that hydrolyses on the surface of the spherical micelles. This is accompanied by the release of ethanol. Ethanol acts as a co-surfactant and becomes intercalated into the hydrophobic PPO core of the micelles. Condensation of the TEOS molecules generates the disordered three-dimensional porous framework of MCF.[125, 126, 127]

In the course of the years, further mesoporous silicas, such as various SBA-type silicas, FDU-1, FDU-12 and KIT-6, haven been developed.[118, 128, 129, 130] However, with respect to its application as a host for immobilized enzymes, SBA-15 as well as MCF are most prominent, as their pore sizes match most enzyme sizes (Chapter 1.5.2).[73, 131, 132, 133]

### 1.5.1 Surface functionalization of mesoporous silicas

Frequently the immobilization of an enzyme is carried out onto the surface of pristine silica. However, in order to introduce specific attractive interaction between the enzyme and the surface of the mesoporous host, it is indispensable to organically functionalize the surface of the host. Due to this modification various

[125] J.S. Lettow, Y.J. Han, P. Schmidt-Winkel, P. Yang, D. Zhao, G.D. Stucky, J.Y. Ying, *Langmuir* **2000**, *16*, 8291-8295.
[126] P. Schmidt-Winkel, W.W. Lukens, P. Yang, D.I. Margolese, J.S. Lettow, J.Y. Ying, G.D. Stucky, *Chem. Mater.* **2000**, *12*, 686-696.
[127] P. Schmidt-Winkel, W.W. Lukens, D.Zhao, P. Yang, B.F. Chmelka, G.D. Stucky, *J. Am. Chem. Soc.* **1999**, *121*, 254-255.
[128] C. Yu, Y. Yu, D. Zhao, *Chem. Commun.* **2000,** 575-576.
[129] J. Fan, C. Yu, F. Gao, J. Lei, B. Tian, L. Wang, Q. Luo, B. Tu, W. Zhou, D. Zhao, *Angew. Chem., Int. Ed.* **2003**, *42*, 3146-3150.
[130] F. Kleitz, S.H. Choi, R. Ryoo, *Chem. Commun.* **2003**, 2136-2137.
[131] R. Reshmi, S. Sugunan, *J. Mol. Catal. B: Enzym.* **2013**, *85-86*, 111-118.
[132] A.S.M. Chong, X.S. Zhao, *Catal. Today* **2004**, *93-95*, 293-299.
[133] K. Kannan, R.V. Jasra, *J. Mol. Catal. B: Enzym.* **2009**, *56*, 34-40.

organic residues can be introduced to the silica surface (Figure 24). Thus, electrostatic, polar, hydrophobic as well as covalent interactions between the enzyme and the organic residues on the surface of the silica can be initiated.

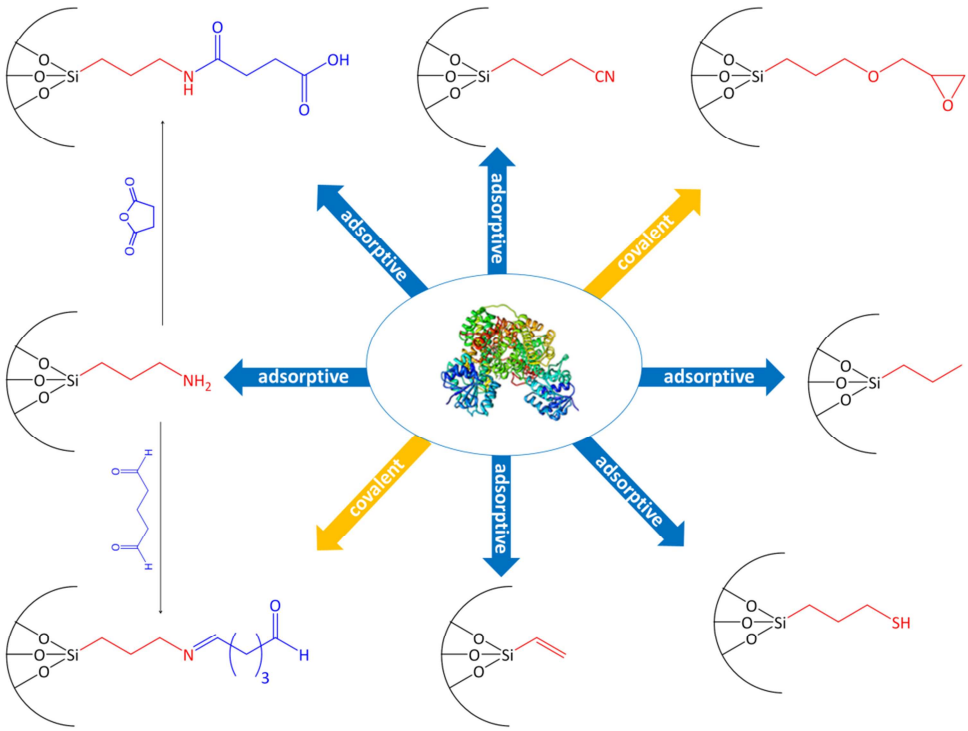


**Figure 24.** Grafting of mesoporous silicas enables the modification of the pore walls with various functional groups. Accordingly the immobilization of an enzyme onto these materials can be initiated by adsorptive (blue arrows) as well as covalent interaction (orange arrows). Copyright Springer-Verlag 2017. Adapted with permission of Springer.[85]

A common and widespread principle to modify the surface of mesoporous silicas is its post-synthetic modification using substituted trialkoxysilanes (*grafting*). In this procedure, the employed substituted trialkoxysilanes is allowed to condense on the surface of the mesoporous silica. Thus, covalent bonds between the silica surface and the silane are formed (Figure 25a). A pronounced drawback of this approach is the frequent inhomogeneous distribution of the organic residues on the pore walls. For instance, this can be provoked by organic residues directly bound at the pore entrances hindering further reactant molecules to enter the porous network.[110]

Capping of the pore entrances can be circumvented by applying the co-condensation method to obtain organically modified mesoporous silicas (Figure 25b). In this method, the substituted trialkoxysilane is incorporated into the actual synthesis of the silica itself, ensuring a homogenous distribution of the organic residues on the pore walls of the obtained mesoporous silica. However,

when exceeding a concentration of 40 mol-% of the substituted trialkoxysilane, a disordered silica material is probable to be formed. Furthermore, under the given reaction conditions, homo-condensation of the functionalization reagent can occur. As the organic residues on the surface of the silica decompose at elevated temperatures, removal of the SDA has to be operated by extraction instead of calcination.[110]

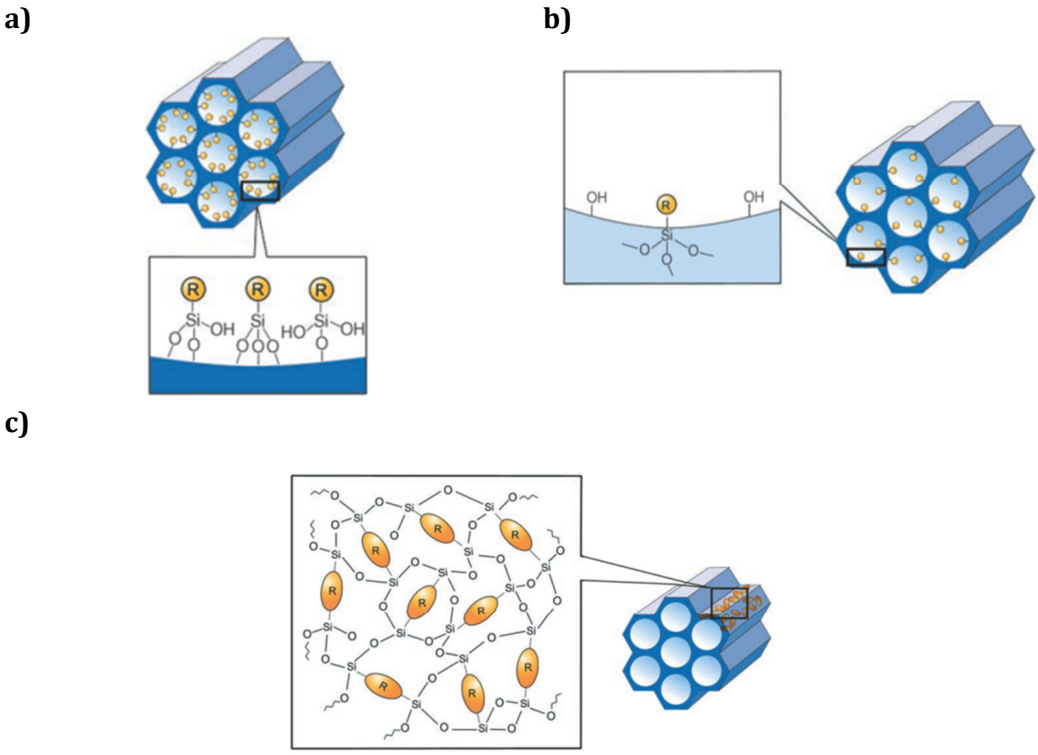


**Figure 25.** Surface functionalization of mesoporous silicas: By using the **a)** grafting or **b)** co-condensation procedure, the organic residues (R) protrude into the pores. **c)** Conversely, in terms of periodic mesoporous organosilicas (PMO), the organic bridges (R) are embedded within the pore walls. Figure reprinted with permission from Wiley-VCH.[110]

A third approach with regard to organically modified silicas is the synthesis of periodic mesoporous organosilicas (PMO). It is conducted in acidic or basic media in the presence of bis-silylated organic compounds ($(R`O)_3$-Si-R-Si-$(OR`)_3$) and a structure directing agent. As a result, the organic bridges are periodically distributed within the pore walls accompanied by a uniform porosity (Figure 25c).[110]

### 1.5.2 Immobilization of enzymes onto mesoporous cellular siliceous foams

Nowadays, the immobilization of enzymes onto MCF with its three-dimensional porous network is state of the art. As the pore sizes of MCF can be tailored up to 50 nm, they match most enzymes sizes. Furthermore, the large

mesopores exhibit sufficient space to become individually modified employing various organically substituted trialkoxysilanes (Figure 24). The efficiency of an immobilization onto mesoporous silicas is highly dependent on the surface properties of the host, which are introduced by functionalization or generated due to the medium of the immobilization, as well as on the pore size in general.

The adsorptive immobilization of lipase from *Rhizopus oryzae* was carried onto the surface of MCF bearing alkyl chains with different carbon chain lengths. The carbon chain length was varied from -$C_3$, -$C_4$ over -$C_8$ up to –$C_{18}$. As a reference, the immobilization was additionally operated onto the surface of pristine MCF. Lipase catalyzes the transesterification of vinyl n-butyrate and (*S*)-glycidol to (*S*)-glycidyl n-butyrate (Scheme 16). The enzymatic assays were performed in isooctane.[73] This clearly demonstrates the successful employment of modified MCFs even in organic solvents.

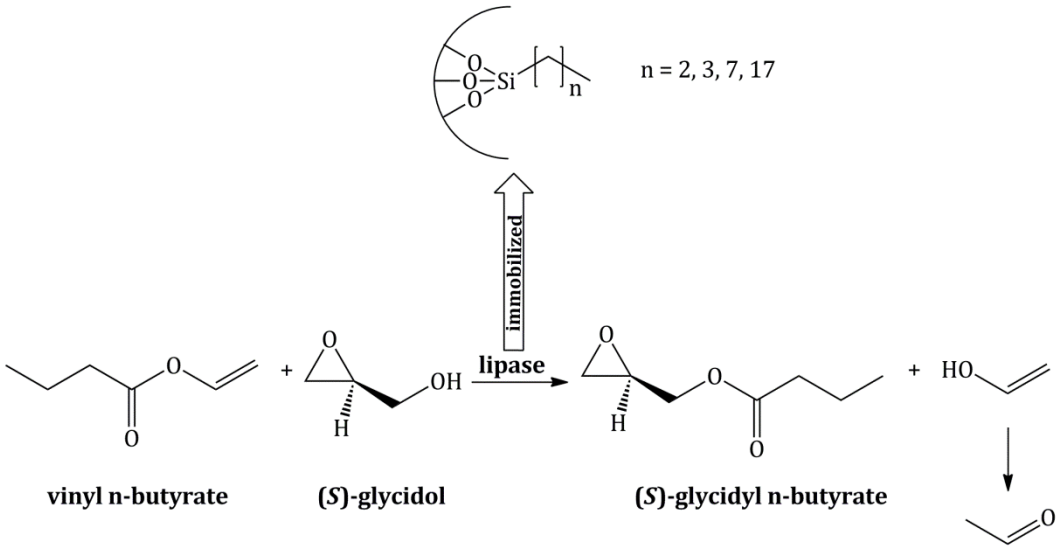


**Scheme 16**. Lipase from *Rhizopus oryzae* was immobilized onto a variety of alkyl functionalized MCFs. The enzyme catalyzes the transesterification of vinyl n-butyrate and (*S*)-glycidol to (*S*)-glycidyl n-butyrate. Reprinted from [73]. Copyright 2008, with permission from Elsevier.

With regard to the alkyl functionalized MCFs, the lipase uptakes increased with increasing alkyl chain length present on the pore walls of the host from 73 % to 87 %, whereas the highest uptake was obtained for the pristine MCF. On one hand electrostatic interactions between the oppositely charged pristine MCF and the lipase were hold responsible for the immobilization. On the other hand, the hydrophobicity of the alkyl modified hosts increases with increasing chain length. Thus, hydrophobic interactions were assumed to be the most predominant interactions when utilizing the alkyl functionalized MCFs for immobilization.[73]

The immobilization of the lipase onto the alkyl functionalized MCFs was identified to be beneficial in terms of its enzymatic activity. As the activity of the native lipase was found to be considerable lower in comparison to the lipase immobilized onto the alkyl functionalized MCFs, the immobilization has effected a certain activation as well as a stabilization of the enzyme. After a reaction time of 40 min, the lipase that was immobilized onto the octadecyl modified MCF had already converted 82 % of the provided substrate. In the further course, the assay was performed over a period of 8 h, whereas the ratio of the substrate conversion was ascertained to descend with decreasing chain length on the pore walls of the MCF (-$C_8$: 82 %; -$C_4$: 50 %; -$C_3$: 40 %; free lipase: ~35 %; MCF: 24 %). The dependency of the enzymatic activity on the hydrophobicity of the host was referred to the preference of the lipase for hydrophobic media. Besides, the enhanced hydrophobic environment of the immobilized enzyme with increasing alkyl chain length, the increased mobility of the enzyme was presumed to be advantageous in terms of longer carbon chain lengths.[73]

The introduced investigations obviously illustrate a clear dependency of the surface polarity of the support material on the efficiency of the immobilization. As lipases prefer unpolar hydrophobic media, the immobilization onto hydrophobic carriers was identified to be beneficial with respect to the enzymatic activity. Furthermore, the immobilization of the lipase onto hydrophobic hosts enhanced the enzymatic activity in comparison to the free enzyme.

Besides the polarity of the host surface, the enzyme-host interactions within an immobilization procedure are highly dependent of the pH value of the reaction medium. Frequently the immobilization is operated at the pI of the enzyme in order to avoid electrostatic repulsion of the enzyme molecules among each other aiming a high enzyme uptake.[56, 69] An immobilization beyond the pI of the enzyme can induce electrostatic interaction between the enzyme and the surface of the carrier. The immobilization of chloroperoxidase (CPO) from *Caldariomyces fumago* was carried out onto the surface of pristine MCM-48, SBA-15 and SBA-16 as well was MCF, whereby the employment of MCF figured out to be most advantageous. CPO catalyzes the peroxidative halogenation of monochlorodimedone to dichlorodimedone (Scheme 17).[134]

[134] Y.J. Han, J.T. Watson, G.D. Stucky, A. Butler, *J. Mol. Catal. B: Enzym.* **2002**, *17*, 1-8.

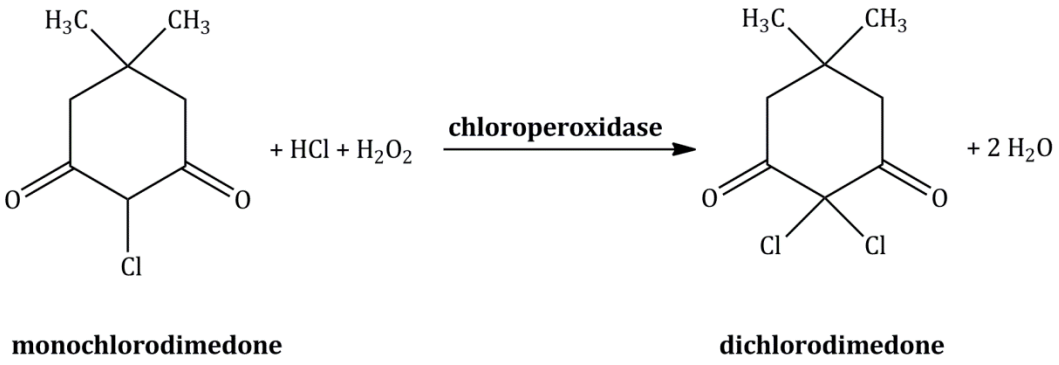


**Scheme 17.** Chloroperoxidase (CPO) from *Caldariomyces fumago* catalyzes the peroxidative halogenation of monochlorodimedone to dichlorodimedone.[134, 135, 136]

The pI of CPO was reported to be at pH ~4.0. Against this backdrop, the immobilization of CPO onto the pore walls of MCF was carried out at pH values ranging from pH 2.75 – 8.0. Thus, the enzyme surface was positively charged at pH values lower than pH 4 as well as negatively charged at pH values higher than pH 4.0, whereas the surface of the silica hosts (pI 2.0) was negatively charged over the entire pH range. The enzymatic activity of the immobilized CPO turned out to be highest after the immobilization at pH 3.4. Subsequently it decreased with decreasing pH of the immobilization (pH <3.4). This was traced back to an enhanced positive surface charge of the enzyme and thus to pronounced electrostatic interactions with the oppositely charged surface of the MCF. However, the enzyme uptake remained constant within this pH range. An increase of the pH of the immobilization (pH >3.4) resulted in a stepwise decrease of the CPO uptakes. Moreover, when exceeding the pI of CPO no immobilization occurred. These findings were referred to electrostatic repulsion arisen between the negatively charged enzyme surface and the likewise negatively charged surface of the MCF.[134]

The immobilization of CPO onto pristine MCF exemplifies the influence of the surface charge of the enzyme and the host on the uptakes and rather on the enzymatic activity of the immobilized enzyme. When an electrostatic immobilization of an enzyme is requested, the strength of the electrostatic interactions are required to be carefully regulated in order to ensure an optimal catalytic activity of the immobilized enzyme.

As indicated above, even the pore size of the host contributes to the efficiency of an immobilization. Having regard to this, the immobilization of aldolase

[135] Sigma-Aldrich: http://www.sigmaaldrich.com/content/dam/sigma-aldrich/docs/Sigma/General_Information/2/chloroperoxidase.pdf, **2017**.
[136] P.F. Hallenberg, L.P. Hagner, *Methods Enzymol.* **1978**, *52*, 521-529.

I antibodies (84G3) owning a hydrodynamic radius of 8 nm was carried out onto the surface of unmodified MCF possessing three different pore sizes. The stability and the catalytic activity of the immobilized antibodies were investigated and the results compared to those obtained for the free 84G3 as well as for antibodies immobilized onto the surface of pristine SBA-15.[137]

The pore sizes of the applied MCFs (window/cell) were determined to amount 21.6/40.2 nm (MCF-21.6), 17.6/29.8 nm (MCF-17.6) and 16.1/23.6 nm (MCF-16.1), whereas the pore diameter of SBA-15 was calculated to amount 7.1 nm. The catalytic activity of the immobilized and the free antibodies was analyzed by means of an aldol reaction employing *p*-nitrobenzaldehyde and acetone (Scheme 18).[137]

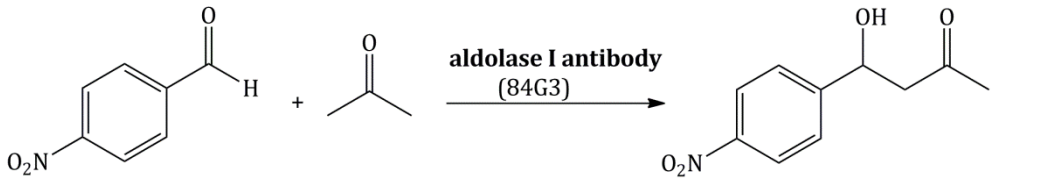


***p*-nitrobenzaldehyde** **acetone** **4-hydroxy-4-(4-nitrophenyl)butan-2-one**

**Scheme 18.** The catalytic activity of the free as well as the immobilized aldolase I antibodies (84G3) was evaluated on the basis of the aldol reaction of *p*-nitrobenzaldehyde and acetone.[137]

When utilizing MCF-16.1 and MCF-17.6 for the immobilization of the protein, an uptake of ~96 % was achieved. Thus, it was twice as high in comparison with the uptakes of MCF-21.6 and SBA-15. In the course of the catalytic reaction, the free antibodies lost most of their activity after 5 min. Conversely, the immobilized proteins were still active after 20 min exhibiting the same enantioselectivity as well as stereoselectivity than the free antibodies. Furthermore, the immobilization of the protein onto the surface of MCF-16.1 led to a ~1.8-fold increase of its catalytic activity with respect to the free antibodies. Hence, the immobilization of the antibodies induced a significant stabilization accompanied by an enhanced catalytic activity. In contrast, the lowest catalytic activity was obtained for the antibodies that were immobilized onto MCF-21.6 (Figure 26).[137]

[137] S. Seelan, A.K. Sinha, K. Kato, Y. Yokogawa, *Adv. Mater.* **2006**, *18*, 3001-3004.

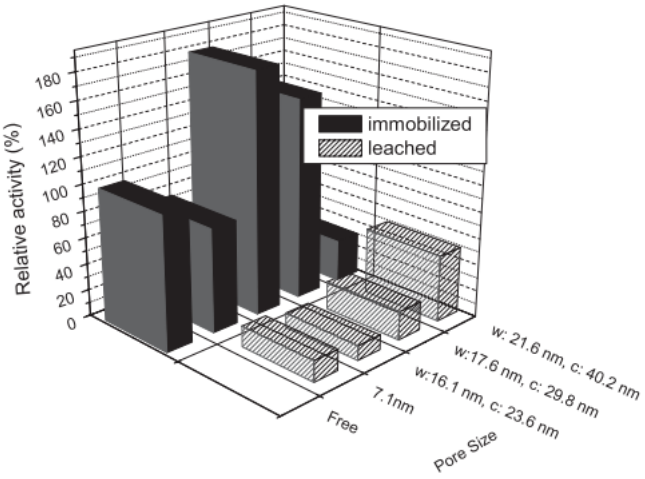


**Figure 26.** Relative activities and percentage leaching of aldolase I antibodies (84G3) immobilized onto MCFs exhibiting different pore sizes as well as SBA-15 in comparison to the free protein. Figure reprinted with permission from Wiley-VCH.[137]

The low activity of the protein immobilized onto the surface of MCF-21.6 was referred to the absence of molecular crowding as well as to denaturation. These assumptions were attributed to the large window and cell sizes of the MCF. Furthermore, this immobilisate exhibited a pronounced leaching behavior in comparison to the silicas possessing smaller pore sizes (Figure 26).[137]

In terms of a pore size in the range of the protein size as well as pore sizes significantly larger than the protein, no stabilization of the immobilized antibodies could be observed. However, pore sizes that were approximately twice as high as the protein size, contribute to a considerably stabilization of the immobilized antibodies.[137]

In conclusion, the previously presented investigations establish a clear connection between the protein/enzyme size, the pore size of the host and the stability or rather catalytic activity of the immobilized biomolecule (*pore-size matching*).

### 1.6 Michaelis-Menten enzyme kinetics

With respect to the incorporation of an immobilized enzyme into a multienzyme cascade it is indispensable to investigate the Michaelis-Menten kinetics of the respective immobilized enzymes. Against the background of an effective enzymatic coenzyme recycling, knowledge concerning the reaction rates of the participating enzymes has to be gained. As a general rule, the coenzyme regeneration step has to be the fastest within the enzyme cascade in order to avoid lack of it within the main reaction. Furthermore, these investigations allow to

deduce the affinity of an (immobilized) enzyme to its substrate and coenzyme. Additionally, it has to be assured that the substrate present in the enzyme cascade does not inhibit the enzymes, as an inhibition is accompanied by a reduction of the reaction rate or at worst with the loss of the entire enzymatic activity.

The first theoretical consideration concerning the investigation of the reaction kinetics of enzymes was established by Leonor Michaelis and Maude L. Menten in 1913.[138] Besides a couple of refinements, their mathematical model of the kinetic investigations of an irreversible enzymatic reaction is widely accepted until today.

The simplest approach is an irreversible enzymatic reaction that was taken as a basis by Michaelis and Menten. Under this assumption, the enzyme (E) binds its substrate (S) with the association constant $k_1$ to compose the enzyme-substrate complex (ES). The formed ES either decomposes back again to E and S with the re-dissociation constant $k_{-1}$ or the substrate becomes converted followed by the release of the product (P). The formation of P is presumed to be irreversible and proceeds with the dissociation constant $k_{cat}$, whereupon $k_{cat}$ is assumed to be considerably smaller than $k_1$ as well as $k_{-1}$. Hence, this reaction step is rate determining (Figure 27).[139, 140, 141]

[138] L. Michaelis, M.L. Menten, *Biochemische Zeitschrift* **1913**, *49*, 333-369.
[139] H. Chmiel, *Bioprozesstechnik*, Spektrum Akademischer Verlag, Heidelberg, **2011**.
[140] A. Rogers, Y. Gibon, *Plant Metabolic Networks*, Springer, New York, **2009**.
[141] H. Bisswanger, *Enzymkinetik: Theorie und Methoden*, 3. Auflage, Wiley-VCH, Weinheim, **2000**.

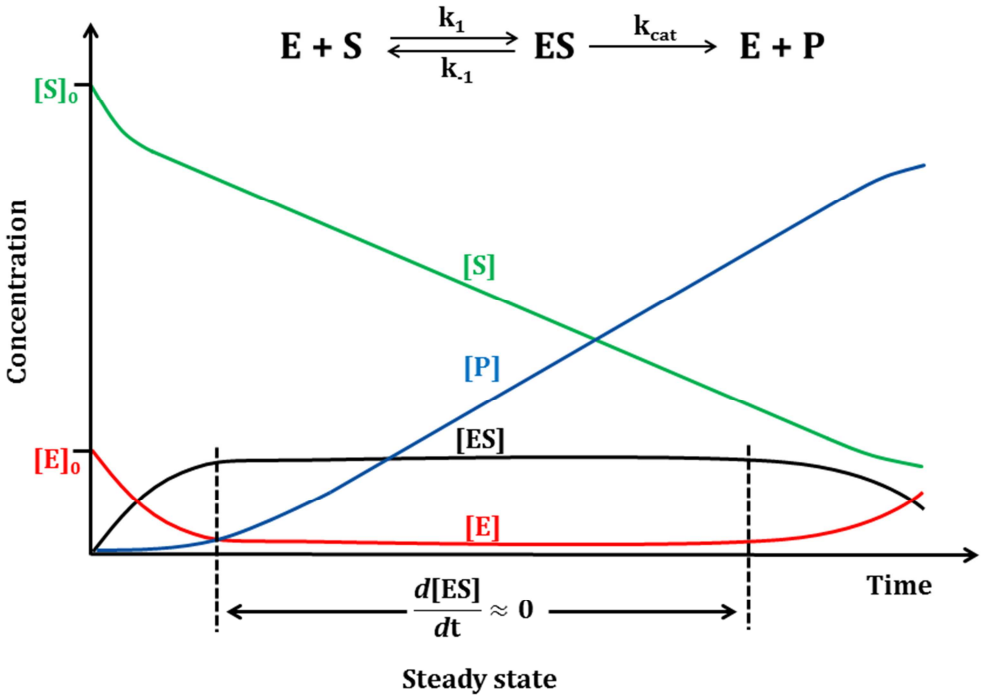


**Figure 27.** Concentration profile of an enzymatic reaction: Shortly after the reaction has started, nearly all enzyme molecules present are incorporated into the enzyme-substrate complex (ES). Within the steady state the concentration of ES ([ES]) remains constant, whereas the concentration of the substrate ([S]) decreases and the product concentration ([P]) increases over time. [ES] decreases and the concentration of the free enzyme ([E]) increases again shortly before a full substrate conversion is achieved. $[S]_0$ as well as $[E]_0$ denote the respective concentrations prior to the introduction of the enzymatic reaction.[139, 140] Copyright Spektrum Akademischer Verlag Heidelberg 2011. Redrawn with permission from Springer.[139]

Once an enzymatic reaction is initiated, the concentration of the free enzyme ([E]) decreases, whereas the concentration of the ES ([ES]) increases. Within the steady state [E] and [ES] remain almost constant, as most of the enzyme molecules are incorporated into the ES. Hence, the concentration of the substrate [S] decreases and the concentration of the product [P] increases in the course of time. Shortly before a complete substrate conversion is reached, [ES] decreases, as not all free enzyme molecules are bound into the ES anymore and thus [E] increases again. The steady state assumption can be referenced to Max Bodenstein and rests upon a quasi-stationary state of the ES. It implies that a constant concentration of ES is reached after a minor initial period in comparison to the total reaction time. Usually, investigations concerning the kinetic of an enzyme are carried out within the steady state.[139, 140, 142]

[142] M. Bodenstein, *Z. Phys. Chem.* **1913**, *85*, 329-397.

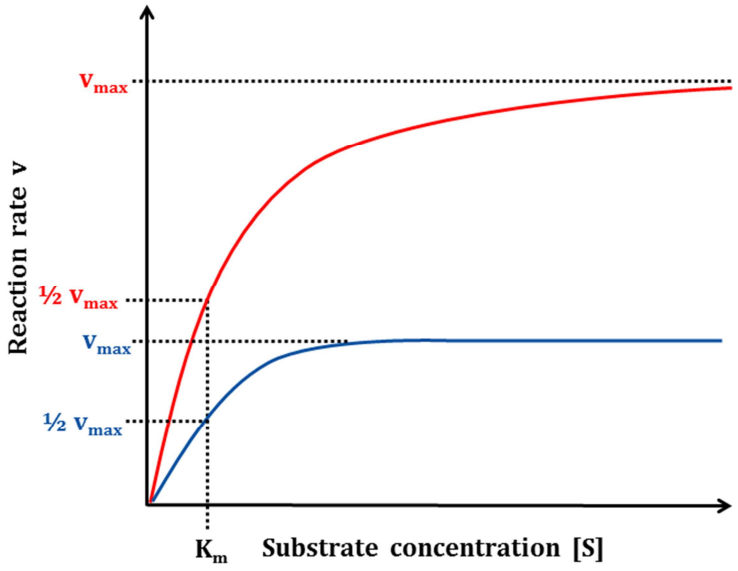


**Figure 28.** Schematic depiction of a common Michaelis-Menten plot in case of a high enzyme concentration (red) as well as a low enzyme concentration (blue): An increasing substrate concentration ([S]) results in an increase of the reaction rate (v). When exceeding a distinct value of [S] no further increase of v can be observed and the maximum reaction rate ($v_{max}$) can be read off. The Michaelis-Menten constant ($K_m$) denotes the substrate concentration that is needed to initiate a half-maximum reaction of the enzyme. It is independent on the enzyme concentration and thus a defined constant of the respective enzyme.[139, 140]

The reaction rate of an enzymatic reaction is dependent on the substrate concentration as well as on the concentration of the enzyme. A rising substrate concentration results in an increase of the reaction rate (v) of the enzyme (Figure 28). However, when exceeding a certain substrate concentration no further increase of the reaction rate can be observed, as all enzyme molecules present are bound into the ES. Aside from the substrate concentration, also high enzyme concentrations contribute to a high reaction rate and vice versa (Eq. 4); whereas the Michaelis-Menten constant ($K_m$) shows no dependency on the enzyme concentration and remains constant. $K_m$ is defined as the substrate concentration that is required to achieve a half-maximum reaction rate of the enzyme. It is a constant of the enzyme and thus it exhibits no dependency on the enzyme concentration. The reaction rate of an enzymatic reaction can be calculated by means of the Michaelis-Menten equation (Eq. 2).[139, 140, 141]

$$v = \frac{d[P]}{dt} = -\frac{d[S]}{dt} = \frac{v_{max}[S]}{K_m + [S]} \qquad \textbf{Eq. 2}$$

with

$$K_m = \frac{k_{-1}}{k_1} \qquad \textbf{Eq. 3}$$

and

$$v_{max} = k_{cat} \cdot [E]_0 \qquad \textbf{Eq. 4}$$

In terms of a high substrate concentration a 0. order reaction is present, as a rising substrate concentration is not accompanied by an increase of the reaction rate (Eq. 5). In the case of a low substrate concentration the enzymatic conversion is based on 1st order reaction. The reaction rate is directly dependent on the substrate concentration (Eq. 5).[139]

| **0. Order reaction** | **1st Order reaction** | |
|---|---|---|
| $[S] >> K_m$ | $[S] << K_m$ | **Eq. 5** |
| $\lim_{[S]\to\infty} v = v_{max}$ | $\lim_{[S]\to\infty} v = \frac{v_{max}}{K_m} \cdot [S]$ | |

Originally Michaelis and Menten presumed the rapid-equilibrium assumption instead of the Bodenstein's steady state assumption. This assumption reveals that the rate constants $k_1$ as well as $k_{-1}$ of the association and re-dissociation of the ES are considerably higher than $k_{cat}$ of the dissociation of ES. Hence, $k_{cat}$ was originally not considered in the calculation of $K_m$ (Eq. 3).[138, 139]

Eq. 3 allows conclusions concerning the affinity of an enzyme towards its substrate. In the case of a high substrate affinity, the substrate is rapidly bound in the enzyme-substrate complex with the rate constant $k_1$ and the dissociation of ES into the direction of the free enzyme and the substrate with the re-dissociation constant $k_{-1}$ is unlikely. Under this assumption $k_{-1}$ is very low in comparison to $k_1$. Consequently, the $K_m$ value is low, too. Thus, a low $K_m$ value implies a high substrate affinity of an enzyme and vice versa.[139, 140]

In 1925 G. Briggs and J. Haldane refined the traditional Michaelis-Menten approach and considered the dissociation rate $k_{cat}$ in their theoretical model (Eq. 6).[143]

$$K_m = \frac{k_{-1} + k_{cat}}{k_1} \qquad \textbf{Eq. 6}$$

Although $k_{cat}$ is generally assumed to be insignificant in comparison to $k_1$ and $k_{-1}$, caution is indicated in terms of a fast decomposition of ES that comes along with a high $k_{cat}$ value. As indicated by Eq. 3, a high $k_{cat}$ value likewise results in a high $K_m$ value and a misinterpretation with respect to the substrate affinity of the enzyme can be attained. In conclusion, $K_m$ as well as $k_{cat}$ are required to be interpreted with caution as $K_m$ indicates the substrate affinity of an enzyme and thus the strength of the binding of the substrate in the ES, whereas no conclusion regarding its conversion can be derived. In contrast, $k_{cat}$ quantifies the conversion of the substrate. However, no statements concerning the binding strength of the substrate within the ES can be derived. Thus, $k_{cat}$ as well as $K_m$ need to be considered in connection.[139]

It is obvious that a precise determination of $v_{max}$ as well as $K_m$ by means of the Michaelis-Menten plot is quite challenging and inaccurate. Therefore, different methods for its linearization have been established in the course of the years (Figure 29). Besides the well know Lineweaver-Burk plot, the Hanes-Woolf plot as well as the Eadie-Hofstee plot were introduced, whereas the double-reciprocal Lineweaver-Burk plot is still most prominent. These plots have in common that basing on the linear regression, $v_{max}$ as well as $K_m$ be determined.[144, 145, 146, 147, 148]

[143] G. Briggs, J.B.S. Haldane, *Biochem. J.* **1925**, *19*, 338-339.
[144] H. Lineweaver, D. Burk, *J. Am. Chem. Soc.* **1934**, *56*, 658-666.
[145] C.S. Hanes, *Biochem. J.* **1932**, *26*, 1406-1421.
[146] J.B.S. Haldane, *Nature* **1957**, *179*, 832.
[147] G.S. Eadie, *J. Biol. Chem.* **1942**, *146*, 85-93.
[148] B.H.J. Hofstee, *Nature* **1959**, *184*, 1296-1298.

**a)**

**Hanes-Woolf plot**

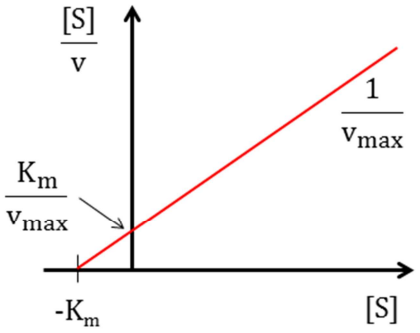


$$\frac{[S]}{v} = \frac{1}{v_{max}} + \frac{K_m}{v_{max}} \cdot [S]$$

**b)**

**Eadie-Hofstee plot**

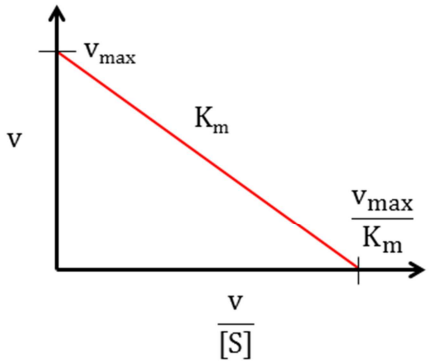


$$v = v_{max} - K_m \cdot \frac{v}{[S]}$$

**c)**

**Lineweaver-Burk plot**

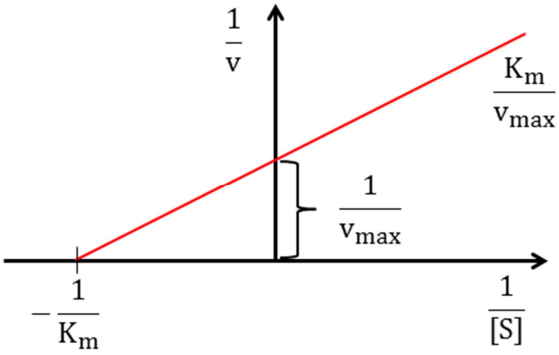


$$v = \frac{d[P]}{dt} = -\frac{d[S]}{dt} = \frac{v_{max}\,[S]}{K_m + [S]}$$

$$\frac{1}{v} = \frac{1}{v_{max}} + \frac{K_m}{v_{max}} \cdot \frac{1}{[S]}$$

**Eq. 1**

**Figure 29.** Depiction of the different principles of the linearization of the Michaelis-Menten plot and its mathematical context: **a)** Hanes-Woolf plot; **b)** Eadie-Hofstee plot; **c)** Lineweaver-Burk plot. [139, 140, 141] Copyright Spektrum Akademischer Verlag Heidelberg 2011. Adapted with permission from Springer.[139]

As these approaches rest upon a mathematical model, they have advantages and disadvantages. The slope of the regression line $\left(\frac{1}{v_{max}}\right)$ in the Hanes-Woolf plot can be calculated without any difficulties. However, the y intercept is mostly located close to the origin. Thus, the determination of $K_m$ is frequently imprecise. Additionally, in the Hanes-Woolf plot as well as in the Eadie-Hofstee plot independent and dependent variables are combined $\left(\frac{[S]}{v}\ ;\ \frac{v}{[S]}\right)$. In some extent, this

contributes to an inaccurate evaluation of the results. With respect to the Lineweaver-Burk plot, these variables are separated. However, due to the reciprocal plot the most precise measurement values are located in close proximity to the origin of the graph; whereas the lowest substrate concentrations possess the major impact on the slope. These values contain experimental errors, as the utilization of microliter pipets (0.500 – 10.00 µL) with higher measurement errors are required for the practical implementation.[139] Nevertheless, in the scope of this thesis, the Lineweaver-Burk plot was used to calculate $v_{max}$ as well $K_m$. This ensures the comparability with results published in the literature, as the Lineweaver-Burk linearization is still most commonly used.

In an experimental investigation of the Michaelis-Menten kinetics, the concentration of the substrate has to be varied, whereupon the concentration of the enzyme and the coenzyme are kept constantly. The kinetic assays are performed for only one minute in order to assure an enzyme performance within the steady state. Needless to say that Michaelis-Menten kinetics can even be elaborated with regard to the coenzyme. In terms of these investigations, the coenzyme concentration is varied while providing a constant enzyme as well as substrate concentration. In the presence of a $NADP^+$ dependent enzyme, the enzymatic activity is determined photometrically with the aid of the increase of the absorbance at a wavelength of $\lambda$ = 340 nm over the measuring time.

As previously mentioned, in consideration of the steady state assumption, the kinetic assays of a $NADP^+$ dependent enzyme are performed over merely one minute and the initial reaction rate ($v_0$) of the enzyme in the presence of a given substrate concentration is calculated by means of the alteration of the absorbance per min ($\Delta abs\ min^{-1}$) as well as the millimolar extinction coefficient of $NADP^+$ ($6.22\ L\ cm^{-1}\ mmol^{-1}$) according to Eq. 8.[139]

$$v_0 = \frac{\Delta abs \cdot min^{-1}}{6.22\ L\ cm^{-1}\ mmol^{-1}} \left[\frac{mmol}{L \cdot min}\right] \qquad \textbf{Eq. 8}$$

After the complete performance of a series of measurements involving a broad range of substrate concentrations, the maximal reaction rate $v_{max}$ of the enzyme, based on the double-reciprocal Lineweaver-Burk plot, can be calculated using Eq. 9, wherein b is the y axis intercept of the linear regression line.

$$v_{max} = \frac{1}{b} \left[\frac{mmol}{L \cdot min}\right] \quad \textbf{Eq. 9}$$

Multiplication of $v_{max}$ with the slope m of the linear regression gives the $K_m$ value.

$$K_m = v_{max} \cdot m \left[\frac{mmol}{L}\right] \quad \textbf{Eq. 10}$$

The quotient of $v_{max}$ and the total enzyme concentration ($c_{enzyme}$) results in the dissociation constant ($k_{cat}$) of the enzyme-substrate complex. $k_{cat}$ is considered as the turnover number of the enzyme and specifies the number of substrate molecules that are converted per active site and per second.[140]

$$k_{cat} = \frac{v_{max}}{c_{enzyme}} \left[\frac{1}{s}\right] \quad \textbf{Eq. 11}$$

The most meaningful parameter with respect to enzyme kinetics is the enzyme efficiency (EE) that is given by the quotient of $k_{cat}$ and $K_m$.[140]

$$EE = \frac{k_{cat}}{K_m} \left[\frac{1}{s} \cdot \frac{1}{\frac{mol}{L}}\right] \quad \textbf{Eq. 12}$$

### 1.7 Mass transport phenomena in porous materials

The application of an enzyme that immobilized onto a (meso)porous host in an aqueous substrate/coenzyme solution is affected by distinct mass transport phenomena. The mass transport of substrate as well as coenzyme molecules into the pore network of a mesoporous host is described by the common principles known from the heterogeneous catalysis. In aqueous media the porous particles are covered by a boundary layer (film) that is composed of the appropriate buffer solution. The thickness of the boundary film can be controlled by means of the flow rate. It is thinner for higher flow rates. On their way to the immobilized enzyme in the porous network of the support material the reactant molecules need to leave the

bulk phase or rather the core flow and pass the boundary layer followed by its diffusion into the pore system (Figure 30).[149, 150]

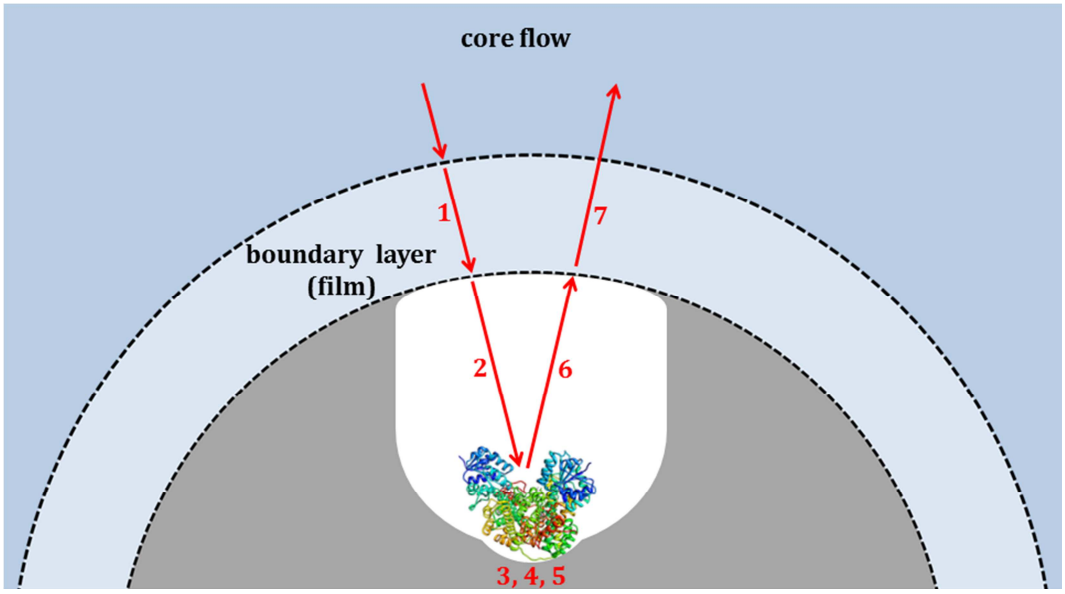


**Figure 30.** Schematic depiction of the sub-steps of the mass transport of substrate as well as coenzyme molecules from the bulk phase to the enzyme that is immobilized within a porous carrier: (1) Film diffusion; (2) Pore diffusion; (3-5) Binding of the substrate/coenzyme molecules; conversion; release of the product and the converted coenzyme; (6) Pore diffusion; (7) Film diffusion. Copyright B. G. Teubner Verlag/GWV Fachverlage GmbH, Wiesbaden 2007. Reproduced with permission from Springer.[149]

Generally, the mass transport of reactant molecules from the bulk phase can be subdivided into seven sub-steps:

(1) Film diffusion. The substrate/coenzyme molecules are transported from the core flow (bulk) through the boundary layer (film) to the outer surface of the porous particle. Within the film the reactant molecules become significantly decelerated to a flow rate of 0.

(2) Pore diffusion. Due to the absence of the fluid flow, the transportation of substrate/coenzyme molecules within the porous network and thus in the direction of the immobilized enzyme is effected by diffusion.

(3) Binding of the substrate as well as the coenzyme in the respective binding sites of the enzyme.

(4) Enzymatic conversion of the substrate and the coenzyme.

(5) Release of the product and the converted coenzyme from the binding sites.

---

[149] E. Müller-Erlwein, *Chemie in der Praxis - Chemische Reaktionstechnik*, 2., überarbeitete und erweiterte Auflage, B.G. Teubner Verlag / GWV Fachverlage GmbH, Wiesbaden, **2007**.
[150] F. Schüth, *Chem. Unserer Zeit* **2006**, *40*, 92-103.

(6) Pore diffusion of the product/coenzyme molecules.
(7) Film diffusion of the product/coenzyme molecules into the core flow (bulk phase).

The employment of immobilized enzymes or carrier-bound catalysts, in general, is frequently accompanied by external and internal mass transport limitations. These effects can be referenced to the ambient conditions of the immobilisate. On one hand the respective velocities of the introduced sub-steps are dependent on the concentration of the substrate and the coenzyme. On the other hand the temperature, the flow conditions as well as the properties of the porous particles possess a major influence on the velocity of the sub-steps. Hence, the respective sub-step exhibiting the lowest velocity is rate-determining (Figure 31).[149]

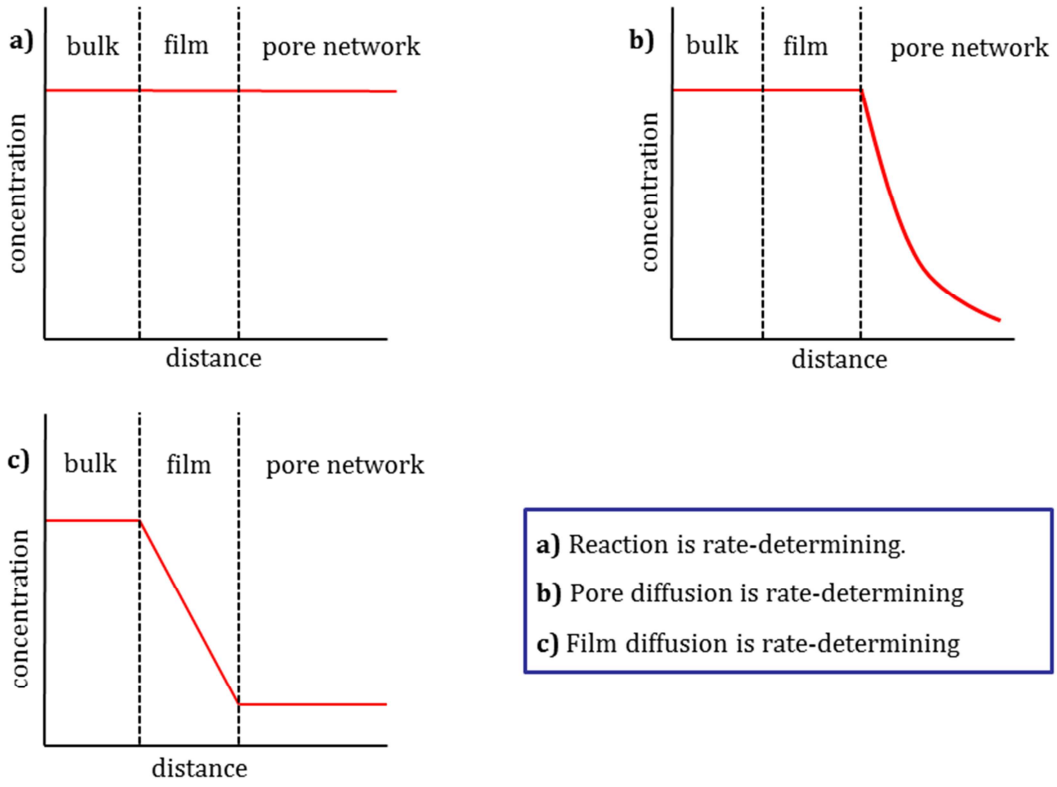


**Figure 31.** Concentration profiles of the substrate/coenzyme in an heterogeneous catalysis: **a)** Low temperature: reaction rate of the enzyme is rate-determining; **b)** Elevated temperature: pore diffusion is rate-determining; **c)** High temperature: film diffusion is rate-determining.[149]

In terms of a low reaction temperature the reaction rate of the enzyme is reduced, whereas the film as well as the pore diffusion proceeds comparatively fast. The concentration of the coenzyme/substrate is nearly constant within all subareas

of the reaction dispersion. Thus, the enzymatic conversion of the substrate/coenzyme is rate-determining (Figure 31a).[149]

An increase of the reaction temperature is accompanied by an enhanced reaction rate of the immobilized enzyme, whereas the diffusion rate remains constant.[66] However, a fast enzymatic conversion of the substrate/coenzyme involves a decrease of the reactant concentration within the porous network of the immobilisate and thus the pore diffusion becomes rate-determining (Figure 31b).[149]

A further increase of the temperature results in a hindered film diffusion. The concentration of the substrate/coenzyme within the boundary layer is decreased in comparison to the bulk phase. Likewise the reaction rate of the enzyme is increased and the reaction preferably occurs on the outer surface of the particles or rather by enzyme molecules that are immobilized in proximity to the pore entrance. Hence, the film diffusion is rate-determining (Figure 31c).[149]

Against the background of mass transport limitations it is important to identify the right balance between an optimal reaction temperature and an ideal enzymatic activity, as elevated reaction temperatures encourage the denaturation of the enzyme.[66]

Dependent on the substrate/coenzyme concentration, the Michaelis-Menten kinetics of immobilized enzymes can be strongly affected by the introduced mass transport limitations. In terms of a high substrate/coenzyme concentration, the influence of mass transport limitations on the enzyme kinetics is negligible and the slope of the regression line in the Lineweaver-Burk plot resembles the slope obtained for the free enzyme. However, mass transport limitations gain in importance in the presence of low substrate/coenzyme concentrations. In this context, the slope of the regression line in the Lineweaver-Burk diagram does not reflect the real kinetics. Accordingly, merely apparent values of $K_m$ ($K_{m,\,app}$) as well as $v_{max}$ ($v_{max,\,app}$) are detected (Figure 32). Thus, mass transport limitations can be responsible for misinterpretations of the kinetic parameters of an immobilized enzyme.[149]

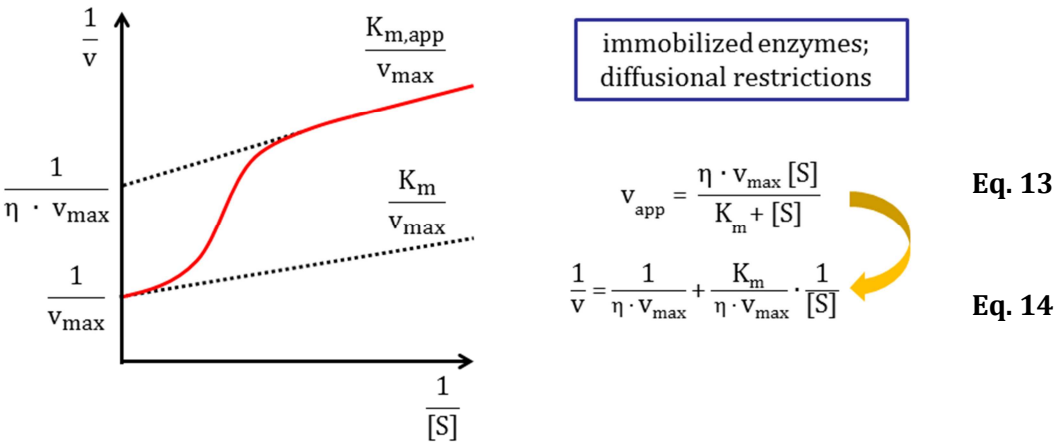


**Figure 32.** Lineweaver-Burk plot: In terms of high substrate/coenzyme concentrations, the slope in the Lineweaver-Burk plot is comparable to that obtained for the free enzyme. When decreasing the substrate/coenzyme concentration, mass transport limitations become increasingly important and merely apparent values of $K_m$ ($K_{m,\,app}$) as well as $v_{max}$ ($v_{max,\,app}$) are detectable. These apparent kinetic parameters can be mathematically corrected by the inclusion of the effectiveness factor (η) into the calculations. Copyright Spektrum Akademischer Verlag Heidelberg 2011. Redrawn with permission from Springer.[139]

It is required to determine the effectiveness factor (η) and to consider it in the calculations of $K_m$ as well $v_{max}$ in order to circumvent the mentioned difficulties (Eq. 13-15).

$$\eta = \frac{v_{max\ (immobilized\ enzyme)}}{v_{max\ (free\ enzyme)}} \qquad \textbf{Eq. 15}$$

However, the determination of η presupposes no alterations of the enzyme properties arisen from the immobilization. In other words, the enzymatic activity or rather the reaction rate of the immobilized enzyme is assumed to be equal to that of the native enzyme. Any deviations from the enzymatic activity as well as reaction rate are exclusively referred to mass transport limitations.[139] However, it is known from the literature that the immobilization of an enzyme is frequently accompanied by a certain loss of the enzymatic activity. Especially in the case of an unspecific adsorptive immobilization, lack of the enzymatic activity and thus an alteration of the kinetic parameters is observed. Thence, splitting of the altered enzymatic activity as well as the kinetic parameters into a portion caused by mass transport limitations and a portion caused by the immobilization procedure is hardly possible and significantly defective. The kinetic properties of a carrier-bound enzyme need to

be considered as a whole, while being aware that diffusion limitations have a contribution on the kinetic behavior of an immobilized enzyme.

A major advantage of porous host for the immobilization of enzymes is its high surface area in comparison with nonporous materials. An interesting approach circumvents the discussed internal mass transport limitations while maintaining a porous host as a carrier. Generally a homogeneous distribution of the immobilized enzyme over the porous support is assumed. However, the immobilization of the respective enzyme merely in the proximity of the pore entrances avoids external mass transport limitations, as these areas own a pronounced accessibility and pore diffusion is negligible. Binding of enzymes close to the pore entrances requires a kinetic control of the immobilization procedure. This can be realized by a low ionic strength of the stock solution employed for the immobilization. With regard to the low ionic strength, the immobilization proceeds very fast and the enzyme immobilizes onto the outer shell and thus preferably on the pore entrances of the support. Consequently, an inhomogeneous distribution of the enzyme on the overall surface of the host is obtained. In contrast, in the presence of a high ionic strength of the stock solution the immobilization proceeds slowly and the enzyme becomes immobilized homogeneously over the entire surface area, whereupon the accessibility of enzyme molecules immobilized in the depths of the porous network is hindered.[66, 151]

### 1.8 Enzyme cascades

In nature, enzymes are participants of complex pathway, for example the introduced pentose phosphate pathway, the citrate cycle as well as the urea cycle and so forth.[20] Thus, an enzymatic reaction has always to be considered related to its natural pathway. The immobilization of an isolated enzyme onto an appropriate support and the subsequent combination of various immobilized enzymes allows a new composition of synthetic pathways. Against this background, access to valuable products can be attained. In the following chapter, impressing recent research concerning carrier-bound biocatalysts and its incorporation into synthetic pathways is represented. The scope spans from immobilized enzymes over immobilized coenzymes to whole cell catalysis.

In 2012, Walde and coworkers published a modular approach of an enzyme cascade aiming a multienzyme system for the quantification of glucose in aqueous

[151] A. Borchert, K. Buchholz, *Biotechnol. Lett.* **1979**, *1*, 15-20.

media. They deposited glucose-oxidase (GOD) from *Aspergillus niger* as well as horseradish peroxidase (HRP) *via* the common avidin-biotin method within a commercially available glass tube, respectively (internal diameter: 1.6 mm, total volume: 280 µL).[152] To prepare the attachment of the enzymes onto the internal surface of the glass tubes, the latter was covered with a polycationic, dendronized polymer (dendripol) followed by its biotinylation and the adsorption of avidin.[153] Prior to the immobilization, the enzymes were biotinylated, too. The immobilization was carried out by avidin-biotin interactions between the introduced biotin residues of the enzymes and the avidin macromolecules attached to the surface of the glass tubes.[148] These non-covalent interactions were identified to be extremely strong possessing a dissociation constant of $10^{-15}$ M.[154]

GOD catalyzes the oxidation of β-D-glucose to glucono-δ-lactone and hydrogen peroxide ($H_2O_2$). In the further course, $H_2O_2$ oxidizes the HRP to the active form HRP* that catalyzes the conversion of two equivalents *o*-phenylenediamine to one equivalent 2, 3-diaminophenazine (Scheme 19).[152]

[152] S. Fornera, T. Bauer, A.D. Schlüter, P. Walde, *J. Mater. Chem.* **2012**, *22* 502-511.
[153] S. Fornera, T.E. Balmer, B. Zhang, A.D. Schlüter, P. Walde, *Macromol. Biosci.* **2011**, *11*, 1052-1067.
[154] J.-L. Guesdon, T. Ternynck, S. Avrameas, *J. Histochem. Cytochem.* **1979**, *27*(8), 1131-1139.

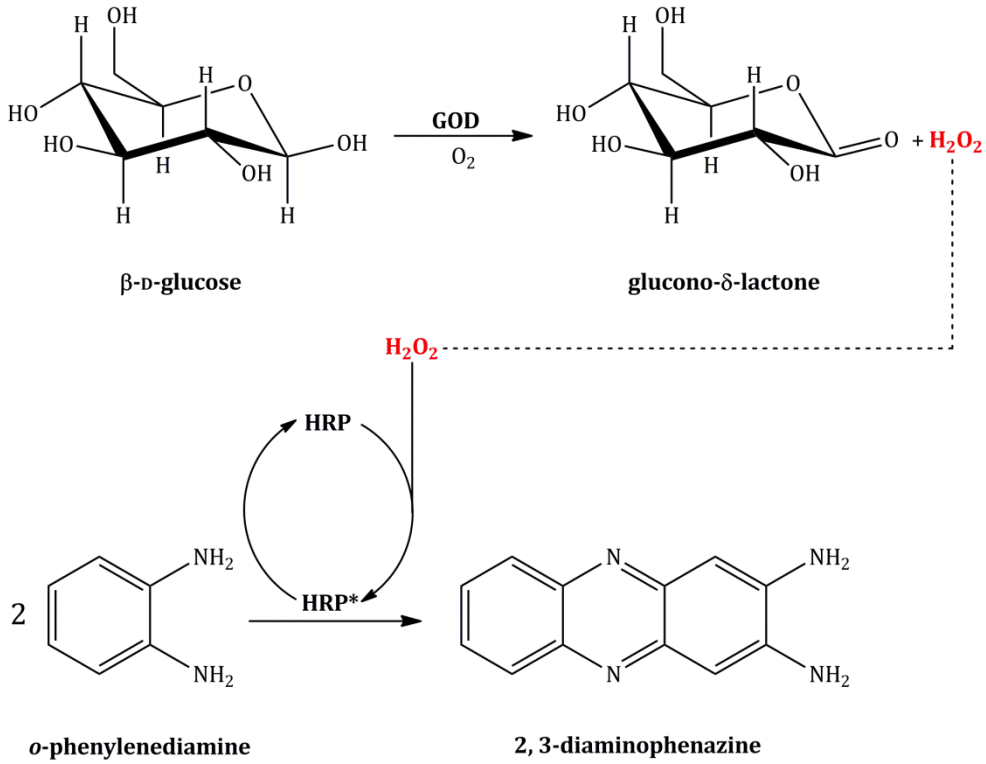


**Scheme 19.** Glucose oxidase (GOD) from *Aspergillus niger* as well as horseradish peroxidase (HRP) were separately immobilized onto the internal surface of dendripol modified glass tubes *via* the avidin-biotin method. GOD catalyzes the oxidation of β-D-glucose to glucono-δ-lactone and hydrogen peroxide ($H_2O_2$), which activates the HRP (HRP*) for the subsequent conversion of *o*-phenylenediamine to 2, 3-diaminophenazine. Reproduced from [152] with permission of The Royal Society of Chemistry.

Both glass tubes possessing the immobilized GOD and HRP, respectively, were connected with a silicon tubing and a buffered substrate solution (0.54 mmol $L^{-1}$ β-D-glucose, 3.14 mmol $L^{-1}$ *o*-phenylenediamine) was pumped through (70 µL $min^{-1}$). The formation of 2, 3-diaminophenazine was detected by means of UV/Vis spectroscopy (λ = 427 nm). A linear dependency on the supplied concentration of β-D-glucose as well as the obtained concentration of 2, 3-diamino–phenazine was found. Hence, the introduced enzyme cascade is a useful approach with regard to the quantification of glucose. Furthermore, by using the avidin-biotin method again, a β-galactosidase was immobilized onto the internal surface of a glass tube and implemented as the first step into the cascade. This three enzyme cascade was capable to convert lactose to 2, 3-diaminophenazine and thus it was possible to even detect the concentration of lactose. The immobilized enzymes exhibited pronounced storage stability in buffer solution. 70 % of the initial activity was retained after 13 days of storage and at least 35 % of the initial activity remained after three months.[152]

This enzyme cascade exemplifies a good manageable approach of an enzyme cascade by using commercially available glass tubes as a host and the well understood avidin-biotin method.

5-Hydroxymethylfurfural (5-HMF) is a valuable platform chemical that is, inter alia, accessible due to the degradation of cellulose. Against this background, a reaction cascade for the conversion of cellulose to 5-HMF has been established. The developed cascade combines an enzymatic reaction sequence employing two immobilized enzymes in aqueous media as well as a chemocatalytic conversion in organic media. The hydrolysis of the cellulose oligomers to glucose as well as its isomerization to fructose was performed by an immobilized cellulase as well as an immobilized isomerase, respectively. The enzymatic part of the cascade was followed by a sulfonic acid catalyzed dehydration of fructose to give 5-HMF (Scheme 20).[155]

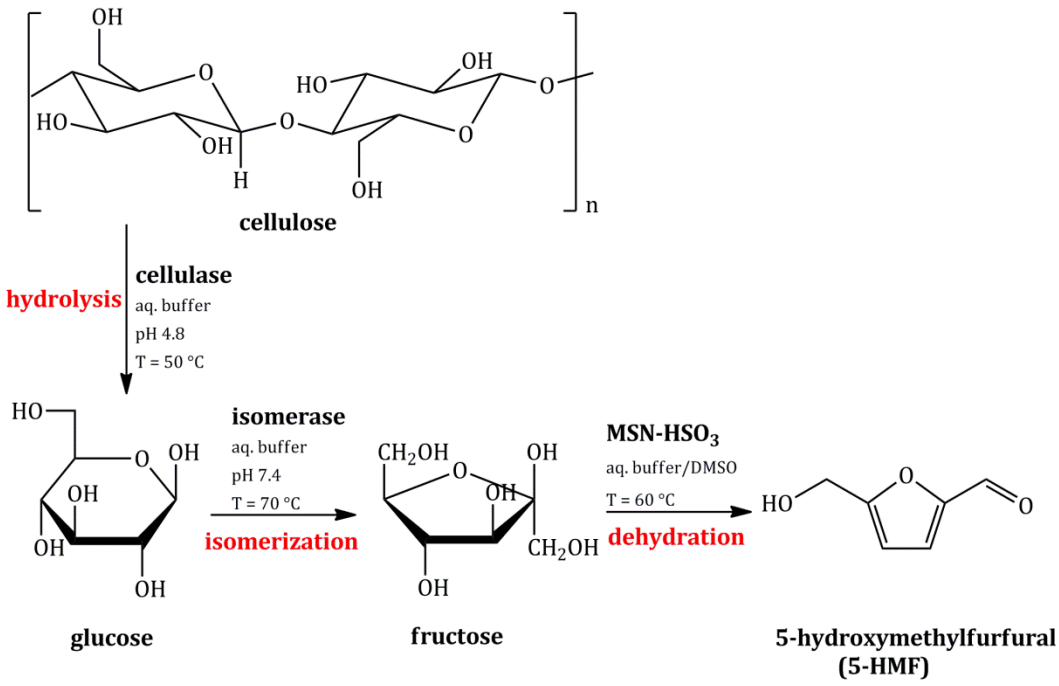


**Scheme 20.** The degradation of cellulose to 5-hydroxymethylfurfural (5-HMF) was put into practice due to a three step reaction cascade combining an enzymatic reaction sequence of two immobilized enzymes and a chemocatalytic reaction. The hydrolysis of cellulose oligomers to glucose monomers is conducted by an immobilized cellulase. Subsequently, an immobilized isomerase initiates the glucose to fructose isomerization. The final conversion of fructose to 5-HMF is catalyzed by sulfonic acid residues grafted onto the surface of mesoporous silica particles. Figure reproduced with permission of Wiley-VCH.[155]

[155] Y.C. Lee, S. Dutta, K.C.-W. Wu, *ChemSusChem* **2014**, *7*, 3241-3246.

To assure a simple and complete separation of the catalysts from the reaction medium, cellulase and isomerase were immobilized onto the surface of magnetic mesoporous silica particles ($d_P$ = 20.2-20.4 nm). Thus, the immobilisates could be recovered from reaction dispersion by using a permanent magnet. Furthermore, mesoporous silica particles bearing sulfonic acid groups on its surface ($d_p$ = 4.7 nm) that were intended for the conversion of fructose to 5-HMF in dimethylsulfoxid (DMSO) were prepared and involved in the third step of the cascade.[155]

Prior to the introduction of the three step cascade, the cellulose was pretreated with 1-butyl-3-methyl-imidazolium chloride as an ionic liquid in order to eliminate hydrogen bonds between the cellulose chains. In a typical cascade experiment, the immobilized cellulase was added to a buffered solution/dispersion containing cellulose (pH 4.8, T = 50 °C). Immediately after the degradation of cellulose to glucose, the cellulase immobilisate was collected and the pH value was increased to pH 7.4 (T = 70 °C). Subsequently, the isomerase immobilisate was added to the reaction mixture in order to initiate the glucose to fructose isomerization. After removal of the immobilized isomerase, the mesoporous silica particles possessing sulfonic acid groups on its internal and external surface were supplied as a solid catalyst for the dehydration of fructose to 5-HMF (T = 50 °C). The addition of the inorganic was accompanied by the addition of DMSO aiming a final ratio of water to the organic solvent of 1:10 (v/v). The dehydration of fructose ended up with a final yield of 45.6 % of 5-HMF. The reaction cascade suffered from a loss of merely 7 % of its origin productivity over five reaction cycles. Hence, the immobilized enzymes were identified to be stable under the given reaction conditions and even the mesoporous silica particles possessing the sulfonic acid functionality on its surface figured out to be reusable without any difficulties.[155]

The cellulose to 5-HMF conversion due to an enzymatic reaction sequence coupled to a chemocatalytic final step paves the way for a reasonable combination of an entire enzymatic approach and a typical “chemical” reaction. On that basis, further development is likely to arise.

A further approach concerning the incorporation of magnetic particles as a potential enzyme host in a modular enzyme cascade was presented by Gu *et al.*. The composition of the magnetic particles is quite sophisticated (Figure 33a). Briefly, the particles are composed of a magnetic core that is cross-liked with layers of amine modified polyethylene glycol (PEG). Finally, the single particles were covered by a robust silica shell, due to the addition of TMOS as well as 3-aminopropyl

triethoxysilane. Uniform spherical particles with diameters in the range of 0.5 – 0.8 nm were obtained.[156]

Pyruvate kinase (PK) and lactate dehydrogenase (LDH) from rabbit muscle were immobilized onto the surface of the presented magnetic particles, respectively. The adsorptive immobilization was followed by cross-linking of the enzyme molecules using glutardialdehyde. The magnetic immobilisates were carefully elaborated regarding its implementation in a modular enzyme cascade. The reaction sequence of phosphoenolpyruvate to lactate was consulted as a model system. Herein, PK catalyzes the dephosphorylation of phosphoenolpyruvate to pyruvate with concomitant phosphorylation of adenosine diphosphate (ADP) to adenosine triphosphate (ATP). The immobilized LDH reduces the formed pyruvate to lactate, whereas NADH becomes oxidized to $NAD^+$ simultaneously (Figure 33b).[156]

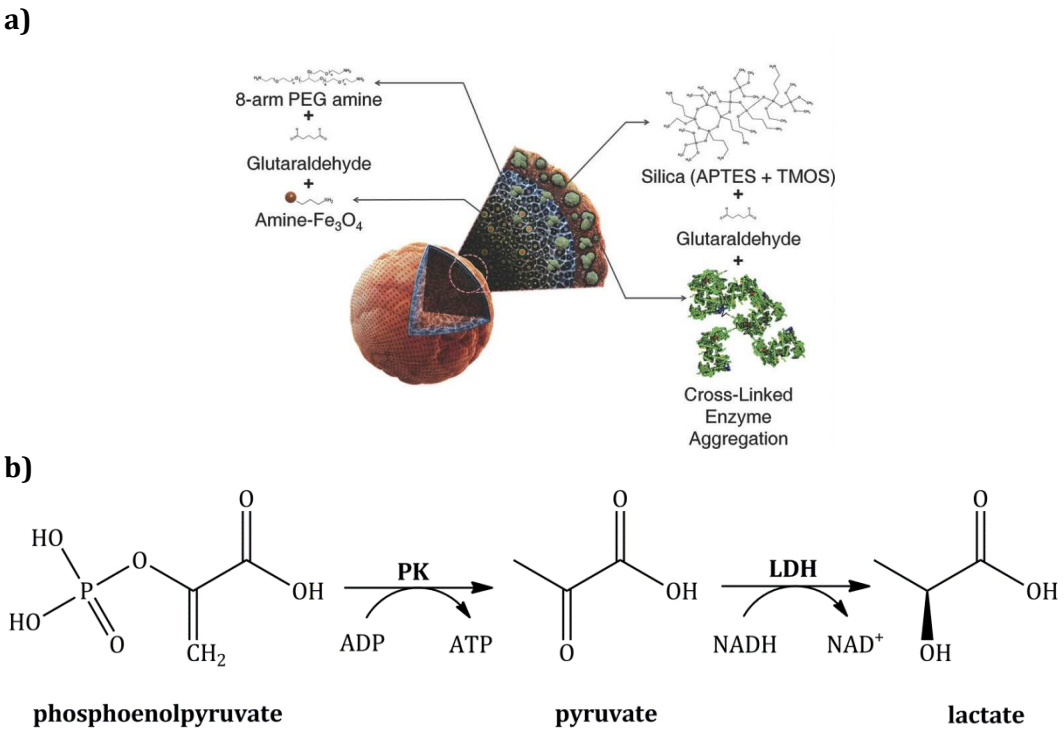


**Figure 33. a)** Schematic depiction of the texture of the magnetic particles used for enzyme immobilization. **b)** The immobilized pyruvate kinase (PK) from rabbit muscles catalyzes the dephosphorylation of phosphoenolpyruvate to pyruvate, which is accompanied by the phosphorylation of adenosine diphosphate (ADP) to adenosine triphosphate (ATP). The second step of the enzyme cascade comes along with the reduction of pyruvate to lactate and the concomitant oxidation of NADH to $NAD^+$ by the immobilized lactate dehydrogenase (LDH). Reprinted from [156] permission from The Royal Society of Chemistry.

[156] J. Chung, E.T. Hwang, J.H. Kim, B.C. Kim, M.B. Gu, *Green Chem.* **2014**, *16*, 1163-1167.

The enzyme cascade was carried out in two separate vessels containing the immobilized PK as well the immobilized LDH, respectively. In an experiment relating to the cycle stability of the immobilized enzymes, the number of the immobilisate particles and thus the ratio of the immobilized PK to the immobilized LDH was varied in nine steps from 0-200 particles and the final lactate concentration was detected, respectively. Within 1000 min, the complete cycle was operated three times, whereby the yield of lactate for a distinct particle amount employed in a certain cycle resembled from cycle to cycle. A substantially dependency on the number of immobilisate particles present in the respective vessel as well as the reaction rate and thus the productivity of the carrier-bound enzymes was ascertained. As expected, both parameters increased with rising particle amount. This opened up the possibility to adjust the reaction rate or rather the productivity of the immobilized PK or LDH in the respective vessel independently, which is a definite advantage in comparison to a one-pot cascade systems.[156]

Also a tandem reaction of two co-immobilized enzymes onto a single carrier can be considered as a cascade reaction. A co-immobilization of two or more enzymes is advantageous, as the catalytic efficiency is increased due to the reduction of the diffusion time of the substrate. A seminal approach was achieved by the entrapment of nitrobenzene nitroreductase (NBNR) from *Pseudomonas pseudoalcaligenes* JS45 and glucose-6-phosphate dehydrogenase (G6PDH) in a mesoporous silica matrix. The $NADP^+$ dependent NBNR catalyzes the conversion of nitrobenzene to hydroxylaminobenzene with concomitant oxidation of NADPH to $NADP^+$. The involvement of G6PDH in the multienzyme system ensures the re-reduction of $NADP^+$ to NADPH, which comes along with the oxidation glucose-6-phosphate (G6P) to 6-phosphoglucono-δ-lactone (6PGDL). Thus, the reuse of NADPH is guaranteed (Scheme 21).[157]

[157] L. Betancor, C. Berne, H.R. Luckarift, J.S. Spain, *Chem. Commun.* **2006**, 3640-3642.

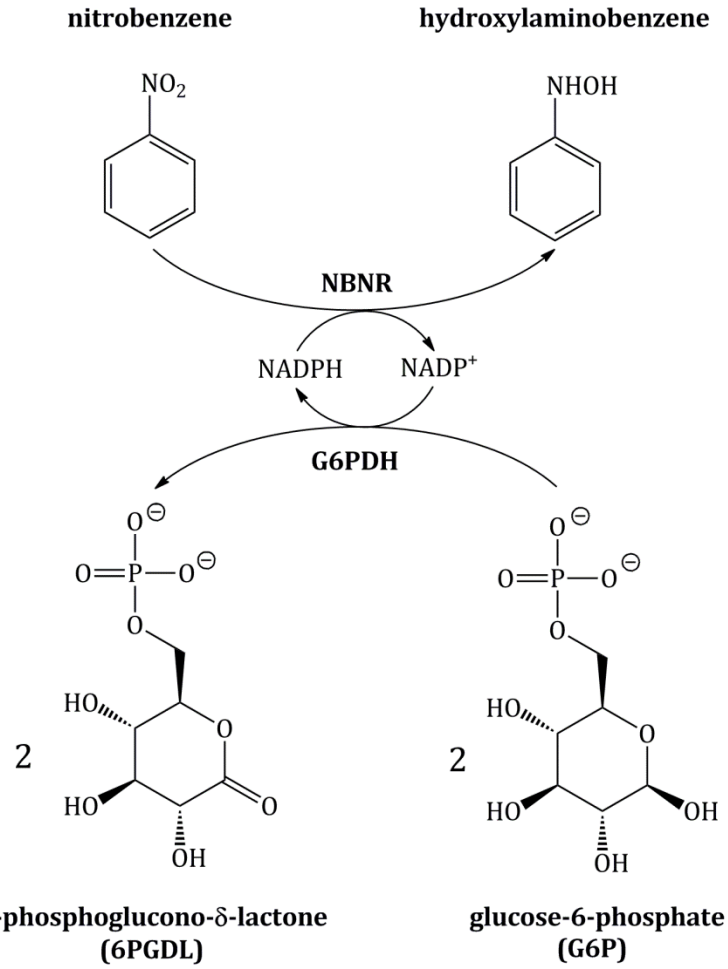


**Scheme 21.** The immobilized nitrobenzene nitroreductase (NBNR) from *Pseudomonas pseudoalcaligenes* JS45 catalyzes the conversion of nitrobenzene to hydroxylaminobenzene. This reaction is accompanied by the oxidation of NADPH to $NADP^+$. The incorporation of a co-immobilized glucose-6-phosphate (G6PDH) ensures the re-reduction of the coenzyme by means of the oxidation of glucose-6-phosphate (G6P) to 6-phosphoglucono-δ-lactone (6PGDL). Reproduced from [157] with permission from The Royal Society of Chemistry.

The synthesis of the host as well as the entrapment of both enzymes within the host was implemented simultaneously in the presence of TMOS as a silica precursor and polyethyleneimine directing the formation of the silica particles. The enzymatic activity of the enzymes has not been affected by the entrapment. Even the $K_m$ value of the immobilized NBNR revealed a similar value than obtained for the native enzyme, whereas the $K_m$ value of the immobilized G6PDH was detected to be three-fold higher than $K_m$ of the free enzyme. An optimal ratio of the incorporated enzymes figured out to be 1 unit (U) of NBNR and 5 U of G6PDH as well as an initial concentration of nitrobenzene of 100 µmol $L^{-1}$. In a long-term experiment, 240 µmol $L^{-1}$ NADPH was supplied uniquely and portions of nitrobenzene (250 µmol $L^{-1}$) were added stepwisely over an interval of 8 h. 3 mmol $L^{-1}$ G6P was

initially provided and a further portion of G6P (3 mmol $L^{-1}$) was added after 3 h. After a total reaction time of 8 h, 90 % of the final substrate amount (1.5 µmol $L^{-1}$) has been enzymatically converted. In further experiments, the substrate concentration was varied up to 10 mmol $L^{-1}$ and even after the conversion of a total amount of 30 mmol $L^{-1}$ nitrobenzene followed by the separation of the co-immobilisate from the reaction dispersion, the immobilized enzymes retained their full activity. Hence, the co-immobilization of NBNR and G6PDH onto a single host resulted in a 125-fold increase of the hydroxylaminobenzene formation in comparison to an uncoupled approach. Furthermore, a TTN of 62 for NADPH was ascertained.[157]

With respect to biomedical applications, a two enzyme cascade has been developed in order to facilitate the detoxification of reactive oxygen species in living cells. With this end in view, superoxide dismutase (SOD) as well as catalase (CAT) were confined in hollow mesoporous silica nanospheres (diameter ~40 nm) and introduced into cells. SOD catalyzes the reduction of hyperoxide ions to hydrogen peroxide that is further reduced to water by CAT (Scheme 22).[158]

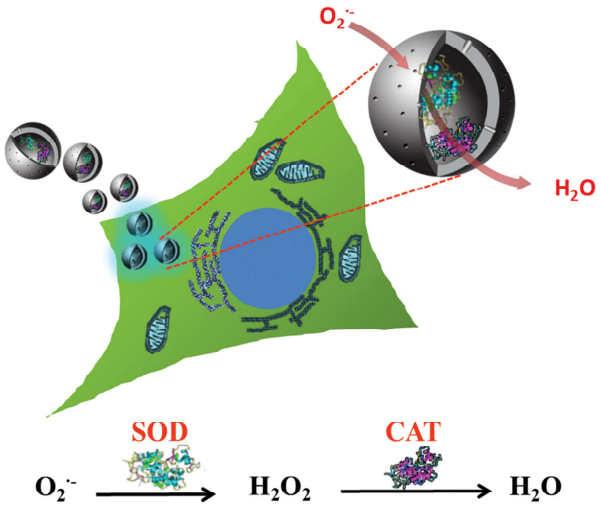


**Scheme 22.** Superoxide dismutase (SOD) and catalase (CAT) were encapsulated into hollow mesoporous silica spheres and introduced into living cells. SOD catalyzes the reduction of hyperoxide ions to hydrogen peroxide that is further reduced to water by CAT. Hence, these synthetic organelles were capable to detoxify reactive oxygen species in organisms. Figure adapted with permission from Wiley-VCH.[158]

Prior to the co-immobilization of SOD and CAT within hollow silica nanoparticles, both enzymes were modified using polyethyleneimine that was

[158] F.-P. Chang, Y.-P. Chen, C.-Y. Mou, *Small* **2014**, *10*, 4785-4795.

covalently attached to the surface of the enzymes. One major advantage of the PEI-coverage of the enzyme surface can be traced back to its positive charge that supports the diffusion of superoxide anions into the hollow nanoparticles and thus in the direction of the SOD. With respect to the co-immobilization of SOD and CAT a synergism between both enzymes in terms of the enzymatic activities turned out. In particular with respect to the native CAT, immobilization exhibited a pronounced stabilizing effect, as the native enzyme was inactivated by superoxide. The enzyme cascade was successfully performed in reaction vials but also in HENRIETTA LACKS (HeLa) cells. Hereby, the hollow silica nanoparticles boasted a high biocompatibility as well as an efficient enzymatic degradation of superoxide by the enzymes entrapped inside the particles. Hence, in the case of diseases caused by oxidative stress an application of these artificial organelles is conceivable.[158]

An entirely different approach in terms of enzyme cascades is the immobilization of the coenzyme instead of the actual enzymes. A simple approach describes the immobilization of $NAD^+$ onto non-porous silica nanoparticles bearing carboxylate groups on its surface. The immobilization of $NAD^+$ onto the organically modified silica particles was initiated by the use of carbodiimide, followed by the integration of the coenzyme immobilisate into a reaction sequence of two free and solubilized $NAD^+$ dependent enzymes (Scheme 23). Within this reaction sequence, pyruvate was reduced to L-lactate with simultaneous oxidation of NADH to $NAD^+$ by a keto reductase (KRD). In a subsequent step, the immobilized coenzyme was *in-situ* recycled due to the oxidation of formate to $CO_2$ with concomitant reduction of $NAD^+$ to NADH catalyzed by a native formate dehydrogenase (FDH).[159]

[159] Y. Li, H. Liang, L. Sun, J. Wu, Q. Yuan, *Biotechnol. Lett.* **2013**, *35*, 915-919.

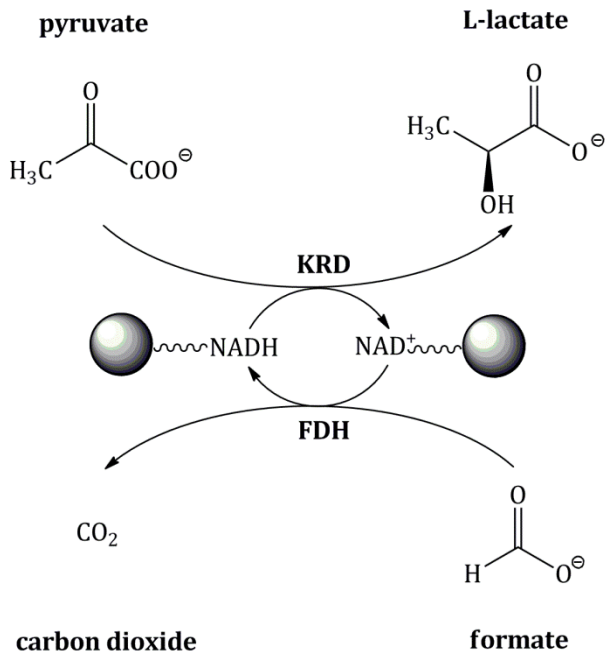


**Scheme 23.** $NAD^+$ was immobilized onto the surface of carboxylate modified non-porous silica particles *via* a carbodiimide initiated route. The immobilized coenzyme was applied in a cascade reaction containing a solubilized keto reductase (KRD) and formate dehydrogenase (FDH). The KRD catalyzed the reduction of pyruvate to L-lactate. Subsequently, the oxidized coenzyme was re-reduced by the free FDH accompanied by the conversion of formate to $CO_2$. Copyright Springer Science + Business Media Dordrecht 2013. Reproduced with permission of Springer.[159]

The functionalization density ($\rho_f$) concerning the carboxylate residues on the surface of the silica particles was detected to amount 0.526 mmol $g^{-1}$ and a total $NAD^+$ uptake of 72.8 mg per gram silica was received. The coenzyme immobilisate was dispersed in buffer solution containing the native KRD as well as FDH and the addition of pyruvate (0.2 mol $L^{-1}$) and formate (3 mol $L^{-1}$) introduced the cascade reaction, resulting in a final L-lactate concentration of 0.16 mol $L^{-1}$. With respect to the cofactor recycling part of the cascade, a TTN of 82.9 $h^{-1}$ was determined, whereas a TTN of 49.9 $h^{-1}$ still retained after six reaction cycles.[159]

This approach clearly highlights the opportunity of an efficient application of immobilized coenzymes in cascade reactions. However, an undesired immobilization of the free enzymes present in the reaction dispersion onto the host of the coenzyme has to be prevented.

One major advantage of the utilization of an immobilized enzyme is its simple separation from the reaction batch. However, a main drawback of the employment of immobilized enzymes is its dependency on appropriate coenzymes. Under consideration of a coenzyme recycling step an enzyme catalyzed reaction path can become rapidly complex. The application of entire cells that are placed in a

teabag-like polyvinylidene fluoride (PVDF) membrane can circumvent these difficulties, as the recycling reaction of the respective coenzyme is involved in the reaction paths of the enzymes within the cells. The reaction of benzaldehyde and acetaldehyde to (*R*)-2-hydroxy-1-phenylpropanone ((*R*)-HPP) and its further conversion to (1*R*, 2*R*)-1-phenylpropane-1,2-diol ((1*R*, 2*R*)-PPD) involving the recycling of the coenzyme NADPH was gathered as a proof of principle for the utilization of entire cells in biocatalysis (Scheme 24). This approach highlights a biocatalytic access to chiral diols. Its chemical syntheses suffer from a lot of disadvantage. Hence, an enzymatic approach seems to be more expediently.[160]

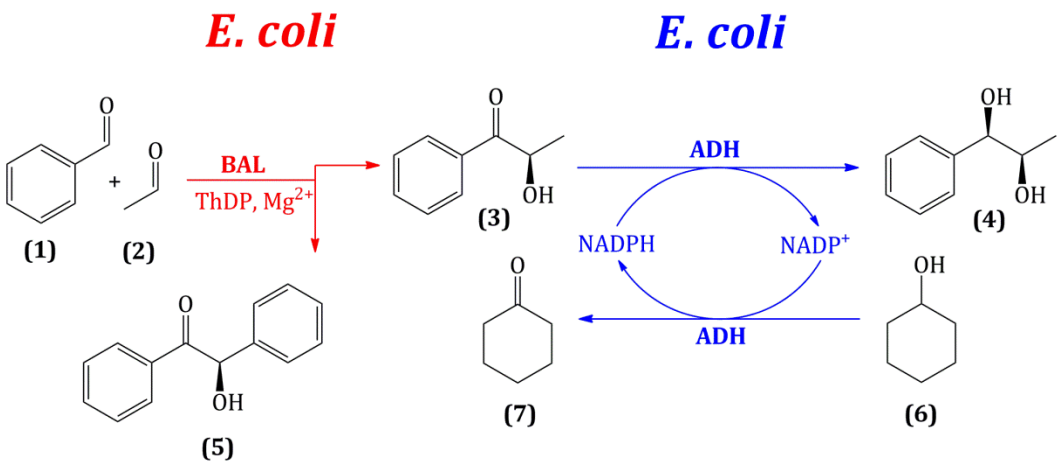


**Scheme 24.** Schematic depiction of a three step model cascade that was realized with the help of *E. coli* cells placed in permeable polyvinyl fluoride membranes. Benzaldehyde lyase (BAL) from *Pseudomonas fluorescens* in *E. coli* cells (red) catalyzes the aldol addition of benzaldehyde **(1)** and acetaldehyde **(2)** to form (*R*)-2-hydroxy-1-phenylpropanone **(3)** in the presence of thiamine diphosphate (ThDP) as well as bivalent magnesium. Hereby, (*R*)-benzoin **(5)** is formed as a side-product. Subsequently, alcohol dehydrogenase (ADH) from *Ralstonia sp.* DSM 6428 in a further type of *E. coli* cells (blue) catalyzes the enantioselective reduction of **(3)** to (1*R*, 2*R*)-1-phenylpropane-1,2-diol **(4)** with concomitant oxidation of NADPH to $NADP^+$. In a final step, $NADP^+$ is re-reduced to NADPH by an ADH-catalyzed oxidation of cyclohexanol **(6)** to cyclohexanone **(7)**. Figure reproduced with permission from Wiley-VCH.[160]

The aldol reaction of benzaldehyde as well as acetaldehyde aiming the formation of (*R*)-HPP was carried within *E. coli* cells by the benzaldehyde lyase (BAL) from *Pseudomonas fluorescens*. In the cascade step, (*R*)-HPP was reduced to (1*R*, 2*R*)-PPD within a further type of *E. coli* cells including alcohol dehydrogenase (ADH) from *Ralstonia sp.* DSM 6428. This final step was accompanied by the oxidation of NADPH to $NADP^+$. Due to the addition of cyclohexanol to the second cascade step $NADP^+$ was re-reduced to NADPH by the ADH, whereby cyclohexanol was oxidized to cyclohexanone.[160]

[160] J. Wachtmeister, A. Jakoblinnert, J. Kulig, H. Offermann, D. Rother, *ChemCatChem* **2014**, *6*, 1051-1058.

The *E. coli* cells were placed in a permeable PVDF membrane that facilitates an uncomplicated removal from the reaction mixture and even ensures its reusability. The enzyme cascade was performed in methyl *tert*-butyl ether (MTBE) with a maximum water content of 7.5 %. Hence, the implementation of whole cells is beneficial, as the cell membrane preserves the enzymes from the organic solvent.[160]

With respect to the presented cascade reaction, three different strategies were inspected in detail. On one hand, the teabags were supplied successively to the substrate solution (sequential mode). On the other hand, they were employed simultaneously for the conversion of the substrates (simultaneous mode). Besides, a mixed approach was forced in order to evaluate the most promising experimental conditions (mixed mode).

With regard to the sequential approach, the teabags were placed consecutively to the substrate solution. After the complete conversion of benzaldehyde as well as acetaldehyde, *E. coli* cells containing the ADH were dipped into the substrate solution. A final concentration of 238 mmol $L^{-1}$ of (1*R*, 2*R*)-PPD was obtained within 16 h. As the ADH is likewise able to convert benzaldehyde and acetaldehyde, which are substrates of the first step, this undesired reaction has been bypassed using the sequential mode. (*R*)-benzoin is a side-product of the BAL catalyzed aldol reaction. However, over time, it decomposed again and thus it was enzymatically converted in the presence of acetaldehyde to (*R*)-HPP. Likewise, this observation was made concerning the simultaneous mode, in which both teabags were dipped into the substrate solution simultaneously. As expected, in this approach, the ADH likewise reduced benzaldehyde (63 mmol $L^{-1}$/11 h). Nevertheless, after 11 h, 235 mmol $L^{-1}$ of (1*R*, 2*R*)-PPD were formed. Therefore, the product yield is comparable to the yield achieved in the sequential mode. In the mixed mode, the teabag containing the *E.coli* cells with BAL that catalyzes the first step of the cascade reaction were dipped into the substrate solution. After 3 h, the second teabag including the *E. coli* cells with the ADH was added to the reaction mixture and a final (1*R*, 2*R*)-PPD concentration of 339 mmol $L^{-1}$ was received after 17 h. However, a certain formation of phenylacohol by the ADH was to be expected (18 mmol $L^{-1}$/17 h). In conclusion, the space-time yield was detected to be best in terms of the simultaneous mode (3.25 g $L^{-1}$ $h^{-1}$) followed by the mixed mode (3.03 g $L^{-1}$ $h^{-1}$) as well as the sequential approach (2.26 g $L^{-1}$ $h^{-1}$).[160]

Dependent on the water content as well as the supplied concentration of acetaldehyde, the productivity of BAL turned out to decrease markedly over three cycles. This was addressed to the toxicity of acetaldehyde that is diminished with increasing water content of the organic reaction medium. Conversely, the

productivity of the ADH remained nearly constant over four cycles an only a minor reduction of 6 % was detected for the fifth cycle.[160]

The application of cells that are placed in a permeable membrane are an impressive example today's scientific knowledge. However, with respect to the poor cycle stability of BAL it is not necessarily superior to the competing utilization of immobilized enzymes for biocatalytic applications. Furthermore, the diffusion limitations arising from the PVDF membrane and additionally from the cell membrane have to be taken into account. Hence, the employment of immobilized enzymes or even whole cells in synthetic reaction paths has manifold assets and drawbacks. The path that needs to be taken regarding the development of a new biocatalytic route has to be chosen on a case-by-case basis.

# 2 CHARACTERIZATION TECHNIQUES

## 2.1 Nitrogen physisorption

Gas physisorption is the major method concerning the surface and pore size analysis of micro- as well as mesoporous materials. Physisorption differentiates from chemisorption by the type of the bond that is formed between the adsorptive and the adsorbent. In terms of chemisorption, a covalent bond is formed making this process irreversible. In contrast, physisorption is characterized by the formation of attractive adsorptive and thus reversible bonds between the adsorptive and the adsorbent. With respect to the investigation of the porosity of mesoporous materials, nitrogen ($N_2$) physisorption has been established as a method of choice. As a general rule, $N_2$ physisorption is performed at 77.4 K, whereat the relative pressure ($p/p_0$) is increased from $p/p_0 = 0$ to $p/p_0 = 1$ initiating the adsorption of $N_2$ molecules onto the surface of the mesoporous solid. Subsequently, the relative pressure is reduced again in order to induce desorption of the gas molecules (pore fluid) from the surface. The relative pressure is composed of two components ($p/p_0$). p defines the equilibrium vapor pressure of $N_2$, whereas $p_0$ designates the saturation pressure of $N_2$ at 77.4 K. The adsorption of gas molecules onto a solid phase can be traced back to van-der-Waals forces that in turn can be subdivided into dipole-dipole interaction (Keesom forces), dipole-induced dipole interactions (Debye forces) as well as interactions between induced dipoles (London forces). Moreover, adsorption of gas molecules onto porous solids is subjected to effects referable to the confinement of the fluid within the porous structure of the adsorbent. This also affects the thermodynamic behavior of the adsorbed fluid. Furthermore, interactions between the fluid molecules among each other play a decisive role within the adsorption procedure (Figure 34). The cooperation of these interactions are indirectly expressed in the shape and type of the physisorption isotherms.[161, 162, 163]

[161] M. Thommes, *Chem. Ing. Tech.* **2009**, *82*(7), 1059-1073.
[162] M. Thommes, *Nanoporous Materials: Science and Ingeneering*, Imperial College Press, London, **2004**.
[163] S. Lowell, J.E. Shields, M.A. Thomas, M. Thommes, Characterization of Porous Solids and Powders: Surface Area, *Pore Size and Density*, Kluwer Academic Publishers, Dordrecht, Boston, London, **2004**.

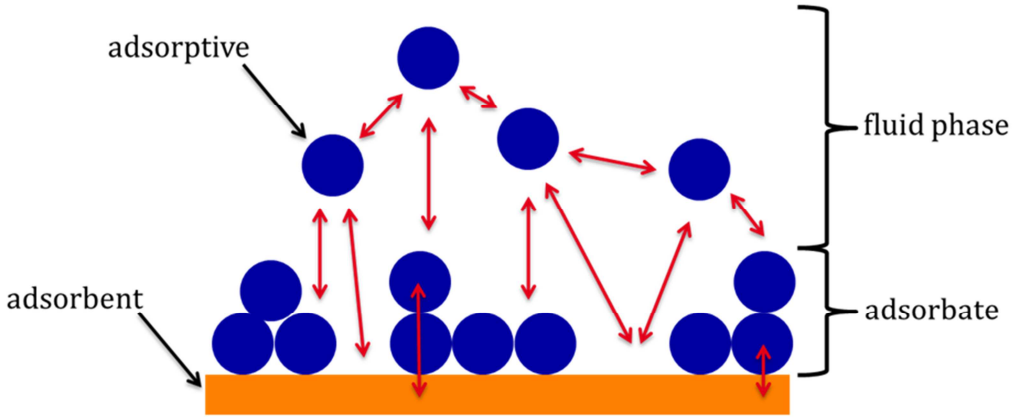


**Figure 34.** In a physisorption experiment, gas molecules (adsorptive) interact with the solid sample material (adsorbent) and among each other *via* comprehensive van-der-Waals forces (red arrows). The gaseous phase of the adsorptive is designated as fluid phase, whereas the adsorbed adsorptive is termed as adsorbate.

The *International Union of Pure and Applied Chemistry* (IUPAC) classified eight common types of physisorption isotherms (Figure 35). Most prominent isotherms are the type I (a)/(b) isotherms that are characteristic for microporous materials possessing pore sizes ≤ 2.5 nm as well as the type IV (a)/(b) isotherms that are relevant in terms of mesoporous materials.[164]

[164] M. Thommes, K. Kaneko, A.V. Neimark, J.P. Oliveir, R. Rodriguez-Reinoso, J. Rouquerol, K.S.W. Sing, *Pure Appl. Chem.* **2015**, 1-19.

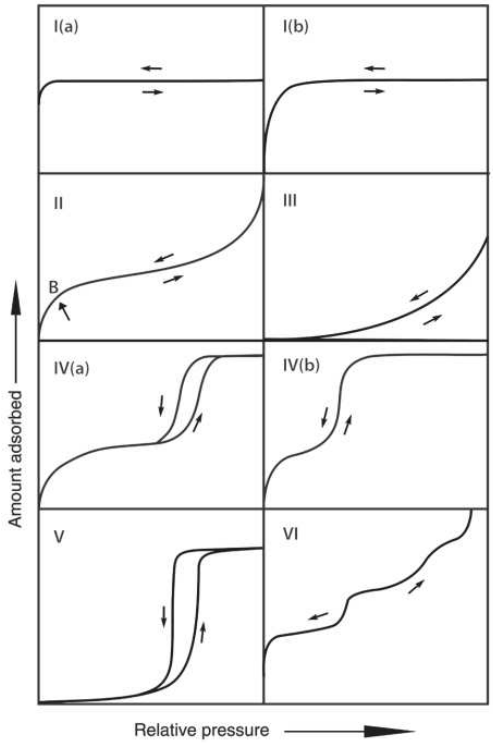


**Figure 35.** Classification of physisorption isotherms in accordance to IUPAC.: Type I(a)/(b): microporous materials; type II: nonporous or macroporous materials; type III: nonporous or macroporous materials (weak adsorbent-adsorbate interactions); type IV(a)/(b): mesoporous materials; type V: nonporous or macroporous materials (weak adsorbent-adsorbate interactions, e.g. water vapor sorption onto hydrophobic porous materials); type VI: uniform nonporous surface (layer by layer adsorption).[164]

The progress of the adsorption of $N_2$ onto mesoporous solids can be separated into several steps. The first step is characterized by the formation of an adsorbate monolayer on the pore walls of the material ($p/p_0 = 0.05 – 0.3$). Within this relative pressure range a statistical monolayer is formed, whereas the extensive formation of multilayers has not yet set in. In the further course, multilayer adsorption is dominant and thus the pore diameter decreases with increasing number of adsorbate layers. Multilayer formation is typical in terms of physisorption, whereas it is absent when chemisorption is present. The multilayers are stabilized by van-der-Waals interactions as well as the surface tension of the adsorbate and the curvature of the adsorbate-adsorptive interface. The influence of the adsorption potential of the pore walls ($\Delta\mu_a$) on the chemical potential difference ($\Delta\mu$) becomes less important with increasing number of adsorbate layers. Conversely, the contribution of the tension and curvature of the adsorbate-adsorptive interface ($\Delta\mu_c$) gains in importance (Eq. 16).

$$\Delta\mu = \Delta\mu_a + \Delta\mu_c \qquad \textbf{Eq. 16}$$

Once the critical film thickness (Kelvin radius) is reached, the adsorption potentials of both pore walls overlap and a further multilayer stabilization is unfeasible. Thus, pore/capillary condensation sets in spontaneously. In this state, the metastable adsorbate undergoes a vapor-liquid phase transition wherein the gaseous adsorbate condenses to a liquid-like phase. Hence, the pore diameter can be calculated basing on the Kelvin equation, as it establishes a connection between the pore diameter and the relative pressure at which capillary condensation occurs. The shift of the phase transition below the saturation pressure of the bulk phase can be referred to attractive adsorbate-pore wall interactions. Generally, pore condensation occurs in the case of contact angles < 90°, whereby a contact angle of 0 ° is assumed in the case of $N_2$ physisorption at 77.4 K (complete wetting). Capillary condensation of the adsorbate comes along with a more or less pronounced steep increase of the adsorption branch and a sudden increase of the amount of adsorbed adsorptive. Hence, the adsorption branch passes over to a plateau indicating a complete filling of the pores. As previously mentioned, physisorption is a reversible process. Thence, desorption can be introduced due to anew reduction of the relative pressure. The pore fluid is separated by a hemispherical meniscus from the bulk gas phase. In the case of desorption, the pore fluid evaporates into the gas phase *via* a receding meniscus at pressures lower than the pressure of the pore condensation.

More precisely, with regard to the metastable behavior of the pore fluid, the adsorption process involves the hindered nucleation of liquid bridges. Hence, this branch is not in thermodynamic equilibrium with the vapor-liquid transition. Conversely, the desorption is not affected from metastabilities. Accordingly, the desorption branch is in thermodynamic equilibrium with the liquid-vapor transition. Thus, a hysteresis loop arises in the isotherms of mesoporous materials when the pores size of the adsorbent exceeds a diameter of 4.2 nm. As mentioned above, the relative pressure, at which pore condensation sets in, is dependent on the pore size of the adsorbent. Consequently, the larger the pore size, the wider the shift of the hysteresis loop towards $p/p_0 = 1$. Furthermore, first indications relating to the pore size distribution can be obtained from the sharpness or rather the steepness of the adsorption as well as the desorption branch. According to this, steep branches indicate a narrow pore size distribution, whereat the width of the hysteresis can be frequently referred to network effects.[161, 162, 163, 164]

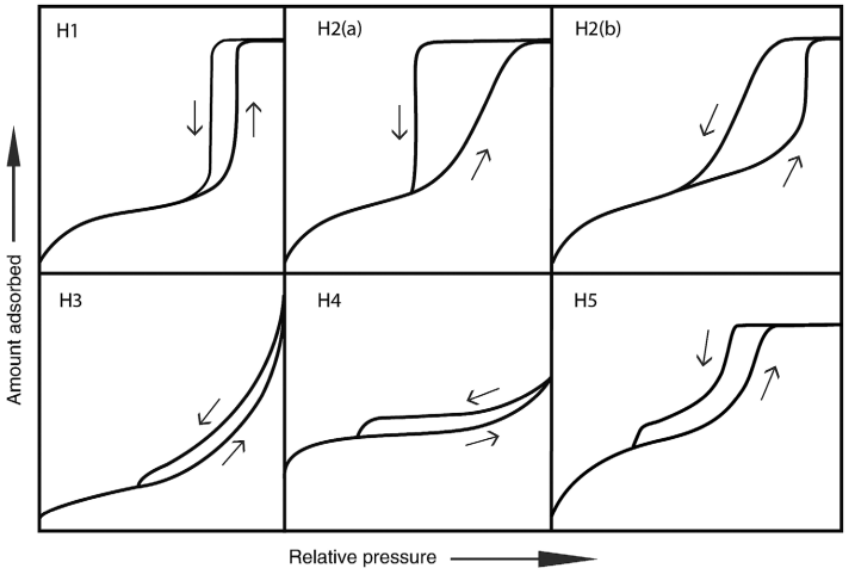


**Figure 36.** Classification of hysteresis loops in according to IUPAC: H1: narrow pore size distribution (PSD; e.g. MCM-41, MCM-48, SBA-15); H2(a)/(b): complex porous networks (e.g. SBA-16, KIT-6, MCF); H3: non-rigid aggregates (e.g. plate-like particles); H4: crystalized zeolites, mesoporous zeolites, microporous-mesoporous carbon; H5: coexistence open and partially blocked mesopores.[164]

Besides the categorization of eight typical isotherms, IUPAC defined six types of commonly occurring hysteresis loops (Figure 36). However, the origin of the hysteresis is still highly discussed and to some extent not fully understood. With respect to mesoporous materials hysteresis H1 as well as H2(a) and H2(b) are most important. The H1 hysteresis is typical for materials possessing open cylindrical mesopores (e.g. MCM-41, SBA-15). In terms of independent cylindrical mesopores, hysteresis is referred to the metastable behavior of the pore fluid and the delayed pore condensation ("*independent pore model*"). In contrast, a metastable phase is absent within the desorption process and thus the desorption is in equilibrium with the vapor-liquid transformation. Conversely, a H2 hysteresis is frequently obtained for complex mesoporous silica networks and it can be attributed to the interconnectivity of the pores effecting a delayed evaporation of the pore fluid ("*network model*"). The steep drop of the desorption branch in hysteresis H2(a) is addressed to pore blocking in terms of narrow pore necks and percolation as well as cavitation effects (e.g. KIT-6, SBA-16). On the contrary, H2(b) hysteresis is present in the case of significantly broader pore necks as partly detected for MCF.[164]

One major outcome of $N_2$ physisorption analysis is the possibility to determine the specific surface area of the adsorbent that is traditionally calculated according to the method of S. Brunauer, P. H. Emmett and E. Teller.[165] The BET

[165] S. Brunauer, P.H. Emmett, E. Teller, *J. Am. Chem. Soc.* **1938**, *60*, 309-319.

model is not only limited to the examination of the specific surface area ($S_{BET}$) of mesoporous materials. It also allows the interpretation of $S_{BET}$ of nonporous materials. However, it is inappropriate in terms of microporous materials. The BET equation takes the formation of an adsorbate monolayer on the surface of the adsorbate as a basis (Eq. 17). A statistical adsorbate monolayer has been formed at a relative pressure of $\leq p/p_0 = 0.3$. Thus, the BET equation is applied in the relative pressure range of $p/p_0 = 0.05 - p/p_0 = 0.3$.[161, 162, 163, 164, 165]

$$\frac{1}{n \cdot \left[\left(\frac{p_0}{p}\right) - 1\right]} = \left(\frac{1}{n_m \cdot C}\right) + \left(\frac{C-1}{n_m \cdot C}\right) \cdot \left(\frac{p}{p_0}\right) \qquad \textbf{Eq. 17}$$

$p_0$ = saturation pressure of the adsorptive

$p$ = vapor pressure of the adsorptive

$n_m$ = monolayer capacity

$n$ = amount of adsorbate

$C$ = empirical BET constant

Some complexity arises from the usage of $N_2$ as a standard adsorptive for mesoporous materials, as the $N_2$ molecule possesses a quadrupole moment. Thus, attractive interactions between the $N_2$ molecules and polar silanol groups on the surface of the material occur. These interactions effect a reduction of the cross-sectional area of $N_2$ from 0.162 $nm^2$ to 0.135 $nm^2$. Hence, in terms of polar adsorptive-adsorbate interactions, the calculation of $S_{BET}$ underlies a more or less pronounced overestimation.[161, 162]

The calculation of the pore size distribution (PSD) of mesoporous materials by means of $N_2$ physisorption was originally merely carried out by methods that correspond to the macroscopic thermodynamic and thus rest upon the Kelvin equation. For instance, the method introduced by E. P. Barrett, L. G. Joyner and P. P. Halenda (BJH) takes a cylindrical pore geometry into account and the calculation of the PSD bases upon a modified form of the Kelvin equation.[166] However, the KELVIN equation neglects inter alia attractive adsorbate-adsorbent interactions as well as the formation of multilayers prior to pore condensation. In the further course, the equation has been altered in order to diminish inadequacies, but primarily the development of microscopic models based upon the density functional theory (DFT) have brought a major breakthrough. The non-local density functional theory (NLDFT) considers the adsorptive-adsorptive interactions as well

[166] E.P. Barrett, L.G. Joyner, P.P. Halenda, *J. Am. Chem. Soc.* **1951**, *73*, 373-380.

as adsorbate-adsorbents interactions, whereas the quenched solid density functional theory (QSDFT) takes wall heterogeneities into consideration. An evaluation according to the DFT methods requires the calculation of theoretical model isotherms ("*kernel*"). Depending on the nature of the material, its pore geometry as well as the chosen adsorptive, various kernels are available allowing a more precise investigation of the porosity.[161, 162]

## 2.2 Enzyme quantification

The immobilization of enzymes onto solid hosts requires a reliable method for the quantification of enzymes. Within the last decades, various principles have established. Besides the notorious Lowry and the biuret assays, in particular the Bradford assay as well as the bicinchoninic assay have established.[167, 168, 169, 170] With respect to immobilized enzymes, these measurements are used in an indirect manner by the detection of the enzyme concentration in the supernatants of the immobilization procedure followed by a recalculation of the real amount of immobilized enzyme. A further method concerning the direct quantification of carrier-bound enzymes by means of infrared spectroscopy (IR) has been developed.[171] However, in the course of this dissertation, the Bradford method as well as the bicinchoninic assay were employed for the indirect determination of enzyme concentrations. Hence, it is obvious to present the scientific background of these measurements.

### 2.2.1 Bradford assay

Major drawbacks concerning the protein quantification according to the Lowry as well as the biuret assays initiated the developed of a more sensitive and less vulnerable method by M. M. Bradford. The quantification of proteins by means of the Bradford method is appropriate for the determination protein concentrations ranging from 1 µg $mL^{-1}$ to 2000 µg $mL^{-1}$.[172] The colorimetric assay bases upon direct binding of the dye coomassie brilliant blue G-250 (CBBG) to distinct amino acid residues of the protein, which is accompanied by a color change und thus a shift of the absorbance (Scheme 25). In particular, CBBG binds to the basic amino acid

[167] A.G. Gornall, S.J. Bardawill, M.M. David, *J. Biol. Chem.* **1949**, *177*(2), 751-766.
[168] O.H. Lowry, N.J. Roseborough, A.L. Farr, R.J. Randall, *J. Biol. Chem.* **1959**, *193*, 265-275.
[169] M.M. Bradford, *Anal. Biochem.* **1976**, *72*, 248-254.
[170] P.K. Smith, R.I. Krohn, G.T. Hermanson, A.K. Mallia, F.H. Gartner, M.D. Provenzano, E.K. Fujimoto, N.M. Goeke, B.J. Olson, D.C. Klenk, *Anal. Biochem.* **1985**, *150*, 76-85.
[171] C. Morhardt, B. Ketterer, S. Heißler, M. Franzreb, *J. Mol. Catal. B.: Enzym.* **2014**, *107*, 55-63.
[172] Thermo Scientific: *Instructions Coomassie (Bradford) Protein Assay Kit*: https://assets.thermofisher.com/TFS-Assets/LSG/manuals/MAN0011181_Coomassie_Bradford_Protein_Asy_UG.pdf, **2017**.

residues of arginine (Arg), histidine (His) and lysine (Lys) as well as to the aromatic amino acids tryptophan (Trp), tyrosine (Tyr) and phenylalanine (Phe). Moreover, the response of CBBG in the presence of arginine was identified to be eight times higher compared to the further previously mentioned amino acid residues. The Bradford reagent consists of 0.01 % (w/v) CBBG, 4.7 % (w/v) ethanol as well as 8.5 % (w/v) phosphoric acid.[169, 173, 174]

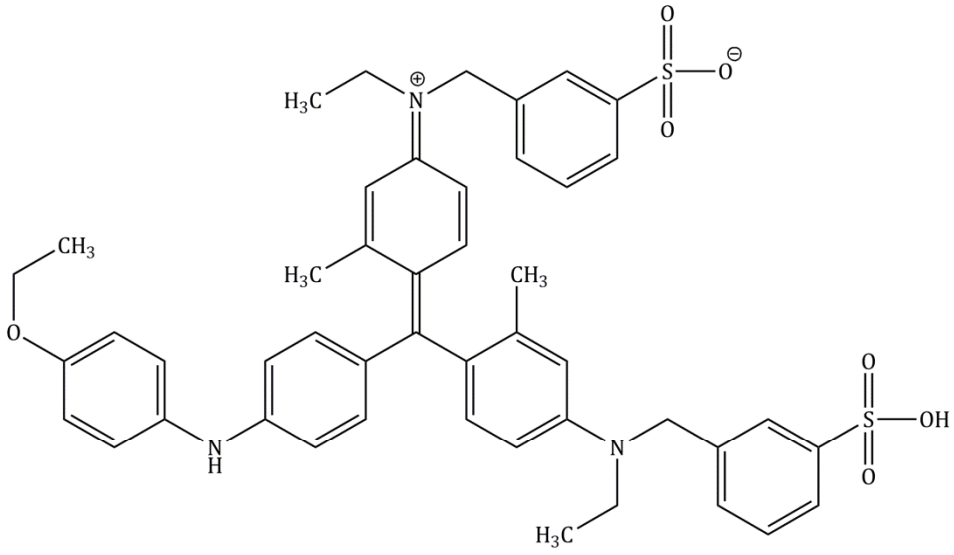

**coomassie brilliant blue G-250 (CBBG)**

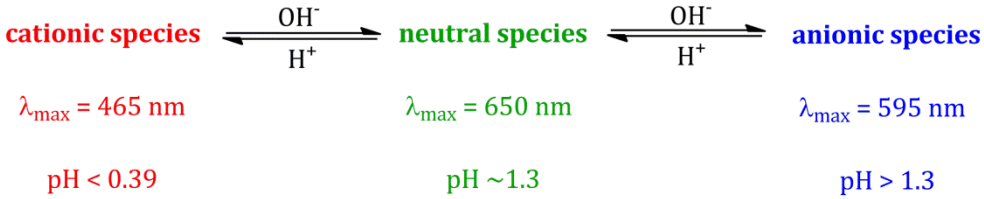


**Scheme 25.** Dependent t on the pH value, coomassie brilliant blue G-250 (CBBG) forms a cationic (pH < 0.39), a neutral (pH ~ 1.3) as well as an anionic (pH > 1.3) species that possess a maximum of the absorbance at different wavelengths respectively.[174, 175] Interactions between the dye and amounts of protein arise between the neutral and the anionic form, whereas the cationic form does not interact with amino acid residues of the protein. The interactions were identified to be electrostatic as well hydrophobic and they are accompanied by a shift of the absorbance maxima, respectively. With respect to the Bradford assay, only the neutral species of CBBG is decisive.[175]

Depending on the pH value, CBBG exists in a cationic (red, $\lambda_{max}$ = 465 nm), neutral (green, $\lambda_{max}$ = 650 nm) or anionic (bue, $\lambda_{max}$ = 595 nm) form (Scheme 25). Initially, it was assumed that merely the anionic form of the dye is able to interact

[173] B.J.S.C. Olson, J. Markwell, Assays for Determination of Protein Concentration. *Current Protocols in Protein Science* **2007**, *48*(3.4), 3.4.1–3.4.29.
[174] S.J. Compton, C.G. Jones, *Anal. Biochem.* **1985**, *151*, 369-374.
[175] C.D. Georgiou, K. Grintzalis, G. Zervoudakis, I. Papapostolou, *Anal. Bioanal. Chem.* **2008**, *391*, 391-403.

with a protein.[174] In the course of time, also the neutral species was identified to interact attractively with proteins, whereas the cationic form does not show any response to the dye. However, with reference to the pH value of the Bradford reagent some confusion arose, as herein mainly the cationic form of CBBG is present that was confirmed not to interact with proteins. Hence, the addition of the Bradford reagent to a protein sample should not initiate any color changes as attractive interactions are absent. However, a sufficient amount of the neutral CBBG species is assumed to be present in the reagent mixture that is able to interact with proteins. These attractive interactions correlate with a shift of the absorbance maximum from $\lambda_{max}$ = 650 nm to $\lambda_{max}$ = 615-625 nm.[175]

With regard to the neutral form of the dye, hydrophobic interactions between aromatic amino acids residues (Trp, Phe) of the protein and hydrophobic areas of CBBG are responsible for its coordination. Furthermore, electrostatic interactions between the negatively charged sulfonic acid residues of the dye and positively charged nitrogen atoms of the basic amino acids (His, Arg, Lys) contribute to the formation of the CBB-protein complex. In terms of the anionic CBBG species, merely electrostatic interactions play a role in the formation of the CBBG-protein complex and a shift of the absorbance maximum from $\lambda_{max}$ = 595 nm to $\lambda_{max}$ = 615 nm has been observed.[175] Nevertheless, the detection of the absorbance in a typical Bradford assay is traditionally operated at a wavelength of $\lambda_{max}$ = 595 nm.[172, 173]

The photometrical detection of the protein concentration requires the erection of a standard curve using bovine serum albumin (BSA). However, in terms of the quantification of arginine-rich proteins, an arginine-rich standard instead of BSA is necessary. Notwithstanding the above, the calibration curve exhibits a certain non-linearity indicating that the absorbance of the standards does not own a linear dependency on the protein concentration and an evaluation by means of linear regression is highly erroneous. Therefore, interpolation utilizing cubical regression is recommended.[169, 173, 176]

After the addition of CBBG to the standards as well as the samples, the formation of the dye-protein complex is completed within 2 min and it is stable over at least 1 h. After the expiration of this time, aggregation of the CBBG-protein complex sets in leading to an inaccurate measurement. The highest stability of the dye-protein complex was reported to be 5-20 min after the addition of CBB. Hence, with respect to a precise protein quantification, it is required to perform the whole

[176] Thermo Scientific: TECH TIP #57: *How to use a protein standard curve*: https://assets.thermofisher.com/TFS-Assets/LSG/Application-Notes/TR0057-Read-std-curves.pdf, **2017**.

series of measurements within this interval.[169] Although the Bradford assay has been reported to be very unsusceptible against a couple of substances, such as buffer salts, buffer additives and detergents as well as chelating agents and organic solvents, it has to be considered not to exceed appropriate concentration, respectively in order to avoid any interferences and thus to gain reliable results.[172, 177]

### 2.2.2 Bicinchoninic acid (BCA) assay

A further widespread and also colorimetric method for the quantification of proteins in aqueous solution is the bicinchoninic acid (BCA) assay that was originally inspired by the LOWRY assay. The BCA assay is performed in alkaline media and it allows the detection of protein concentrations up to 2000 µg $mL^{-1}$. Here again, the erection of a calibration employing BSA is indispensable.[168, 170, 178, 179]

The addition of the BCA reagent mixture to a protein sample induces a two-step reaction mechanism. Initially, bivalent copper ions ($Cu^{2+}$) are reduced to $Cu^{+}$ (green) by cysteine (Cys), cystine (a Cys dimer), tryptophan (Trp) as well as tyrosine (Tyr) residues of the protein. Even the peptide bonds of the protein contribute to the reduction of $Cu^{2+}$, which, however, only occurs when incubation is carried out at 37 °C or rather at 60 °C instead of exposing the samples to room temperature. In a subsequent second step, two equivalents of BCA coordinate one $Cu^{+}$ ion forming the purple BCA-$Cu^{+}$ complex that possesses an absorbance maximum at $\lambda_{max}$ = 562 nm and thus it is photometrical detectable (Scheme 26). With respect to the BCA assay, the absorbance at a wavelength of 562 nm shows a nearly linear dependency on the protein concentration. Hence, the protein amount can be calculated by means of linear regression.[168, 170, 179, 180]

[177] Sigma-Aldrich: *Bradford Reagent Technical Bulletin*: http://www.sigmaaldrich.com/content/dam/sigma-aldrich/docs/Sigma/Bulletin/b6916bul.pdf, **2017**.
[178] Merck-Millipore: *Novagen® BCA Protein Assay Kit*: http://www.merckmillipore.com/DE/de/product/BCA-Protein-Assay-Kit,EMD_BIO-71285, **2017**.
[179] Thermo Sientific: *Instructions: Pierce® BCA Protein Assay Kit*: https://tools.thermofisher.com/content/sfs/manuals/MAN0011430_Pierce_BCA_Protein_Asy_UG.pdf, **2017**.
[180] K.J. Wiechelmann, R.D. Braun, J.D. Fitzpatrick, *Anal. Biochem.* **1988**, *175*, 231-237.

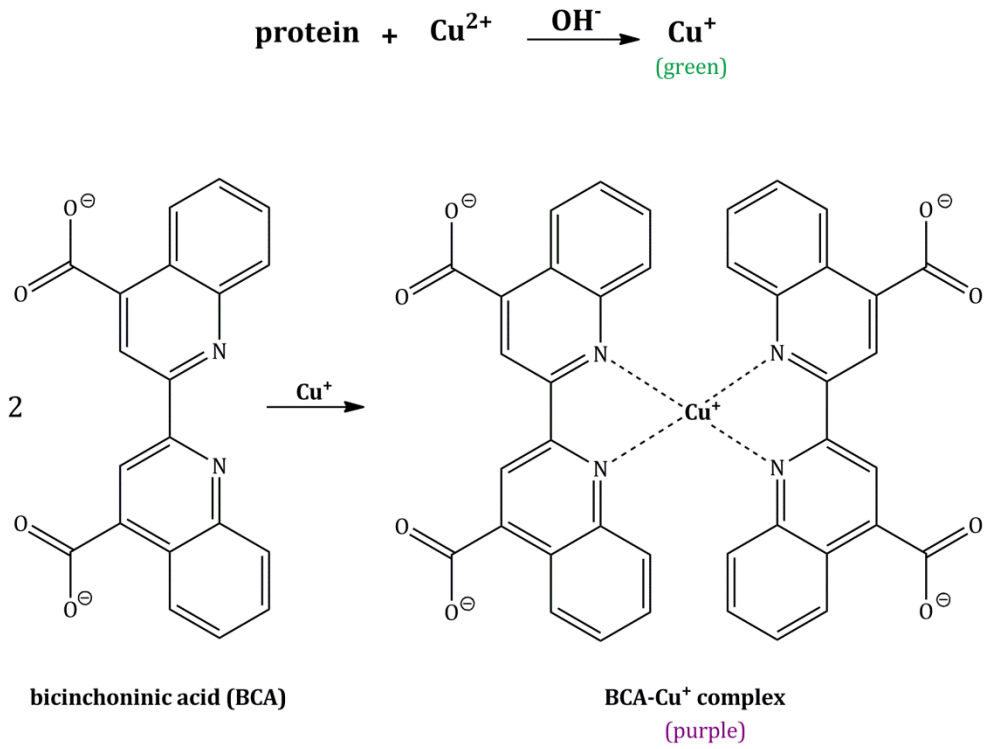


**Scheme 26.** Schematic depiction of the protein quantification according to the bicinchoninic assay (BCA). The BCA reagent mixture contains bivalent copper ions ($Cu^{2+}$) that are reduced to $Cu^{+}$ (green) by distinct amino acid residues of the protein. Subsequently, the formed $Cu^{+}$ ions are coordinated by two equivalents BCA, respectively. The arising purple BCA-$Cu^{+}$ complex possesses an absorbance maximum at $\lambda = 562$ allowing a photometrical determination of the protein concentration. Reprinted from [170]. Copyright 1985, with permission from Elsevier.

The BCA reagent mixture is composed of two solutions: Solution A (pH 11.25): 1 % BCA, 2 % sodium carbonate monohydrate, 0.16 % sodium tartare, 0.4 % sodium hydroxide, 0.95 % sodium hydrogen carbonate and solution B: 4 % copper sulfate pentahydrate in distilled water. Prior to the performance of the assay, both solutions are freshly mixed in a volume ratio of 100:2 (solution A:solution B).[170] Most protocols recommend an incubation at 37 °C for 30 min or at 60 °C for 15 min, after the BCA reagent is added to the BSA standards as well as the protein samples.[178, 179] Incubation at room temperature has to be excluded, as the reduction of $Cu^{2+}$ by peptide bonds is absent at 25 °C.[173] The formed BCA-$Cu^{+}$ complex was reported to be stable over time. However, when incubation was conducted at 37 °C for 30 min a further increase of the absorbance of 0.25 % per min was observed during and after cooling the samples to room temperature. This can be traced back to an incomplete reduction of $Cu^{2+}$.[170] Hence, with respect to reliable results, incubation at 60 °C for 15 min is highly recommended.[173]

However, even the BCA assay is subjected to certain restrictions. Thence, in the presence of substances that to reduce $Cu^{2+}$ to $Cu^{+}$ the BCA assay is limited. Furthermore, caution has to be paid in the presence of chelating agents and when exceeding certain concentrations of buffer salts, organic solvents as well as detergents. In addition, the juxtaposition of BCA and glucose, mercaptoethanol or dithiothreitol results in an increase of the absorbance at a wavelength of 562 nm, whereas it is diminished in the presence of ammonium sulfate.[178, 179, 181]

[181] R.E. Brown, K.L. Jarvis, K.J.Hyland, *Anal. Biochem.* **1989**, *180*, 136-139.

# 3 MOTIVATION

Enzymes are efficient biocatalysts, as they specifically convert their substrate under mild conditions accompanied by a high selectivity. Furthermore, an enzyme catalyzed approach is generally characterized by the absence of unrequested side products. Thus, enzyme catalytic routes have always attracted the attention of preparative working chemists. However, the separation of a solved enzyme from a reaction batch is quite challenging and frequently accompanied by its denaturation. Hence, a significant cost factor arises, as the reusability of the enzyme is not ensured.

The immobilization of the required enzyme onto a suitable carrier circumvents these difficulties. Besides various porous and nonporous hosts, mesoporous silicas have established themselves as adequate support materials for the immobilization of proteins within the last decades. However, most enzymes are dependent on a cofactor or coenzyme. Out of this, another cost factor arises concerning the application of immobilized enzymes in laboratory as well as industrial scale. The costs of a coenzyme frequently exceed the costs of an enzyme. Accordingly, when intending a reaction sequence employing immobilized enzymes, a cofactor recycling step should be considered and incorporated. On one hand, the immobilization of an enzyme assures its reusability and enhances the efficiency a biocatalytic approach. On the other hand, the recycling of necessary coenzymes additionally contributes to an efficient application of immobilized enzymes in organic chemistry.

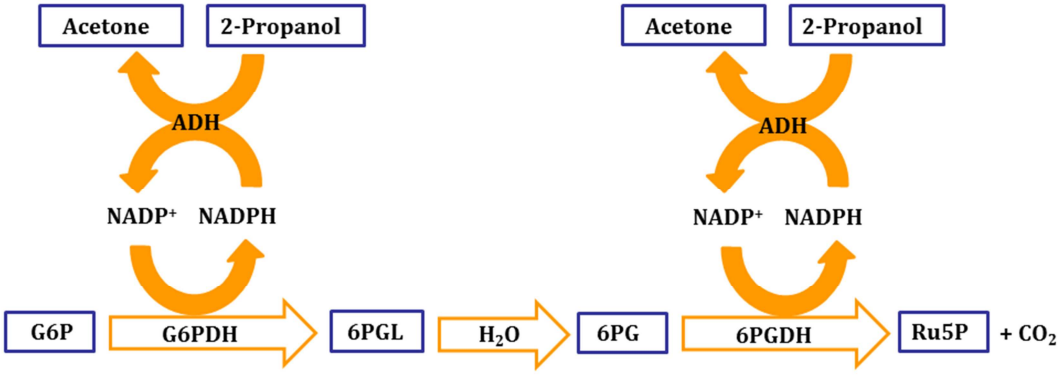


**Figure 37.** Modular enzyme cascade consisting of a reaction sequence of the pentose phosphate pathway, linked to a cofactor recycling system. The immobilized glucose-6-phosphate dehydrogenase (G6PDH) catalyzes the oxidation of glucose-6-phoshate (G6P) to give 6-phosphoglucono-δ-lactone (6PGL), which immediately hydrolyzes to 6-phosphogluconate (6PG); whereas the carrier bound 6-phosphogluconate dehydrogenase (6PGDH) enables the oxidation of 6PG to ribulose-5-phosphate (Ru5P) and $CO_2$. Both enzymatic reaction steps are accompanied by the reduction of an equivalent nicotinamide adenine dinucleotide phosphate ($NADP^+$) to NADPH, respectively. $NADP^+$ becomes be regenerated from NADPH by an alcohol dehydrogenase (ADH)-catalyzed oxidation with concomitant reduction of acetone to 2-propanol.

The aim of this thesis was the investigation of the efficiency of immobilized nicotinamide adenine dinucleotide phosphate ($NADP^+$) dependent oxidoreductases with respect to a cascade reaction, associated with investigations concerning the regeneration of the reduced coenzyme. Thus, a modular enzyme cascade was constructed (Figure 37).

As a model system, a reaction sequence of the pentose phosphate pathway was interlinked to a cofactor recycling system. In the first reaction step of the multienzyme cascade, the immobilized glucose-6-phosphate dehydrogenase (G6PDH) oxidizes glucose-6-phosphate (G6P) to 6-phosphoglucono-δ-lactone (6PGL), which immediately hydrolyzes to 6-phoshogluconate (6PG). 6PG becomes converted by an immobilized 6-phosphate-dehydrogenase (6PGDH) to ribulose-5-phosphate (Ru5P) and $CO_2$. Both reaction steps are accompanied by the reduction of one equivalent $NADP^+$ to NADPH, respectively. Due to the adaption of an immobilized alcohol dehydrogenase (ADH), NADPH becomes re-oxidized to $NADP^+$ and thus, it can be re-employed into the cascade. The ADH-catalyzed oxidation of NADPH is accompanied by the reduction of acetone to 2-propanol.

The introduced oxidoreductases were immobilized onto differently organically modified MCFs. Besides extensively investigations regarding the immobilization conditions as well as long-term stabilities, a special focus was placed onto the Michaelis-Menten kinetics of the immobilized enzymes. With respect to the

requested enzyme cascade, it was mandatory to gain detailed information concerning the kinetics of the immobilized enzymes and in particular its maximum reaction rate ($v_{max}$), respectively. $v_{max}$ of an enzyme is highly dependent on the concentration of the substrate as well as coenzyme. A lack of substrate or coenzyme will decelerate $v_{max}$ of the respective enzyme. Special attention was paid to the ADH-catalyzed recycling of NADPH to $NADP^+$, as a complete regeneration of $NADP^+$ was required. This approach is very promising, since a high-grade coenzyme can be recycling by simply using the bulk chemical acetone as a substrate for the ADH.

# 4 RESULTS AND DISCUSSION

For the composition of the aimed modular enzyme cascade, involving G6PDH, 6PGDH as well as ADH, it was necessary to immobilize these oxidoreductases onto a suited host material (Figure 37). The benefits of carrier bound enzymes are obvious. On one hand, the immobilization of an enzyme ensures its reusability, as the immobilisate can simply be recovered by filtration or centrifugation. On the other hand, an immobilization is frequently accompanied by a certain stabilization of the enzyme. Within the last years, mesoporous silicas have established themselves as adequate host materials for the immobilization of larger enzymes. Especially MCF with its 3-dimensional porous structure consisting of spherical cells interconnected by smaller windows has been proven to be a promising host material. Furthermore, an organic modification of the surface of MCF is essential in order to initiate attractive interactions between the surface of the enzyme and the surface of the modified MCF during the immobilization process. Dependent on the respective surface functionalization of the MCF, the immobilization can be governed by different attractive interactions as well as covalent bonds. For instance, hydrophobic organic residues on the surface of MCF can initiate hydrophobic interactions with hydrophobic areas on the surface of the enzyme, whereas polar residues are able to provoke electrostatic interactions. However, within this discussion the pH value of the immobilization has always been taken into account.

The immobilization of 6PGDH was carried out onto aminoalkyl as well as alkyl modified MCFs with varying carbon chain lengths, whereas the immobilization of G6PDH and ADH was exclusively conducted by employing aminopropyl functionalized MCF (MCF-$C_3$-$NH_2$). Figure 38 displays schematically the surface modifications of the MCFs that were applied for the immobilization of the three enzymes and its respective abbreviations used in the following discussion.

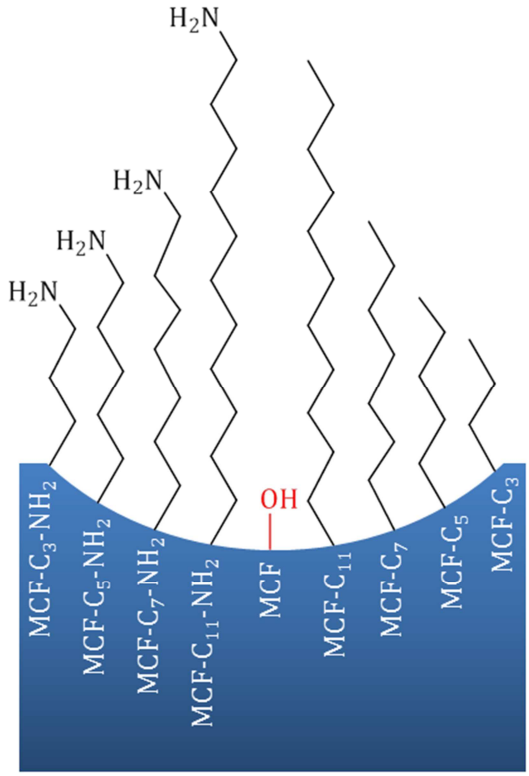


**Figure 38.** Schematic representation of the organic surface modifications of MCF that was employed for the immobilization of 6PGDH, G6PDH and ADH as well as the respective abbreviations used in the discussion.

Prior to the incorporation of the respective immobilisates into the enzyme cascade, the immobilizations of G6PDH, 6PGDH and ADH were studied in detail. Besides, the elaboration of the optimal immobilization conditions, investigations concerning the long-term stabilities and the Michaelis-Menten kinetics of the immobilized enzymes were necessary, respectively. Using the most promising immobilization conditions, the introduced modular enzyme cascade was constructed (Figure 37). The first two steps of the enzyme cascade are characterized by the reduction of two equivalents of the coenzyme $NADP^+$ to NADPH by the immobilized G6PDH as well as the immobilized 6PGDH. These two reaction steps are followed by an ADH-catalyzed re-oxidation of NADPH to $NADP^+$. It will turn out that by using an immobilized ADH, $NADP^+$ can be completely recovered. With respect to an effective recycling of NADPH to $NADP^+$, the immobilized ADH represents an advantageous recycling system, which can easily be implemented into modular enzyme cascades containing $NADP^+$/H dependent enzymes.

## 4.1 Characterization of the nanoporous enzyme hosts

### 4.1.1 Characterization of MCF

Prior to the immobilization of G6PDH, 6PGDH as well as ADH, it was fundamental to fully characterize the employed support materials. It was indispensable to guarantee pore sizes matching the enzyme sizes, thus allowing the respective enzyme to enter the porous system. With regard to a high enzymatic activity matched with ideal kinetics, the immobilized enzyme needs to be enabled to undergo conformational changes during catalysis. Moreover, the functionalization densities of the organic residues on the surface of the host materials had to be determined, as strong interactions between the enzyme and the surface of the organically modified MCFs within the immobilization procedure were required. With respect to the prevailing interactions, knowledge concerning the surface charge of the respective enzyme and the host at a certain pH of immobilization was essential. As the focus of an immobilized enzyme is placed on its long-term reusability, it was additionally mandatory to examine closely the stability of MCF when storing it in buffer solution.

#### Nitrogen physisorption

$N_2$ physisorption is the most significant characterization method for the investigation of the porosity of mesoporous materials. To that effect it allows an investigation of the porosity of the respective host materials. In terms of the pristine MCF with its spherical cells that are interconnected by smaller windows, typical type IV(a) isotherms exhibiting a H1 hysteresis were obtained (Figure 39). With respect to the 3D pore network of MCF that is frequently affected by pore blocking or network effects in general, a H2(a)/(b) hysteresis was expected. However, the appearance of a H1 hysteresis implies the presence of only minimal network effects.[164] Moreover, the hysteresis is shifted to high relative pressures, indicating a large pore size, whereas the narrow hysteresis can be referred to a narrow pore size distribution (PSD). According to the BET equation, the BET surface area ($S_{BET}$) of the non-functionalized MCF was calculated to amount to 453 $m^2\ g^{-1}$.[165] The total pore volume ($V_p$) of all MCF samples was calculated at a relative pressure of $p/p_0 = 0.99$ and it values 2.71 $cm^3\ g^{-1}$ for pure MCF (Table 3).[163]

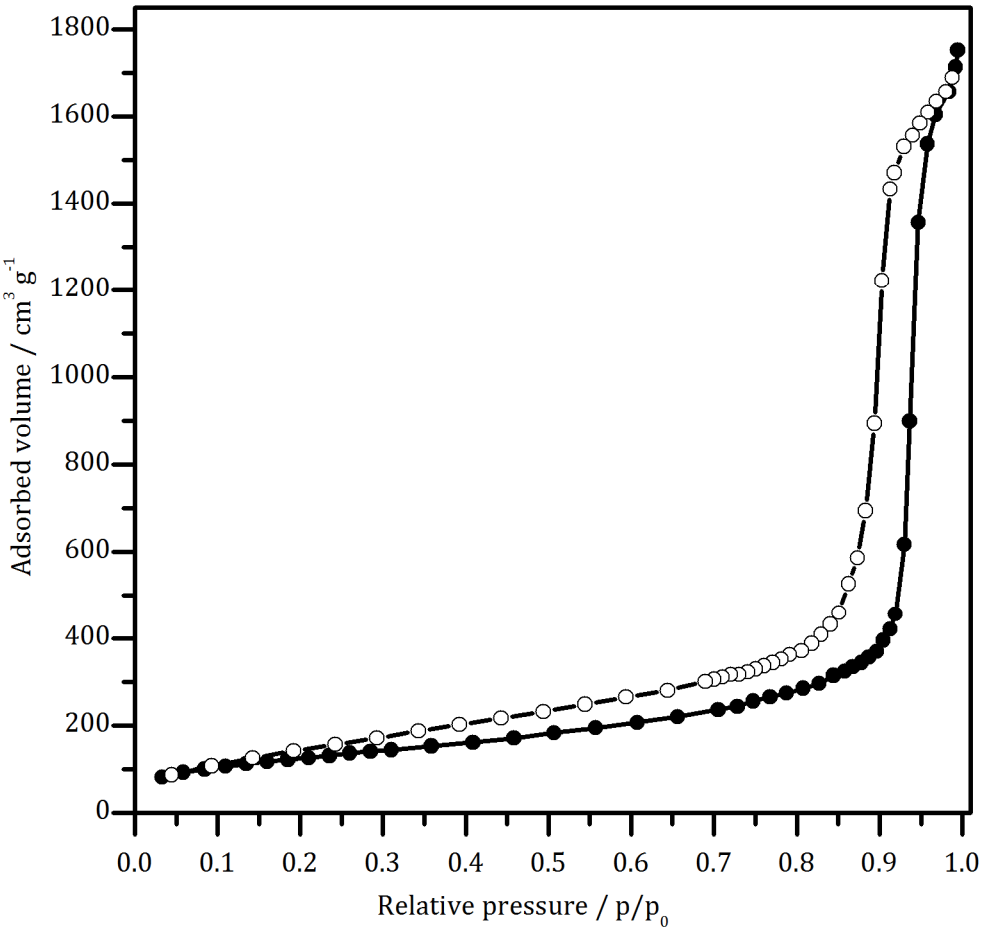


**Figure 39.** Type IV(a) $N_2$ physisorption isotherms (77 K) of pure MCF displaying a H1 hysteresis with adsorption branch (filled symbols) and desorption branch (empty symbols).

For comparison, the evaluation of the PSD of the pristine MCF was performed by utilizing the NLDFT as well as the traditional BJH method. BJH bases upon a modified form of the Kelvin equation and presumes cylindrical pore geometry. It is generally known to underestimate pore sizes < 10 nm by 20 – 30 % due to disregarding the thickness of pre-adsorbed adsorbate layers on the surface of the adsorbent. Moreover, the assumption of a cylindrical pore geometry results in further inaccuracies when employing BJH for the determination of the PSD of MCF, since MCF consists of spherical pores instead. Furthermore, this classical method does not consider the critical point shift, the freezing point as well as the triple point shift of the pore fluid in its calculation. In contrast, NLDFT rests upon statistical mechanics and circumvents the disadvantages of the traditional methods. Thus, NLDFT enables the prediction of the relative pressure, at which capillary condensation occurs as well as the evaporation transition of $N_2$ in spherical or cylindrical pores. Merely an appropriate kernel has to be chosen according to the respective material and its expected pore geometry.[161, 162]

Under consideration of the above mentioned limitations, BJH was exemplarily used to evaluate the PSD of the spherical cells as well as of the interconnecting windows of MCF by employing the adsorption or desorption branch for computation, respectively. Independent on the branch used for calculation; on the basis of NLDFT solely the PSD of the cells can be obtained. Figure 40 compares the PSDs of the pristine MCF obtained according to the NLDFT as well as to the BJH method.

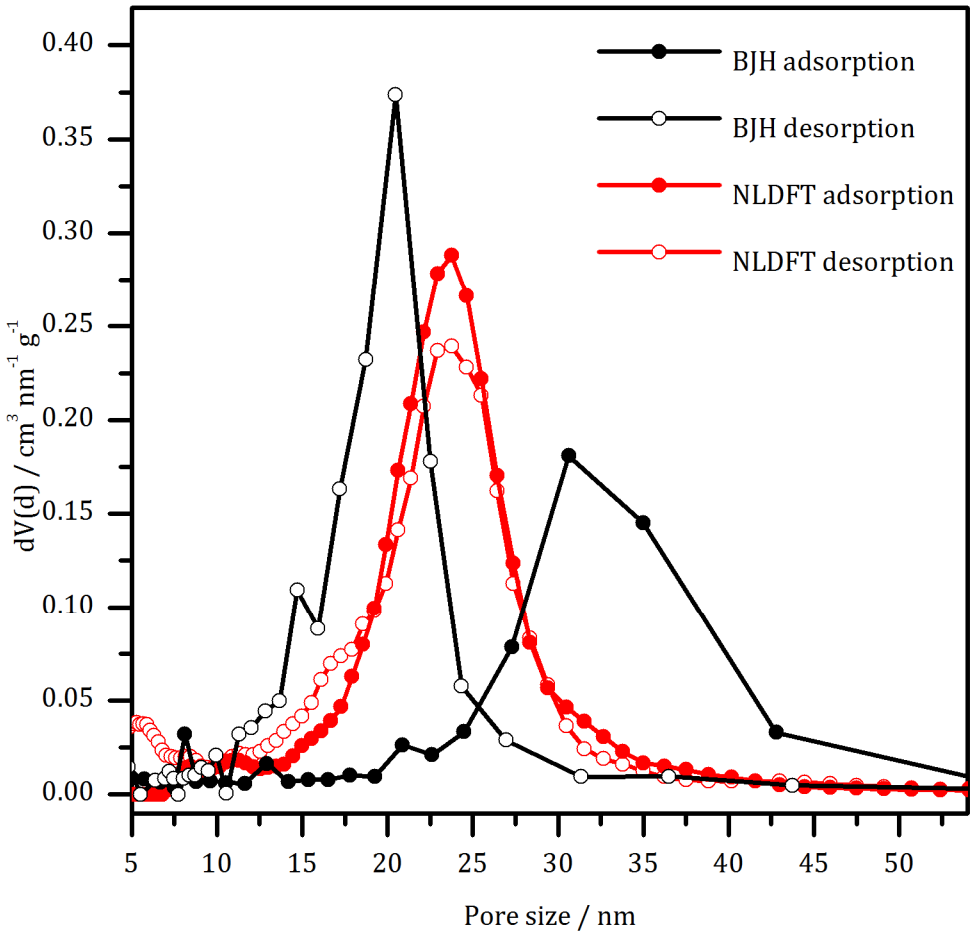


**Figure 40.** Comparison of the pore size distributions based on the calculations according to NLDFT (red)(kernels: silica cylindrical pores, adsorption / silica cylindrical pores, equilibrium model) as well as BJH (black).

The evaluation of the PSD according to BJH resulted in an average cell size of 33 nm by using the adsorption branch for calculation. Measured by means of the desorption branch, the size of the interconnecting windows amounted to 20 nm. Hence, according to BJH the width of the windows as well as the spherical cells was sufficient to let the three enzymes enter the porous structure of MCF or rather host them (maximum enzyme diameters: 8.5 – 12.3 nm). However, the above mentioned

inadequacies of BJH need to be considered, especially against the background of the presumed cylindrical pore geometry instead of a spherical geometry.

Referring to NLDFT, a main pore diameter of 24 nm was obtained. Thus, by using NLDFT the cells were likewise identified to be large enough to host the enzymes. As the determined pore size is independent on the branch that was used for the evaluation of the pore size, pore blocking figured out to be absent. Additionally, this result confirms that the interconnecting windows of MCF do not possess a specific surface area and thus their diameter cannot be determined by means of $N_2$ physisorption. In conclusion, it can be stated that, contrary to expectations, by employing BJH an overestimation of the pore size arose, whereby an underestimation was expected. However, these findings are in accordance with the literature.[182] With respect to the above mentioned drawbacks and the presented results, an accurate investigation of the PSD of MCF by applying the BJH method is questionable or rather defective. Thence, in the further course, merely the NLDFT method was used to determine the width of the cells. Thereby, it is crucial to mention that all pore sizes were determined from the mean of the full width at half maximum (FWHM) of the PSD, respectively.

In comparison to pristine MCF, grafting resulted in a decrease of $S_{BET}$ as well as $V_p$ of all organically modified samples. This can be assigned to a mass increase due to the functionalization as well as to a decrease of $D_p$, as the organic residues protrude from the pore walls into the pores (Table 3). Correspondingly, the pore condensation step in the $N_2$ physisorption isotherms is shifted to lower relative pressures in comparison to pure MCF (Figure 41).

[182] D. Gaffney, *Tailored Adsorption of Enzymes onto Mesoporous Silicates*, Dissertation, University of Limerick, **2010**.

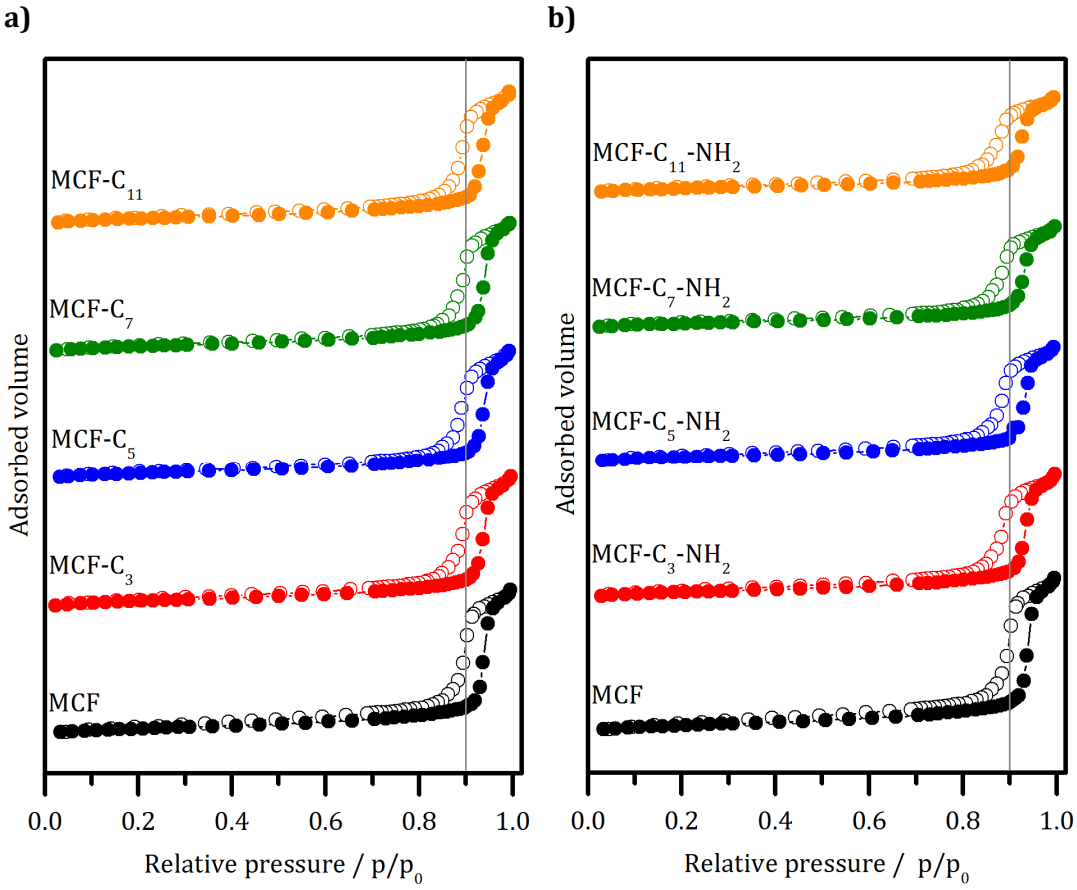


**Figure 41.** Type IV(a) $N_2$ physisorption isotherms (77 K) of **a)** alkyl (MCF-$C_x$) as well as **b)** aminoalkyl (MCF-$C_x$-$NH_2$) modified MCFs in comparison to pristine MCF with adsorption branch (filled symbols) and desorption branch (empty symbols). The grey line at $p/p_0$ = 0.9 acts as guide to the eyes.

Post-synthetic modification of MCF using alkyltrialkoxysilanes led to a slight decrease of $S_{BET}$ and $V_p$, providing a first hint towards a low functionalization density of this material. This was later on additionally proven by TG-DTA-MS. Furthermore, $D_p$ decreased merely slightly in comparison to the pristine MCF, too. The smallest $D_p$, considering the alkyl modified MCFs, was obtained for MCF-$C_{11}$ (22 nm), which was attributed to the expansion of the long undecyl chain inside the pores. Whereas the decrease of $D_p$ from the unmodified MCF to MCF-$C_3$/$C_5$/$C_7$ was less pronounced due to the shorter carbon chains (Figure 42a, Table 3).

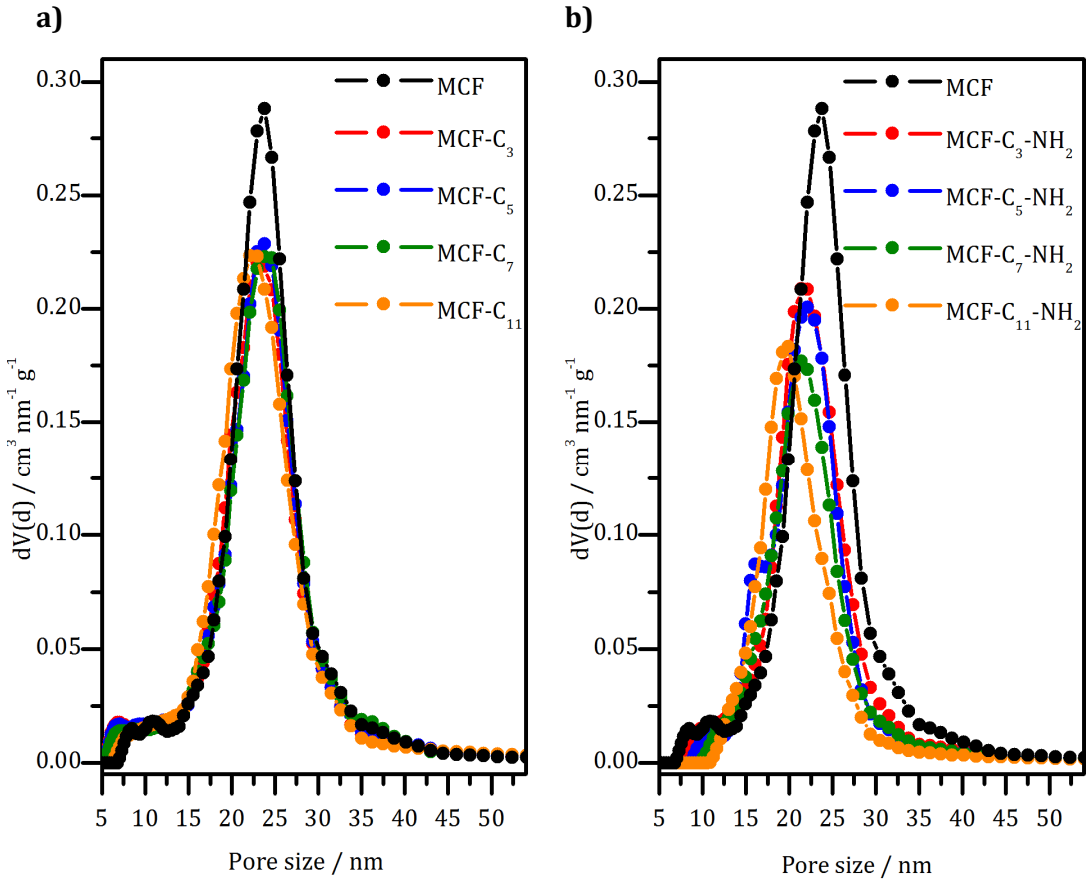


**Figure 42.** Pore size distributions of **a)** the alkyl modified MCFs (MCF-$C_x$) and **b)** the aminoalkyl modified MCFs (MCF-$C_x$-$NH_2$) in comparison to the pristine MCF (kernel: silica cylindrical pores, adsorption). The pore sizes were determined from the mean of the full width at half maximum (FWHM), respectively.

Conversely, a clear distinction of the porosity of the aminoalkyl functionalized MCFs was gained (Figure 42b, Table 3). In this case, $S_{BET}$ decreased with increasing chain length of the functionalization reagent. Thus, $S_{BET}$ of MCF-$C_{11}$-$NH_2$ (265 $m^2\ g^{-1}$) was lowest and reduced by 42 % compared to pure MCF (453 $m^2\ g^{-1}$). Evidently, this suggests a higher functionalization density of aminoalkyl residues compared to alkyl residues, which was confirmed later on by thermal analysis. Accordingly, $V_p$ was reduced in the same order. This can be explained by an increasing expansion of the aminoalkyl residues within the pores, attributed to an increasing carbon chain length. $D_p$ of MCF-$C_{11}$-$NH_2$ (20 nm) decreased around 4 nm in comparison to the non-functionalized MCF (24 nm). Regarding the length of the respective carbon chains, the decrease of $D_p$ of MCF-$C_3$/$C_5$/$C_7$-$NH_2$ was less distinct.

**Table 3.** Overview of the material properties of the pristine MCF in comparison to the alkyl (MCF-$C_x$) as well as aminoalkyl (MCF-$C_x$-$NH_2$) modified MCFs.

| sample | $S_{BET}$ [$m^2 g^{-1}$] | $V_P$ [$cm^3 g^{-1}$] | $D_p$ [nm] | $\rho_f$ [mmol $g^{-1}$] | pI |
|---|---|---|---|---|---|
| **MCF** | 453 | 2.71 | 24 | --- | 3.7 |
| **MCF-$C_3$** | 447 | 2.46 | 23 | 0.84 | 3.4 |
| **MCF-$C_5$** | 447 | 2.43 | 24 | 0.57 | 3.6 |
| **MCF-$C_7$** | 444 | 2.44 | 24 | 0.46 | 3.6 |
| **MCF-$C_{11}$** | 447 | 2.49 | 22 | 0.27 | 3.7 |
| **MCF-$C_3$-$NH_2$** | 356 | 2.16 | 22 | 1.16 | 8.6 |
| **MCF-$C_5$-$NH_2$** | 353 | 2.03 | 22 | 1.33 | 9.6 |
| **MCF-$C_7$-$NH_2$** | 285 | 1.78 | 22 | 1.64 | 10.1 |
| **MCF-$C_{11}$-$NH_2$** | 265 | 1.67 | 20 | 1.48 | 9.9 |

Modification of MCF utilizing alkyl as well as aminoalkyl residues resulted in a decrease of $S_{BET}$, $V_p$ and $D_p$. However, the pores of the obtained support materials were still large enough to host 6PGDH, G6PDH as well as ADH, as the proteins possess maximal diameters of 8.5 - 12.3 nm.

**IR spectroscopy**

For a qualitative investigation of MCF-$C_x$ as well as MCF-$C_x$-$NH_2$, IR spectroscopy was applied. The IR spectrum of MCF possesses the typical bands expected for mesoporous silicas (Figure 43). Correspondingly, broad OH stretching vibrations (ν) at 3434 $cm^{-1}$, weaker H-O-H (1637 $cm^{-1}$) as well as strong Si-O-Si deformation vibrations (δ) (1084$cm^{-1}$) were detected. The IR spectra of the alkyl functionalized MCFs in comparison to the non-modified MCF are shown in Figure 43. The spectra of MCF-$C_x$ were standardized to the Si-O-Si deformation vibration of the non-modified MCF (1084 $cm^{-1}$).

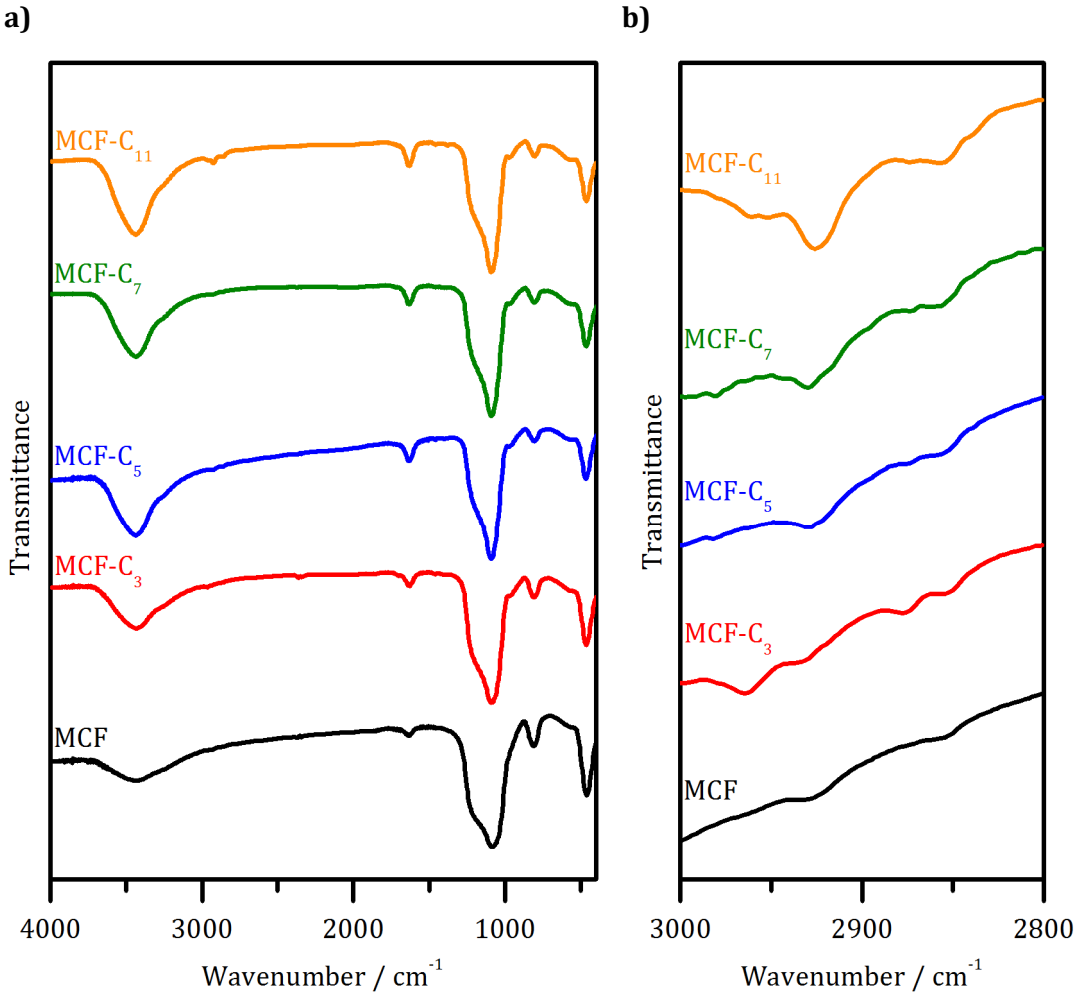


**Figure 43. a)** IR spectra of MCF-$C_x$ in comparison to the non-modified MCF (KBr pellet). **b)** Enlarged depiction of the wavenumber range from 3000 to 2800 $cm^{-1}$ exhibiting stretching vibrations of $CH_2$.

Besides the typical silica bands, the comparison of the IR spectra of MCF-$C_x$ among each other illustrate an increasing intensity of $\nu(CH_2)$ with increasing length of the carbon chain in the wavenumber range between 3000 and 2800 $cm^{-1}$. Hence, the intensity of $\nu(CH_2)$ is at highest for MCF-$C_{11}$ and at lowest for MCF-$C_3$ . Merely in the case of MCF-$C_3$ $\nu(CH_3)$ were detected (2964 $cm^{-1}$, 2873 $cm^{-1}$). This can be attributed to the largest proportion of the $CH_3$ group related to the $CH_2$ groups of the respective alkyl chain. With increasing carbon chain length, the proportion of $CH_3$ related to the $CH_2$ groups minimizes and $\nu(CH_3)$ decreases, whereas $\nu(CH_2)$ increases. Table 4 summarizes all $\nu(CH_2/CH_3)$ of the alkyl modified MCFs.

**Table 4.** Overview of the detected $\nu(CH_2)$ and $\nu(CH_3)$ of MCF-$C_x$.

| sample | wavenumber [$cm^{-1}$] | band |
|---|---|---|
| **MCF-$C_3$** | 2964 | $\nu(CH_3)$ |
| | 2929 | $\nu(CH_2)$ |
| | 2873 | $\nu(CH_3)$ |
| | 2858 | $\nu(CH_2)$ |
| **MCF-$C_5$** | 2929 | $\nu(CH_2)$ |
| | 2854 | $\nu(CH_2)$ |
| **MCF-$C_7$** | 2929 | $\nu(CH_2)$ |
| | 2856 | $\nu(CH_2)$ |
| **MCF-$C_{11}$** | 2926 | $\nu(CH_2)$ |
| | 2858 | $\nu(CH_2)$ |

The IR spectra of the aminoalkyl modified MCFs in comparison to the non-modified MCF are shown in Figure 44. The spectra of MCF-$C_x$-$NH_2$ were standardized to the Si-O-Si deformation vibration of the unfunctionalized MCF (1084 $cm^{-1}$).

The IR spectra of MCF-$C_x$-$NH_2$ exhibit a clear dependency of the carbon chain length on the intensity of $\nu(CH_2)$. Thus, the intensity of $\nu(CH_2)$ increases from MCF-$C_3$-$NH_2$ to MCF-$C_{11}$-$NH_2$ in the wavenumber range between 3000 and 2800 $cm^{-1}$ (Figure 44, Table 5). Moreover, the IR spectra of MCF-$C_5$-$NH_2$, MCF-$C_7$-$NH_2$ as well as MCF-$C_{11}$-$NH_2$ represent an unambiguously emerging formation of two bands caused by $CH_2$ stretching vibrations in this area (Figure 44b). However, bands induced by $NH_2$ or NH vibrations are covered by typical bands expected for silica materials (1650 – 1560 $cm^{-1}$ $\delta(-NH_2)$, 3500 – 3300 $cm^{-1}$ $\nu(-NH)$ ).[183]

[183] M. Hesse, H. Meier, B. Zeeh, Spektroskopische Methoden in der organischen Chemie, 5., überarbeitete Auflage, Stuttgart, New York, **1995**.

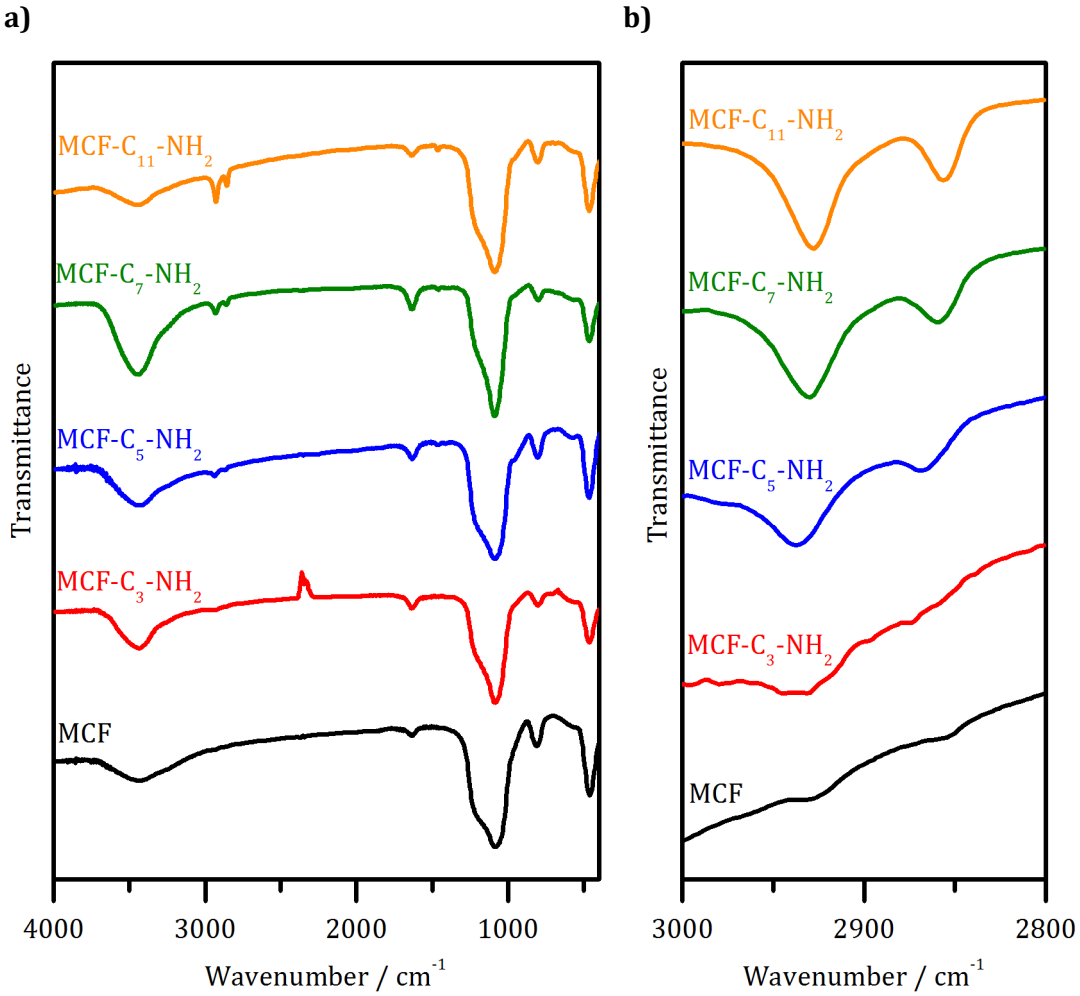


**Figure 44. a)** IR spectra of MCF-$C_x$–$NH_2$ in comparison to the unmodified MCF (KBr pellet). **b)** Enlarged depiction of the wavenumber range from 3000 to 2800 $cm^{-1}$ exhibiting stretching vibrations of $CH_2$.

Table 5 summarizes $\nu(CH_2)$ and $\delta(CH_2)$ detected for MCF-$C_x$-$NH_2$

**Table 5.** Overview of the detected $\nu(CH_2)$ and $\delta(CH_2)$ of MCF-$C_x$-$NH_2$.

| sample | wavenumber [$cm^{-1}$] | band |
|---|---|---|
| **MCF-$C_3$-$NH_2$** | 2933 | $\nu(CH_2)$ |
| **MCF-$C_5$-$NH_2$** | 2937 | $\nu(CH_2)$ |
| | 2868 | $\nu(CH_2)$ |
| | 1462 | $\delta(CH_2)$ |
| **MCF-$C_7$-$NH_2$** | 2929 | $\nu(CH_2)$ |
| | 2858 | $\nu(CH_2)$ |
| | 1460 | $\delta(CH_2)$ |
| **MCF-$C_{11}$-$NH_2$** | 2927 | $\nu(CH_2)$ |
| | 2856 | $\nu(CH_2)$ |
| | 1465 | $\delta(CH_2)$ |

As IR spectroscopy is rather a qualitative method, it does not allow a quantitative investigation of the functionalization density of MCF-$C_x$ and MCF-$C_x$-$NH_2$. Thus, thermal analyzes was consulted.

**Thermal analyses**

Thermal analyses of the modified MCFs (TG-DTA-MS) were performed in order to evaluate the respective functionalization densities ($\rho_f$) of MCF-$C_x$ as well as MCF-$C_x$-$NH_2$. Figure 43 comparatively represents the TG-DTA-MS results of MCF-$C_3$ and MCF-$C_3$-$NH_2$. The results of both measurements were summarized in Table 6. The TG-DTA-MS depictions of the further alkyl and aminoalkyl modified MCFs resemble each other in appearance and can be found in the appendix (Appendix 7.2).

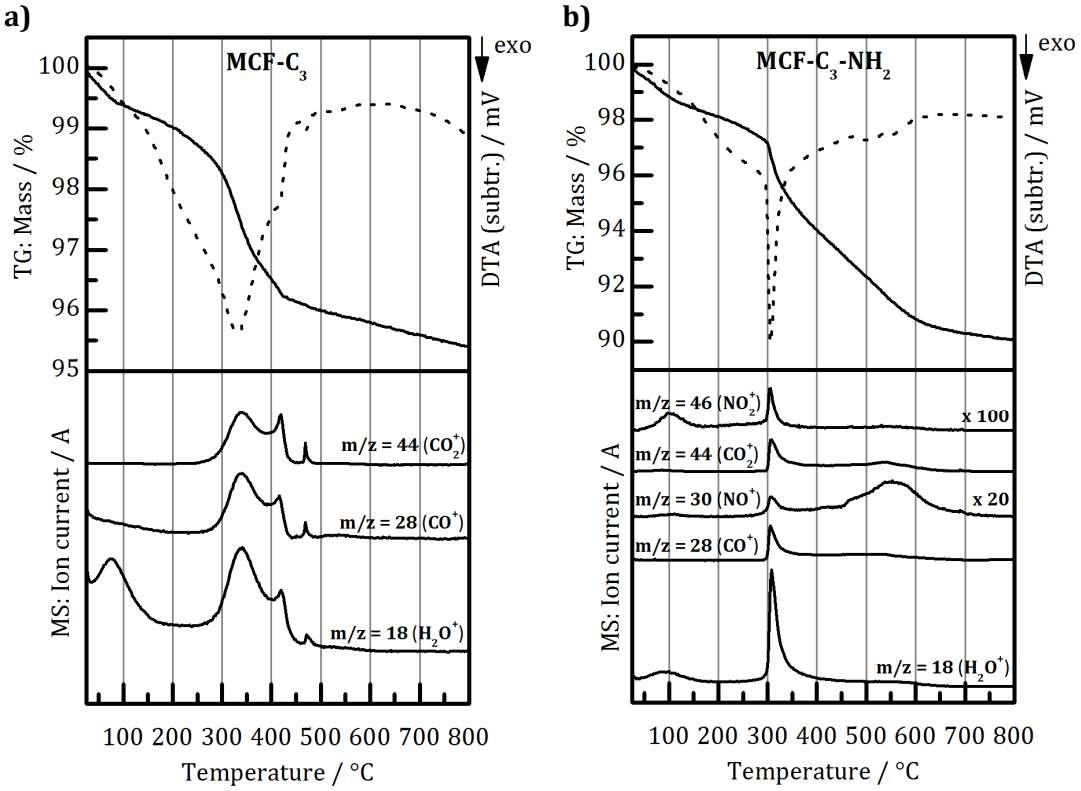


**Figure 45.** TG-DTA-MS of **a)** MCF-$C_3$ and **b)** MCF-$C_3$-$NH_2$ in an $Ar/O_2$ atmosphere (8:2). The diagram at the top shows the TG (solid line) and DTA (dashed line) curve, whereas the ion currents detected by a mass spectrometer are depicted at the bottom.

The TG curve of MCF-$C_3$ as well as MCF-$C_3$-$NH_2$ displays three steps of the combustion in the range from rt to 800 °C. The first step (rt – 200 °C) is characterized by the release of loosely attached water molecules from the surface of MCF-$C_3$ and MCF-$C_3$-$NH_2$. Due to the porous network of MCF, the release of water (m/z = 18) is hindered and delayed. Thus, it was detected up to 200 °C. The mass

loss addressed to the evaporation of water molecules amounts to 1.0 % for MCF-$C_3$ and 1.9 % in the case of MCF-$C_3$-$NH_2$ (Table 6). This observation can be referenced to a higher hydrophilicity of the surface of MCF-$C_3$-$NH_2$ compared to MCF-$C_3$. The second step of the combustion can be attributed to the decomposition of the alkyl as well as aminoalkyl residues on the surface of the respective MCF. The degradation of the propyl residues on the surface of MCF-$C_3$ was detected due to the molecule ions of CO (m/z = 28) and $CO_2$ (m/z = 44). In contrast, the combustion of the aminopropyl chains on the surface of MCF-$C_3$-$NH_2$ was detected by means of the molecule ions of CO (m/z = 28), $CO_2$ (m/z = 44), NO (m/z = 30) as well as $NO_2$ (m/z = 46). The thermal decomposition of the propyl functionalization of MCF-$C_3$ was completed at 550 °C (mass loss: 3.1 %), whereas the decomposition of the organic residues of MCF-$C_3$-$NH_2$ was detected up to 750 °C (mass loss: 7.9 %). Post-condensation of the silica network resulted in a minor mass loss in the third step of the respective thermogram (mass loss: 0.1 – 0.5 %).

On the basis of the respective mass loss caused by the combustion of the alkyl or aminoalkyl residues on the surface of MCF-$C_x$ and MCF-$C_x$-$NH_2$, $\rho_f$ was calculated (Table 3). The principle of the calculations can be found in the appendix (Appendix 7.2.1).

**Table 6.** Comparison of the results of TG-DTA-MS measurements of MCF-$C_3$ and MCF-$C_3$-$NH_2$.

| sample | step | ΔT [°C] | mass loss [%] | classification |
|---|---|---|---|---|
| **MCF-$C_3$** | 1 | rt - 200 | 1.0 | adsorbed water |
| | 2 | 200 - 550 | 3.1 | decomposition -$C_3$ chain |
| | 3 | 550 - 800 | 0.5 | post-condensation silica |
| **MCF-$C_3$-$NH_2$** | 1 | rt - 200 | 1.9 | adsorbed water |
| | 2 | 200 - 750 | 7.9 | decomposition -$C_3$-$NH_2$ chain |
| | 3 | 750 - 800 | 0.1 | post-condensation silica |

The thermal analytical measurements reveal a significant impact of the carbon chain length on $\rho_f$ (Table 3). $\rho_f$ of the alkyl modified MCFs decreases consistently from MCF-$C_3$ (0.84 mmol $g^{-1}$) to MCF-$C_{11}$ (0.27 mmol $g^{-1}$). It was recently proven that an increasing carbon chain length leads to an increase of the

hydrophobicity of the respective functionalized materials.[184] A view on the functionalization densities of the aminoalkyl functionalized materials displays an increase of $\rho_f$ from MCF-$C_3$-$NH_2$ (1.16 mmol $g^{-1}$) to MCF-$C_7$-$NH_2$ (1.64 mmol $g^{-1}$), whereas the value obtained for MCF-$C_{11}$-$NH_2$ (1.48 mmol $g^{-1}$) is slightly reduced. As already implied by nitrogen physisorption measurements, thermal analysis confirmed that $\rho_f$ of the aminoalkyl modified MCFs is higher than $\rho_f$ of the alkyl functionalized MCFs. This observation can be assigned to hydrogen bridges formed during the grafting process between the amine groups of the organosilanes and the silanol groups on the surface of the MCF (Figure 46). The first intermediate reaction step of the post-synthetic functionalization with aminoalkyltrialkoxysilanes is the formation of a hydrogen bond between the amino nitrogen atom of the silane and a hydrogen atom of a surface silanol group. In this case, the silanol oxygen atom becomes partial negatively charged and is able to attack the silicon atom of the aminoalkyl substituted silane nucleophilically.[185]

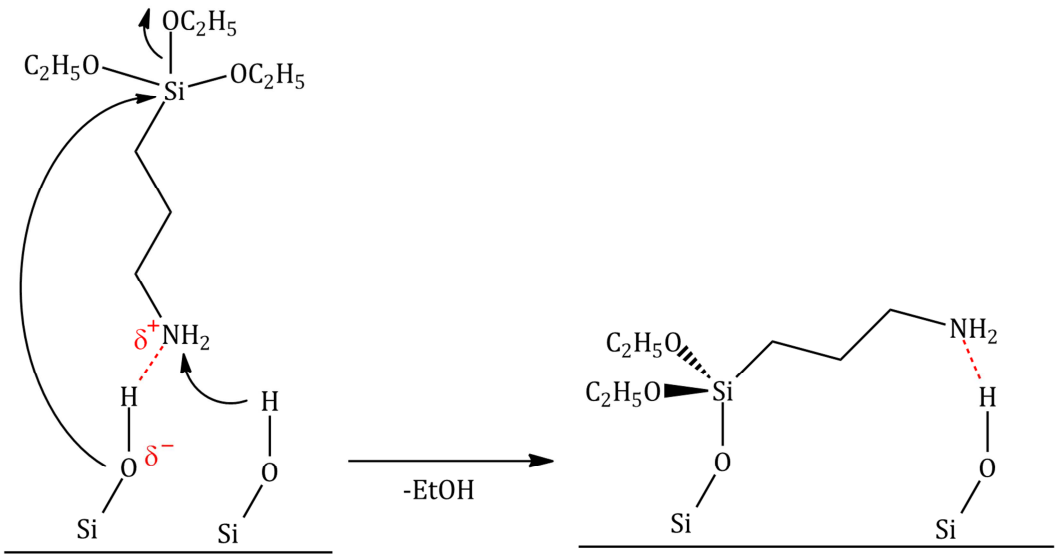


**Figure 46.** The surface modification of mesoporous silicas employing aminoalkyltrialkoxysilanes is strongly influenced by the formation of initial hydrogen bridges between the amino group of the amino silane and hydrogen atoms of the silanol groups on the surface of the mesoporous silica. These attractive interactions result in a high functionalization density of the mesoporous silica. Reprinted with permission from [185]. Copyright 2002 American Chemical Society.

The absence of an amino function in alkyltriethoxysilanes accompanied by a higher hydrophobicity reduces these initial interactions. Thus, modification with alkyltrialkoxysilanes resulted in lower functional densities in comparison to the aminoalkyl functionalization. The hydrophobicity of the surface of the alkyl modified

[184] D.I. Fried, D. Bednarski, M. Dreifke, F.J. Brieler, M. Thommes, M. Fröba, *J. Mater. Chem. B* **2015**, *3*, 2341-2349.
[185] S.M. Kanan, W.T.Y. Tze, C.P. Tripp, *Langmuir* **2002**, *18*, 6623-6627.

MCFs rises with increasing carbon chain length.[73, 184] Also, the hydrophobicity is dependent on $\rho_f$: The higher $\rho_f$, the higher the hydrophobicity.

Thermal analysis confirmed higher $\rho_f$ values for the aminoalkyl modified MCFs compared to the alkyl functionalized hosts. However, the post-synthetic modification was successful in both cases. Thus, each support material possessed functionalities to interact with the surface of enzymes by hydrophobic as well as electrostatic interactions.

**Zeta potential titrations**

To evaluate possible electrostatic interactions between the surface of the respective enzyme and the surface of the host material at the pH of the immobilization, zeta potential titrations were performed and the isoelectric point (pI) of each material was determined (Table 3). As expected, due to countless silanol groups on the surface of the pristine MCF its pI is in the acidic range at pH 3.7. Figure 45 exemplarily displays the zeta potential curves of MCF, MCF-$C_3$ as well as MCF-$C_3$-$NH_2$. The titration curves of the further materials can be found in the appendix (Appendix 7.3).

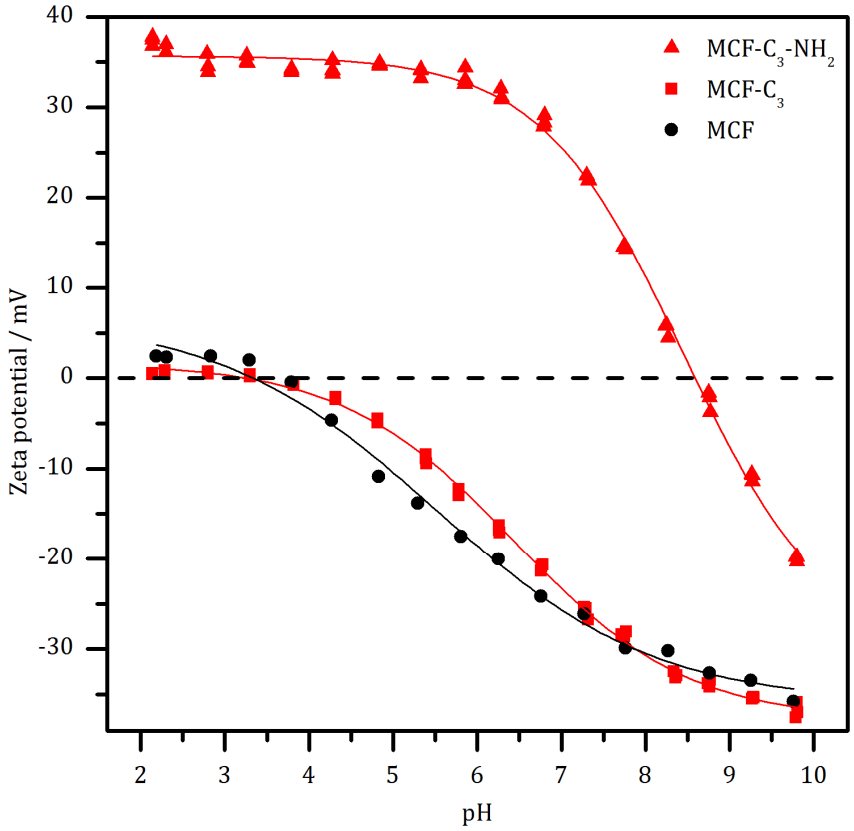


**Figure 47.** Exemplary depiction the zeta potential titration curves of MCF, MCF-$C_3$ as well as MCF-$C_3$-$NH_2$.

As thermal analysis confirmed, the surfaces of the modified support materials were not fully covered with organic residues. Thus, residual silanol groups have an influence on the zeta potential titrations. Discussing the zeta potential titrations of the alkyl modified MCFs, it has to be considered that only remaining silanol groups on the surface of the alkyl modified MCFs can be protonated or deprotonated by means of HCl and NaOH, respectively. In the case of a completely functionalized silica surface and accordingly in the absence of silanol groups, no pI should be detectable, as a protonation or deprotonation of the alkyl residues is not possible. Generally, the pI values of the alkyl modified MCFs are in the acidic range, thus the surface of these hosts is negatively charged at the pH values of the immobilizations (pH 6.5 – 7.5). Regarding the aminoalkyl modified materials; a higher $\rho_f$ indicates a higher density of amino groups on the surface. Hence, a larger amount of base is necessary to deprotonate the amino groups and the pI increases with increasing $\rho_f$. MCF-$C_7$-$NH_2$, exhibiting the highest $\rho_f$ value, reveals a pI of 10.1 and correspondingly MCF-$C_3$-$NH_2$, having the lowest $\rho_f$ of the aminoalkyl modified MCFs, possesses a pI at pH 8.6. Due to the amino functions, the pI of all aminoalkyl modified materials is in the alkaline range. Accordingly, the surface of these materials is positively charged at the pH values of the immobilizations (pH 6.5 – 7.5).

Zeta potential titrations of the alkyl as well as of the aminoalkyl modified MCFs clarified a correlation between $\rho_f$ of the respective host material and the pI. As the surfaces of the alkyl functionalized materials are negatively charged and the surfaces of the aminoalkyl modified MCFs are positively charged at the pH values of immobilization (pH 6.5 – 7.5), electrostatic interactions between the surface of the host materials and oppositely charged areas of the respective enzyme surface were possible.

**Structure stability of MCF-$C_3$-$NH_2$**

One major criterion of a potential host material for enzymes is its storage stability in the buffer solution of the immobilization over a couple of days. Thus, it was important to elaborate the resistance of the porous structure of MCF as well as its organic surface functionalization against the buffer deployed for storage. This was exemplarily investigated for MCF-$C_3$-$NH_2$ that was stored in potassium phosphate buffer solution (50 mM, pH 6.5) over a period of seven days.

In accordance to a common immobilization procedure, MCF-$C_3$-$NH_2$ was dispersed in an enzyme-free potassium phosphate buffer solution (50 mM, pH 6.5) and shaken for 24 h at 25 °C and 350 rpm. Subsequently, the host was washed four

times with potassium phosphate buffer solution and stored in the buffer solution for seven days at 4 °C. After this period, the MCF-$C_3$-$NH_2$ was separated by centrifugation and washed four times by using ultrapure water in order to remove any residual buffer salts. $N_2$ physisorption as well as thermal analysis was applied to the untreated MCF-$C_3$-$NH_2$ prior to the experiment (day -1) and to the MCF-$C_3$-$NH_2$ after seven days of storage in the buffer solution (day 7). The $N_2$ isotherms are depicted in Figure 48.

With respect to the host that was stored in the buffer solution, a distinct decrease of the volume of adsorbed nitrogen was detected. At a first glance, this can be referred to an incomplete removal of buffer salts within the purification step after seven days of storage. Additionally, this assumption is underpinned by a decrease of $V_p$, whereas $S_{BET}$ remained nearly constant (Table 7).

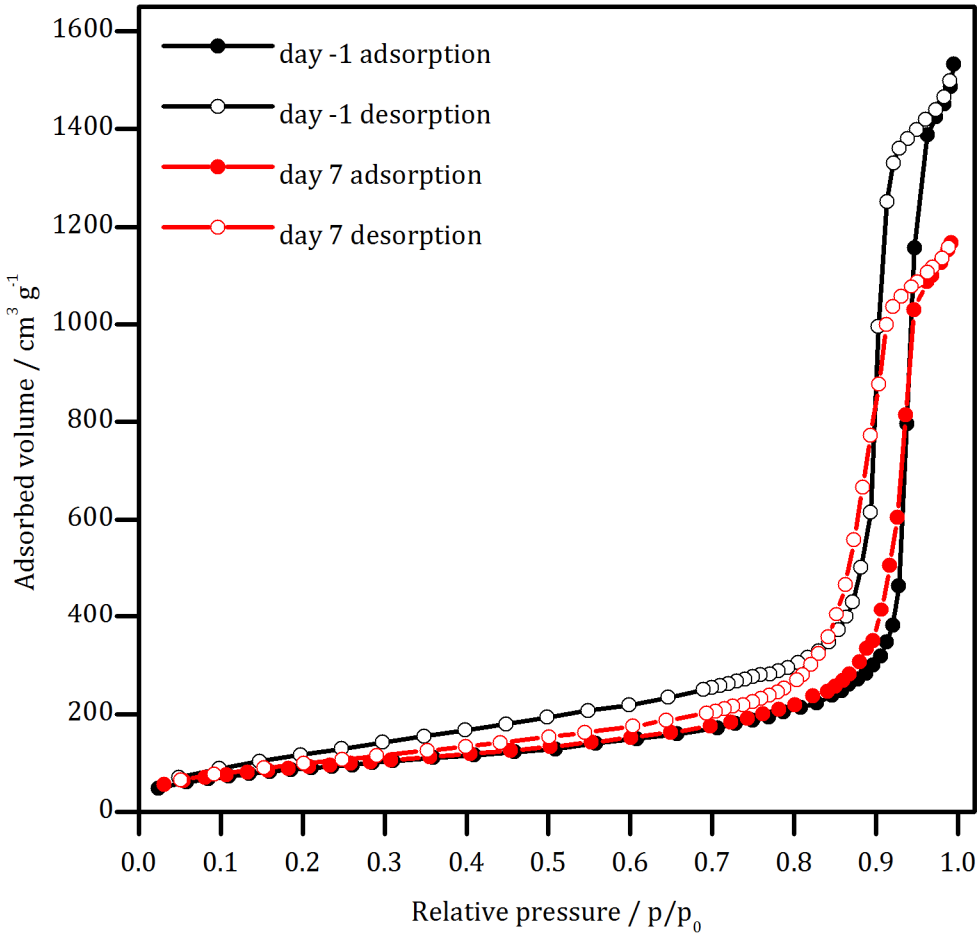


**Figure 48.** Type IV(a) $N_2$ physisorption isotherms (77 K) of MCF-$C_3$-$NH_2$ displaying a H1 hysteresis with adsorption branch (filled symbols) and desorption branch (empty symbols). Black isotherms (day -1): MCF-$C_3$-$NH_2$ prior to storage in potassium phosphate buffer solution (50 mM, pH 6.5). Red isotherms (day 7): MCF-$C_3$-$NH_2$ after storage in potassium phosphate buffer solution (50 mM, pH 6.5) over period of seven days

Likewise the PSD of the MCF-$C_3$-$NH_2$ that was stored in buffer solution has been broadened and is shifted to lower pore sizes in comparison to the PSD of the untreated MCF-$C_3$-$NH_2$ (Figure 49). This was addressed to a partial occupation of the pores due to residual buffer ions. Once again, the pore sizes were detected on the respective full width at half maximum. A value of 24 nm was found for the untreated MCF-$C_3$-$NH_2$ and a value of 21 nm after seven days of storage in buffer solution. Hence, storage in buffer solution resulted in a decrease of the pore size. Finally, this can be traced back to residual buffer ions within the porous structure. Correspondingly, $V_p$ decreased from 2.4 $cm^3g^{-1}$ for the untreated host to 1.8 $cm^3g^{-1}$ for the material stored in buffer solution.

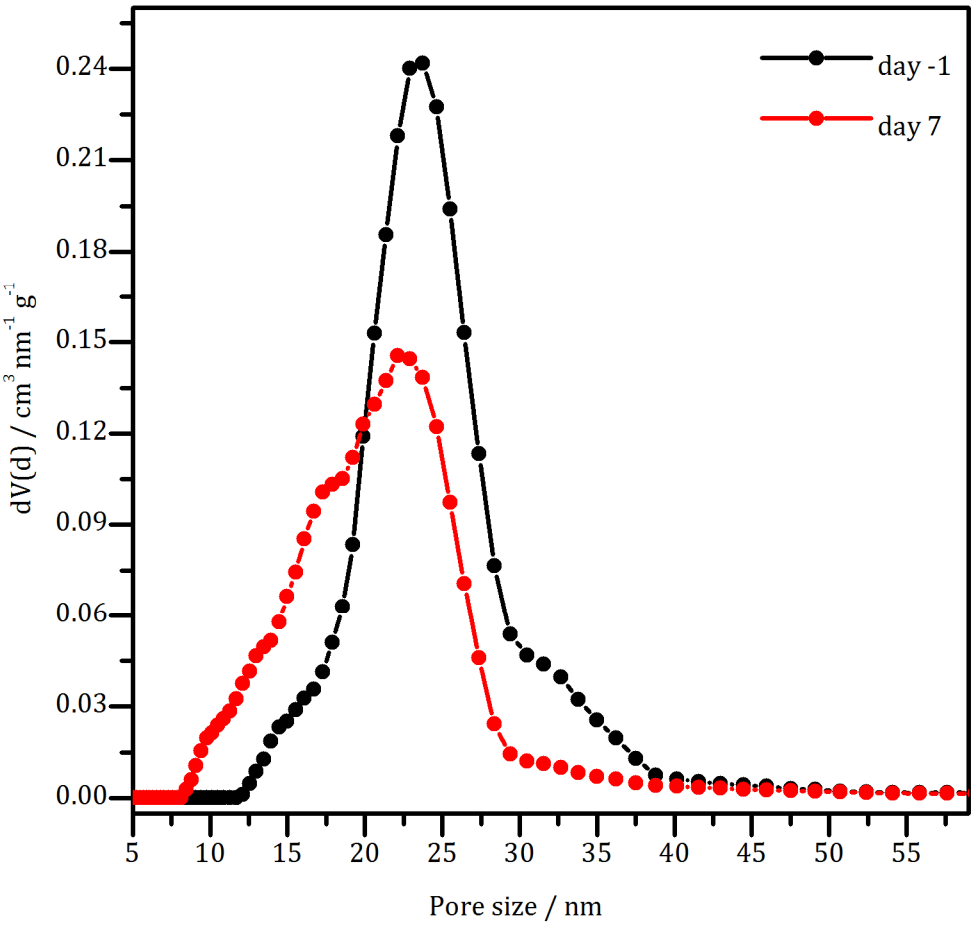


**Figure 49.** Black (day-1): Pore size distribution of the untreated MCF-$C_3$-$NH_2$; Red (day 7): Pore size distribution of MCF-$C_3$-$NH_2$ stored in potassium phosphate buffer solution (50 mM, pH 6.5) over a period of 7 days (kernel: silica cylindrical pores, adsorption). The pore sizes were determined from the mean of the full width at half maximum (FWHM), respectively.

Thermal analysis was applied to both samples in order to gain information concerning possible changes of $\rho_f$ due to the storage in buffer solution. The

untreated material possessed a $\rho_f$ value of 1.2 mmol $g^{-1}$ (Table 7). After seven days of storage in buffer solution a $\rho_f$ of 1.1 mmol $g^{-1}$ was calculated by means of thermal analysis. In fact, $\rho_f$ was slightly decreased by 0.1 mmol $g^{-1}$. However, this reduction is in the range of possible measurement errors. Thus, the $\rho_f$ values were considered to be equal and the storage in buffer solution has not negatively affected the aminopropyl residues on the surface of MCF-$C_3$-$NH_2$.

**Table 7.** Comparison of the material properties of untreated MCF-$C_3$-$NH_2$ in comparison to MCF-$C_3$-$NH_2$ stored in potassium phosphate buffer solution (50 mM, pH 6.5) over a period of seven days.

| MCF-$C_3$-$NH_2$ | $S_{BET}$ [$m^2 g^{-1}$] | $V_P$ [$cm^3 g^{-1}$] | $D_p$ [nm] | $\rho_f$ [mmol $g^{-1}$] |
|---|---|---|---|---|
| **day -1** | 330 | 2.4 | 24 | 1.2 |
| **day 7** | 333 | 1.8 | 21 | 1.1 |

Storage of MCF-$C_3$-$NH_2$ in potassium phosphate buffer solution (50 mM, pH 6.5) over a seven day period resulted in a decrease of $D_p$ as well as $V_p$. These findings were referenced to an uncomplete removal of the buffer salts prior to the $N_2$ physisorption measurement. Furthermore, $\rho_f$ of the aminopropyl residues on the surface of the host was calculated to be equal before and after storage in buffer solution. As the pore network of MCF-$C_3$-$NH_2$ has not been negatively affected by the storage in buffer solution, organically modified MCFs are very well suited to host enzymes.

Contrary to possible expectations, in the following, the discussion on the immobilizations of the three enzymes is introduced with the immobilization of 6PGDH (Chapter 4.2) and subsequently followed by the immobilization of the ADH (Chapter 4.4). Only then the focus is placed upon the immobilization of G6PDH (Chapter 4.5). This may seem confusing to the reader, however, the immobilization of G6PDH was extensively discussed by D. Fried.[26] Hence, merely supplementary studies were necessary in order to optimize the immobilization of G6PDH for its implementation into the intended enzyme cascade. Furthermore, some of these additional experiments arose from the results obtained for the immobilization of 6PGDH or ADH. Consequently, it is reasonable to discuss the immobilization of G6PDH at last, before the discussion is focused on the construction of the enzyme cascade.

## 4.2 Immobilization of 6PGDH from *Geobacillus stearothermophilus* (*G.s.*6PGDH)

Parts of this chapter have already been published.[186]

6PGDH is the third enzyme of the oxidative path of the pentose phosphate pathway. It catalyzes the oxidation of 6PG to Ru5P and $CO_2$ with concomitant reduction of one equivalent $NADP^+$ to NADPH (Scheme 4). Within the scope of the strived enzyme cascade, the immobilized 6PGDH catalyzes the second NADPH providing reaction step (Figure 37). Its substrate, 6PG, is generated in a former reaction step by an immobilized G6PDH. This reaction including the immobilization of the G6PDH will be discussed later on (Chapter 4.5).

For the application of *G.s.*6PGDH in a modular multienzyme cascade, it was indispensable to carefully investigate the enzyme in terms of its adsorptive immobilization onto the surface of organically modified MCFs (Figure 50). MCF was applied as an adequate support material for the immobilization of *G.s.*6PGDH, as it consists of a large mesoporous network enabling the immobilized enzyme to enter the pores as well as to undergo necessary conformational changes during catalysis, with a view to ensure high enzymatic activity matched with ideal kinetics.

[186] M. Dreifke, D. I. Fried, F. J. Brieler, M. Fröba, *J. Mol. Catal. B: Enzymatic* **2016**, *132*, 5-15.

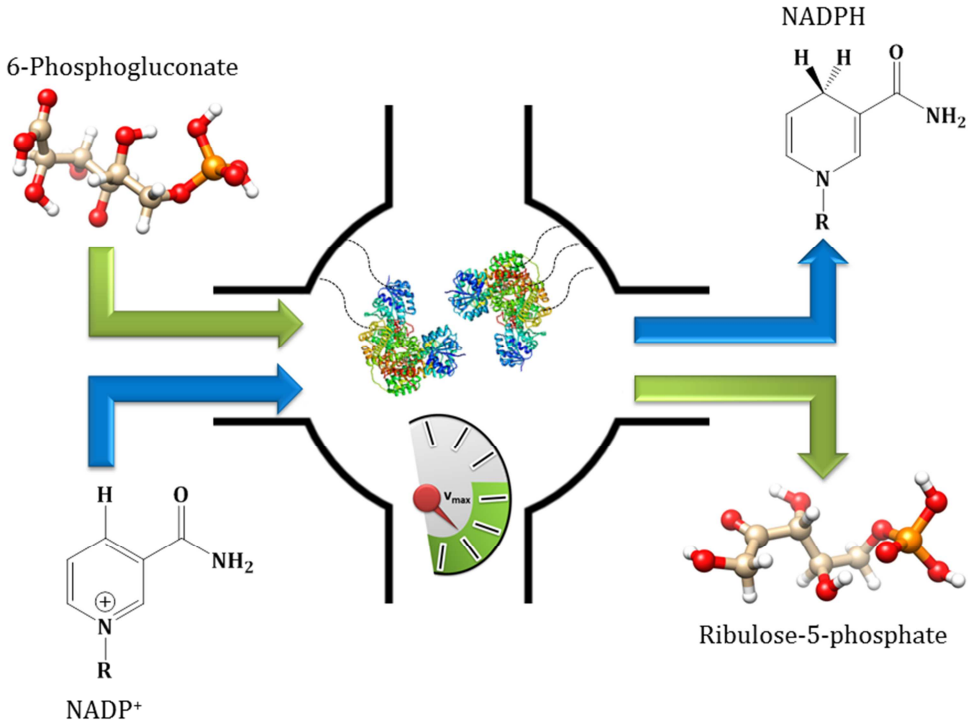


**Figure 50.** Adsorptive immobilization of *G.s.*6PGDH onto organically functionalized MCF. 6PGDH catalyzes the oxidation of 6-phosphogluconate to ribulose-5-phosphate. A special focus was placed onto the enzyme kinetics of the immobilized enzyme.

The immobilization of *G.s.*6PGDH was not very promising when using pristine MCF as a support material, as it only retained 27 % of its original catalytic activity. Thus, the immobilization of *G.s.*6PGDH was carried out onto the surface of aminoalkyl modified MCFs. The carbon chain lengths of the aminoalkyl residues on the surface of the MCFs was varied from -$C_3$-$NH_2$, -$C_5$-$NH_2$, -$C_7$-$NH_2$ to -$C_{11}$-$NH_2$ in order to verify the optimal distance between the enzyme and the pore walls. Rounding this approach, *G.s.*6PGDH was additionally immobilized onto simply alkyl functionalized MCFs owning the same carbon chain lengths (-$C_3$, -$C_5$, -$C_7$, $C_{11}$; Figure 38). Herewith, the influence of a terminal amino function on the surface of the functionalized MCFs concerning the immobilization behavior of *G.s.*6PGDH was investigated. Accordingly, the enzyme uptakes and long-term stabilities of the immobilized as well as free *G.s.*6PGDH were elaborated and compared among each other.

In a previous chapter, the surface properties of *G.s.*6PGDH were depicted (Figure 7). As the surface of this enzyme is mainly covered by hydrophilic amino acids, polar interactions between the aminopropyl modified MCFs and polar amino acids on the surface of *G.s.*6PGDH were presumed. Whereas hydrophobic

interactions between the alkyl modified MCFs and hydrophobic surface areas of *G.s.*6PGDH were supposed. Thus, detailed investigations of the predominating interactions were essential.

With respect to the utilization of the immobilized *G.s.*6PGDH in a modular enzyme cascade, it was mandatory to carefully investigate the Michaelis-Menten kinetics of the immobilized as well as of the native enzyme. In return, details concerning its substrate and coenzyme affinities were obtained. These investigations were applied to all alkyl and aminoalkyl functionalized MCFs carrying the immobilized enzyme. Thus, the most appropriate host material regarding the Michaelis-Menten kinetics of the immobilized *G.s.*6PGDH was identified.

### 4.2.1 Investigation of the adsorptive immobilization of *G.s.*6PGDH onto alkyl and aminoalkyl functionalized MCFs

The immobilization of *G.s.*6PGDH onto the alkyl as well as aminoalkyl modified MCFs was carried out in phosphate buffer solution (50 mM, pH 6.5) for 24 h at 25 °C. An enzyme to host ratio of 1:10 was chosen (~0.5 mg 6PGDH + 5 mg MCF), unless otherwise stated.

To ensure optimal catalytic power of the immobilized enzyme, a high uptake coupled with a high retained activity is generally required. Certainly it is obvious that the immobilization of an enzyme is examined foremost onto the pristine host, prior to its immobilization onto complex modified support materials. Hence, in first instance, the immobilization of *G.s.*6PGDH was performed onto the surface of the unmodified MCF. The immobilization of *G.s.*6PGDH onto pristine MCF resulted in an enzyme uptake of 94.3 % (Appendix 7.4.1; Table 8). Initially, this was a satisfactorily result concerning the amount of immobilized enzyme. However, the immobilized *G.s.*6PGDH retained only 27 % of its original activity (Table 9). Therefore, it was self-evident to organically modify the surface of the MCF by employing alkyl- as well aminoalkyl-trialkoxysilanes in order to improve the retained enzymatic activity. Additionally, the carbon chain length of the alkyl and aminoalkyl modified MCFs was varied from $-C_3(-NH_2)$ and $-C_5(-NH_2)$, over $-C_7(-NH_2)$ to $-C_{11}(-NH_2)$, in order to evaluate the optimal distance between the immobilized *G.s.*6PGDH and the pore walls of the MCF. A too short distance between the pore walls and the immobilized enzyme was assumed to hinder the enzyme to undergo conformational changes during the catalytic process later on. Whereas a long spacer was supposed to allow the immobilized enzyme to additionally interact with further alkyl or aminoalkyl chains on the surface of the respective modified MCF resulting in a decrease of the

enzymatic activity, too. Thus, the optimal distance between the pore walls of the MCFs and the enzyme had to be verified.

**Uptakes.** In first instance, the immobilization of *G.s.*6PGDH onto the surface of the alkyl and aminoalkyl modified MCFs was assumed to be carried out by adsorption, governed by hydrophobic as well as electrostatic interactions between the surface of the functionalized MCFs and the surface of the enzyme (Figure 51). According to the pI of *G.s.*6PGDH (pH 6.5), the immobilization was performed at pH 6.5 to ensure a neutral net charge of the protein surface and hence reduced electrostatic repulsion of the enzyme molecules among each other. This is particularly relevant to obtain a high enzyme uptake. Although pH 6.5 is the pI of *G.s.*6PGDH, dissolving the enzyme in a phosphate buffer solution of this pH did not lead to precipitation of enzyme aggregates. Moreover, no precipitation of *G.s.*6PGDH was observed in the stock solution over a period of 53 days, indicating pH 6.5 is convenient for the immobilization of *G.s.*6PGDH.

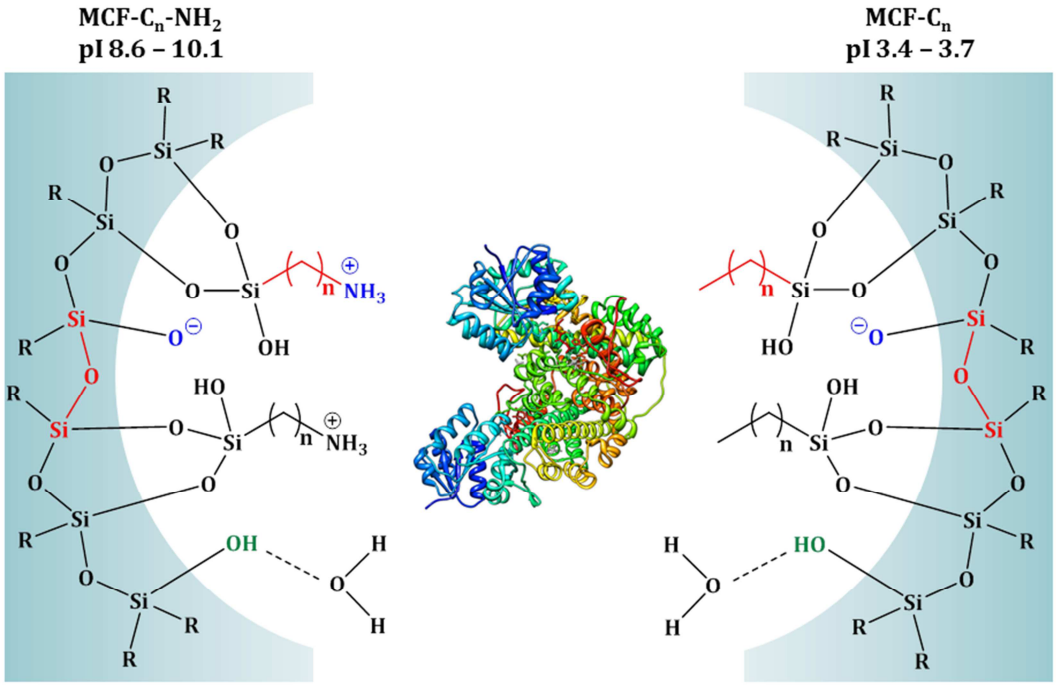


**Figure 51.** Schematic depiction of possible interactions between *G.s.*6PGDH and the aminoalkyl (MCF-$C_x$-$NH_2$) as well as alkyl (MCF-$C_x$) modified MCFs at an immobilization pH of 6.5. Hydrophobic interaction (red) can arise between siloxane bridges within in the pore walls or carbon chains of the surface functionalization of the respective MCF and hydrophobic surface areas of *G.s.*6PGDH. Electrostatic interactions (blue) can occur between protonated surface amino groups of MCF-$C_x$-$NH_2$ or deprotonated silanol groups and oppositely charged groups on the surface of the enzyme. An immobilization *via* hydrogen bridges (green) is negligible.

By using the alkyl modified MCFs as hosts an enzyme uptake of 100 % (~ 0.5 mg *G.s.*6PGDH) was obtained, independent on the carbon chain length (Table 8). This can be referred to percentages of 6.5 –9.3 wt-% *G.s.*6PGDH on the immobilisate (immobilisate = support + enzyme; Table 8). The immobilization process itself was figured out to be very fast and completed after 15 minutes at latest (Figure 52). Even if the surface of *G.s.*6PGDH is mainly covered by hydrophilic amino acids (Figure 7b), hydrophobic interactions between the alkyl residues on the support material and hydrophobic areas on the *G.s.*6PGDH surface were assumed to be the dominating interactions within the immobilization procedure (Figure 51).

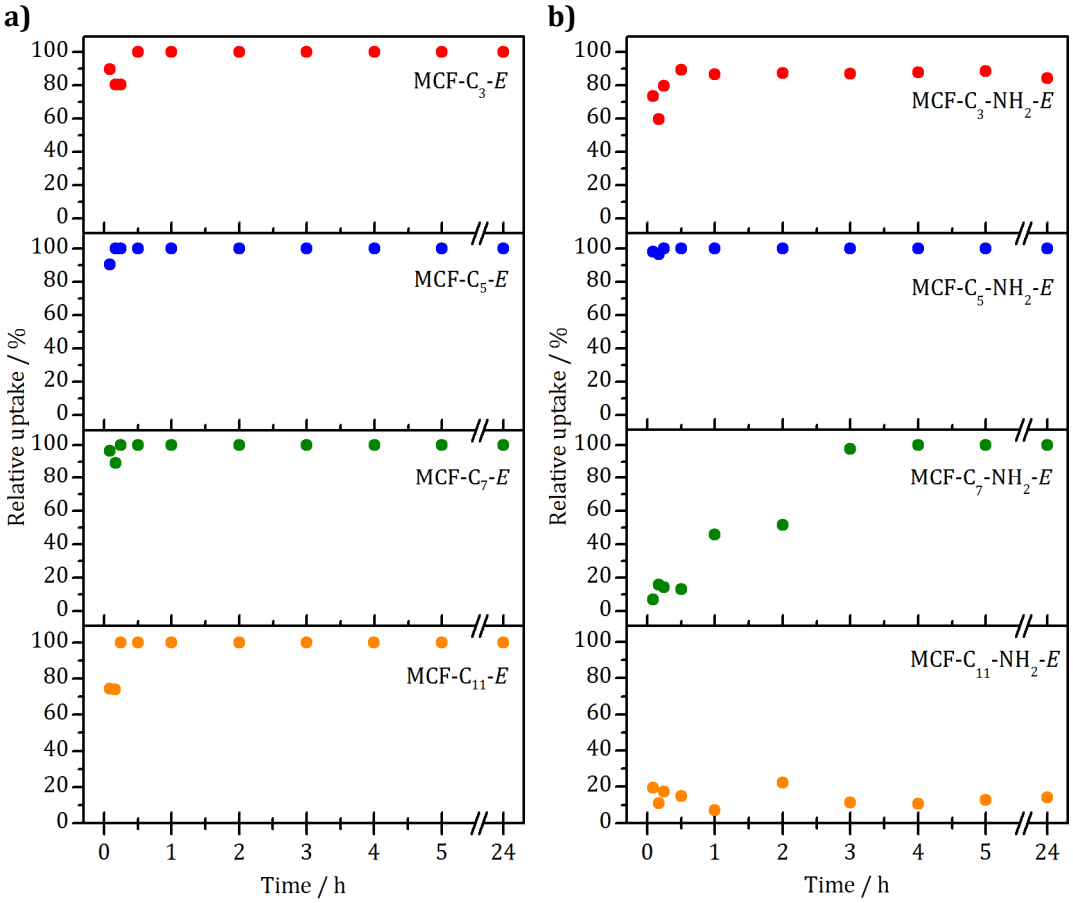


**Figure 52.** Relative uptakes of *G.s.*6PGDH versus immobilization time by **a)** using alkyl modified MCFs and **b)** aminoalkyl modified MCFs as host materials. An uptake of 100 % was obtained when using the alkyl functionalized MCFs and MCF-C5-NH2 as well as MCF-C7-NH2 as a host material.

As thermoanalytical data confirmed (Table 6), modification of MCF with alkyltrialkoxysilanes did not lead to full coverage of the silica surface with organic residues, leading to numerous free silanol groups still remaining on the surface of the MCFs. According to zeta potential titrations, the surface of these materials is negatively charged at the pH of immobilization (pH 6.5). Thus, attractive

electrostatic interactions between the charged oxygen atoms and the hydrophilic surface of the enzyme are also possible (Figure 51). However, to verify or falsify these predictions further investigations concerning the predominating interactions present in the immobilization were necessary.

Likewise an enzyme uptake of 100 % (~ 0.5 mg *G.s.*6PGDH) was obtained by using MCF-$C_5$-$NH_2$ and MCF-$C_7$-$NH_2$ as support materials for the immobilization of *G.s.*6PGDH (Table 8). This corresponds to 6.3 as well as 6.4 wt-% of *G.s.*6PGDH, respectively. Employing MCF-$C_3$-$NH_2$ and MCF-$C_{11}$-$NH_2$ as hosts, the uptakes were reduced (79.4 % for MCF-$C_3$-$NH_2$, 13.9 % for MCF-$C_{11}$-$NH_2$). The comparatively low uptake onto MCF-$C_{11}$-$NH_2$ can be referred to the high hydrophobicity of this material, associated with a low dispersibility in the aqueous buffer solution, accompanied by a hindered diffusion of the protein into the porous structure of the host. Thus, the immobilization is presumed to be carried out preferentially onto the outer surface of MCF-$C_{11}$-$NH_2$. The uptake of MCF-$C_3$-$NH_2$ is reduced by 21 % compared to MCF-$C_3$. However, the percent by weight of *G.s.*6PGDH (7.1 wt-%) is in the same range as calculated for MCF-$C_5$-$NH_2$ and MCF-$C_7$-$NH_2$ with an uptake of 100 %. As ascertained by zeta potential titrations, the dispersion of the aminoalkyl functionalized MCFs in phosphate buffer solution possessing pH 6.5 results in a positively charged host surface. At a first glance, immobilization of *G.s.*6PGDH onto these MCFs can be addressed to electrostatic interactions between the positively charged amino groups on the silica surface and the large amount of hydrophilic areas on the outer surface of the enzyme (Figure 7c). Furthermore, hydrophobic interactions between the carbon chains of the aminoalkyl residues and hydrophobic surface areas of the enzyme are likely to participate in the immobilization process.

**Table 8.** Comparative survey of the *G.s.*6PGDH uptakes and percentages by weight when using MCF, MCF-$C_x$ as well as MCF-$C_x$-$NH_2$ as host materials.

| sample | uptake [%] | percent by weight [wt-%] |
|---|---|---|
| **MCF** | 94.3 | 5.2 |
| **MCF-$C_3$** | 100 | 9.3 |
| **MCF-$C_5$** | 100 | 6.5 |
| **MCF-$C_7$** | 100 | 6.5 |
| **MCF-$C_{11}$** | 100 | 9.0 |
| **MCF-$C_3$-$NH_2$** | 79.4 | 7.1 |
| **MCF-$C_5$-$NH_2$** | 100 | 6.3 |
| **MCF-$C_7$-$NH_2$** | 100 | 6.4 |
| **MCF-$C_{11}$-$NH_2$** | 13.9 | 1.4 |

**Driving interactions resulting in immobilization.** For a detailed investigation of the prevailing interactions that are present in the immobilization of *G.s.*6PGDH onto the alkyl as well as the aminoalkyl modified MCFs, the concentration of potassium phosphate in the buffer solution of the immobilization was varied from 50 mmol $L^{-1}$ to 1000 mmol $L^{-1}$. The electrostatic shielding of an enzyme increases with increasing ionic strength of the respective buffer solution (Figure 53). The higher the ionic strength of the buffer solution, the lower the radius of the sphere in which a sufficient amount of corresponding counter ions are present to compensate the surface charge of the enzyme. Hence, in the presence of electrostatic interactions, the enzyme uptake decreases with increasing ionic strength of the buffer solution.

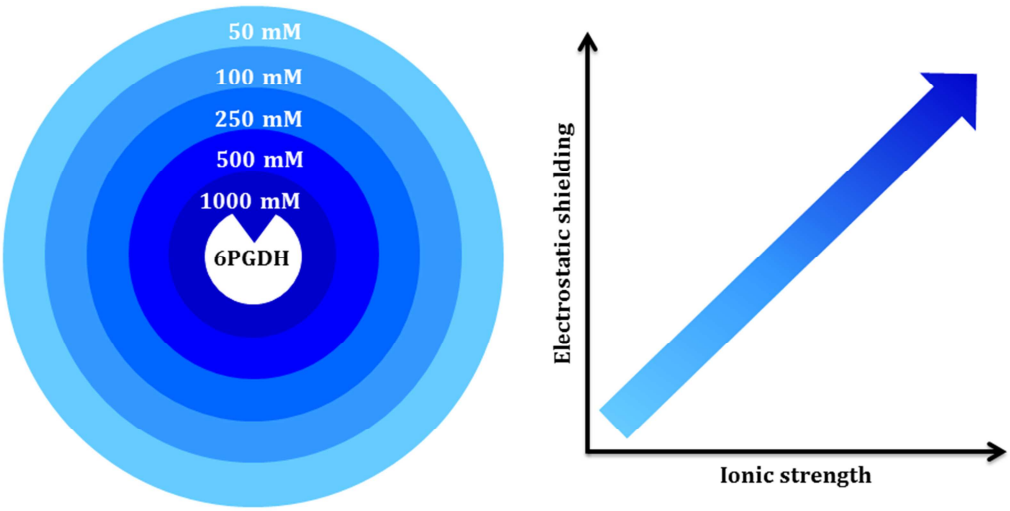


**Figure 53.** The ionic strength of the phosphate buffer solution employed for immobilization was varied from 50 mmol $L^{-1}$ up to 1000 mmol $L^{-1}$. The electrostatic shielding of an enzyme increases with increasing ionic strength of the respective buffer solution. In the presence of hydrophobic interactions within the immobilization process, the enzyme uptake is not affected by the ionic strength. However, in the existence of electrostatic interactions, the uptake decreases with increasing ionic strength of the buffer solution.

These investigations were exemplarily conducted for the alkyl modified supports using MCF-$C_5$ as well as for the aminoalkyl functionalized MCFs consulting MCF-$C_5$-$NH_2$ as a host material. An enzyme uptake of 100 % onto MCF-$C_5$ and MCF-$C_5$-$NH_2$ was obtained, respectively, independent on the ionic strength of the buffer solution (Appendix 7.4.2). This indicates that the immobilization of *G.s.*6PGDH onto these MCFs is exclusively governed by hydrophobic interactions between hydrophobic residues on the surface of *G.s.*6PGDH and the hydrophobic alkyl chains on the surface of the supports. Hydrophobic interactions play an important role within the immobilization process, as they reduce the free energy of the system. Displacement of coordinated, and consequently, in their mobility restricted water molecules on the contact points between the hydrophobic surface area of the enzyme and the hydrophobic surface of the MCF leads to an increase in the entropy and thus to a reduction of the free energy (Figure 54). The increased mobility of the displaced water molecules enables them to form a maximum quantity of hydrogen bridges. In accordance, the number of hydrogen bridges in the reaction volume ascends. Hence, the increase in entropy is the driving force of hydrophobic interaction.[8, 9, 10]

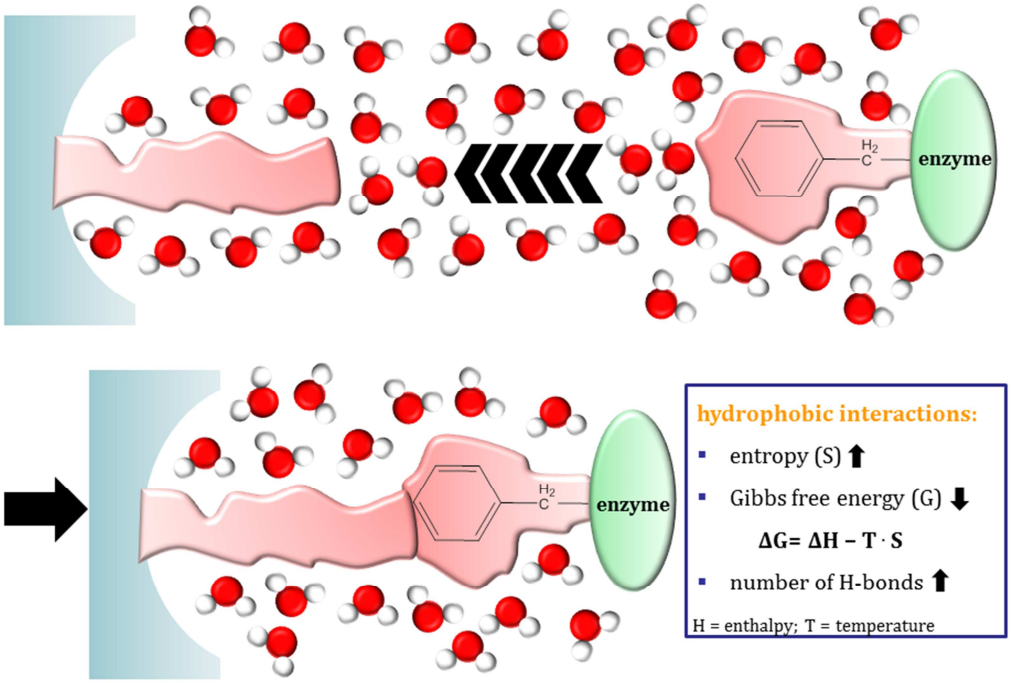


**Figure 54.** Schematic illustration of hydrophobic interactions. A hydrophobic phenylalanine residue on the surface of an enzyme gets in contact with a hydrophobic alkyl residue on the surface of a porous host. Water molecules solvating the contact points become displaced and the entropy increases. The blue box explains the mathematical background.

The formation of hydrogen bridges between the silanol functions on the surface of the functionalized MCFs and *G.s.*6PGDH is highly questionable, as water molecules from the phosphate buffer are in a huge excess and thus forming hydrogen bonds to the silanol hydrogen atoms preferentially.[69] However, siloxane bridges (Si-O-Si groups) exhibit a markedly hydrophobic character enabling them to interact with hydrophobic regions on the enzyme surface, too. Hence, the immobilization can additionally be carried out due to these hydrophobic groups and likewise hydrophobic areas on the surface of the enzyme (Figure 51).

**Proportion of $\rho_f$ of the hosts and the amounts of immobilized *G.s.*6PGDH.** It is irremissible to create a relationship between $\rho_f$ of the organic residues on the surface of MCF-$C_x$ as well as MCF-$C_x$-$NH_2$ and the amounts of *G.s.*6PGDH immobilized, respectively (final immobilization ratio). Accordingly, the quotient of $\rho_f$ and the amount of immobilized enzyme (AIE) needs to be introduced (Eq. 18).

$$\text{final immobilization ratio} = \frac{\rho_f}{\text{AIE}} \left[\frac{\text{mmol} \cdot \text{g}^{-1}}{\text{mmol} \cdot \text{g}^{-1}}\right] \qquad \textbf{Eq. 18}$$

The final immobilization ratio describes the ratio of the amounts of organic residues on the surface of the modified MCFs and the respective enzyme loadings (Table 9). High values of the quotient indicate a huge excess of organic residues on the modified surface of the MCFs compared to the amount of immobilized enzyme and vice versa. This approach presupposes that one enzyme molecule interacts with merely one organic residue on the surface of the host. However, a multipoint attachment of the enzyme cannot be excluded, which can be referenced to a significantly larger dimension of the enzyme in comparison to the size of the organic residues on the surface of the functionalized MCFs. Thus, the final immobilization ratio needs to be considered as a theoretical point of view and gives a first impression regarding the ratio between $\rho_f$ as well as AIE.

The values calculated for the alkyl modified MCFs are lowest for MCF-$C_{11}$ (311), which is addressed to the low $\rho_f$ (0.27 mmol $g^{-1}$) of this material. However, even the comparatively low quotient of $\rho_f$ and AIE of MCF-$C_{11}$ reveals that the organic residues are in a 311-fold excess related to the enzyme amount immobilized. The highest ratios for the alkyl modified MCFs were obtained for MCF-$C_3$ (931) and MCF-$C_5$ (934). For the aminoalkyl modified MCFs, final immobilization ratio increases from MCF-$C_3$-$NH_2$ (1742) to MCF-$C_{11}$-$NH_2$ (11935). The markedly high value of MCF-$C_{11}$-$NH_2$ can be traced back to the low enzyme uptake (13.9 %) combined with a high $\rho_f$ (1.48 mmol $g^{-1}$). The huge excess of the organic residues in all samples compared to the enzyme loadings ensures a comparability of all immobilisates, independent of the respective $\rho_f$ of the host material.

**Activity retention.** In order to distinguish in the following discussion between pristine host materials and host materials with immobilized enzyme the latter was additionally designated as MCF-$C_x$-($NH_2$)–*E*.

An important aspect concerning the immobilization of enzymes is the retention of the enzymatic activity immediately after 24 h of immobilization as well as the long-time stability over a defined period of days. The enzymatic activity of the native as well as the immobilized *G.s.*6PGDH was investigated by means of the conversion of 6-phosphogluconate to ribulose-5-phosphate with concomitant reduction of $NADP^+$ to NADPH. For the aminoalkyl modified supports, the activity retention after 24 h of immobilization was 56 % for MCF-$C_3$-$NH_2$-*E* and thus highest in comparison of the aminoalkyl as well as to the alkyl functionalized MCFs (Table 9). It is apparent that the retention of activity depends on the aminoalkyl chain length. Accordingly, MCF-$C_5$-$NH_2$-*E* retained merely 30 % and MCF-$C_7$-$NH_2$-*E* 17 % of the origin enzymatic activity prior to immobilization. The immobilization of

*G.s.*6PGDH onto MCF-$C_{11}$-$NH_2$ led to complete denaturation of the enzyme. Thus, no enzymatic activity was detectable. As mentioned above the immobilization of *G.s.*6PGDH onto the aminoalkyl modified hosts was initially implemented due to hydrophobic interactions. Thus, the enzyme interacts with the alkyl chains bearing the amino group. The extent of these hydrophobic interactions is stronger with increasing chain length and thus increasing hydrophobicity. These strong interactions possibly lead to an unfolding of the tertiary structure of the enzyme in order to lower its free energy. This is accompanied by a decrease of the retained activity, as the fixation of substrate or coenzyme molecules is constricted. Accordingly, the hydrophobic interactions were strongest for MCF-$C_{11}$-$NH_2$-*E*. Hence, the enzyme is completely denatured. Additionally, with respect to the low dispersibility of MCF-$C_{11}$-$NH_2$ in the aqueous buffer solution, *G.s.*6PGDH was assumed to be primarily immobilized onto the outer surface of the host. Hereby, the immobilized enzyme was exposed to external forces, like shear forces etc., as a protective confinement of a pore was missing. Lack of this stabilization led to a rapid denaturation of the enzyme.

**Table 9.** Overview of the retained enzymatic activities after 24 h of immobilization as well as $\rho_f$/AIE values for the immobilization of *G.s.*6PGDH onto MCF-$C_x$ and MCF-$C_x$-$NH_2$.

| sample | activity retention [%] | $\rho_f$ / AIE |
|---|---|---|
| **free *G.s.*6PGDH** | 92 | --- |
| **MCF-*E*** | 27 | --- |
| **MCF-$C_3$-*E*** | 47 | 931 |
| **MCF-$C_5$-*E*** | 23 | 934 |
| **MCF-$C_7$-*E*** | 19 | 754 |
| **MCF-$C_{11}$-*E*** | 13 | 311 |
| **MCF-$C_3$-$NH_2$-*E*** | 56 | 1742 |
| **MCF-$C_5$-$NH_2$-*E*** | 30 | 2270 |
| **MCF-$C_7$-$NH_2$-*E*** | 17 | 2742 |
| **MCF-$C_{11}$-$NH_2$-*E*** | 0 | 11935 |

When employing the alkyl functionalized MCFs for the immobilization of *G.s.*6PGDH, the same dependency between the chain length and the retained enzymatic activity was observed. Accordingly, the highest retention of activity was obtained for MCF-$C_3$-*E* (47 %) and the activities of MCF-$C_5$-*E* as well as MCF-$C_7$-*E* were correspondingly lower. As mentioned above, hydrophobic interactions between the alkyl modified MCFs and the hydrophobic surface area of *G.s.*6PGDH are responsible for the immobilization, as they are accompanied by an increase in entropy. Therefore, interactions with remaining surface silanol groups are negligible. In terms of MCF-$C_3$ as well as MCF-$C_5$, the absence of terminal amino groups on the surface of the hosts led to a stronger decrease of the retained activity due to lack of interactions stabilizing the enzyme. In contrast to MCF-$C_{11}$-$NH_2$-*E* with no residual activity, MCF-$C_{11}$-*E* retained 13 % of its origin enzymatic activity. As the thermoanalytical data revealed, $\rho_f$ of MCF-$C_{11}$ is very low, whereas the uptake of *G.s.*6PGDH was 100 %. Due to the low $\rho_f$ of MCF-$C_{11}$ in comparison to MCF-$C_{11}$-$NH_2$-*E*, the former is less hydrophobic and thus more dispersible in the buffer leading to a minor residual activity of the enzyme.

Generally the orientation of the immobilized 6PGDH plays a decisive role in terms of the retained activity. The active sites of the immobilized enzyme can be orientated towards the surface of the MCF and thus the accessibility and the fixation of 6PG and/or $NADP^+$ can be hindered. Thus, the capability to undergo conformational changes during the catalysis can be reduced and result in a lower activity compared to the free enzyme.

**Variation of the initial *G.s.*6PGDH concentration.** To survey whether the initial *G.s.*6PGDH concentration ($c_{i,6PGDH}$) employed for immobilization has an impact on the uptake as well as on the activity retention, $c_{i,6PGDH}$ was varied from ~ 0.100 mg $mL^{-1}$ to ~ 1.90 mg $mL^{-1}$ (Table 10). The quantity of the support material was set to 5 mg, respectively.

**Table 10.** Enzyme activity maintenance on MCF-$C_3$ as well as MCF-$C_3$-$NH_2$ when varying the initial concentration of *G.s.*6PGDH ($c_{i,6PGDH}$).

| sample | $c_{i,6PGDH}$ [mg mL$^{-1}$] | uptake [%] | activity retention [%] | percent by weight [wt-%] |
|---|---|---|---|---|
| **MCF-$C_3$** | 0.112 | 100 | 29 | 2.2 |
| **MCF-$C_3$** | 0.277 | 100 | 30 | 5.2 |
| **MCF-$C_3$** | 0.544 | 100 | 47 | 9.3 |
| **MCF-$C_3$** | 1.082 | 100 | 34 | 17.8 |
| **MCF-$C_3$** | 1.962 | 100 | 32 | 27.8 |
| **MCF-$C_3$-$NH_2$** | 0.101 | 78 | 25 | 1.5 |
| **MCF-$C_3$-$NH_2$** | 0.250 | 54 | 42 | 2.5 |
| **MCF-$C_3$-$NH_2$** | 0.544 | 79 | 56 | 7.1 |
| **MCF-$C_3$-$NH_2$** | 1.109 | 32 | 57 | 6.4 |
| **MCF-$C_3$-$NH_2$** | 1.845 | 34 | 47 | 10.4 |

When using MCF-$C_3$ as an exemplary support for the alkyl functionalized MCFs independent on the initial *G.s.*6PGDH concentration an enzyme uptake of 100 % was obtained. The plot of the adsorbed enzyme amount as a function of $c_{i,6PGDH}$ shows linear behavior (Figure 55). Employing a stock solution possessing a *G.s.*6PGDH concentration of 1.962 mg mL$^{-1}$, it took two hours until the immobilization was completed. Due to the lower enzyme concentration, the immobilization of the enzyme from the further stock solutions was already completed after 1 hour at latest (Appendix 7.4.3). The enzymatic activity retention compared to the activity of the enzyme in the stock solution before immobilization was about 30 % for nearly all samples. However, as discussed above the, activity retention of *G.s.*6PGDH immobilized from a stock solution with an enzyme concentration of 0.544 mg mL$^{-1}$ amounted to 47 % and is thus highest for this series of measurements. As expected, the percentages by weight of the immobilized enzyme increase with increasing initial enzyme concentration, as the uptake is 100 % in every case.

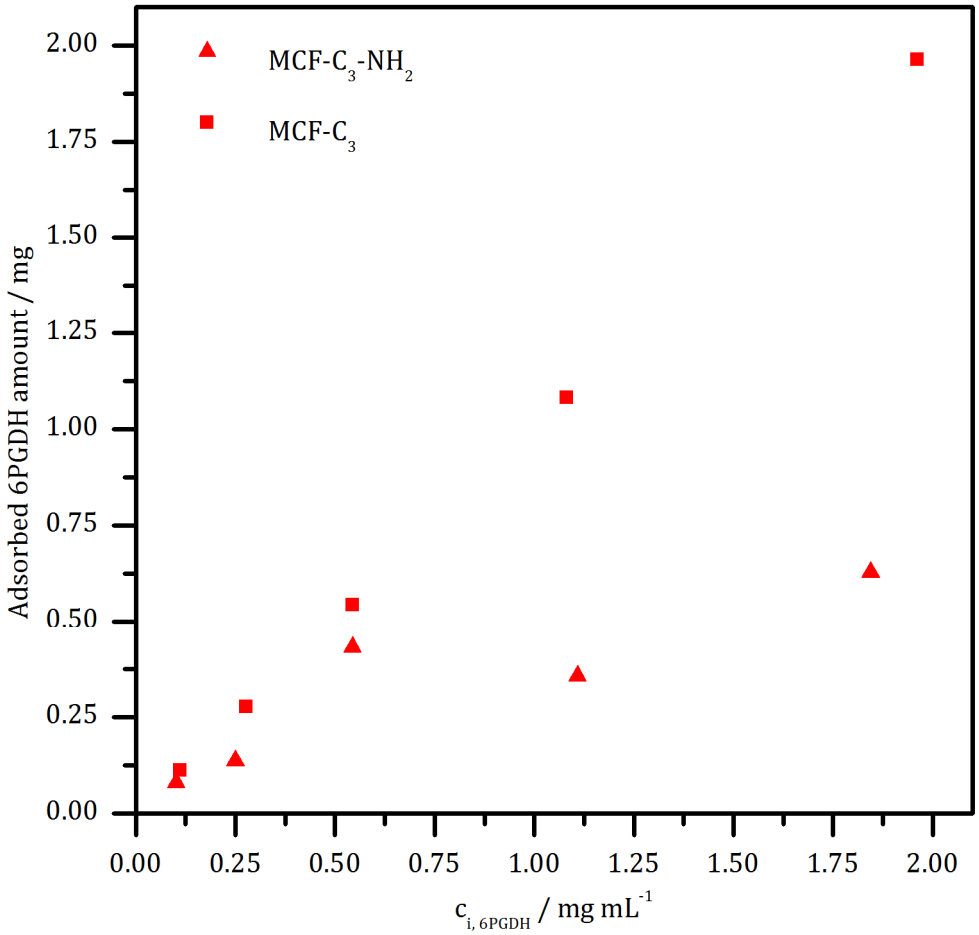


**Figure 55.** Variation of the initial *G.s.*6PGDH amount ($c_{i,6PGDH}$) employed for the immobilization onto MCF-$C_3$ and MCF-$C_3$-$NH_2$. $c_{i,6PGDH}$ was varied from ~ 0.100 mg $mL^{-1}$ to ~ 1.90 mg $mL^{-1}$, whereas the applied amount of MCF-$C_3$ and MCF-$C_3$-$NH_2$ was set to 5 mg, respectively. In case of MCF-$C_3$ the adsorbed enzyme amount increases linearly with increasing $c_{i,6PGDH}$. However, when using MCF-$C_3$-$NH_2$ as a support material no distinct trend was observed.

The variation of $c_{i,6PGDH}$ in the immobilization of *G.s.*6PGDH onto MCF-$C_3$-$NH_2$ resulted in comparatively lower uptakes than obtained for the immobilization onto MCF-$C_3$ (Table 10; Appendix 7.4.3). The uptakes do not show any distinct trend. They were found to be lowest for the highest $c_{i,6PGDH}$. However, the activity retention was by far lowest when using a $c_{i,6PGDH}$ of 0.101 mg $mL^{-1}$ (25 %). The main reason for the high loss of activity in this sample can be addressed to spreading. Due to the lower enzyme concentration, each immobilized enzyme molecule has the ability to expand its contact to the pore walls in order to lower its free energy. This circumstance results in an unfolding of the protein's tertiary structure and is affiliated with a loss of enzymatic activity.[69] The values of the activity retentions of the further samples range between 42 % and 57 %. The utilization of an origin *G.s.*6PGDH concentration of 0.544 mg $mL^{-1}$ yielded in a promising result (56 %), as a further increase of the enzyme concentration did not lead to a markedly increase of

the retained activity. This behavior was observed for MCF-$C_3$ as well as MCF-$C_3$-$NH_2$ and confirms an optimum ratio of enzyme to host of 1:10.

**Leaching experiments.** To evaluate the strength of the attractive interactions between *G.s.*6PGDH and the organo modified MCFs as well as the pristine MCF, leaching experiments were performed. The respective immobilisates were dispersed twice in the buffer of the immobilization and shaken at room temperature, respectively. Under the given conditions and independent on the surface functionalization, *G.s.*6PGDH could not be eluted neither after 24 h nor after 48 h from the material. The outcome indicates strong attractive interaction between the enzyme and the alkyl as well aminoalkyl functionalized host materials.

**Long-term stability of the immobilized *G.s.*6PGDH.** A major advantage of an immobilized enzyme is its reusability. Hence, a special focus was placed on the long-term stability of the immobilized *G.s.*6PGDH. The long-time stability of the free *G.s.*6PGDH and all immobilisates was investigated over a period of 53 days (Figure 56). Therefore, the respective samples were stored in potassium phosphate buffer (pH 6.5, 50 mM) at 4 °C. For the long-time stability studies, the retained activity after 24 h of immobilization was set to 100 % relative activity.

In comparison to the immobilized enzyme, the free *G.s.*6PGDH still possessed 87 % relative activity after six days. Within the first week after immobilization, the activity decreased significantly, most likely attributed to time-spreading, which is associated with the unfolding of the enzyme's tertiary structure and therefore accompanied by loss of enzymatic activity (Figure 15).[69] The residual enzymatic activity after six days for the enzyme immobilized onto the alkyl modified MCFs was 21 – 22 % and with 24 – 31 % slightly higher for *G.s.*6PGDH immobilized onto the aminoalkyl modified MCFs. The further decay of the activity over a period of 53 days was similar for all samples, whereupon the residual activity of *G.s.*6PGDH immobilized onto the aminoalkyl modified MCFs was slightly higher compared to the respective alkyl functionalized materials. Apparently, during storage time, the amino groups exert a stabilizing effect on the immobilized enzyme. This observation is addressed to stronger adsorptive bonds between the enzyme and the aminoalkyl modified MCFs and thus minor mobility of the enzyme. The native *G.s.*6PGDH possessed the best long-term stability under given conditions. However, for prospective applications in the introduced multienzyme cascade, *G.s.*6PGDH has to be used in an immobilized manner, even though immobilization did not lead to a stabilization of the enzyme (Figure 37).

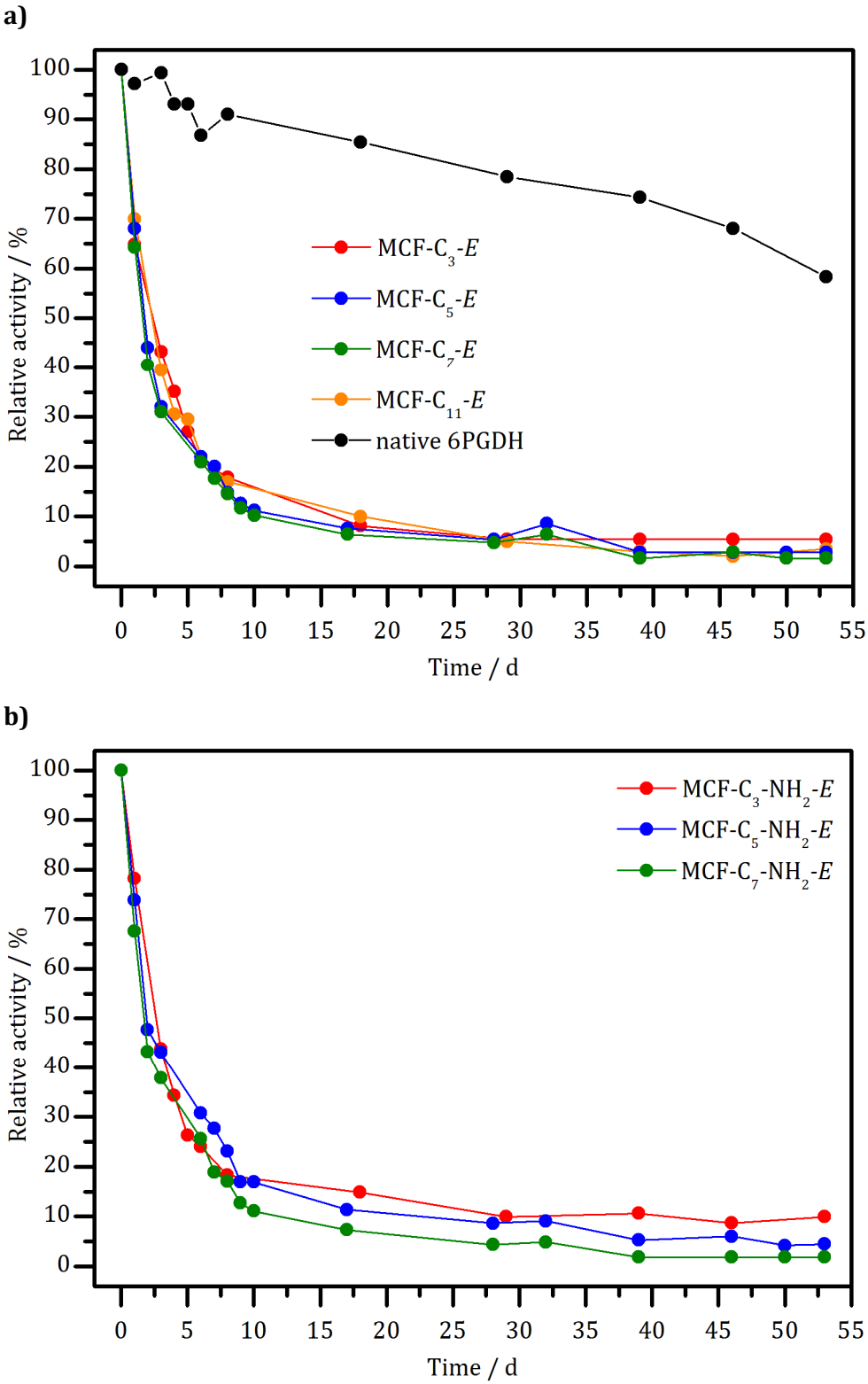


**Figure 56.** Long-term stabilities of the free and the immobilized *G.s.*6PGDH. **a)** *G.s.*6PGDH immobilized onto MCF-$C_x$; **b)** *G.s.*6PGDH immobilized onto MCF-$C_x$-$NH_2$. A dependency on the enzyme activity, the carbon chain length and the existence of a terminal amino function was observed. Over a period of 53 days the enzyme immobilized onto the aminoalkyl modified MCFs was slightly higher as of the enzyme immobilized onto the respective alkyl functionalized MCFs.

**Intermediate summary.** The immobilization of *G.s.*6PGDH was exclusively carried out by hydrophobic interactions. Employing the alkyl modified MCFs for immobilization, an enzyme uptake of 100 % was obtained independent on the carbon chain length. Whereas the uptakes onto the aminoalkyl functionalized MCFs varied between 13.9 % (MCF-$C_{11}$-$NH_2$) and 100 % (MCF-$C_{5/7}$-$NH_2$). The proportion of $\rho_f$ and AIE confirmed the considerable excess of organic residues on the surface of the functionalized MCFs compared to the respective enzyme loadings. This ensures a comparability of all immobilisates independent on the respective $\rho_f$ of the host material. The variation of the initial *G.s.*6PGDH concentration applied for immobilization illustrated that in terms of the uptakes as well as the retained activity of the immobilized *G.s.*6PGDH, a *G.s.*6PGDH to host ratio of 1:10 within the immobilization procedure is most promising (0.5 mg *G.s.*6PGDH + 5 mg MCF-$C_x$-($NH_2$)). The immobilization of *G.s.*6PGDH onto MCF-$C_3$-$NH_2$ as well as MCF-$C_3$ led to the highest retentions of activity. The retained activity amounted to 56 % and 47 %, respectively, and was considerably higher than for the enzyme immobilized onto the unmodified MCF (27 %). The retained activity was strongly affected by the carbon chain length of the modified MCFs: The longer the carbon chain, the higher the hydrophobicity and thus the lower the retention of enzymatic activity. Moreover, the retained activity was slightly higher for the enzyme immobilized onto the aminoalkyl modified host than compared to the enzyme immobilized onto the respective alkyl functionalized MCFs. The long-time stability of the enzyme was evaluated over a period of 53 days, whereupon the dependency on declining activity and chain lengths as well as on the existence of a terminal amino group persisted.

### 4.2.2 Michaelis-Menten kinetics of the immobilized *G.s.*6PGDH

Against the background of the aspired modular enzyme cascade, it was important to gain information regarding the Michaelis-Menten kinetics of each immobilized enzyme. As the immobilized *G.s.*6PGDH was intended to be a part of a multienzyme complex, it was important that the former reaction step provides a sufficient amount of substrate and coenzyme in order to ensure ideal kinetics. Although the long-time stability and activity of an immobilized enzyme are important parameters, they do not allow conclusions relating to its substrate as well as its coenzyme affinity and finally its catalytic efficiency. Investigations of Michaelis-Menten kinetics shed light on these issues. However, this is quite ambitious when examining immobilized enzymes, as diffusion plays an important role when employing porous carriers. On their way to the immobilized enzyme

within mesopores, substrate as well as coenzyme molecules need to diffuse from the core flow of the buffer through a barrier film, which covers the outer surface of the silica particles. Within this surface layer the current velocity of the substrate and coenzyme molecules becomes decelerated. Thus, the mass transport can be hindered due to film or diffusional resistance and result in a decrease of substrate or coenzyme affinity.[58, 139, 149, 187, 188] Moreover, microenvironmental effects can play a decisive role. In accordance to the surface properties of the host material, buffer salts can enrich within the porous structure, resulting in divergent salt concentration compared to the bulk buffer and correspondingly to a different pH value within the pores. Interactions between substrate or coenzyme molecules and the silica surface, covered with organic residues, can compete with the active center or the coenzyme binding sites of the enzyme, thus leading to an influence on the affinities, too.[58, 62, 69, 139, 184, 188] In order to elaborate these effects for the immobilized *G.s.*6PGDH, Michaelis-Menten kinetics were investigated employing the oxidation of 6PG to Ru5P with concomitant reduction of $NADP^+$ to NADPH. In a first step, the concentration of 6PG was varied, while keeping the $NADP^+$ constant. In a second step the $NADP^+$ concentration was varied, while providing a constant concentration of 6PG. The initial reaction rate ($v_0$) was detected over a period of 1 min at 25 °C (potassium phosphate buffer solution, 50 mM, pH 6.5). Moreover, the Michaelis-Menten constant of the substrate ($K_{m,\,6PG}$) and the coenzyme ($K_{m,\,NADP^+}$), the maximum reaction rate ($v_{max}$) as well as the dissociation rate ($k_{cat}$) of the enzyme substrate complex and finally the enzymatic efficiency (EE) of the immobilized *G.s.*6PGDH were determined and compared to the values obtained for the free enzyme (Table 11). For the calculation of $v_{max}$ as well as $K_m$, a linearization of the Michaelis-Menten plot is indispensable (Figure 57). Here the Lineweaver-Burk plot was applied. The Lineweaver-Burk plot is a double reciprocal plot of the substrate or coenzyme concentration and the initial reaction rate ($v_0$). The y intercept of the regression line gives the reciprocal of $v_{max}$, whereas the slope is characterized by the ratio of $K_m$ and $v_{max}$ (Figure 57, Appendix 7.5).[139, 140]

The Michaelis-Menten constant $K_m$ is defined as the respective substrate or coenzyme concentration that induces, under certain reaction conditions (pH, temperature, ionic strength, etc.), a half-maximum reaction rate of the enzyme (Eq. 10). For free enzymes $K_m$ can be considered as the affinity of an enzyme towards its substrate or coenzyme. Low $K_m$ values indicate a high substrate or coenzyme affinity and vice versa. However, a high rate of the decomposition of the

[187] V. Kasche, *Enzyme Microb. Technol.* **1983**, *5*, 2-13.
[188] A. Liese, L. Hilterhaus, *Chem. Soc. Rev.* **2012**, *42*, 6236-6249.

enzyme substrate complex also results in a high $K_m$ value. Thus, $K_m$ is not necessarily appropriate to make statements concerning substrate or coenzyme affinities.[139, 140] When elaborating $K_m$ values of immobilized enzymes it has to be kept in mind that the obtained $K_m$ values are apparent values, as the diffusion of the substrate or coenzyme to the immobilized *G.s.*6PGDH can strongly be influenced by the texture of the host material's surface. In the case of high substrate/coenzyme concentrations, the enzyme kinetics are almost unaffected, as limitations of the mass transport are negligible. However, in the presence of merely low substrate or coenzyme concentrations, the kinetics of the immobilized enzyme are distinctly dependent on the mass transport.[139] Therefore, $K_m$ of an immobilized enzyme combines diffusion resistance of substrate/coenzyme molecules to the immobilized enzyme and an altered substrate/coenzyme affinity of the immobilized enzyme due to structural changes affected by immobilization.

**Table 11.** Overview of the kinetic parameters of the free *G.s.*6PGDH as well as of *G.s.*6PGDH immobilized onto MCF-$C_x$ and MCF-$C_x$-$NH_2$.

| sample | $K_{m\ 6PG}$ [µM] | $K_{m\ NADP^+}$ [µM] | $v_{max}$ [µmol $L^{-1}$ $min^{-1}$] | $k_{cat}$ [$s^{-1}$] | EE [$s^{-1}$ (µmol $L^{-1}$)$^{-1}$] |
|---|---|---|---|---|---|
| **native *G.s.*6PGDH** | 82.2 | 3.4 | 51.4 | 22.1 | $269 \cdot 10^9$ |
| **MCF-$C_3$-*E*** | 205 | 14 | 2.32 | 1.03 | $5.04 \cdot 10^9$ |
| **MCF-$C_5$-*E*** | 95.5 | 36 | 6.16 | 3.04 | $31.8 \cdot 10^9$ |
| **MCF-$C_7$-*E*** | 134 | 19 | 3.22 | 1.88 | $14.0 \cdot 10^9$ |
| **MCF-$C_{11}$-*E*** | 214 | 13 | 2.32 | 0.517 | $2.41 \cdot 10^9$ |
| **MCF-$C_3$-$NH_2$-*E*** | 102 | 15 | 3.76 | 2.11 | $20.7 \cdot 10^9$ |
| **MCF-$C_5$-$NH_2$-*E*** | 92.9 | 20 | 6.60 | 3.25 | $35.0 \cdot 10^9$ |
| **MCF-$C_7$-$NH_2$-*E*** | 154 | 19 | 5.40 | 3.63 | $23.6 \cdot 10^9$ |
| **MCF-$C_{11}$-$NH_2$-*E*** | --- | --- | --- | --- | --- |

$K_{m,\ 6PG}$ for the free *G.s.*6PGDH was calculated to be 82.2 µM, whereas $K_{m,\ NADP^+}$ amounts to 3.4 µM. These values are the least compared to the respective $K_m$ values obtained for the immobilized enzyme (Table 11). Initially, this indicates an influence of the immobilization on the enzyme's substrate/coenzyme affinity or rather diffusional restrictions of these molecules from the bulk buffer solution into the porous network of MCF until finally reaching the binding sites of the immobilized enzyme. $K_{m,\ 6PG}$ of the immobilized *G.s.*6PGDH is up to 2.5-fold higher compared to

the free enzyme. The $K_{m,\ 6PG}$ values decrease from MCF-$C_3$-$NH_2$-*E* (102 µM)/MCF-$C_3$-*E* (205 µM) to MCF-$C_5$-$NH_2$-*E* (92.9 µM)/MCF-$C_5$-*E* (95.5 µM), however, in the further course $K_{m,\ 6PG}$ increases with increasing chain length independent of the existence of an amino group. Thus, the lowest $K_{m,\ 6PG}$ value, about 13/16 % higher compared to the free enzyme, was determined for MCF-$C_5$-$NH_2$-*E* (92.9 µM) and MCF-$C_5$-*E* (95.5 µM). Except MCF-$C_7$-$NH_2$-*E* (154 µM), $K_{m,\ 6PG}$ of *G.s.*6PGDH immobilized onto the amino functionalized materials were generally lower compared to *G.s.*6PGDH immobilized onto the alkyl modified MCFs. Regardless of the existence of an terminal amino group on the silica surface, the carbon chain length obviously has an impact on $K_{m,\ 6PG}$. The $K_{m,\ 6PG}$ values of *G.s.*6PGDH, immobilized *via* carbon chains containing three, seven or eleven carbon atoms, are considerably higher than obtained for free *G.s.*6PGDH. Hence, a chain length of five carbon atoms is recommendable for the immobilization of *G.s.*6PGDH, as the substrate affinity has only been slightly reduced or rather diffusional restrictions or a possible unbefitting orientation of the active site are negligible.

In contrast, $K_{m,\ NADP^+}$ is 4- to 10-fold higher than for the free enzyme. The lowest $K_{m,\ NADP^+}$ value was observed for MCF-$C_{11}$-*E* (13 µM), though the divergence from $K_{m,\ NADP^+}$ of the free enzyme is 382 %. No correlation between the chain length of the organic residues on the silica surface as well as the existence of an amino function could be ascertained. The comparatively high $K_{m,\ NADP^+}$ values indicate significant diffusion resistance of $NADP^+$ into the porous network, but also attractive interactions of the coenzyme and the functionalized pore walls are likely. Fried *et al.* proposed electrostatic interactions between the negatively charged phosphate atom of $NADP^+$ and positively charged nitrogen atoms of the aminoalkyl modified MCFs resulting in an immobilization of the coenzyme.[184] This aspect gains in importance with increasing hydrophilicity of the host material. However, by way of comparison, the total amount of $NADP^+$ adsorbed onto the positively charged surface of MCF-$C_x$-$NH_2$ was assumed to be rather low. In fact the immobilization of *G.s.*6PGDH can also be affected by amino acids of the coenzyme binding site and thus limiting the $NADP^+$ fixation. Hence, the access to the coenzyme binding site can be restrained due to its possible orientation in direction to the pore walls.

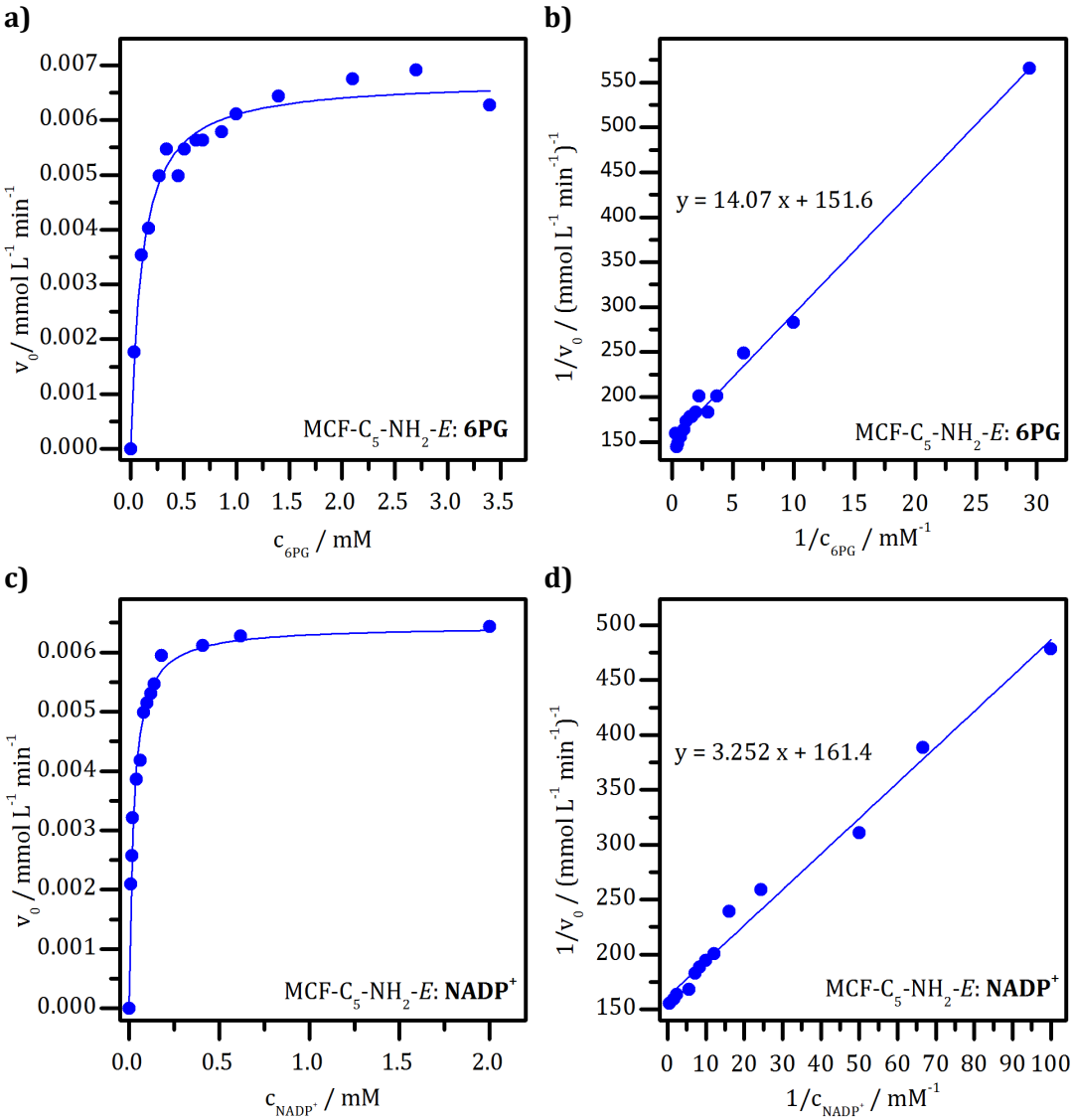


**Figure 57.** Exemplary depiction of the Michaelis-Menten and Lineweaver-Burk plots of *G.s.*6PGDH immobilized onto MCF-$C_5$-$NH_2$ with varied concentrations of 6PG (**a)** and **b)**) or $NADP^+$ (**c)** and **d)**) at 25 °C. All further Michaelis-Menten as well as Lineweaver-Burk plots can be found in the appendix (Appendix 7.5).

Assuming that all enzyme molecules are bound in the enzyme substrate complex within the steady-state, $v_{max}$ can be calculated (Eq. 9). A further increase of the substrate or coenzyme concentration would not yield in an increase of $v_{max}$ (Figure 57).[139, 140] Discussing the enzyme immobilized onto the alkyl modified MCFs, $v_{max}$ increases from MCF-$C_3$–*E* (2.32 µmol $L^{-1}$ $min^{-1}$) to MCF-$C_5$-*E* (6.16 µmol $L^{-1}$ $min^{-1}$) and further decreases for MCF-$C_7$-*E* (3.22 µmol $L^{-1}$ $min^{-1}$) and MCF-$C_{11}$-*E* (2.32 µmol $L^{-1}$ $min^{-1}$; Table 11). A similar development of $v_{max}$ was obtained when using the aminoalkyl modified MCFs as hosts. *G.s.*6PGDH immobilized on the surface of these materials possesses a higher reaction rate than the enzyme immobilized onto the alkyl functionalized materials. Here again,

MCF-$C_5$-$NH_2$-*E* (6.60 µmol $L^{-1}$ $min^{-1}$) and MCF-$C_5$-*E* (6.16 µmol $L^{-1}$ $min^{-1}$) displayed the highest $v_{max}$, respectively. However, it has not to be concealed that $v_{max}$ of the free enzyme in stock solution was calculated to amount to 51.4 µmol $L^{-1}$ $min^{-1}$ and is appropriately much higher than the values determined for the immobilized enzymes. An important reason for these observations can be found in diffusional restrictions of 6PG and $NADP^+$. Furthermore, the release of Ru5P as well as NADPH after conversion can be hindered. These hindrances can be attributed to an inappropriate orientation of the immobilized enzyme in the porous network of MCF. Potentially, the substrate and/or coenzyme binding sites can be orientated towards the pore walls impeding the release of the product and/or reduced coenzyme. Furthermore, $v_{max}$ can be affected by comprehensive time-spreading of the immobilized *G.s.*6PGDH. Time-spreading is mostly accompanied by a creeping denaturation of the immobilized enzyme (Figure 15). Hence, it is associated with the restricted ability to fix the substrate or coenzyme within the respective binding sites.

The rate-determining step of an enzymatic reaction is the decay of the enzyme substrate complex, which is characterized by the rate constant $k_{cat}$, also known as the turnover-number. The higher $k_{cat}$, the higher the number of substrate molecules converted per second and active site (Eq. 11).[140] One active center of the free *G.s.*6PGDH oxidizes 22.1 6PG molecules per second. Again, the $k_{cat}$ values of *G.s.*6PGDH immobilized onto the aminoalkyl modified MCFs are higher than the ones determined for the enzyme immobilized onto the respective alkyl modified MCFs (Table 11). This can be referenced to the higher $v_{max}$ values, as $k_{cat}$ is defined by the ratio of $v_{max}$ and the enzyme concentration. On closer examination, the $k_{cat}$ values of MCF-$C_3$-$NH_2$-*E* (2.11 $s^{-1}$) and MCF-$C_7$-$NH_2$-*E* (3.63 $s^{-1}$) are twice as high as calculated for the respective alkyl modified MCFs (MCF-$C_3$-*E*: 1.03 $s^{-1}$; MCF-$C_7$-*E*: 1.88 $s^{-1}$). This indicates a considerably faster decay of the enzyme substrate complex for the enzyme immobilized onto these aminoalkyl modified MCFs, accompanied by a fast release of Ru5P and NADPH from the respective binding sites. The $k_{cat}$ values of MCF-$C_5$-$NH_2$-*E* (3.25 $s^{-1}$) and MCF-$C_5$-*E* (3.04 $s^{-1}$) differ only by 7 %, illustrating only a slight influence of the amino group at a chain length of five carbon atoms on the enzyme kinetics.

The enzyme efficiency (EE) is the most meaningful kinetic parameter of an enzyme, as it describes the catalytic efficiency expressed as quotient of $k_{cat}$ and $K_m$. The higher EE, the higher the catalytic efficiency (Eq. 12).[140] As $k_{cat}$ and $K_m$ depend on $v_{max}$, the same regularities for EE were observed than obtained for $v_{max}$. Hence, *G.s.*6PGDH immobilized onto the aminoalkyl functionalized silicas shows higher EE

values than determined for the enzyme on the respective alkyl modified hosts. MCF-$C_5$-$NH_2$-*E* reveals the highest EE ($35.0 \cdot 10^9$ $s^{-1}(\mu mol\ L^{-1})^{-1}$) of all immobilized enzyme samples (Table 11). However, this value corresponds to only 13 % of the catalytic efficiency of the free enzyme meaning immobilization has a strong impact on the catalytic efficiency of *G.s.*6PGDH.

**Intermediate summary.** With regard to the kinetic data ($v_{max}$, $K_m$) MCF-$C_5$-*E* as well as MCF-$C_5$-$NH_2$-*E* displayed best kinetic conditions for usage as host materials for *G.s.*6PGDH immobilization with respect to its utilization in a modular enzyme cascade (Table 11, Figure 58).

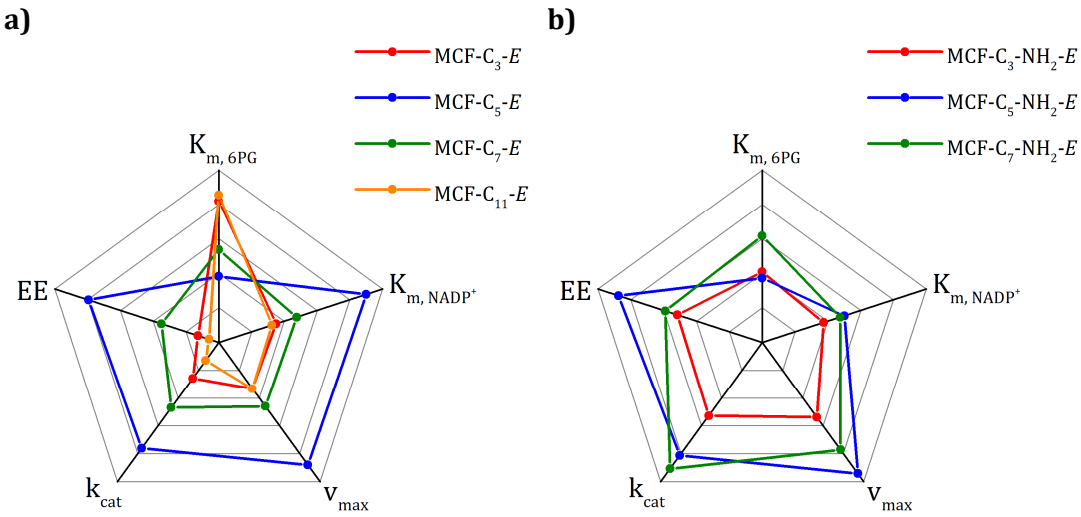


**Figure 58.** Spider charts of the calculated kinetic parameters obtained for the *G.s.*6PGDH immobilized onto **a)** MCF-$C_x$ as well as **b)** MCF-$C_x$-$NH_2$. The scaling is the same for both charts. The respective absolute values of the kinetic parameters can be found in Table 11.

Obviously, a carbon chain length of five carbon atoms on the host material's surface is most eligible to ensure ideal kinetic behavior of the immobilized *G.s.*6PGDH. To some extend this can be refined by using aminopentyl instead of pentyl residues, as immobilization via aminoalkyl residues exhibited slightly better kinetic results. However, the catalytic efficiency of *G.s.*6PGDH immobilized via (amino)propyl or (amino)heptyl as well as undecyl residues is considerably lower, implying immobilization via (amino)pentyl residues ensures an optimal distance between the protein and the pore walls and thus best conditions for the diffusion of 6PG and $NADP^+$ to the respective binding sites.

### 4.2.3 Immobilization of *G.s.*6PGDH: Summary

Grafting of MCF by using aminoalkyltrialkoxysilanes as well as alkyltrialkoxysilanes, consisting of different carbon chain lengths, led to host materials which were successfully employed for the adsorptive immobilization of *G.s.*6PGDH. Addressed to the surface amino groups of the aminoalkyl functionalized MCFs, these materials possess a positively charged surface at the pH of the immobilization (pH 6.5), whereas the surface of the alkyl modified MCFs is negatively charged at pH 6.5, which is attributed to the remaining silanol groups on the surface of these host materials. However, experiments confirmed that solely hydrophobic interactions contribute to the immobilization of *G.s.*6PGDH onto these materials (Figure 59). In addition, a significant excess of (amino)alkyl residues on the surface of the modified MCFs related to the respective *G.s.*6PGDH uptakes was confirmed. With respect to the activity retention after 24 h of immobilization, an enzyme to host ratio of 1:10 turned out to be ideal.

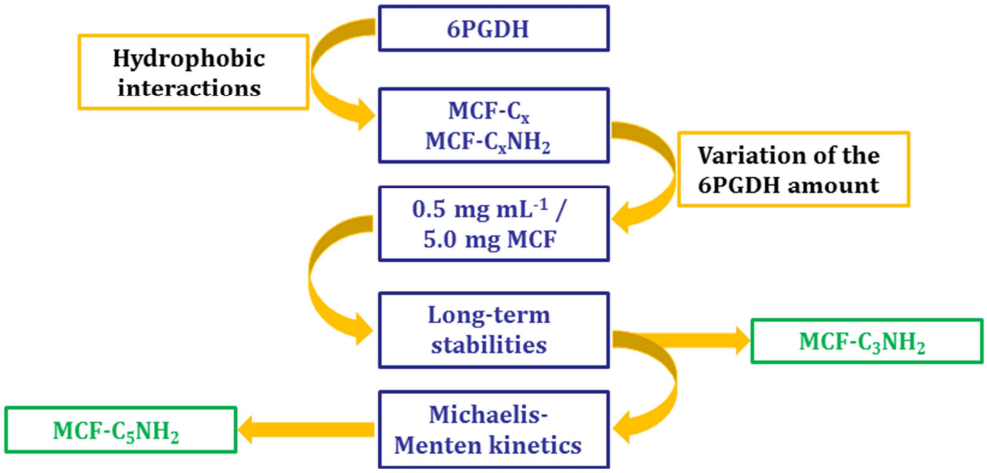


**Figure 59.** Graphical summary of the parameters that were investigated concerning the immobilization of *G.s.*6PGDH onto MCF-$C_x$ as well as MCF-$C_x$-$NH_2$. The immobilization was exclusively governed by hydrophobic interactions. By the variation of the initial *G.s.*6PGDH amount employed for immobilization, an enzyme to host ratio of 1:10 was proven. With regard to the long-term stability of the immobilized *G.s.*6PGDH, an immobilization onto MCF-$C_3$-$NH_2$ is preferable. If the focus is placed on the kinetic behavior of the enzyme, an immobilization onto MCF-$C_5$-$NH_2$ is recommendable.

The retained enzymatic activity after 24 h of immobilization was highest for MCF-$C_3$-$NH_2$-*E* and MCF-$C_3$-*E*. In general, the activity retention reflects a dependency on the carbon chain length of the modified MCFs and thus the hydrophobicity of the support. The retained activity was the higher, the shorter the carbon chain on the surface of the support and, hence, the lower its hydrophobicity. Furthermore, the

long-time stability of the immobilized *G.s.*6PGDH was investigated over a period of 53 days. The enzymatic activity of all samples was reduced in the same extend over this period. However, the activity of the enzyme immobilized onto the aminoalkyl modified MCFs was slightly higher as of the enzyme immobilized onto the respective alkyl functionalized MCFs. Likewise, Michaelis-Menten kinetics of the immobilized enzyme were affected by the immobilization. A decrease of the substrate as well as coenzyme affinity accompanied by diffusional resistance into the porous network for the immobilized *G.s.*6PGDH, expressed in an increase of $K_{m,\,6PG}$ and $K_{m,\,NADP^+}$, was observed. Moreover, the $v_{max}$, $k_{cat}$ and EE values were reduced compared to the free enzyme. However, these parameters were slightly better for the enzyme immobilized onto the aminoalkyl functionalized MCFs. Under kinetic aspects, immobilization onto MCF-$C_5$ and MCF-$C_5$-$NH_2$ has to be preferred. With respect to an optimal long-term stability of the immobilized, *G.s.*6PGDH MCF-$C_3$-$NH_2$ represents a preferable host. Regarding the incorporation of the immobilized enzyme into the aspired modular enzyme cascade, MCF-$C_3$-$NH_2$ and MCF-$C_5$-$NH_2$ were selected for the short list.

### 4.3 Immobilization of 6PGDH from *Saccharomyces cerevisiae* (*S.c.*6PGDH)

The *G.s.*6PGDH, which was used so far for the immobilization onto MCF-$C_x$ as well as MCF-$C_x$-$NH_2$ with respect to its incorporation in a multienzyme cascade, was provided from the research group of Professor Andreas Liese from the *Hamburg University of Technology* (TUHH). In 2016 it was suddenly no longer available. However, an immobilized 6PGDH was indispensable to realize the aimed enzyme cascade (Figure 37). Hence, it was necessary to resort to a commercially available 6PGDH from *Saccharomyces cerevisiae* from *Sigma-Aldrich* (Figure 60). As the immobilized enzyme was intended to participate in a modular enzyme cascade employing the second and the third reaction step of the pentose phosphate pathway accompanied by a coenzyme recycling step, it was mandatory to recap the most important experiments concerning the immobilized *S.c.*6PGDH. Correspondingly, it was essential to recapitulate the investigations regarding the long-term stability and the Michaelis-Menten kinetics of the immobilized *S.c.*6PGDH.

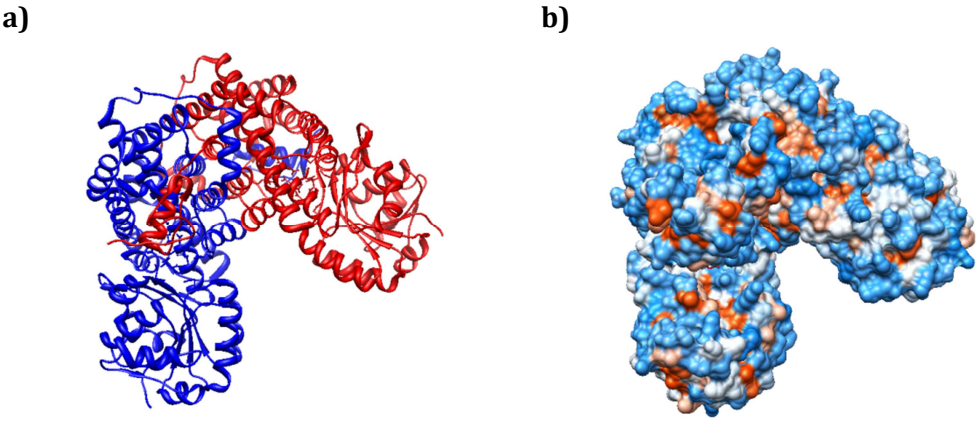


**Figure 60.** Graphical depiction of *S.c.*6PGDH (PDB ID: 2P4Q): a) Ribbon model: Monomer A (red) and monomer B (blue); b) Surface mapping: Hydrophilic surface areas (blue) and hydrophobic areas (red).[27]

*S.c.*6PGDH is a homodimeric oxidoreductase composed of two monomeric units (Figure 60a). Each monomer consists of 476 amino acids and its molecular weight amounts 56 kDa.[189] The pI of *S.c.*6PGDH is at pH 6.5 and its diameter was measured to be 14.7 nm. Compared to *G.s.*6PGDH, the surface of S.c.6PGDH is likewise created by predominantly hydrophilic amino acids (Figure 60b). The immobilization of *S.c.*6PGDH was carried out onto the surface of MCF-$C_3$-$NH_2$, as the best long-term stability was obtained when using this material for the immobilization of *G.s.*6PGDH (Table 12).

**Table 12.** Overview of the material properties of MCF-$C_3$-$NH_2$ employed for the immobilization of *S.c.*6PGDH.

| sample | $S_{BET}$ [$m^2 g^{-1}$] | $V_P$ [$cm^3 g^{-1}$] | $D_p$ [nm] | $\rho_f$ [mmol $g^{-1}$] | pI |
|---|---|---|---|---|---|
| **MCF-$C_3$-$NH_2$** | 360 | 2.30 | 23 | 1.2 | 8.4 |

The amino acid sequence of *S.c.*6PGDH is similar to that of *G.s.*6PGDH; thus, hydrophobic interactions between the surface of the enzyme and the functionalized MCF were assumed.[28, 189]

**Uptake and long-term-stability.** The immobilization procedure of *S.c.*6PGDH rested upon on the same procedure applied for the immobilization of *G.s.*6PGDH (phosphate buffer solution, 50 mM, pH 6.5, 25 °C, 24 h).

[189] W. He, Y. Wang, W. Liu, C.-Z. Zhou, *BMC Structural Biology* **2007**, *7*(38), 1-9.

The immobilization of *S.c.*6PGDH onto MCF-$C_3$-$NH_2$ proceeded very fast and was completed after 10 min (Figure 61a) but it resulted in an absolute uptake of only 25.7 % (Table 13). This value is considerably lower than the value obtained for the immobilization of *G.s.*6PGDH onto the same host (79.4 %). This observation can be attributed to a faster immobilization of *S.c.*6PGDH in comparison to *G.s.*6PGDH (Figure 61a). In terms of *S.c.*6PDH, the maximum uptake (25.7 %) was reached after ~10 min of immobilization, whereas the immobilization of *G.s.*6PGDH was completed after ~30 min (79.4 %). Generally, a fast immobilization is accompanied by the attachment of enzyme molecules onto the outer regions of the pores.[66, 151] This circumstance results in blocked pore entrances and the diffusion of further enzyme molecules into the porous host is unfeasible. Thus, a rapid immobilization of an enzyme comes along with lower enzyme uptakes. According to the uptakes, the appropriate percentage by weight regarding the immobilization of *S.c.*6PGDH is lower (2.3 wt-%), too. However, the activity retention of *S.c.*6PGDH after 24 h of immobilization amounted to 74 %, whereas the retained activity of the immobilized *G.s.*6PGDH was distinctly lower (56 %). This observation can be referenced to the low uptake of *S.c.*6PGDH onto MCF-$C_3$-$NH_2$. The higher enzymatic activity of the immobilized *S.c.*6PGDH can be traced back to its adsorptive immobilization close to the pore entrances. Hence, diffusion limitations of substrate/coenzyme molecules are of no consequence.[66, 151] Furthermore, due to the low enzyme loading, each immobilized enzyme molecule possesses a sufficient area of freedom to undergo conformational changes within catalysis. These effects are reflected by the activity retention after 24 h of immobilization.

**Table 13.** Comparison of the immobilization properties of *G.s.* and *S.c.*6PGDH onto MCF-$C_3$-$NH_2$.

| MCF-$C_3$-$NH_2$ | uptake [%] | activity retention [%] | percentage by weight [wt-%] |
|---|---|---|---|
| ***G.s.*6PGDH** | 79.4 | 56 | 7.1 |
| ***S.c.*6PGDH** | 25.7 | 74 | 2.3 |

To further compare the immobilized *G.s.6PGDH* to the *S.c.*6PGDH, the long-term stabilities of the immobilized enzymes were examined (Figure 61). The remained activity immediately after 24 h of immobilization was set to 100 % and the decrease of the activity was monitored over a period of six days, respectively. It is

obvious that within the first six days after immobilization the activity of the immobilized *G.s.*6PGDH subsided markedly. During this time, 75 % of the origin activity was lost. Conversely, the enzymatic activity of the immobilized *S.c.*6PGDH decreased very slowly within the first five days, prior to a significant descent six days after immobilization. At least, 45 % of the origin activity remained even six days after immobilization. Consequently, the enzymatic activity of the immobilized *S.c.*6PGDH was considerably higher than the remained activity of the immobilized *G.s.*6PGDH after a period of six days. By reason of these results, it was unproblematic or rather advantageous to replace *G.s.*6PGDH by *S.c.*6PGDH.

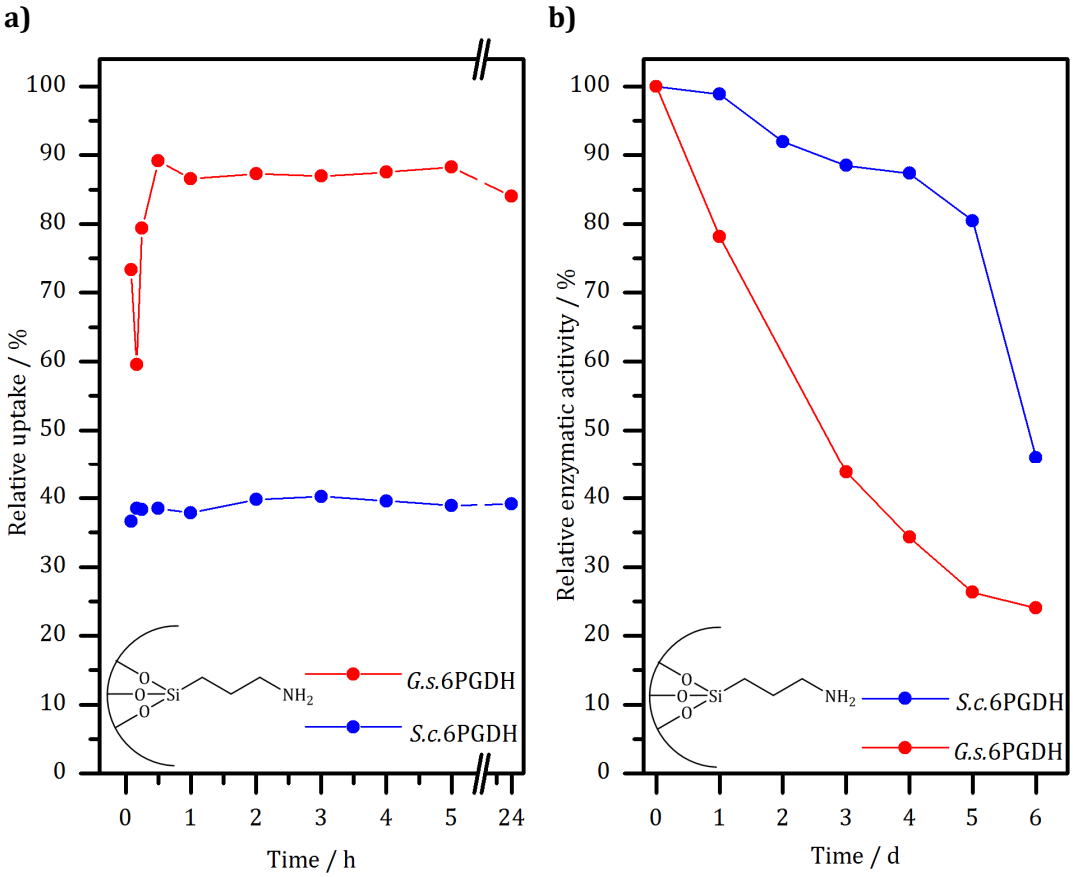


**Figure 61. a)** Comparative representation of the relative uptakes of *G.s.* as well as *S.c.*6PGDH onto MCF-$C_3$-$NH_2$. **b)** Comparative depiction of the relative enzymatic activities of *G.s.* and *S.c.*6PGDH immobilized onto MCF-$C_3$-$NH_2$ over a period of 6 days. The retained activity immediately after 24 h of immobilization was set to 100 %, respectively (day 0). The relative activity of the immobilized *S.c.*6PGDH was considerably higher in contrast to the relative activity of the immobilized *G.s.*6PGDH.

**Michaelis-Menten kinetics.** Of course it was very important to additionally elaborate the Michaelis-Menten kinetics of the native and in particular of the

immobilized *S.c.*6PGDH. The received results were compared to the data obtained for the free as well as the immobilized *G.s.*6PGDH (Table 14).

$K_{m,\,6PG}$ (282 µM) and $K_{m,\,NADP^+}$ (17.4 µM) of the immobilized *S.c.*6PGDH are significantly lower than the $K_m$ values of the free *S.c.*6PGDH ($K_{m,\,6PG}$ = 328 µM; $K_{m,\,NADP^+}$ = 96.5 µM). Thus, minor substrate and coenzyme concentrations are required to preserve a half-maximum reaction rate of the immobilized enzyme, in contrast to the free enzyme. In this case, immobilization had a benefitting impact on the substrate as well as the coenzyme affinity and diffusional restrictions were apparently non-existent. However, $v_{max}$ of the immobilized *S.c.*6PGDH was reduced by nearly 90 % (12.0 µmol $L^{-1}$ $min^{-1}$) with respect to $v_{max}$ of the free *S.c.*6PGDH (108 µmol $L^{-1}$ $min^{-1}$). As the substrate/coenzyme affinity of the immobilized enzyme was increased and $v_{max}$ decreased, it has to be assumed that the release of Ru5P or NADPH after catalysis is hindered. This is attributed to a disadvantageous orientation of the immobilized *S.c.*6PGDH on the pore walls of MCF-$C_3$-$NH_2$.

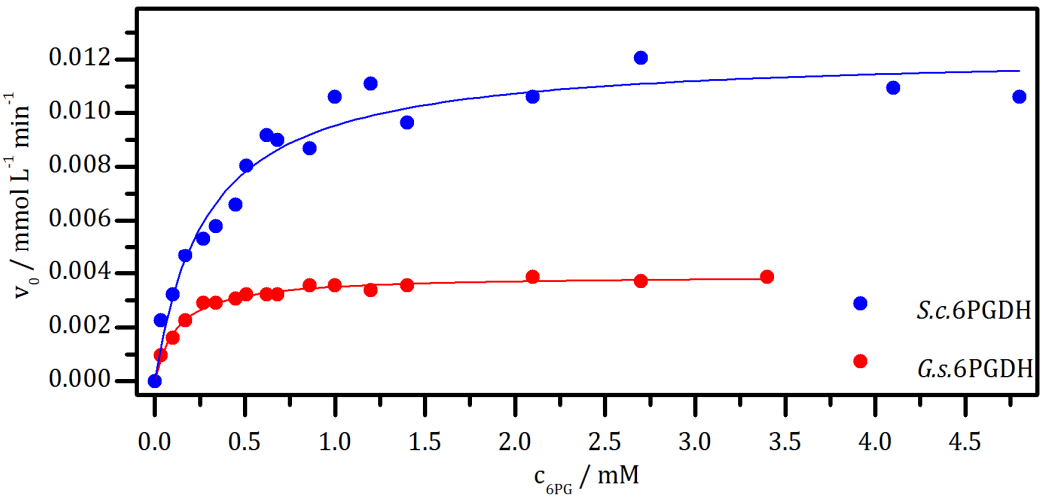


**Figure 62.** Comparison of the Michaelis-Menten diagrams of *S.c.*6PGDH and *G.s.*6PGDH immobilized onto MCF-$C_3$-$NH_2$, respectively. It illustrates that $v_{max}$ of the immobilized *S.c.*6PGDH is distinctly higher compared with $v_{max}$ of the immobilized *G.s.*6PGDH. All further Michaelis-Menten as well as Lineweaver-Burk plots can be found in the appendix (Appendix 7.6).

$v_{max}$ of the immobilized *S.c.*6PGDH has indeed decreased in comparison to $v_{max}$ of the free S.c.6PGDH; but, at a second glance, it is almost threefold higher than $v_{max}$ of the immobilized *G.s.*6PGDH (3.76 µmol $L^{-1}$ $min^{-1}$; Figure 62).

**Table 14.** Comparison of the enzyme kinetic parameters of *G.s.* as well as *S.c.*6PGDH immobilized onto MCF-$C_3$-$NH_2$.

| | $K_{m,\ 6PG}$ [µM] | $K_{m,\ NADP^+}$ [µM] | $v_{max}$ [µmol $L^{-1}$ $min^{-1}$] | $k_{cat}$ [$s^{-1}$] | EE [$s^{-1}$ (µmol $L^{-1}$)$^{-1}$] |
|---|---|---|---|---|---|
| **MCF-$C_3$-$NH_2$** | | | | | |
| *G.s.*6PGDH | 102 | 15 | 3.76 | 2.11 | $20.7 \cdot 10^9$ |
| *S.c.*6PGDH | 282 | 17.4 | 12.0 | 30.6 | $109 \cdot 10^9$ |
| **native 6PGDH** | | | | | |
| *G.s.*6PGDH | 82.2 | 3.4 | 51.4 | 22.1 | $269 \cdot 10^9$ |
| *S.c.*6PGDH | 328 | 96.5 | 108 | 59.5 | $181 \cdot 10^9$ |

The decay of the enzyme-substrate complex of the carrier bound *S.c.*6PGDH, which is characterized by $k_{cat}$, was simply reduced by 50 % (30.6 $s^{-1}$ vs. 59.5 $s^{-1}$), whereas EE at least amounts 60 % of the free *S.c.*6PGDH ($109 \cdot 10^9$ $s^{-1}$ (µmol $L^{-1}$)$^{-1}$ vs. $181 \cdot 10^9$ $s^{-1}$ (µmol $L^{-1}$)$^{-1}$). Despite the lower $v_{max}$ value of the immobilized *S.c.*6PGDH, in contrast to the native *S.c.*6PGDH, the results of $k_{cat}$ and EE are quite promising.

With exception of $K_{m,\ NADP^+}$ of the immobilized *S.c.*6PGDH, the further $K_m$ values of the free as well as the immobilized *S.c.*6PGDH are higher in comparison to the respective $K_m$ values of the *G.s.*6PGDH. This implies a higher substrate and coenzyme affinity of the free/immobilized *G.s.*6PGDH. However, $v_{max}$, $k_{cat}$ and EE of the free/immobilized *S.c.*6PGDH are considerably higher compared to the free/immobilized *G.s.*6PGDH. This once again confirms the advantageous replacement of *G.s.*6PGDH by *S.c.*6PGDH.

**Intermediate summary.** Due to the lack of further *G.s.*6PGDH, it was necessary to resort to *S.c.*6PGDH, as an immobilized 6PGDH was essential to realize the aspired enzyme cascade. Thus, studies concerning the long-term stability and the Michaelis-Menten kinetics of the immobilized *S.c.*6PGDH were required. It figured out that the immobilization of *S.c.*6PGDH onto MCF-$C_3$-$NH_2$ yielded in a better long-term stability of the immobilized enzyme in comparison to the immobilized *G.s.*6PGDH. This can be referenced to a lower enzyme loading in terms of the immobilized *S.c.*6PGDH, associated with the possibility to undergo unhindered conformational changes within the catalytic conversion of 6PG. Moreover, the immobilization of *S.c.*6PGDH was assumed to be carried out primarily on the outer regions of the pores. Hence, diffusion restrictions were presumed to be negligible. Additionally, the maximum reaction rate of the immobilized *S.c.*6PGDH was detected

to be much higher than $v_{max}$ calculated for the immobilized *G.s.*6PGDH. Hence, the immobilized *S.c.*6PGDH is well suited to be alternatively incorporated into the introduced enzyme cascade.

### 4.4 Immobilization of ADH from *Escherichia coli* (*E.c.*ADH)

Parts of this chapter have already been published.[190]

Among the conversion of G6P to Ru5P and $CO_2$, the first two reaction steps of the aimed modular enzyme cascade are characterized by the reduction of two equivalents $NADP^+$ to NADPH (Figure 37). Within a third reaction step, it was requested to re-oxidize these amounts of NADPH to $NADP^+$. This cofactor recycling step was implemented by an immobilized $NADP^+$/H dependent ADH. ADH catalyzes the oxidation of 2-propanol to acetone with concomitant reduction of $NADP^+$ to NADPH (forward reaction). Generally, enzymes are additionally able to catalyze the respective back reaction. Hence, ADH likewise catalyzes the reduction of acetone to 2-propanol accompanied by the oxidation of NADPH to $NADP^+$.[2] The utilization of an immobilized ADH concerning the recycling of $NADP^+$ or NADPH is very attractive, as a high-grade coenzyme can be regenerated by a simple employment of a low-cost bulk chemical like 2-propanol or acetone.

In the first instance, it was indispensable to carefully investigate the ADH in terms of its immobilization. As the immobilization of 6PGDH onto the surface of MCF-$C_3$-$NH_2$ was very promising in terms of its long-term stability as well as its Michaelis-Menten kinetics, the immobilization of ADH was conducted on the surface of this material, too. Besides, the immobilization was additionally carried out onto pristine MCF to prove or disprove the necessity of a surface functionalization. As the immobilization of ADH is impossible at its pI (pH = 6.1), because the enzyme crystallizes at that pH, several pH values were on trial to verify the ideal pH of the immobilization. Furthermore, the ADH to MCF-$C_3$-$NH_2$ ratios in the immobilization procedure were varied in order to determine the most suitable MCF-$C_3$-$NH_2$ amount necessary for the immobilization. The loading capacities as well as the long-term stabilities regarding the forward as well as the back reaction were compared, respectively.

The surface of the ADH is likewise composed by mostly hydrophilic amino acids, suggesting polar interactions between the surface of the enzyme and the surface of MCF-$C_3$-$NH_2$ (Figure 9b). Nevertheless, the dominating interactions were investigated in detail.

[190] M. Dreifke, F. J. Brieler, M. Fröba, *ChemCatChem* **2017**, *9*, 1148-1163.

As the ADH-catalyzed reduction of acetone to 2-propanol with concomitant re-oxidation of NADPH to $NADP^+$ was intended to be incorporated as the cofactor recycling step in the enzyme cascade, an extensive investigation of the Michaelis-Menten kinetics of the native as well as of the immobilized enzyme was conducted. It had to be assured that the cofactor recycling step is the fastest reaction step within the enzyme cascade in order to avoid a lack of $NADP^+$.

### 4.4.1 Characteristics of the immobilization of ADH

The immobilization of ADH was carried out onto the surface of MCF-$C_3$-$NH_2$, as this host material turned out as a suitable or rather beneficial host for G6PDH as well as 6PGDH (Table 15).

**Table 15.** Overview of the material properties of MCF and MCF-$C_3$-$NH_2$ employed for the immobilization ADH.

| sample | $S_{BET}$ [$m^2 g^{-1}$] | $V_P$ [$cm^3 g^{-1}$] | $D_p$ [nm] | $\rho_f$ [mmol $g^{-1}$] | pI |
|---|---|---|---|---|---|
| **MCF** | 528 | 2.8 | 24 | --- | 3.7 |
| **MCF-$C_3$-$NH_2$** | 346 | 2.1 | 22 | 1.4 | 8.4 |

Frequently, the immobilization of an enzyme is performed at its pI in order to prevent electrostatic interactions between the enzyme molecules itself. However, the immobilization of ADH at its pI (pH 6.1) is not possible, as the enzyme crystallizes at that pH. The crystallization can be addressed to the association of hydrophobic surface areas of the protein, accompanied by a decrease of the water solubility and followed by a precipitation of the enzyme.[139] Thus, several pH values (potassium phosphate buffer, 50 mM, pH 6.5/7.0/7.5) were evaluated as the possible immobilization pH. In addition, the amount of MCF-$C_3$-$NH_2$ provided for immobilization was varied from 6.7 mg over 10 mg up to 20 mg while always applying 1 mL of a 2 mg $mL^{-1}$ buffered ADH solution. Thus, the ADH proportion employed for immobilization amount to 10 % when using 20 mg MCF-$C_3$-$NH_2$, 20 % when applying 10 mg of the host material and 30 % when providing 6.7 mg of the carrier. Frequently, an enzyme proportion of average 10 % can be found in the literature as the most suitable enzyme amount for immobilization.[191, 192, 193] For

[191] M. Vittorini, E. Dumitriu, G. Barletta, F. Secundo, *Bioprocess Biosyst. Eng.* **2011**, *34*, 247-251.
[192] D.I. Fried, K. Tropp, M. Fröba, *ChemCatChem* **2013**, *5*, 931-938.
[193] A. Schlossbauer, D. Schaffert, J. Kecht, E. Wagner, T. Bein, *J. Am. Chem. Soc.* **2008**, *130*, 12558-12559.

each pH value and each ADH proportion, the uptake after 24 h of immobilization was monitored (Figure 63).

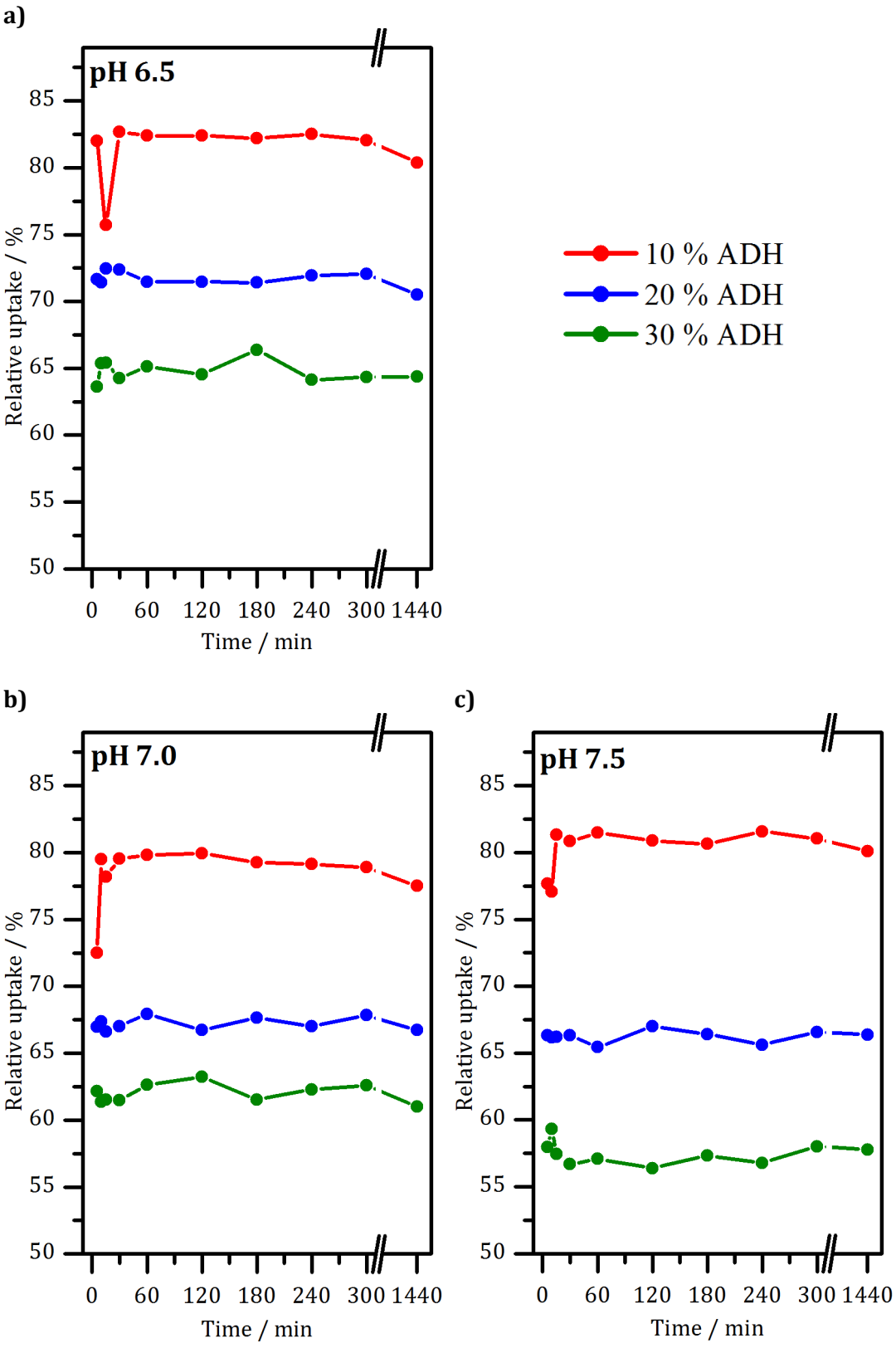


**Figure 63.** Uptake diagrams of the immobilization of ADH onto MCF-$C_3$-$NH_2$. The pH of the immobilization was varied from pH 6.5 to pH 7.5 while additionally varying the ADH to MCF-$C_3$-$NH_2$ proportions employed for immobilization.

**Uptakes.** Irrespective of the pH, the immobilization proceeded very fast and was completed after 30 min at latest (Figure 63). As expected for each immobilization pH, the relative as well as the absolute uptake decreased with increasing ADH amount deployed for immobilization (Table 16). Hence, the highest relative uptake (64 %) after four washing steps was obtained when using a pH 6.5 buffer and an enzyme proportion of 10 % for immobilization, whereas the lowest uptake (46 %) was achieved when employing an ADH amount of 30 % and a pH 7.5 buffer for immobilization. However, when comparing the absolute uptakes of the different immobilization pHs it is clear that the enzyme uptakes nearly remained the same for equal ADH ratios independent on the pH, respectively. As a pH of 6.5 is close to the pI of the ADH (pH 6.1), the electrostatic repulsion between the ADH molecules was lowest when using a pH 6.5 buffer for immobilization. It might be expected that the lower repulsion of the ADH molecules at a pH of 6.5 would lead to a higher absolute uptake. However, this phenomenon was not observed when comparing the absolute uptakes despite the increase of the positive surface charge of MCF-$C_3$-$NH_2$ with decreasing pH (Table 16). The percentages by weight specify the percentage amount of ADH on the immobilisate. It is quite evident that the percentages by weight increase with increasing ratio of ADH or rather decreasing amount of MCF-$C_3$-$NH_2$ present in the immobilization. Therefore, the highest percentages by weight were received using an ADH proportion of 30 % for the immobilization (11-12 wt-%).

**Table 16.** Recapitulation of the relative and absolute ADH uptakes and percentages by weight when varying the pH of the buffer solution as well as the ADH proportions applied for immobilization.

| pH | ADH proportion [%] | relative uptake [%] | absolute uptake [mg] | percentage by weight [wt-%] |
|---|---|---|---|---|
| **6.5** | 10 | 64 | 1.1 | 5.3 |
| | 20 | 54 | 0.94 | 8.6 |
| | 30 | 51 | 0.89 | 12 |
| **7.0** | 10 | 57 | 0.98 | 4.6 |
| | 20 | 51 | 0.87 | 8.0 |
| | 30 | 48 | 0.83 | 11 |
| **7.5** | 10 | 60 | 1.2 | 5.7 |
| | 20 | 49 | 0.97 | 9.0 |
| | 30 | 46 | 0.93 | 12 |

**Driving interactions resulting in immobilization.** At a first glance, electrostatic interactions may be estimated as predominant interactions of the immobilization. The pI of the ADH is at pH 6.1 and the pI of MCF-$C_3$-$NH_2$ was detected at pH 8.4. Thus, both components are oppositely charged at the three pHs of immobilization (Figure 64).

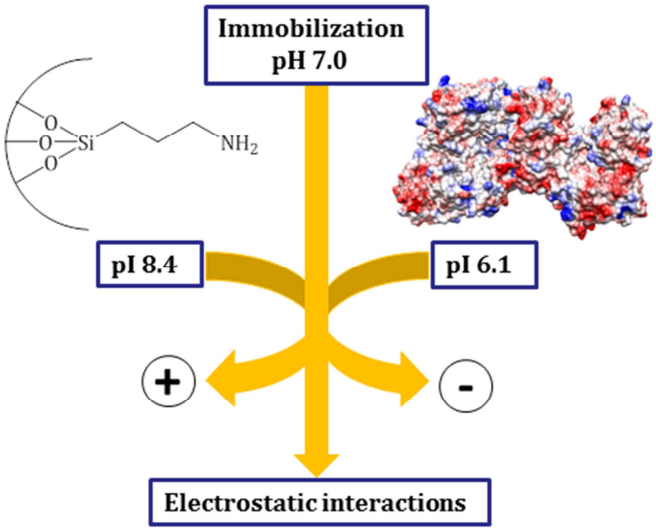


**Figure 64.** At an immobilization pH of 7.0 the surface of MCF-$C_3$-$NH_2$ is positively charged, whereas the surface of the ADH possesses a negatively charged surface. In accordance of the opposite charge, electrostatic interactions were supposed to prevail within immobilization. Figure reprinted with permission from Wiley-VCH.[190]

In order to verify the dominating interactions of the immobilization process the ionic strength of the phosphate buffer deployed for immobilization was varied from 50 mM up to a 1000 mM. The higher the ionic strength of the immobilization buffer, the better the shielding of the electrostatic surface of the ADH (Figure 9c). If a high ionic strength is present in the buffer of immobilization, the ADH does not necessarily need to interact with the, likewise electrostatically shielded, positively charged amino residues on the surface of MCF-$C_3$-$NH_2$ in order to compensate its surface charge. Hence, if electrostatic interactions are causal for the immobilization an increase of the ionic strength results in a decrease of the uptake (Figure 53). Conversely, if hydrophobic interactions induce the immobilization, the increase of the ionic strength of the buffer solution will have no influence on the uptake. To explore the enzyme-host interactions an ADH to MCF-$C_3$-$NH_2$ ratio of 1:10 (2 mg ADH : 20 mg MCF-$C_3$-$NH_2$) and a buffer solution possessing a pH of 7.0 was used exemplarily (Figure 65.).

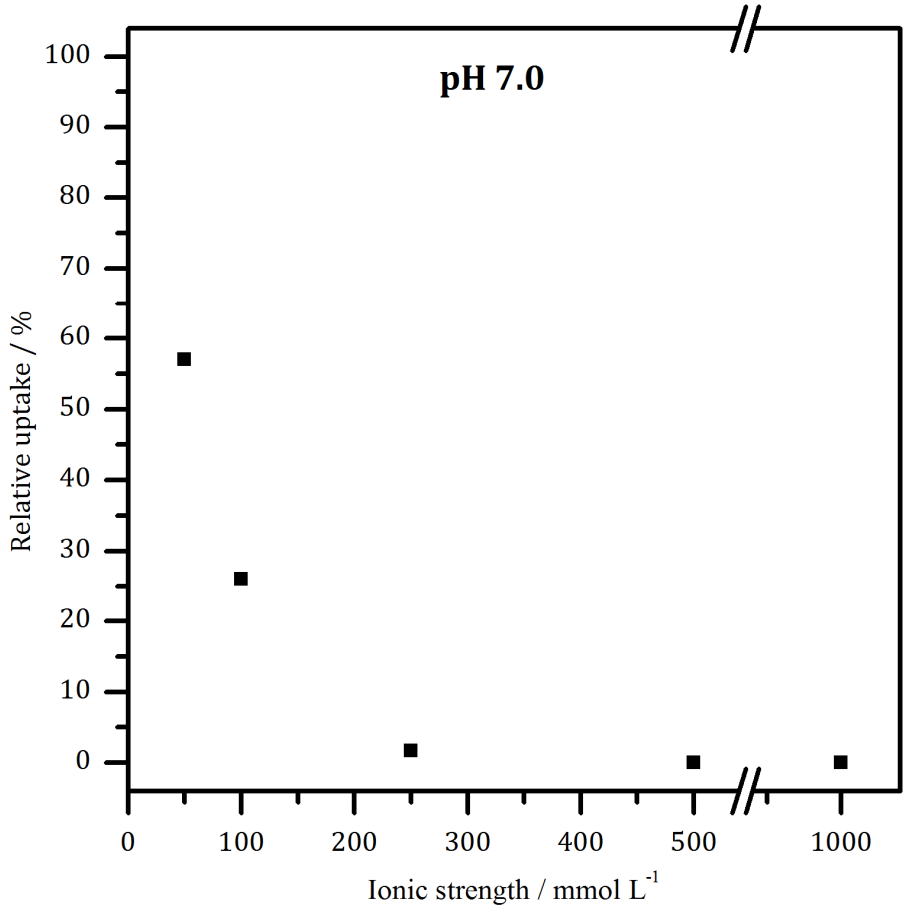


**Figure 65.** Relative ADH uptakes when varying the ionic strength of the phosphate buffer solution employed for immobilization (pH 7.5, 25 °C). The increase of the ionic strength resulted in a decrease of the relative uptake. This implies electrostatic interactions between the negatively charged surface of the ADH and the positively charged surface of MCF-$C_3$-$NH_2$ as prevailing interactions within the immobilization procedure.

The increase of the ionic strength of the buffer solution was accompanied by a strong decrease of the ADH uptake. The highest uptake (57 %) was obtained when a 50 mM buffer solution was present in the immobilization process. However, no ADH uptake was observed when employing a 500 mM or 1000 mM phosphate buffer solution as an immobilization buffer, as the negatively charged surface of the ADH as well as the positively charged surface of the host were strongly electrostatically shielded. This confirms the presumption that the immobilization of the ADH onto MCF-$C_3$-$NH_2$ was carried out through electrostatic interactions (Figure 66).

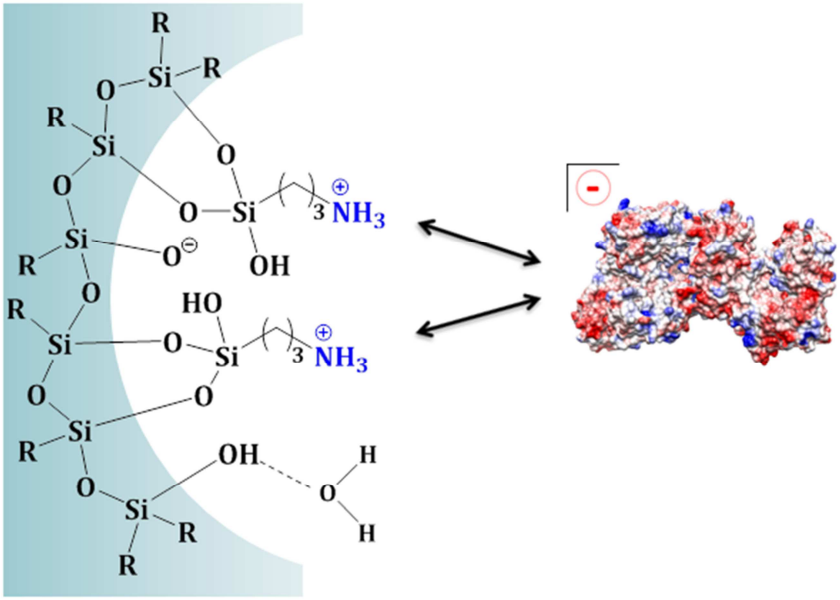


**Figure 66.** Schematic depiction of electrostatic interactions between MCF-$C_3$-$NH_2$ and ADH. At pH 6.5, 7.0 and 7.5 the surface of MCF-$C_3$-$NH_2$ is positively charged (pI 8.4 ), whereas the surface of ADH is negatively charged at these pH values (pI 6.1). The coulomb surface of ADH illustrates positively charged amino acid residues (blue), negatively charged areas (red) as well as neutral areas (white) at pH 7.0.

**Leaching experiments.** To survey the strength of the electrostatic interactions between the ADH and the support material, leaching experiments were conducted. Neither after 24 h nor after 48 h of shaking (350 rpm) the immobilisate at room temperature could free ADH be detected in the supernatant. This indicates strong electrostatic interaction between the ADH and the host. Correspondingly, this circumstance enables the immobilized ADH to be used in the introduced enzyme cascade, as after the removal of the immobilisate from the reaction batch no free ADH will be left in the reaction mixture.

**Intermediate summary.** The immobilization of ADH onto the surface of MCF-$C_3$-$NH_2$ was carried out through electrostatic interactions. These interactions were identified to be very strong, as no leaching was observed. The increase of the enzyme amount in the immobilization procedure led to a decrease of the uptake. However, no dependency of the uptake and the pH of the buffer employed for immobilization was identified. Hence, the absolute uptakes for equal ADH ratios but varying pH values were detected to be almost the same, respectively.

### 4.4.2 Enzymatic activity and long-term stabilities of the immobilized ADH

Evidently, the advantage of an immobilized enzyme is its reusability. Thus, it is required that the enzymatic activity is not greatly affected by the immobilization. Instead, a high retention of the enzymatic activity after the immobilization is required. Moreover, an optimal long-term stability is essential to ensure the long use of the immobilisate. Therefore, besides the activity retention after 24 h of immobilization, the long-term stabilities of the immobilized ADH were monitored over a period of seven days. Without exception and independent on the pH values of the immobilizations, all enzymatic activity assays were carried out in pH 7.5 buffer (50 mM). As a basic principle, enzymes are not only able to catalyze the respective forward reactions but also the back reactions. Hence, the retained activities and the long-term stabilities of the immobilized ADH were investigated for the conversion of 2-propanol to acetone (forward reaction) as well as the transformation of acetone to 2-propanol (back reaction). Each reaction step is accompanied by either the reduction of $NADP^+$ (forward reaction) or the oxidation of NADPH (back reaction). Consequently, when applying the immobilized ADH as a cofactor recycling system the recycling of $NADP^+$ or NADPH can be regulated by the choice of the substrate.

**Conversion of 2-propanol to acetone (forward reaction).** Employing a pH 6.5 buffer for immobilization the retained activity of the ADH decreased with increasing ADH amount used (Table 17). Thus, the highest retention of enzymatic activity (72 %) was obtained when using an ADH proportion of 10 %, whereas the activity was at lowest (51 %) when using an ADH proportion of 30 % for the immobilization. The pH optimum of the ADH with reference with the enzymatic activity was reported to be at pH 7.0.[49] The activity of the ADH immobilized at that pH did not show any dependency on the enzyme amount used for immobilization. The activity retention amounted 59 % in every case. Likewise, when immobilizing the ADH at pH 7.5, no distinct trend of the retained activity was observed. Quite low

activity retentions were obtained applying ADH proportions of 10 and 30 %, whereas the highest activity was detected providing an enzyme amount of 20 % (56 %). Conversely, after 24 h, the activity of the free ADH in the respective stock solutions remained nearly unaltered.

**Table 17.** Retained enzymatic activities of the immobilized ADH after 24 h of immobilization for the forward (2-propanol → acetone) as well as the back reaction (acetone → 2-propanol).

| pH | ADH proportion [%] | activity retention 2-propanol → acetone [%] | activity retention acetone → 2-propanol [%] |
|---|---|---|---|
| **6.5** | 10 | 72 | 87 |
| | 20 | 59 | 83 |
| | 30 | 51 | 70 |
| **7.0** | 10 | 59 | 71 |
| | 20 | 59 | 68 |
| | 30 | 59 | 58 |
| **7.5** | 10 | 43 | 62 |
| | 20 | 56 | 58 |
| | 30 | 37 | 42 |

The immobilization of an enzyme can lead to significant changes of its microenvironment. An enzyme possesses its highest activity under conditions that correlate to its natural environment. Thus, immobilization mostly results in a decrease of the enzymatic activity. Furthermore, diffusional restrictions of substrate or coenzyme molecules caused by the properties of the host can induce a decrease of the retained activity of an immobilized enzyme.[62, 139, 188]

The long-term stabilities of the immobilized ADH as well as of the free ADH were examined over a period of one week after immobilization (Figure 67). Within the first couple of days after immobilization, a considerable loss of the activity of the immobilized ADH was monitored. This can be attributed to the incidence of time-spreading (Figure 15). As mentioned above, the immobilization of the ADH onto MCF-$C_3$-$NH_2$ was implemented due to electrostatic interactions initially. However, it is supposable that after the electrostatic immobilization the ADH additionally interacts hydrophobically with the propyl chains bearing the amino groups as well

as siloxane bridges in the pore walls of the silica host in order to lower its free energy. These hydrophobic interactions are accompanied by the displacement of complexed water molecules on the contact areas. Thus, the entropy of the system increases and this can be deemed as the driving force of these hydrophobic interactions. The outcome of this is an unfolding of the tertiary structure of the enzyme. These structural changes are known to impede the fixation of the substrate or coenzyme resulting in a loss of the enzymatic activity.[8, 10, 69]

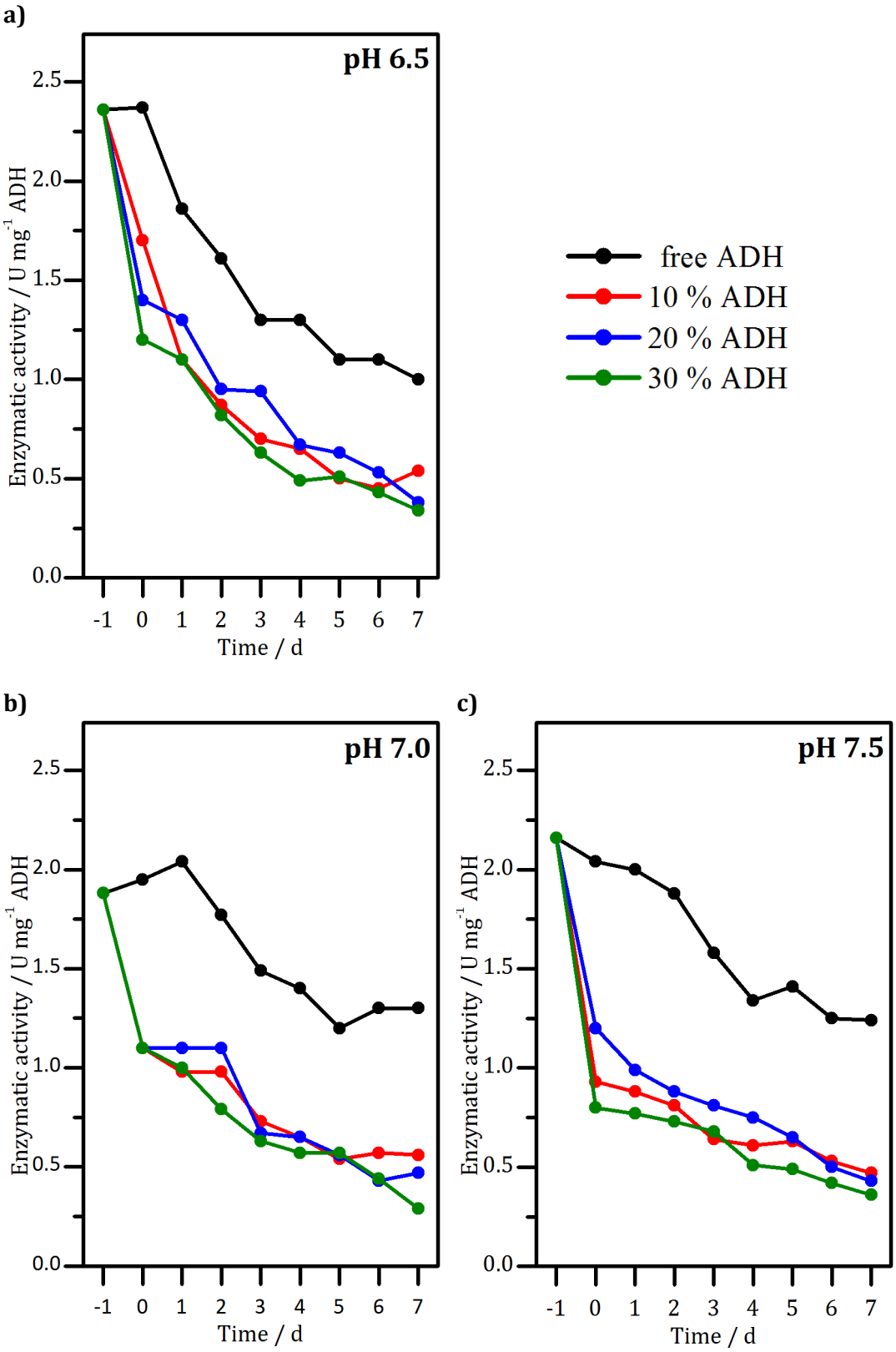


**Figure 67.** Long-term stabilities of the immobilized as well as of the free ADH for the conversion of 2-propanol to acetone (forward reaction). Day -1 denotes the activity of the native ADH before immobilization, whereas day 0 marks the activity immediately after 24 h of immobilization.

The long-term stabilities of the immobilisate did not show a marked trend with the respective pH of the immobilization buffer. Within the first five days after

immobilization the activity was highest for the immobilisates employing an ADH proportion of 10 % for immobilization. However, after seven days, a distinct dependency on the ADH ratio applied for immobilization and the residual activity was detected. One week after immobilization, the remaining enzymatic activity was higher with the lower ADH ratio used for immobilization. Thus, the highest remaining activity was observed for the samples using an ADH amount of 10 % for immobilization, whereas the lowest residual activity was noticed applying an ADH proportion of 30 %. With respect to the forward reaction, an ADH proportion of 10 % turned out to be the optimum amount for the immobilization. Even if the enzymatic activity of the free ADH decreases over time, too, it is still higher as detected for the immobilized enzyme.

**Conversion of acetone to 2-propanol (back reaction).** In comparison to the forward reaction, when looking at the back reaction a correlation between the ADH ratios employed for immobilization and the activity retention after 24 h of immobilization was observed, too (Table 17). For each immobilization pH the retained activity of the ADH decreased with increasing ADH ratio of the immobilization. Moreover, the respective retained activities decreased with increasing immobilization pH. Thus, the highest activity retention was detected using a pH of 6.5 and an ADH amount of 10 % for immobilization (87 %). The lowest remaining activity was received when employing an enzyme proportion of 30 % at pH 7.5 for immobilization (42 %).

With respect to the forward reaction, it was natural to expect a definite loss of the residual activity of the immobilized ADH over one week. However, for the back reaction a distinct trend of the enzymatic activity and the ADH ratio applied for immobilization was observed for each pH (Figure 68). Independent on the pH the highest activities were obtained for the immobilization using an ADH proportion of 10 % and the lowest activities were received when using an enzyme amount of 30 % for immobilization. This trend continues over the whole period of the measurement series. It is evident that the absolute enzymatic activities were distinctly higher when using acetone/NADPH as substrate/coenzyme instead of 2-propanol/$NADP^+$. As these findings were simultaneously observed for the free ADH it can be ruled out that an alteration of the diffusion conditions is responsible. Hence, a preference of the ADH for the back reaction can be assumed.

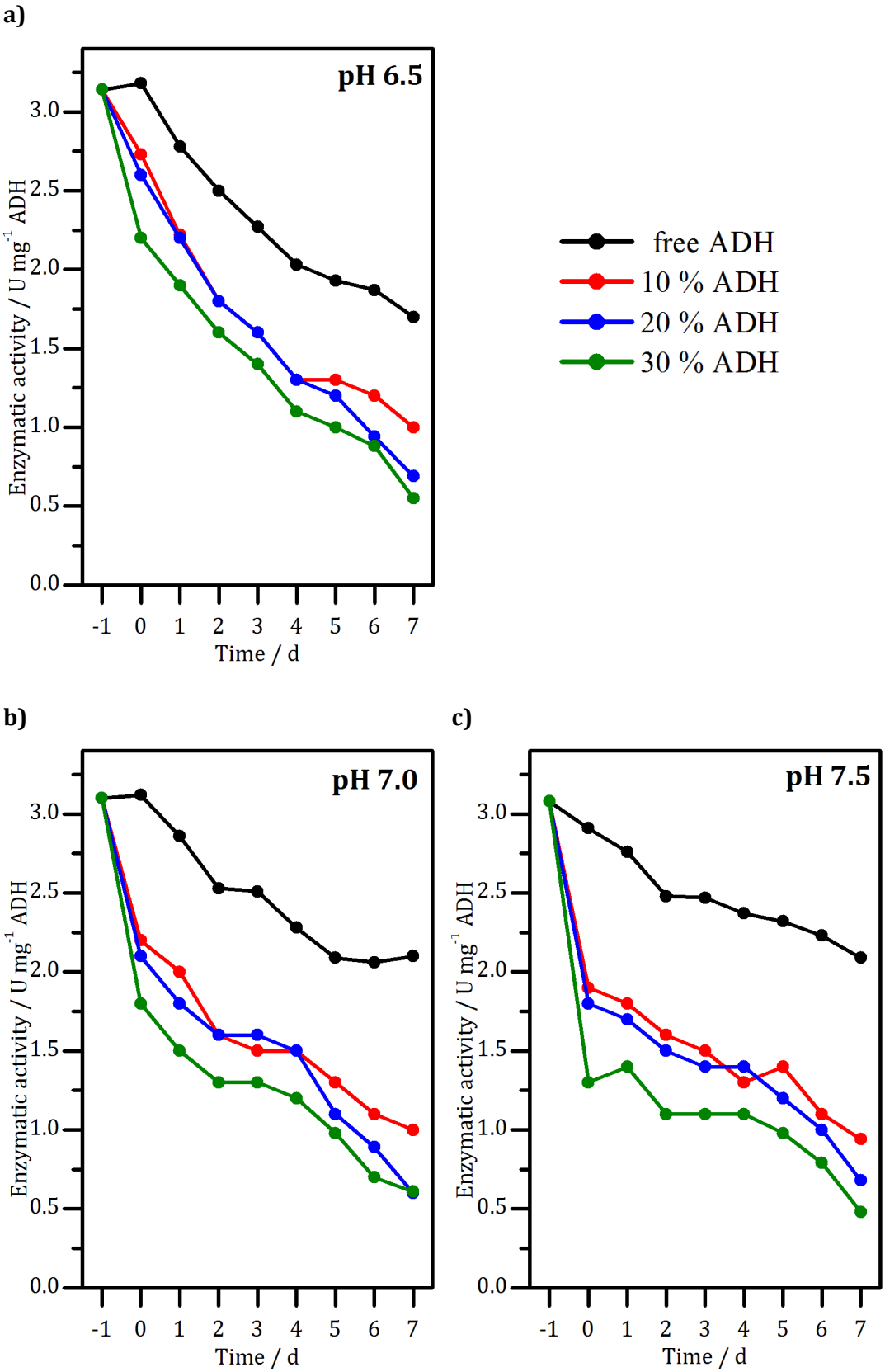


**Figure 68.** Long-term stabilities of the immobilized as well as of the free ADH for the conversion of acetone to 2-propanol (back reaction). Day -1 denotes the activity of the native ADH before immobilization, whereas day 0 marks the activity immediately after 24 h of immobilization.

As a reference, the ADH was additionally immobilized onto pristine MCF (Table 18). An enzyme proportion of 10 % was exemplarily deployed for this study (potassium phosphate buffer, 50 mM, pH 7.0).

**Table 18.** Overview of the material properties of the pristine MCF employed for the immobilization of ADH.

| sample | $S_{BET}$ [$m^2 g^{-1}$] | $V_P$ [$cm^3 g^{-1}$] | $D_p$ [nm] | pI |
|---|---|---|---|---|
| **MCF** | 528 | 2.8 | 24 | 3.7 |

After 24 h of immobilization an ADH uptake of 99 % was obtained (Figure 69a). Hence, the enzyme uptake was considerably increased compared to the uptakes obtained for the utilization of MCF-$C_3$-$NH_2$ as a host material. However, the activity retention for the conversion of 2-propanol to acetone amounted to only 19 % and for the reduction of acetone to 2-propanol it was detected to be just 26 %. These findings were accompanied by a marked loss of the absolute activity over a period of seven days (Figure 69b).

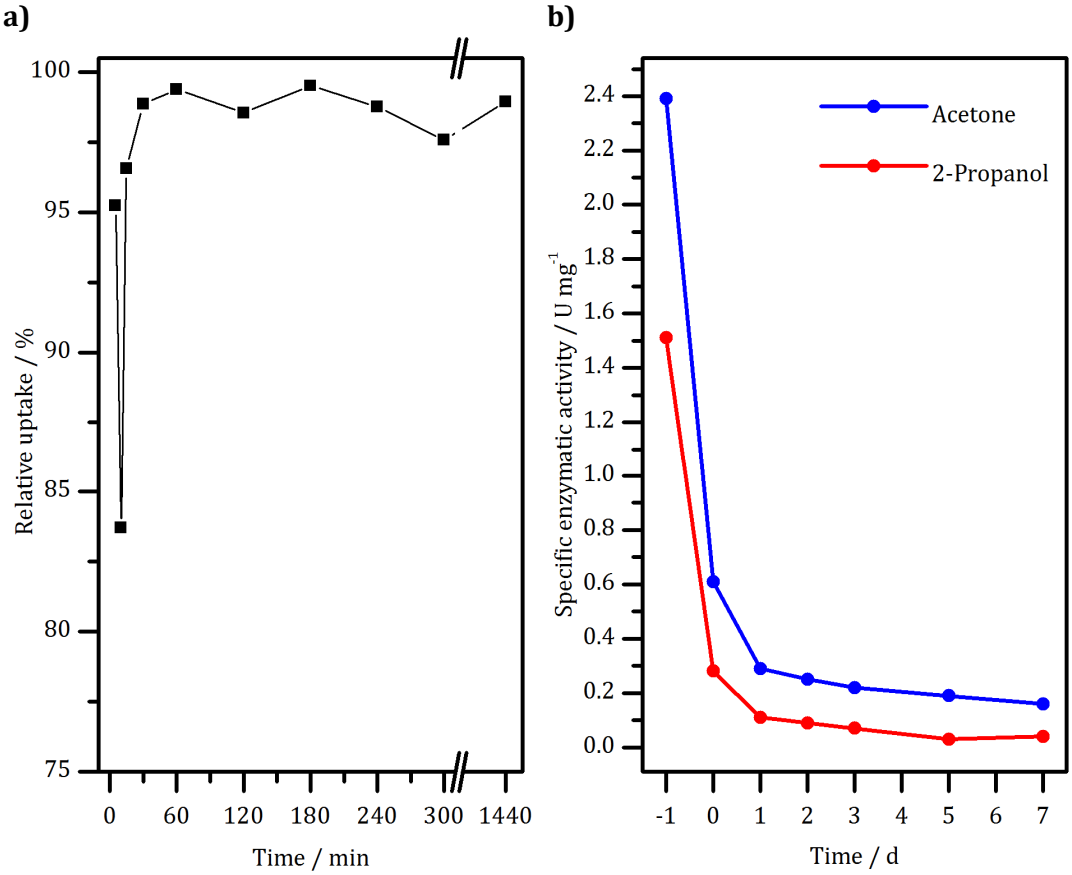


**Figure 69. a)** Uptake diagram of the immobilization of ADH onto pristine MCF (10 % ADH, pH 6.5, 25 °C); **b)** Long-term stabilities of ADH immobilized onto pristine MCF: 2-propanol (forward reaction), acetone (back reaction).

When using MCF-$C_3$-$NH_2$ as a support material the aminopropyl chains on the MCF surface protrude into the pores, behaving as spacers between the immobilized enzyme and the pore walls. The distance between the ADH and the pore walls enable the enzyme to undergo conformational changes in the catalysis and decelerate the time-spreading. As the ADH is directly immobilized onto the pore walls of the MCF, time-spreading is strongly pronounced (Figure 15). Furthermore, conformational changes of the enzyme necessary for the catalytic activity were hindered. Thus, the retained activity after immobilization as well as the long-term stability of the immobilized ADH were significantly lower than those obtained when applying MCF-$C_3$-$NH_2$ as a host. Accordingly, it is highly recommended to immobilize the ADH onto MCF-$C_3$-$NH_2$.

**Intermediate summary.** With regard to the forward reaction, the highest activity retention was found when using a pH 6.5 buffer and an ADH amount of 10 % for immobilization, whereas the lowest remaining activity was observed when employing an immobilization buffer of pH 7.5 and an enzyme proportion of 30 %. With a view of the conversion of 2-propanol to acetone, the best long-term stabilities and thus the highest activity of the immobilized ADH was obtained by using an ADH proportion of 10 % for immobilization. With respect to the long-term stability, no dependency on the immobilization pH was found. Regarding the back reaction, a considerable trend of the retained activity after 24 h of immobilization was detected. The remaining activity decreased with increasing ADH ratio applied for immobilization and additionally with increasing pH of the immobilization. Moreover, a distinct trend was observed for the long-term stabilities. Independent on the pH of immobilization, the immobilizations using an ADH amount of 10 % offered the highest activity.

As the best long-time stabilities of the immobilized ADH were obtained when employing an ADH amount of 10 % for the immobilization the Michaelis-Menten kinetics of these immobilisates were investigated.

### 4.4.3 Michaelis-Menten kinetics of the immobilized ADH

With respect to an incorporation of the immobilized ADH as a cofactor regeneration system into a multienzyme cascade, it was necessary to carefully investigate the Michaelis-Menten kinetics of the immobilized enzyme (Figure 37). It had to be ascertained that $v_{max}$ of the immobilized ADH is significantly higher compared to $v_{max}$ of the further participating immobilized enzymes in order to avoid

lack of the reduced or oxidized coenzyme within the cascade. A deficit of the respective coenzyme in a multienzyme complex is attended by a decrease of $v_{max}$ of the enzymes that are dependent on this coenzyme. The long-term stabilities of the immobilized ADH only give a first impression of the remained activity and stability of the immobilized enzyme. However, no connections concerning the kinetic behavior of the immobilized ADH can be drawn. Hence, it was important to further investigate the immobilized ADH under kinetic aspects.

Immobilized enzymes represent complex systems. Thus, the reaction kinetics of an immobilized enzyme distinguish themselves substantially from those of a free enzyme. An immobilization is frequently accompanied by structural changes of the enzyme's tertiary structure. This impacts not only the enzymatic activity but also the enzyme kinetics. When applying a porous support, mass transport limitations of coenzyme/substrate molecules into the porous system of the host can arise due to hindered diffusion.[139, 149] Therefore, the concentration of the coenzyme/substrate in the pore system can differ strongly from the respective concentration in the bulk buffer. Furthermore, attractive interactions between functional groups on the surface of the support material and substrate/coenzyme molecules can occur and compete with the active sites of the enzyme. Moreover, an accumulation of buffer salts within the porous system of the support material can change the pH value within the pores. This additionally contributes to an alteration of the microenvironment of the immobilized enzyme. These phenomena can have an influence on the kinetics of an immobilized enzyme.[62, 69, 70, 71, 72, 188] To gain insight into these facts, the Michaelis-Menten kinetics of the immobilized ADH were investigated.

With respect to the forward as well as the back reaction, the Michaelis-Menten constants ($K_m$, Eq. 10), the maximum reaction rates ($v_{max}$, Eq. 9), the inhibition constants ($K_i$) and the dissociation constant ($k_{cat}$, Eq. 11) of the enzyme substrate complex of the immobilized ADH were determined. Finally, the enzyme efficiency (EE, Eq. 12) and the effectiveness factor ($\eta$, Eq. 15) were calculated. All kinetic parameters were referenced to the results obtained for the free ADH.

The Michaelis-Menten constant $K_m$ is a meaningful enzyme constant. $K_m$ expresses the coenzyme/substrate concentration necessary to induce the half-maximum reaction rate of an enzyme. If $K_m$ is very low, only small amounts of coenzyme/substrate are needed to reach the half-maximum reaction rate. Thus, the affinity of the enzyme to its coenzyme/substrate is high and vice versa. Hence, $K_m$ is also a measure of the affinity of an enzyme to its coenzyme/substrate. However, a very fast decomposition of the enzyme-substrate complex likewise results in a high

$K_m$. Therefore, $K_m$ is not necessarily suitable in every case to make statements concerning the affinity of an enzyme to its coenzyme/substrate. Moreover, apparent $K_m$ values were obtained when elaborating immobilized enzyme as diffusional restrictions and structural changes of the enzyme influence $K_m$ strongly.[139, 140, 141]

**Conversion of 2-propanol to acetone (forward reaction).** To examine the enzyme kinetics of the forward reaction the concentrations of 2-propanol as well as $NADP^+$ were varied, respectively, and the initial reaction rates detected. Foremost, to have a reference, the enzyme kinetics of the free ADH stored in buffer solutions with different pH values (pH 6.5/7.0/7.5) were investigated.

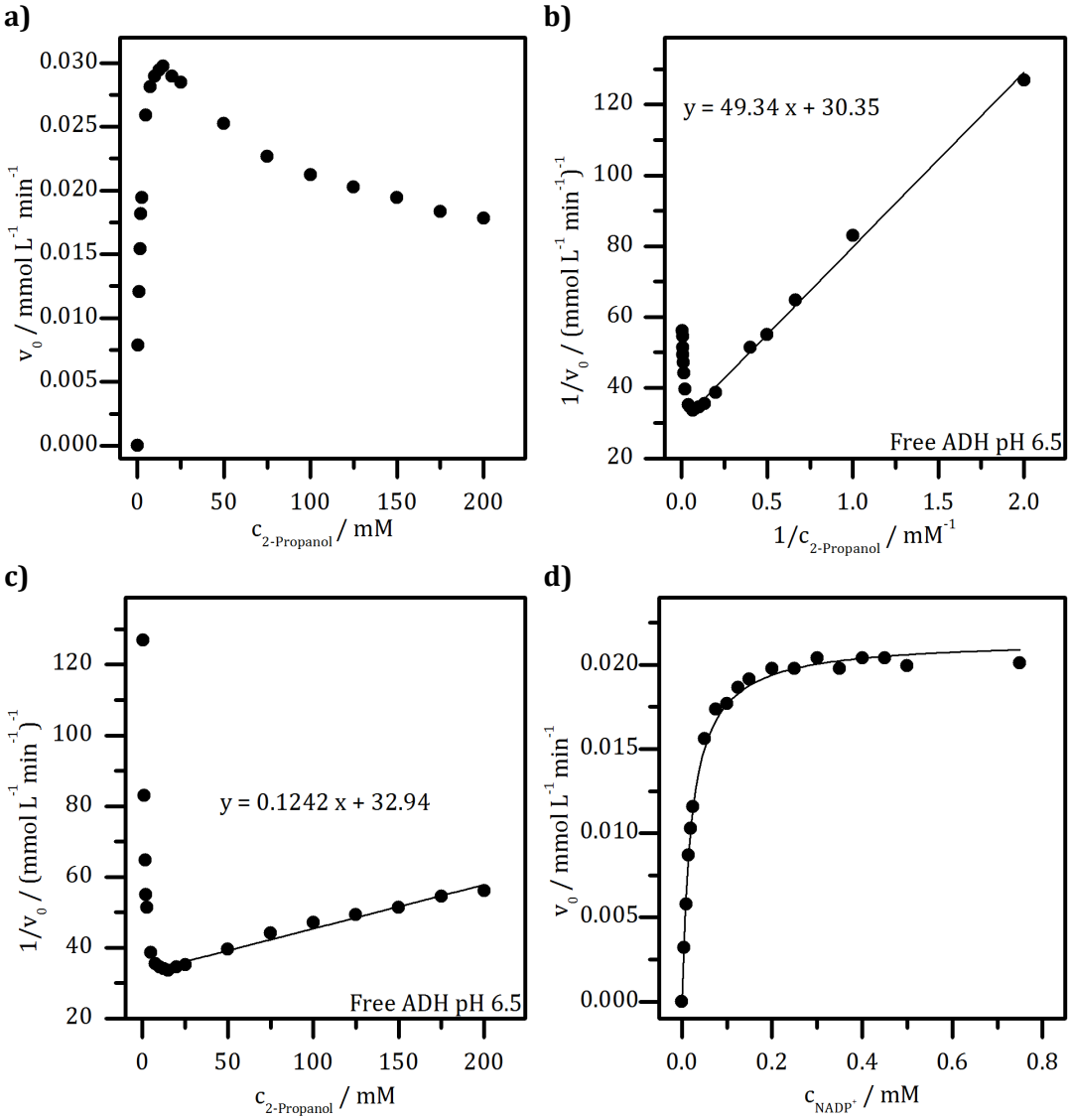


**Figure 70.** Exemplary depiction of the graphical evaluation of the enzyme kinetics of the free ADH stored in pH 6.5 buffer: **a)** Michaelis-Menten plot (2-propanol); **b)** Lineweaver-Burk plot (2-Propanol); **c)** Dixon plot (2-propanol); **d)** Michaelis-Menten plot ($NADP^+$). All further Michaelis-Menten, Lineweaver-Burk as well as Dixon plots can be found in the appendix (Appendix 7.7).

The increase of the 2-propanol concentration resulted in a very steep rise of the initial reaction rate of the free ADH. After reaching a certain concentration of 2-propanol, a further increase led to a decrease of the initial reaction rate (Figure 70a). This indicates that a substrate inhibition arises when exceeding a certain concentration of 2-propanol. In contrast, when varying the concentration of $NADP^+$ and keeping the 2-propanol concentration constant, no inhibition due to the coenzyme occurred (Figure 70d). The determination of $v_{max}$ and $K_m$ by using the Michaelis-Menten plot is problematic and unusual. Again, the Lineweaver-Burk method was used for the linearization of the Michaelis-Menten plot. As an inhibition is present, no overall linearity was observed within the Lineweaver-Burk plot. Thus, only the linear area of the plot was considered for the linear regression. In the Lineweaver-Burk diagram the y intercept is the reciprocal of $v_{max}$ and the slope gives the ratio of $K_m$ and $v_{max}$ (Figure 70b). However, it has to be taken into account if an inhibition is present, only an apparent value of $v_{max}$ will be obtained, although $K_m$ remains unaffected.[139, 140, 141]

$K_{m,\ 2\text{-Propanol}}$ of the free ADH does not show a distinct dependency on the pH of the buffer solution used for enzyme storage. The $K_{m,\ 2\text{-Propanol}}$ values vary only slightly between 1.58 mM (pH 7.0), 1.63 mM (pH 6.5) and 1.68 mM (pH 7.5). In addition, owing the variation of the $NADP^+$ concentration $K_{m,\ NADP^+}$ was examined. The alteration of $K_{m,\ NADP^+}$ over the pH range pH 6.5-7.5 is marginal, too. The $K_m$ values of the substrate and the coenzyme were lowest at pH 7.0. Thus, the highest substrate and coenzyme affinities were observed at pH 7.0. This correlates with the pH optimum of the free ADH.[49] However, $K_{m,\ NADP^+}$ was detected to be in the µM range whereas $K_{m,\ 2\text{-Propanol}}$ was identified to be in the mM range (Table 19). This illustrates the strong dependency of the ADH on $NADP^+$, as only a small concentration of the coenzyme is necessary to induce the half-maximum reaction rate.

With regard to the reaction rate, $v_{max,\ 2\text{-Propanol}}$ decreases from 33.0 µmol $L^{-1}$ $min^{-1}$ (pH 6.5) over 29.9 µmol $L^{-1}$ $min^{-1}$ (pH 7.0) to 28.6 µmol $L^{-1}$ $min^{-1}$ (pH 7.5). Thus, likewise $v_{max,\ 2\text{-Propanol}}$ shows only a slight dependency on the pH of the buffer solution used for ADH storage. Moreover, the dissociation constant of the decay of the enzyme-substrate complex ($k_{cat}$) was evaluated. The decomposition of the enzyme-substrate complex is generally assumed to be very slow. Hence, it is the rate-determining step of an enzymatic reaction. The $k_{cat}$ value can be considered as the turnover number of the enzyme. It describes the number of substrate molecules converted per enzyme molecule and second.[140] It was found that $k_{cat}$ merely varies very slightly when increasing the pH. The highest value of $k_{cat}$ was obtained when

storing the ADH in pH 6.5 buffer (3.85 $s^{-1}$) and the lowest $k_{cat}$ value was found for the ADH stored in pH 7.0 buffer (3.52 $s^{-1}$; Table 19).

As an inhibition is present when exceeding a certain concentration of 2-propanol, the inhibition constant $K_i$ was calculated. $K_i$ characterizes the concentration of the inhibitor that is necessary to occupy 50 % of the active sites of all enzyme molecules present. Thus, the higher the $K_i$ value the higher the inhibitor concentration needed to block 50 % of the binding sites of the enzyme. In the case of a substrate inhibition, the inhibition is classified to be uncompetitive. In an uncompetitive inhibition, a second substrate molecule binds to the enzyme-substrate complex and thus the release of the product is hindered (Figure 71).[139, 140, 141]

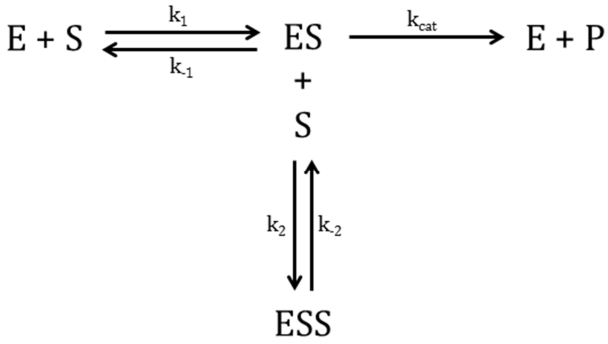


**Figure 71.** Schematic illustration of an uncompetitive inhibition of an enzyme. The enzyme (E) fixes its substrate (S) within the active site to create the enzyme-substrate-complex (ES). A second substrate molecule binds to the ES impeding the release of the product (P). Generally, an inhibition is associated with a decrease of $v_{max}$. However, an uncompetitive inhibition is reversible.[141]

The inhibition of an enzyme is accompanied by a reduction of the reaction rate when exceeding a certain concentration of the inhibitor. However, the respective $K_m$ values remain unaffected.[141]

By using the Dixon plot $K_i$ was determined (Figure 70c). The Dixon plot has the reciprocal of the initial reaction rate on the y axis as well as the inhibitor concentration on the x axis. As, once again, no overall linearity of the plot was observed; only the linear region of the plot was used for the linear regression. The x intercept yields the negative value of $K_i$.[139, 141] The inhibition of ADH is less pronounced when using a pH 7.5 buffer for storage (340 mM) and most distinctive when storing it in a pH 7.0 buffer (229 mM). However, $K_i$ of the free ADH varies merely in a small range. Collectively for the enzyme kinetics of the free ADH solved in buffer solutions possessing pH 6.5-7.5 no distinct dependency between the kinetics and the pH was monitored.

**Table 19.** Overview of the kinetic parameters of the ADH-catalyzed oxidation of 2-propanol to acetone.

| pH | $K_{m,\ 2\text{-Propanol}}$ [mM] | $K_{m,\ NADP^+}$ [µM] | $v_{max,\ 2\text{-Propanol}}$ [µmol $L^{-1}$ $min^{-1}$] | $k_{cat,\ 2\text{-Propanol}}$ [$s^{-1}$] | $K_{i,\ 2\text{-Propanol}}$ [mM] |
|---|---|---|---|---|---|
| **immobilized ADH** | | | | | |
| **6.5** | 12.0 | 128 | 15.0 | 2.64 | 693 |
| **7.0** | 6.24 | 94.6 | 10.7 | 2.34 | 168 |
| **7.5** | 2.92 | 44.0 | 6.53 | 1.52 | 293 |
| **free ADH** | | | | | |
| **6.5** | 1.63 | 29.8 | 33.0 | 3.85 | 265 |
| **7.0** | 1.58 | 28.6 | 29.9 | 3.52 | 229 |
| **7.5** | 1.68 | 34.0 | 28.6 | 3.60 | 340 |

Investigating the Michaelis-Menten kinetics of the immobilized ADH $K_{m,\ NADP^+}$ decreases with increasing immobilization pH from 128 µM (pH 6.5) to 44.0 µM (pH 7.5). Likewise, $K_{m,\ 2\text{-Propanol}}$ decreases in the same manner from 12.0 mM (pH 6.5) to 2.92 (pH 7.5). Hence, the lowest coenzyme and substrate affinities of the immobilized ADH were gained by using a pH 6.5 buffer for immobilization (Table 19). The $K_{m,\ NADP^+}$ and $K_{m,\ 2\text{-Propanol}}$ values are apparently higher than those calculated for the free enzyme. On one hand, these observations may be attributed to diffusional restrictions of the coenzyme/substrate into the porous system of the host.[139] On the other hand, structural changes of the enzyme's tertiary structure resulting from the immobilization can impede the ability to bind the coenzyme/substrate or the release of the reduced coenzyme/product.[69] However, all kinetic assays were carried out in pH 7.5 buffer. Thus, the diffusion behavior can be assumed to be the same, independent on the pH employed for immobilization. Attractive interactions between $NADP^+$ and the aminopropyl chains on the surface of MCF-$C_3$-$NH_2$ can be excluded. Therefore, the dependency of $K_{m,\ NADP+}$ and $K_{m,\ 2\text{-Propanol}}$ on the pH of immobilization can be attributed to the accessibility of the coenzyme/substrate molecules to the respective binding sites as well as the requirement to fix these molecules within the active sites. Hence, the accessibility to the active site and the capability to bind the substrate/coenzyme is best when using a pH 7.5 buffer for immobilization as the lowest $K_m$ values were obtained for these immobilisates.

However, the maximum reaction rate of the immobilized ADH ($v_{max,\ 2\text{-Propanol}}$) decreases with increasing pH of the immobilization. It is highest (15.0 µmol $L^{-1}$ $min^{-1}$) when using a pH 6.5 buffer for immobilization. In this case, $v_{max,\ 2\text{-Propanol}}$ is halved compared with the free ADH stored in pH 6.5 buffer. In the

case of an immobilization at pH 7.0 and pH 7.5 $v_{max,\ 2\text{-Propanol}}$ has been reduced by two-third and three-fourths compared with the free ADH, respectively (Table 19). As $v_{max,\ 2\text{-Propanol}}$ was highest for the ADH immobilized at pH 6.5, also $k_{cat}$ was obtained to be highest for this sample (2.64 $s^{-1}$). In accordance with $v_{max,\ 2\text{-Propanol}}$, $k_{cat}$ decreases with increasing pH of the immobilization (pH 6.5: 2.64 $s^{-1}$; pH 7.0: 2.34 $s^{-1}$; pH 7.5: 1.52 $s^{-1}$). Although immobilization of the ADH at pH 6.5 resulted in the highest $K_m$ values and accordingly the lowest affinities for $NADP^+$/2-propanol, this immobilisate possessed the highest $v_{max,\ 2\text{-Propanol}}$. In spite of a low accessibility of coenzyme/substrate molecules to the active site and a hindered fixation of these molecules, the conversion of 2-propanol as well as the release of acetone is assumed to be comparatively fast. These findings were supported by the course of the activity retentions detected immediately after 24 h of immobilization (Table 17). It was highest immobilizing the ADH onto MCF-$C_3$-$NH_2$ by using a pH 6.5 buffer (72 %).

It is striking that $K_i$ of the ADH immobilized at pH 6.5 is considerably higher (693 mM) than $K_i$ of the free enzyme stored in pH 6.5 buffer (265 mM). Thus, besides a high $v_{max,\ 2\text{-Propanol}}$ value, immobilization of the ADH at pH 6.5 has additionally a positive effect in terms of the substrate inhibition. The $K_i$ values of the ADH immobilized at pH 7.0 (168 mM) and pH 7.5 (293 mM) are distinctly lower as the values obtained for the free ADH. This indicates that immobilization has negatively affected the inhibition behavior of the ADH and inhibitions appears already at lower concentrations of 2-propanol.

**Conversion of acetone to 2-propanol (back reaction).** To determine the Michaelis-Menten kinetics of the back reaction the concentrations of acetone as well as NADPH were varied and the initial reaction rates were measured. Once again, the kinetics of the free ADH stored in buffer solutions exhibiting pH 6.5, pH 7.0 or pH 7.5 were used as a reference for the immobilized ADH. A specific focus is placed on the kinetic investigations of the back reaction of the ADH as this reaction path was necessary to be implemented into the modular enzyme cascade.

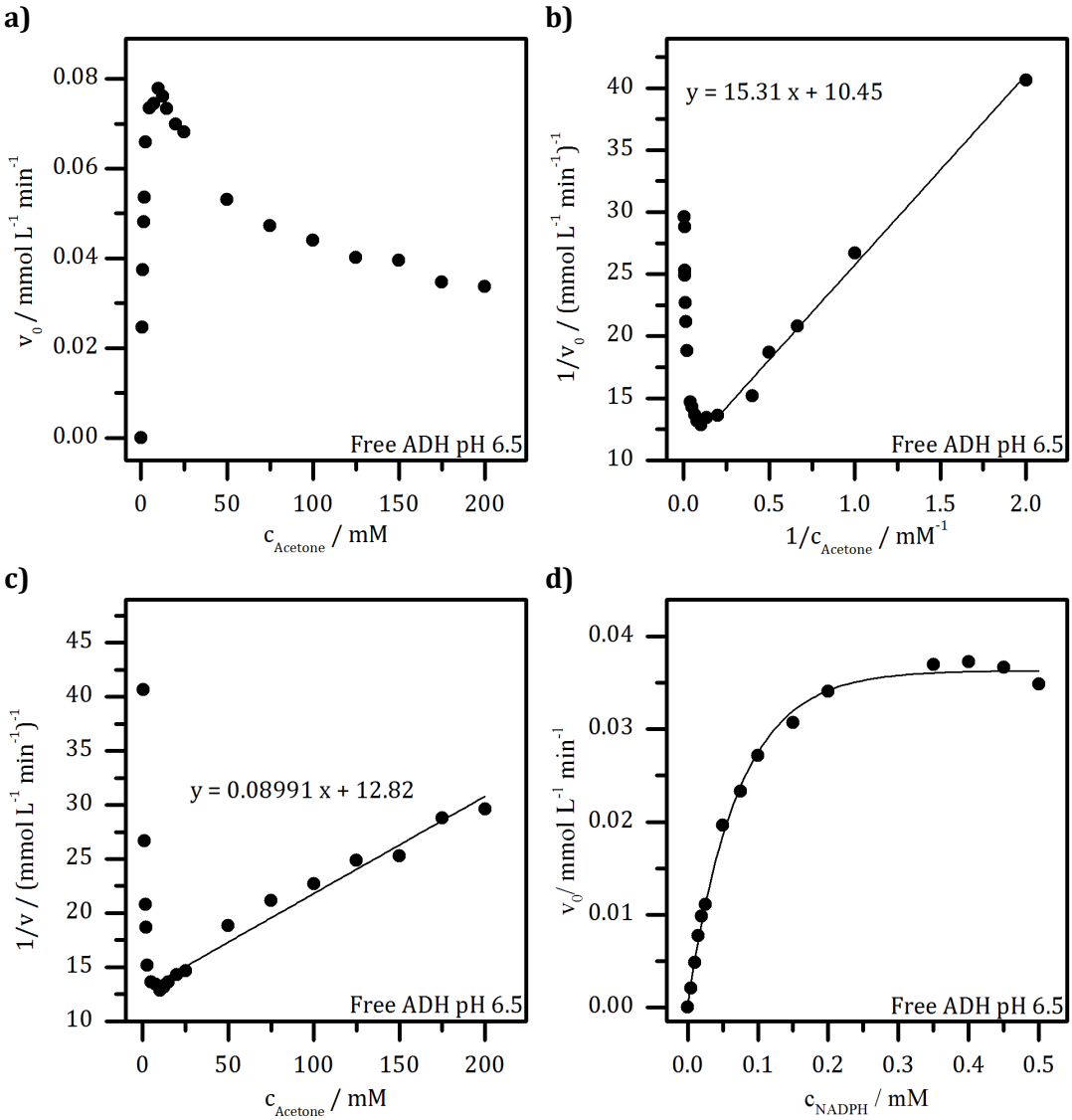


**Figure 72.** Exemplary depiction of the graphical evaluation of the enzyme kinetics of the free ADH stored in pH 6.5 buffer: **a)** Michaelis-Menten plot (acetone); **b)** Lineweaver-Burk plot (acetone); **c)** Dixon plot (acetone); **d)** Michaelis-Menten plot (NADPH). All further Michaelis-Menten, Lineweaver-Burk as well as Dixon plots can be found in the appendix (Appendix 7.7).

By means of the Lineweaver-Burk plot, $K_m$ and $v_{max}$ were calculated. $K_{m,\ NAPDH}$ of the free ADH increases from pH 6.5 (87.6 µM) to pH 7.0 (115 µM) and decreases in the further course to pH 7.5 (72.5 µM). A similar development was received for $K_{m,\ Acetone}$. Consequently, the highest NADPH/acetone affinities of the free ADH were obtained storing the ADH in pH 7.5 buffer (Table 20). Corresponding to the pH optimum of the free ADH (pH 7.0), the highest $v_{max,\ Acetone}$ was found to be at pH 7.0 (132 µmol $L^{-1}$ $min^{-1}$), too. However, $v_{max,\ Acetone}$ of the enzyme stored in pH 6.5 as well as pH 7.5 buffer is slightly reduced to 96.2 µmol $L^{-1}$ $min^{-1}$ and 82.0 µmol $L^{-1}$ $min^{-1}$, respectively. Accordingly, $k_{cat}$ follows the same trend and increases from pH 6.5 (11.2 $s^{-1}$) to pH 7.0 (15.5 $s^{-1}$) and decreases in the further course to pH 7.5 (10.3 $s^{-1}$). Compared to 2-propanol, acetone is an inhibitor of the ADH, too (Figure 72). The

inhibition was less pronounced when employing pH 7.5 for storage ($K_i$ = 568 mM) and most distinctive when storing the enzyme in pH 7.0 buffer ($K_i$ = 134 mM).

**Table 20.** Overview of the kinetic parameters of the ADH-catalyzed reduction of acetone to 2-propanol.

| | $K_{m,\ Acetone}$ | $K_{m,\ NADPH}$ | $v_{max,\ Acetone}$ | $k_{cat,\ Acetone}$ | $K_{i,\ Acetone}$ |
|---|---|---|---|---|---|
| **pH** | **[mM]** | **[µM]** | **[µmol $L^{-1}$ $min^{-1}$]** | **[$s^{-1}$]** | **[mM]** |
| **immobilized ADH** | | | | | |
| **6.5** | 1.88 | 97.7 | 38.2 | 6.74 | 238 |
| **7.0** | 9.44 | 133 | 61.3 | 15.6 | 178 |
| **7.5** | 11.4 | 52.8 | 57.5 | 14.4 | 294 |
| **free ADH** | | | | | |
| **6.5** | 1.47 | 87.6 | 96.2 | 11.2 | 143 |
| **7.0** | 2.44 | 115 | 132 | 15.5 | 134 |
| **7.5** | 1.17 | 72.5 | 82.0 | 10.3 | 568 |

Regarding the immobilized ADH, $K_{m,\ NADPH}$ exhibits the same dependency on the pH of the immobilization than obtained for the free ADH (pH 6.5: 97.7 µM; pH 7.0: 133 µM; pH 7.5: 52.8 µM). Thus, the highest NADPH affinity was gained when immobilizing the ADH at pH 7.5. In addition, $K_{m,\ NADPH}$ is reduced compared with $K_{m,\ NADPH}$ of the free ADH stored in pH 7.5 buffer. This indicates an enhanced coenzyme affinity of the immobilized enzyme with respect to the free ADH. In comparison to the free ADH, the further $K_{m,\ NADPH}$ values of the immobilized enzyme are slightly increased. This implies a reduced coenzyme affinity of the immobilized ADH but also only a slight impact of the diffusion. However, $K_{m,\ Acetone}$ increases from 1.88 mM (pH 6.5) to 11.4 mM (pH 7.5) with increasing pH employed for immobilization. Accordingly, the highest acetone affinity was obtained by immobilization of the ADH at pH 6.5. As all kinetic assays were conducted at pH 7.5, the diffusion limitations of all three immobilisates can be assumed to be similar. Thus, once again, the clear variation of the $K_m$ values can be assigned to alteration of the accessibility of the respective binding sites of the immobilized ADH as well as a possible disability in terms of the fixation of NADPH/acetone. The hindered binding of these molecules can be traced back to time-spreading, which accompanied the immobilization (Figure 15).[69]

The reaction rate $v_{max,\ Acetone}$ increases with increasing pH of the immobilization from pH 6.5 (38.2 µmol $L^{-1}$ $min^{-1}$) to pH 7.0 (61.3 µmol $L^{-1}$ min-$^{1}$) and decreases in the further course to pH 7.5 (57.5 µmol $L^{-1}$ $min^{-1}$). Thus, immobilization of the ADH at pH 7.0 led to the highest $v_{max,\ Acetone}$. This corresponds to the pH

optimum of the free ADH at pH 7.0.[49] However, the dissociation constant $k_{cat}$ of the enzyme-substrate complex increases with increasing pH of the immobilization from 6.74 $s^{-1}$ (pH 6.5) over 12.6 $s^{-1}$ (pH 7.0) to 14.4 $s^{-1}$ (pH 7.5). Thus, after the reduction of acetone, the ADH immobilized at pH 7.5 releases the 2-propanol molecule quickest. As acetone is also an inhibitor of the ADH, $K_{i,\ Acetone}$ was calculated. The lowest value of $K_{i,\ Acetone}$ (178 mM) was detected for the ADH immobilized at pH 7.0 whereas the highest $K_{i,\ Acetone}$ of the ADH (294 mM) was obtained when using a pH 7.5 buffer for immobilization. Compared with $K_{i,\ Acetone}$ of the free ADH, the values of the ADH immobilized at pH 6.5 and pH 7.0 are considerably increased. Thus, concerning the immobilization at pH 6.5 and pH 7.0, the inhibition of the ADH is less pronounced and higher concentrations of acetone are necessary to introduce a substrate inhibition. This is an important side effect of the immobilization.

It is clear that $v_{max,\ Acetone}$ is considerably higher than $v_{max,\ 2\text{-}Propanol}$. Immobilizing the ADH onto MCF-$C_3$-$NH_2$ at pH 6.5, $v_{max}$ of the back reaction proceeds twice as fast as the forward reaction. Employing an immobilization pH of 7.0, the back reaction is nearly six times faster than the forward reaction. If a pH of 7.5 was present in the immobilization, $v_{max,\ Acetone}$ is nearly ten times faster than $v_{max,\ 2\text{-}Propanol}$. This implies a preference for the back reaction. Hence, it is important to evaluate the enzyme efficiencies (EE) and the effectiveness factor (η) of the free and as well as the immobilized ADH.

**Enzyme efficiency (EE) and effectiveness factor (η).** EE is defined as the quotient of $k_{cat}$ and $K_m$. It is a meaningful kinetic parameter as the higher EE, the higher the catalytic efficiency of an (immobilized) enzyme.[140]

Concerning the forward reaction, $EE_{2\text{-}Propanol}$ of the immobilized ADH increases with increasing pH of the immobilization from $2.20 \cdot 10^8$ $s^{-1}$ $(\mu mol\ L^{-1})^{-1}$ (pH 6.5) to $5.21 \cdot 10^8$ $s^{-1}$ $(\mu mol\ L^{-1})^{-1}$ (pH 7.5, Table 21). Thus, the best catalytic efficiency of the ADH was obtained when using a pH 7.5 buffer for the immobilization. However, it is the other way round when looking at the $EE_{2\text{-}Propanol}$ values obtained for the free ADH. $EE_{2\text{-}Propanol}$ decreases from $2.36 \cdot 10^9$ $s^{-1}$ $(\mu mol\ L^{-1})^{-1}$ to $2.14 \cdot 10^9$ $s^{-1}$ $(\mu mol\ L^{-1})^{-1}$ with increasing pH of the buffer solution used for ADH storage. On one hand, immobilization has reversed the $EE_{2\text{-}Propanol}$ values of the ADH. On the other hand, $EE_{2\text{-}Propanol}$ of the immobilized ADH is reduced by one decimal power.

Conversely, the $EE_{Acetone}$ values of the back reaction calculated for the immobilized ADH decrease with increasing pH of the immobilization from $3.58 \cdot 10^9$ $s^{-1}$ $(\mu mol\ L^{-1})^{-1}$ to $1.27 \cdot 10^9$ $s^{-1}$ $(\mu mol\ L^{-1})^{-1}$. These values are one decimal

power higher than the $EE_{2\text{-propanol}}$ values obtained for the forward reaction. This indicates, once again, a preference of the ADH for the back reaction. In the case of the free ADH no distinct trend of the $EE_{Acetone}$ values was observed. However, $EE_{Acetone}$ is two- to three-fold higher as $EE_{2\text{-Propanol}}$ of the forward reaction. Additionally, it is conspicuous that $EE_{Acetone}$ of the ADH immobilized at pH 6.5 is only reduced by 50 % in comparison to the free ADH stored in pH 6.5 buffer.

**Table 21.** Recapitulation of the enzyme efficiencies (EE) and the efficiency factor (η) of the immobilized as well as of the free ADH.

| pH | $EE_{2\text{-Propanol}}$ [$s^{-1}$ (µmol $L^{-1}$)$^{-1}$] | $\eta_{2\text{-Propanol}}$ [%] | $EE_{Acetone}$ [$s^{-1}$ (µmol $L^{-1}$)$^{-1}$] | $\eta_{Acetone}$ [%] |
|---|---|---|---|---|
| **immobilisate** | | | | |
| **6.5** | $2.20 \cdot 10^8$ | 45 | $3.58 \cdot 10^9$ | 40 |
| **7.0** | $3.74 \cdot 10^8$ | 36 | $1.33 \cdot 10^9$ | 46 |
| **7.5** | $5.21 \cdot 10^8$ | 23 | $1.27 \cdot 10^9$ | 70 |
| **free ADH** | | | | |
| **6.5** | $2.36 \cdot 10^9$ | --- | $7.64 \cdot 10^9$ | --- |
| **7.0** | $2.23 \cdot 10^9$ | --- | $6.36 \cdot 10^9$ | --- |
| **7.5** | $2.14 \cdot 10^9$ | --- | $8.83 \cdot 10^9$ | --- |

The effectiveness factor η is specified by the quotient of $v_{max}$ of the immobilized enzyme and $v_{max}$ of the free enzyme. However, η does not consider alterations of the enzyme characteristics resulting from the immobilization. The reduction of $v_{max}$ of the immobilized enzyme is merely traced back to diffusion limitations of substrate/coenzyme molecules into the porous network of the host. Therefore, this parameter has to be interpreted with caution.[139]

Discussing the forward reaction $\eta_{2\text{-Propanol}}$ decreases with increasing pH of the immobilization. Thus, the effectiveness of the immobilized ADH is reduced by 55 % (pH 6.5), 64 % (pH 7.0) as well as 77 % (pH 7.5) as a result of the immobilization. With respect to the largest possible $\eta_{2\text{-Propanol}}$, immobilization at pH 6.5 has to be preferred.

The effectiveness of the ADH of the back reaction shows an opposing trend: $\eta_{Acetone}$ increases with increasing pH of the immobilization. It is reduced by 60 % (pH 6.5), 54 % (pH 7.0) and 30 % (pH 7.5). Hence, with regard to the conversion of

the back reaction and a high $\eta_{Acetone}$, an immobilization pH of 7.5 is most promising as $\eta_{Acetone}$ is highest (70 %).

**Intermediate summary.** The immobilization of the ADH onto the surface of MCF-$C_3$-$NH_2$ had an impact on the Michaelis-Menten kinetics of the immobilized enzyme. The variation of the pH of the immobilization has additionally affected the enzyme kinetics. Amongst others, the coenzyme or substrate affinity of the immobilized ADH as well as $v_{max}$ has been decreased as a result of the immobilization. Furthermore, 2-propanol and acetone were identified to be inhibitors of the ADH. Pertaining to the forward reaction, the highest $v_{max, 2\text{-Propanol}}$ was found when immobilization of the ADH was carried out at pH 6.5. However, the highest 2-propanol affinity was detected for the ADH immobilized at pH 7.5 (Figure 73).

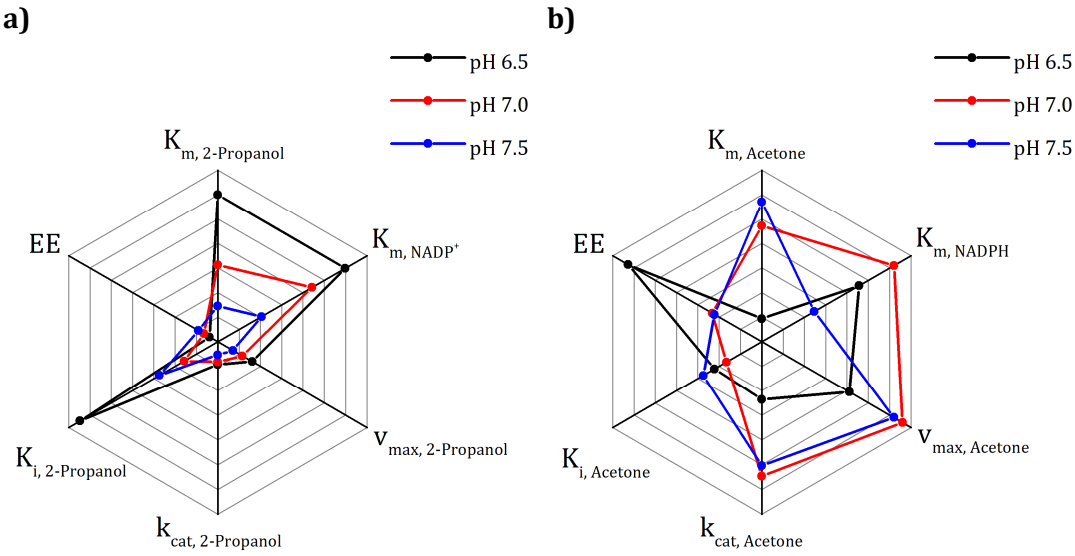


**Figure 73.** Spider charts of the calculated kinetic parameters obtained for the ADH that was immobilized at three different pH values (pH 6.5, 7.0, 7.5) for **a)** forward reaction (2-propanol → acetone) and **b)** back reaction (acetone → 2-propanol). The scaling is the same for both charts. The respective absolute values of the kinetic parameters can be found in Table 19 (forward reaction) as well as in Table 20 (back reaction). The absolute EE values are summarized in Table 21.

The back reaction of the ADH turned out to be preferred, as in comparison to $v_{max,\ 2\text{-Propanol}}$, $v_{max,\ Acetone}$ was considerably enhanced. The highest $v_{max,\ Acetone}$ was gained employing an immobilization pH of 7.0. However, the highest acetone affinity of the immobilized ADH was found when using a pH 6.5 buffer for immobilization.

### 4.4.4 Immobilization of ADH: Summary

ADH from *E. coli* was successfully immobilized onto the surface of MCF-$C_3$-$NH_2$. As an immobilization of the ADH at its pI (pH 6.1) was not possible, three different pH values (6.5/7.0/7.5) were tested as the possible pH of the immobilization (Figure 74). At these pH values the ADH is negatively and the surface of MCF-$C_3$-$NH_2$ is positively charged. Thus, electrostatic interaction between the enzyme and the host were expected as predominant interactions and this was experimentally confirmed. To identify the most appropriate enzyme amount for the immobilization, the proportions of the ADH and MCF-$C_3$-$NH_2$ were varied from 10 - 30 % of ADH. As expected, the ADH uptakes decreased with increasing ADH proportion. Regarding the conversion of 2-propanol to acetone (forward reaction), the retained enzymatic activity after 24 h of immobilization was found to be highest (72 %) when an ADH proportion of 10 % and an immobilization pH of 6.5 were used. With respect to the reduction of acetone to 2-propanol (back reaction), a maximum activity retention of 87 % was obtained by employing an ADH proportion of 10 % in a pH 6.5 buffer for immobilization.

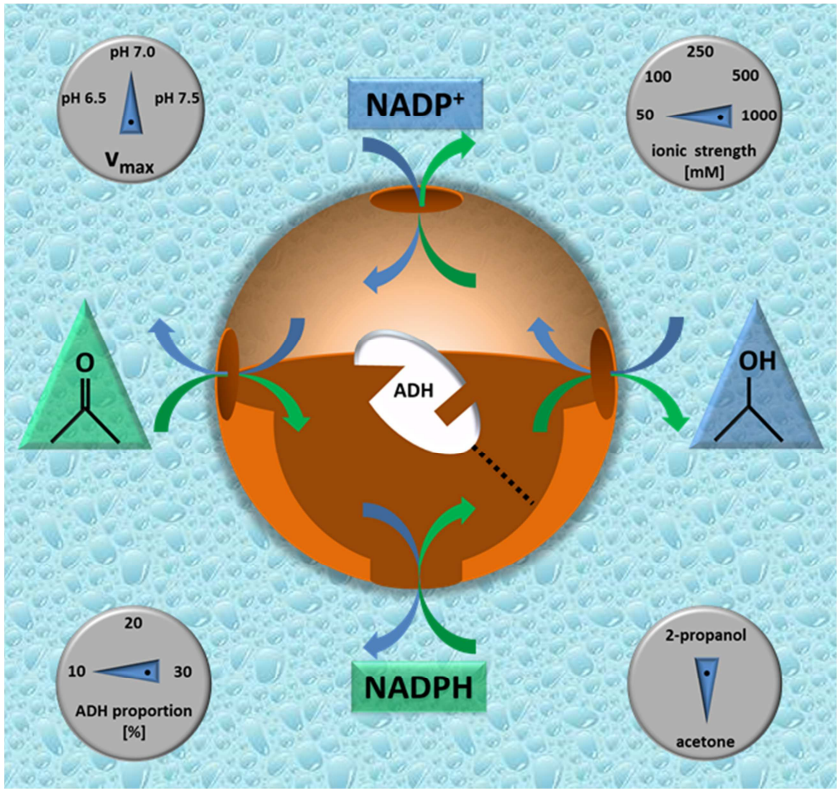


**Figure 74.** Graphical abstract of the immobilization of ADH. The four indication instruments in the corners display the parameters that were varied in the immobilization experiments. The indicator needle points towards the optimum, respectively.

The long-term stabilities of the immobilized ADH were monitored over a period of seven days, for both the forward and the back reaction. No significance dependence between the pH of the immobilization and the course of the remaining activity of the immobilized ADH over this time was observed. However, after seven days, the residual activity of the ADH was higher for the lower ADH amounts used for immobilization. In terms of the long-term activity an ADH proportion of 10 % turned out to be ideal for the immobilization. Thus, the Michaelis-Menten kinetics of these immobilisates for the three pH values of immobilization were investigated.

Independent of the pH of immobilization, the $K_m$ values for the coenzyme and the substrate were increased compared with the free ADH. That applies to the forward as well as the back reaction (Figure 75). It implies a reduction of the coenzyme/substrate affinity of the ADH. These findings were assigned to diffusion limitations and structural changes of the tertiary structure of the ADH due to immobilization.

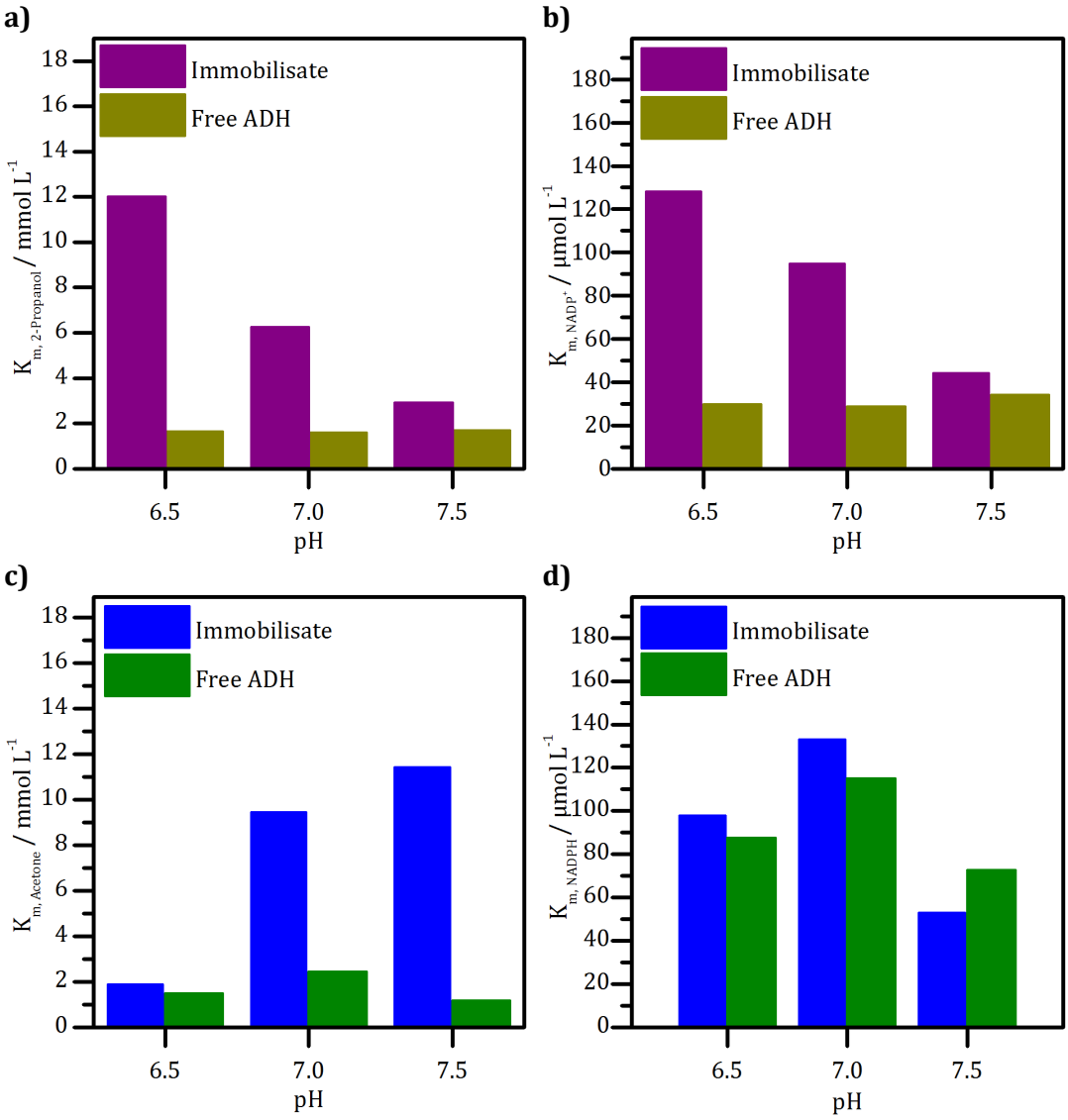


**Figure 75.** Comparative bar graphs of the $K_m$ values for 2-propanol (**a)**) and $NADP^+$ (**b)**) of the free and the immobilized ADH (forward reaction) as well as of the $K_m$ values for acetone (**c)**) and NADPH (**d)**) of the free and the immobilized ADH (back reaction).

Generally, the $v_{max,\ Acetone}$ values of the (immobilized) ADH of the back reaction were determined to be considerably higher than the $v_{max,\ 2\text{-Propanol}}$ values of the forward reaction. This indicates a preference of the (immobilized) ADH for the back reaction. The highest $v_{max,\ 2\text{-Propanol}}$ value of the forward reaction was gained by immobilizing the ADH at pH 6.5, whereas the highest $v_{max,\ Acetone}$ value of the back reaction was received from the immobilization of the ADH at pH 7.0 (Figure 76). Hence, depending on the coenzyme that needs to be recycled ($NADP^+$ or NADPH), the immobilization pH of the ADH has to be selected.

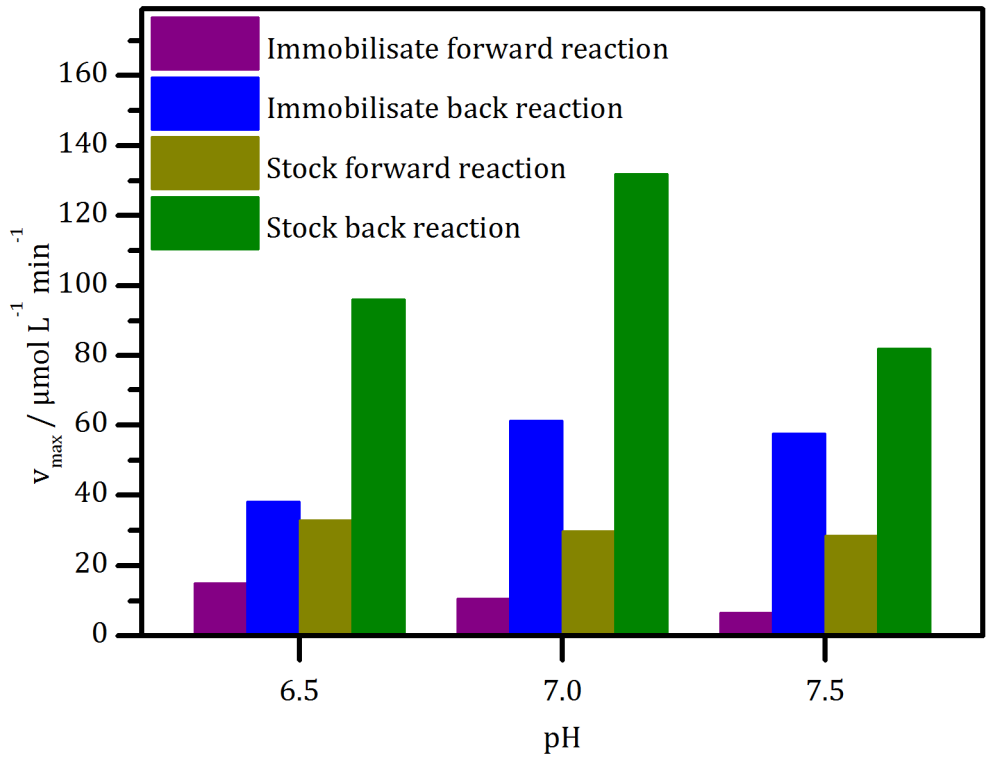


**Figure 76.** Comparison of the $v_{max}$ values of the free ADH of the stock solution and the immobilized ADH obtained for the forward as well as the back reaction, respectively.

The EE of the back reaction was found to be one decimal power higher compared with the forward reaction. Consequently, the immobilized ADH is particularly suitable to re-oxidize NADPH to $NADP^+$.

In comparison with the $v_{max}$ values of the immobilized G6PDH (35.6 µmol $L^{-1}$ $min^{-1}$; Chapter 4.2.2) as well as the immobilized *S.c.*6PGDH (12.0 µmol $L^{-1}$ $min^{-1}$; Chapter 4.3), $v_{max}$ of the back reaction of the immobilized ADH (pH 7.0) is significantly higher (61.3 µmol $L^{-1}$ $min^{-1}$) and thus a rapid re-oxidation of NADPH to $NADP^+$ within the multienzyme cascade is ensured.

## 4.5 Immobilization of glucose-6-phosphate dehydrogenase from *Leuconostoc mesenteroides* (G6PDH)

G6PDH is the first NADPH providing enzyme of the aspired multienzyme cascade (Figure 37). It catalyzes the oxidation of G6P to 6PGDL with subsequent reduction of $NADP^+$ to NADPH. 6PGDL immediately hydrolyzes in the aqueous reaction medium to give 6PG, which is the substrate of 6PGDH (Scheme 2).

A lot of research has been done on the field of the immobilization of G6PDH onto mesoporous silicas and macroporous carbons as well. It was found out that the immobilization of this enzyme onto the surface of MCF-$C_3$-$NH_2$ has high potential in

terms of the long-term stability of the immobilized enzyme.[67, 184, 192] Thus, it was resorted to MCF-$C_3$-$NH_2$ as a host material for the immobilization of G6PDH. Originally, G6PDH was immobilized in a 4-(2-Hydroxyethyl)piperazine-1-ethanesulfonic acid (HEPES) buffer solution (200 mM) possessing pH 7.4. As the enzyme cascade had to be performed at pH 7.5, the immobilization was additionally carried out in phosphate buffer solution (50 mM, pH 7.5). Both buffer systems were compared in terms of its suitability for the G6PDH immobilization (uptakes, long-term stabilities). Likewise, against this background, the Michaelis-Menten kinetics of the immobilized G6PDH was elaborated, too.

According to the literature, the enzymatic assay of G6PDH contains a distinct amount of $MgCl_2 \cdot 6\ H_2O$.[194] However, with respect to the enzyme cascade, as little as possible reagents were required to be present in order to prevent the further participating enzymes from a possible inhibition. Hence, the necessity of the presence of $MgCl_2 \cdot 6\ H_2O$ in the activity assay of G6PDH was evaluated.

### 4.5.1 Characteristics of the immobilization of G6PDH

Within the last years, numerous organically functionalized MCFs, and in particular MCF-$C_3$-$NH_2$, have established as beneficial carriers for the immobilization of G6PDH.[184, 192] Accordingly, for further investigations of the immobilized G6PDH with respect to its employment in the multienzyme cascade, MCF-$C_3$-$NH_2$ was chosen as a host material (Table 22).

**Table 22.** Overview of the material properties of MCF-$C_3$-$NH_2$ employed for the immobilization of G6PDH.

| sample | $S_{BET}$ [$m^2 g^{-1}$] | $V_P$ [$cm^3\ g^{-1}$] | $D_p$ [nm] | $\rho_f$ [mmol $g^{-1}$] | pI |
|---|---|---|---|---|---|
| **MCF-$C_3$-$NH_2$** | 360 | 2.30 | 23 | 1.2 | 8.4 |

**Uptake.** The immobilization of G6PDH onto MCF-$C_3$-$NH_2$ was carried out in HEPES (200 mM, pH 7.4) as well as in potassium phosphate (50 mM, pH 7.5) buffer solution for 24 h at 25 °C, respectively (~1 mg G6PDH + 14 mg MCF-$C_3$-$NH_2$). Independent on the buffer system that was used for the immobilization, an enzyme uptake of 100 % was achieved (Table 23). Furthermore, the immobilization

[194] Sigma-Aldrich: http://www.sigmaaldrich.com/technical-documents/protocols/biology/enzymatic-assay-of-glucose-6-phosphate-dehydrogenase.html **2017**.

procedure turned out to be very fast, as the immobilization of G6PDH was completed after five minutes at latest. This indicates strong attractive interactions between the host material and the enzyme. Fried *et al.* proposed electrostatic interactions between the positively charged surface of MCF-$C_3$-$NH_2$ (pI 8.4) and the negatively charged surface of G6PDH (pI 4.6) to be the driving interactions of the immobilization at pH 7.4.[192] Naturally, this also applies to the immobilization at pH 7.5 in the presence of a phosphate buffer solution (50 mM).

**Table 23.** Summary of the G6PDH uptakes onto MCF-$C_3$-$NH_2$ and percentages by weight in the presence of different immobilization buffers.

| buffer solution | uptake [%] | percent by weight [wt-%] |
|---|---|---|
| HEPES, 200 mM, pH 7.4 | 100 | 7.1 |
| potassium phosphate, 50 mM, pH 7.5 | 100 | 6.9 |

The percentages by weight describe the proportion of enzyme with respect to the immobilisate. It was calculated to amount to 7.1 wt-% when using HEPES (200 mM, pH 7.4) and 6.9 wt-% by using phosphate buffer (50 mM, pH 7.5) solution as a medium of the immobilization. These values cannot be exceeded, as an uptake of 100 % was obtained, respectively.

#### 4.5.1.1 Activity retention after 24 h of immobilization

A meaningful parameter concerning the efficiency of an enzyme immobilization is the retained enzymatic activity after immobilization. Against this background, the activity retention of the G6PDH that was immobilized onto MCF-$C_3$-$NH_2$ was determined immediately after 24 h of immobilization. The enzymatic assays were conducted in the respective buffer solution that was used for the immobilization or rather enzyme storage (stock solutions). In addition, the activity assays were performed with or without the addition of $MgCl_2 \cdot 6\ H_2O$, as the common assay proposes the presence of a final $MgCl_2 \cdot 6\ H_2O$ concentration of 10.0 mM.[194] However, with respect to an application of the immobilized G6PDH in a multienzyme cascade, it was important to additionally elaborate the effect of $MgCl_2 \cdot 6\ H_2O$ on the enzymatic activity. With reference to the enzyme cascade, as little as possible reactants are required in order to avoid any inhibition of the

incorporated immobilized enzymes. All measurements were conducted by using a 1:10 dilution of the immobilized or free enzyme in HEPES (200 mM, pH 7.4) or phosphate buffer solution (50 mM, pH 7.5), respectively (100 µL sample + 900 µL buffer). A dilution of the samples was indispensable in order to match the operating range of the photometer, as the absolute activity of the G6PDH was very high. The enzymatic activities of the dilutions were extrapolated to the undiluted samples. The activity retentions of the G6PDH after 24 h of immobilization (immobilisates) or rather after 24 h of incubation (stock solutions) are presented in Table 24.

**Table 24.** Comparison of the retained activities of the free as well as the immobilized G6PDH immediately after 24 h of immobilization or rather incubation (stock solutions) at 25 °C.

| medium of the enzymatic assay | activity retention [%] |
|---|---|
| **free G6PDH** | |
| HEPES, 200 mM, pH 7.4 | 103.2 |
| HEPES, 200 mM, pH 7.4 / $MgCl_2 \cdot 6\ H_2O$ | 103.6 |
| phosphate, 50 mM, pH 7.5 | 105.4 |
| phosphate, 50 mM, pH 7.5/ $MgCl_2 \cdot 6\ H_2O$ | 105.7 |
| **immobilized G6PDH** | |
| HEPES, 200 mM, pH 7.4 | 20.3 |
| HEPES, 200 mM, pH 7.4 / $MgCl_2 \cdot 6\ H_2O$ | 28.6 |
| phosphate, 50 mM, pH 7.5 | 54.2 |
| phosphate, 50 mM, pH 7.5/ $MgCl_2 \cdot 6\ H_2O$ | 44.2 |

**Immobilization in HEPES/activity assays in HEPES.** After 24 h of immobilization in HEPES (200 mM, pH 7.4), the immobilized G6PDH possessed only 20.3 % of its origin activity (Table 24). By adding $MgCl_2 \cdot 6\ H_2O$ to the activity assay ($c_{final}$ = 11.5 mM), an activity retention of 28.6 % of the immobilized enzyme was obtained. Hence, the presence of $MgCl_2 \cdot 6\ H_2O$ has an activating effect regarding the remained activity of the immobilized enzyme. This effect was not observed for the free enzyme. After 24 h of incubation at 25 °C, the activity of the free enzyme was increased by 3.2 % (without $MgCl_2 \cdot 6\ H_2O$) and 3.6 % (with $MgCl_2 \cdot 6\ H_2O$), respectively. The markedly loss of the enzymatic activity of the immobilized G6PDH in comparison to the native enzyme in the stock solution can be attributed to time-

spreading. Within the immobilization procedure, the enzyme starts to unfold its tertiary structure in order to increase its contact areas with the pore walls (Figure 15). The driving force of this unfolding is the reduction of the intrinsic energy of the enzyme, which is accompanied by an increase of the entropy of the system. Due to the unfolding of the enzyme, the binding of substrate and/or coenzyme molecules can be restricted.[8, 10, 69] Thus, the enzymatic activity of the immobilized G6PDH is reduced.

**Immobilization in phosphate buffer/activity assays in phosphate buffer.** The immobilization of G6PDH in phosphate buffer solution (50 mM, pH 7.5) resulted in an activity retention of 54.2 % (without $MgCl_2 \cdot 6\ H_2O$) as well as 44.2 % (with $MgCl_2 \cdot 6\ H_2O$; Table 24). In this case, the presence of $MgCl_2 \cdot 6\ H_2O$ in the activity assay led to a decrease of the retained activity of the immobilized G6PDH and thus $MgCl_2 \cdot 6\ H_2O$ was supposed to possess a deactivating effect concerning the enzymatic activity. Once again, the reduction of the enzymatic activity after immobilization can be assigned to time-spreading. However, it is less pronounced compared with the immobilization in HEPES (200 mM, pH 7.4), as the activity retention is twice as high regarding the immobilization in HEPES (200 mM, pH 7.4). The activity of the free enzyme after 24 h of incubation at 25 °C in phosphate buffer (50 mM, pH 7.5) was increased to 105.4 % (without $MgCl_2 \cdot 6\ H_2O$ ) and 105.7 % (with $MgCl_2 \cdot 6\ H_2O$), respectively. Hence, the presence of $MgCl_2 \cdot 6\ H_2O$ has no considerable effect in terms of the activity of the free G6PDH in the stock solution.

In the following, the discussion is focused on the long-term stabilities of the immobilized G6PDH. Two different series of measurements were performed (study 1 and study 2). Study 1 was introduced immediately after the immobilization of G6PDH onto the surface of MCF-$C_3$-$NH_2$; whereas study 2 started six days after the immobilization of the enzyme. As already discussed, a dilution of the original immobilisates by employing the buffer of the immobilization was necessary in order to match the operating range of the photometer, respectively.

#### 4.5.1.2 Long-term stability of the immobilized G6PDH (study 1)

An extensive study concerning the long-term stabilities of G6PDH immobilized onto various modified MCFs including MCF-$C_3$-$NH_2$ has been published by Fried *et al*. and is not required at this point.[192] Thus, the long-term stabilities of the free as well as the G6PDH immobilized onto MCF-$C_3$-$NH_2$ were merely monitored

over a five day period immediately after immobilization. The daily activity assays were performed in the buffer solution that was used for the immobilization, respectively.

**General observations.** Proceeding from the absolute enzymatic activity detected immediately after 24 h of immobilization, two days after immobilization or rather after diluting the immobilisates, the activity of the G6PDH increased significantly. The increase was independent on the buffer solution that was used for immobilization and likewise independent on the presence of $MgCl_2 \cdot 6\ H_2O$ (Figure 77). However, this effect was not observed for the native G6PDH in the stock solution. Due to the dilution of the immobilized as well as the free G6PDH by using the respective buffer solution (100 µL sample + 900 mL buffer), more buffer ions per enzyme molecule were available resulting in an additional stabilization of the enzyme. The stabilization of the free G6PDH set in immediately after dilution. Hence, its enzymatic activity remained nearly constant over the period of five days. However, in the case of the immobilized enzyme, the buffer ions needed to diffuse into the mesoporous structure of MCF-$C_3$-$NH_2$ leading to a delayed stabilization of the immobilized enzyme. After a certain stabilization of the immobilized G6PDH was reached, the enzymatic activity remained nearly unaltered over a period of three days, too. This fact confirms an immobilization of the G6PDH within the porous network of MCF-$C_3$-$NH_2$ and not on the outer surface of the host. Over a period of five days, the enzymatic activities follow the general trend that was found for the retained activities after 24 h of immobilization and discussed above.

**Immobilization in HEPES/activity assays in HEPES.** Regarding the long-term stability of G6PDH immobilized in HEPES (200 mM, pH 7.4), the comparatively lowest enzymatic activities were obtained (Figure 77). However, as mentioned above, the presence of $MgCl_2 \cdot 6\ H_2O$ in the activity assays resulted in a minor increase of the activity. This suggests that $MgCl_2 \cdot 6\ H_2O$ has a stabilizing effect in terms of the enzymatic activity when employing HEPES buffer (200 mM, pH 7.4) for the enzymatic assays. With respect to the free G6PDH stored in HEPES (200 mM, pH 7.4), it is the other way round. The native G6PDH possessed a slightly higher activity in the absence of $MgCl_2 \cdot 6\ H_2O$ over a period of five days. Thus, when an immobilization in HEPES (200 mM, pH 7.4) is required, it is preferable to add $MgCl_2 \cdot 6\ H_2O$ to the activity assay of the immobilized G6PDH in order to assure an optimal enzymatic activity.

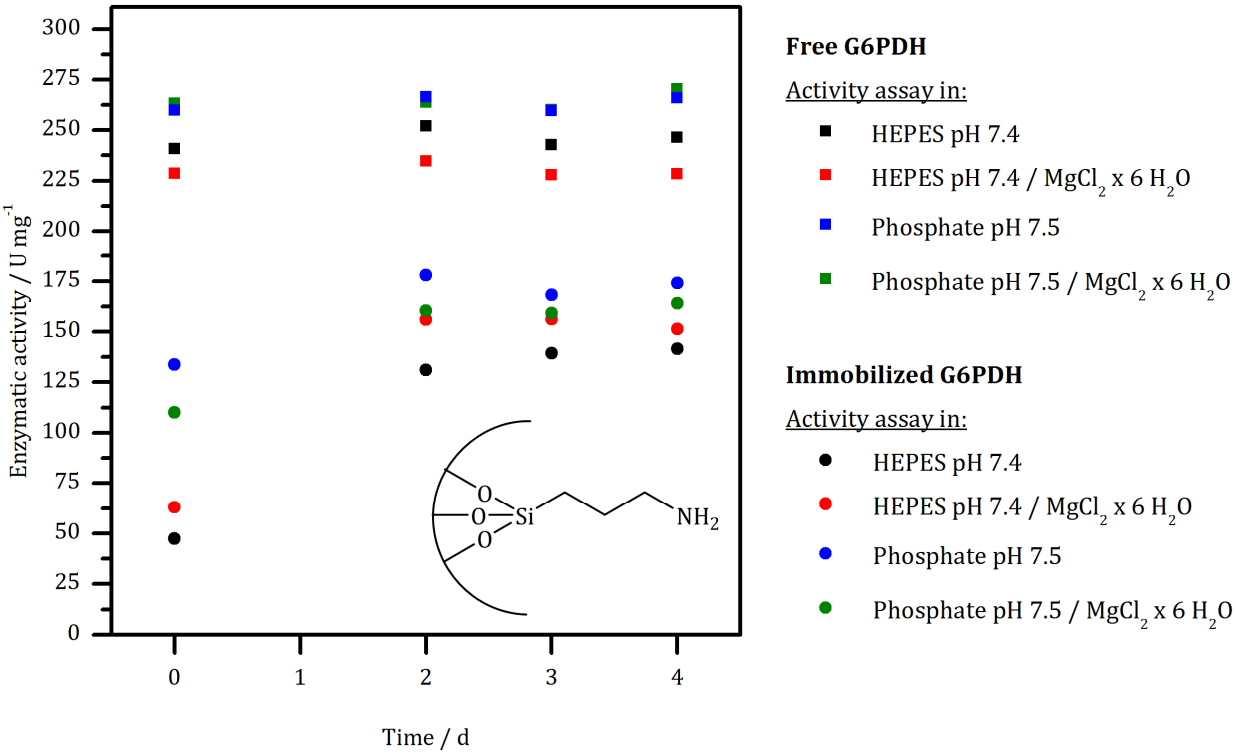


**Figure 77.** Long-term stability of the free as well as of the immobilized G6PDH over a period of five days. Day 0 denotes the day after 24 h of immobilization. The activity assays were performed in the respective buffer solutions of the immobilization (immobilisates) or rather the buffer used for enzyme storage (stock solutions), either with addition of $MgCl_2 \cdot 6\ H_2O$ ($c_{final}$ = 11.5 mM) or without addition of $MgCl_2 \cdot 6\ H_2O$.

**Immobilization in phosphate buffer/activity assays in phosphate buffer.** Over a period of five days, the G6PDH immobilized in phosphate buffer (50mM, pH 7.5) exhibited higher enzymatic activities compared to the enzyme immobilized in HEPES (200 mM, pH 7.4). However, in contrast, the presence of $MgCl_2 \cdot 6\ H_2O$ in the activity assays resulted in a decrease of the enzymatic activities compared to the assays that were performed without the addition of $MgCl_2 \cdot 6\ H_2O$. In this case, the presence of $MgCl_2 \cdot 6\ H_2O$ possessed a destabilizing effect. This effect was observed over the entire 5 day period. With respect to the free G6PDH in phosphate buffer (50 mM, pH 7.5), no correlation between the presence of $MgCl_2 \cdot 6\ H_2O$ in the activity assay and the enzymatic activity could be drawn. However, the activity of the native enzyme in the phosphate buffer solution was apparently higher than the activity of the immobilized G6PDH. It is even higher than the enzymatic activity of the free enzyme in HEPES. Up to here, the long-term stability was best when immobilizing the G6PDH in a phosphate buffer solution (50 mM, pH 7.5). Thus, this buffer system can be recommended for the immobilization of this enzyme. When assaying the immobilized G6PDH in phosphate

buffer (50 mM, pH 7.5) an addition of $MgCl_2 \cdot 6\ H_2O$ should be avoided in order to gain ideal enzymatic activities.

#### 4.5.1.3 Long-term stability of the immobilized G6PDH (study 2)

Six days after immobilization, a new measurement series of long-term stability studies was introduced. As previously mentioned, by reason of the comparatively high absolute enzymatic activity of the immobilized G6PDH, a dilution of the immobilisates was indispensable in order to match the operating range of the photometer. Hence, six days after immobilization, the original immobilisates were again diluted by 1:10 using the respective buffer of the immobilization (100 µL immobilisate + 900 µL buffer). Here, too, the enzymatic activities that were detected for the diluted immobilisates were extrapolated to the undiluted immobilisate.

Once again, the long-term stabilities of the immobilized enzymes were monitored over a period of five days. The daily activity assays of G6PDH immobilized in HEPES (200 mM, pH 7.4) were carried out in HEPES (200 mM, pH 7.4) as well as additionally in phosphate buffer solution (50 mM, pH 7.5). In accordance, the activity assays of G6PDH immobilized in phosphate buffer (50 mM, pH 7.5) were performed in phosphate buffer (50 mM, pH 7.5) and additionally in HEPES (200 mM, pH 7.4). Through this, a connection between the optimal medium of the immobilization as well as the buffer of the enzymatic assay could be drawn. Finally, the activity assays were performed in the presence and in the absence of $MgCl_2 \cdot 6\ H_2O$ ($c_{final}$ = 11.5 mM) in the above mentioned buffer systems. These investigations allow an insight into the importance of $MgCl_2 \cdot 6\ H_2O$ in the enzymatic assay. Furthermore, the enzyme cascade was intended to be performed in phosphate buffer solution (50 mM, pH 7.5), as this buffer system has turned out to be beneficial concerning the immobilized 6PGDH as well as ADH. Hence, the long-term stability of the carrier bound G6PDH had to be investigated in this buffer, independent on the buffer that was originally used for the immobilization of this enzyme.

**Immobilization in HEPES/activity assays in HEPES.** It is striking that the enzymatic activity of G6PDH immobilized in HEPES (200 mM, pH 7.4) increased over a period of three days when likewise assaying it in HEPES (200 mM, pH 7.4; Figure 78). In contrast, in study 1, immediately after immobilization, the activity merely increased within two days after diluting the immobilisate by 1:10

(study 1; Figure 77). However, in this study, which was introduced six days after immobilization, the activity of the freshly diluted sample increased over three days (study 2; Figure 78). As mentioned above, due to the dilution, a larger portion of buffer ions per G6PDH molecule was present. Thus, the dilution led to a pronounced stabilization of the immobilized enzyme. The stabilization was delayed, which can be referred to diffusion limitations of the buffer ions into the porous structure of MCF-$C_3$-$NH_2$. The distinct loss of the original activity of the immobilized enzyme was addressed to time-spreading (Figure 15). This procedure continues over time. Hence, six days after immobilization broad areas of the tertiary structure of G6PDH were unfolded in order to undergo attractive interactions with the pore walls of MCF-$C_3$-$NH_2$. The dilution, and thus the higher ratio of HEPES molecules to enzyme molecules, reversed these adsorptive bonds and contributed to a stabilization of the immobilized G6PDH again. In this study, three days after the dilution, a maximum activity of the immobilized enzyme was obtained. Here again, a considerably higher activity of the immobilized G6PDH was obtained in the presence of $MgCl_2 \cdot 6\ H_2O$ ($c_{final}$ = 11.5 mM) in the enzymatic assays than in its absence. However, this correlation diminished three to four days after dilution. Generally, the maximal activities of the immobilized G6PDH in study 2 were in the same range than detected in study 1 immediately after immobilization (study 1; Figure 77). Thus, it can be stated that no enzymatic activity has been lost during the storage of the immobilized enzyme over six days at 4 °C.

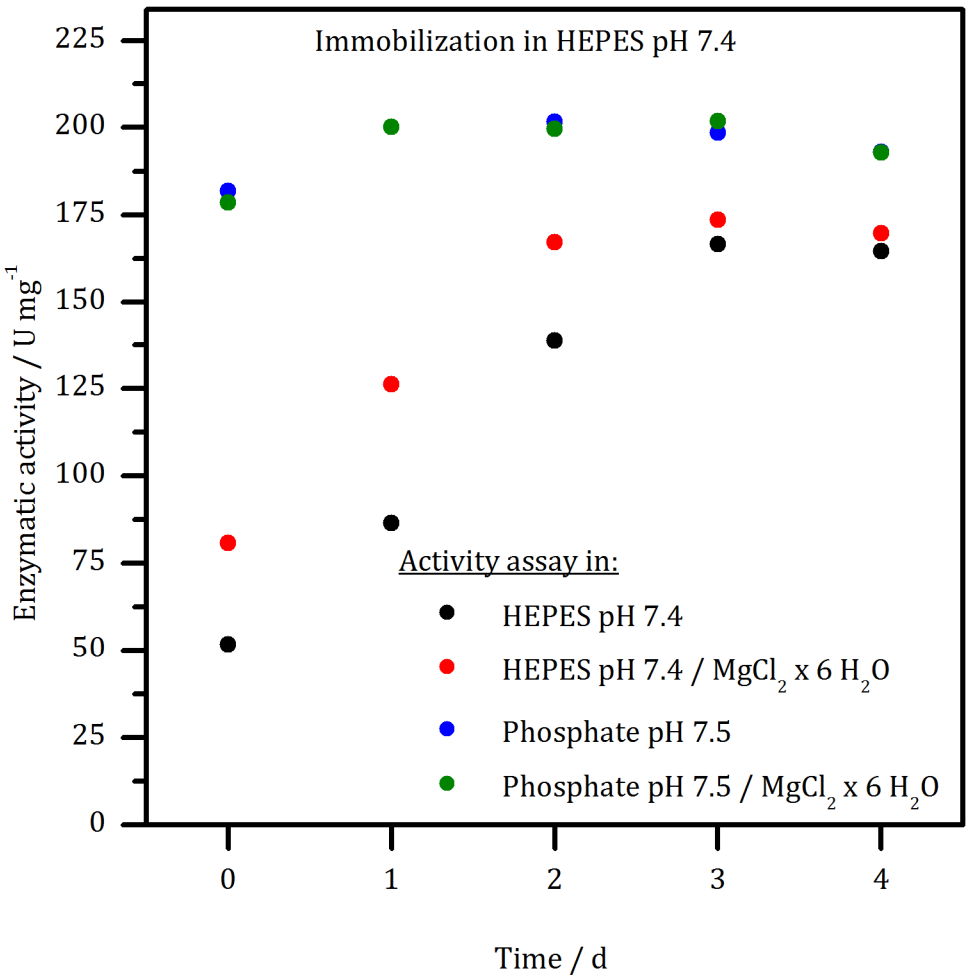


**Figure 78.** Long-term stabilities of G6PDH immobilized onto MCF-$C_3$-$NH_2$ in HEPES (200 mM, pH 7.4) over a period of five days. The dilutions (1:10) of the samples employed for this study were prepared six days after immobilization. Day 0 denotes the day of the dilution. The activity assays were carried out in HEPES (200 mM, pH 7.4) as well as in phosphate buffer solution (50 mM, pH7.5) and performed in the presence or absence of $MgCl_2 \cdot 6\ H_2O$ ($c_{final}$ = 11.5 mM), respectively. The enzymatic activities were extrapolated to the undiluted samples.

**Immobilization in HEPES/activity assays in phosphate buffer.** In study 2, the G6PDH immobilized in HEPES (200 mM, pH 7.4) was additionally assayed in phosphate buffer solution (50 mM, pH 7.5) in order to elaborate the effect of the change of the buffer system (Figure 78). At a first glance, the activity of the G6PDH immobilized in HEPES possessed higher activities when employing phosphate buffer instead of HEPES for the enzymatic assays. Here again, the activity increased within the first day after dilution in HEPES (200 mM, pH 7.4) and reached a maximum of the activity that remained constant over the further period of time. As the immobilized enzyme already reached its maximal activity one day after dilution instead of three days, the ascent of the activity when assaying the immobilized enzyme in HEPES cannot exclusively be referenced to a hindered diffusion of HEPES

molecules into the porous host (cf. paragraph above). Apparently, the phosphate buffer solution owns a distinct stabilizing effect on the immobilized G6PDH. Potentially, it contributed to a fast recovery of the immobilized G6PDH that was affected by time-spreading. This is additionally reflected by the higher activities obtained when using phosphate buffer instead of HEPES for the enzymatic assays. Furthermore, the presence of $MgCl_2 \cdot 6\ H_2O$ ($c_{final}$ = 11.5 mM) in the activity assay had no influence on the enzymatic activity.

**Immobilization in phosphate buffer/activity assays in phosphate buffer.** In study 2, the activity of G6PDH immobilized in phosphate buffer solution (50 mM, pH 7.5) increased over a period of three days when likewise assaying it in phosphate buffer solution (50 mM, pH 7.5). Obviously, regarding this immobilisate, that was stored for six days at 4 °C prior to its introduction into study 2, time-spreading was more pronounced than in terms of using HEPES as an immobilization buffer. Thus, its reversion, and thereby the stabilization of the immobilized G6PDH, was only completed three days after the original immobilisate was diluted again. Accordingly, in the further course, the enzymatic activity remained constant (Figure 79). The presence of $MgCl_2 \cdot 6\ H_2O$ ($c_{final}$ = 11.5 mM) in the activity assay led to slightly lower activities of the immobilized enzyme. This indicates a deactivating effect of $MgCl_2 \cdot 6\ H_2O$ on the immobilized enzyme. However, four days after diluting the original immobilisate in phosphate buffer (50 mM, pH 7.5), the enzymatic activity did not show a dependency on the existence of $MgCl_2 \cdot 6\ H_2O$ in the assay. The maximum enzymatic activity that was obtained in this study corresponds or rather is slightly higher than the activity detected in study 1 immediately after immobilization (study 1; Figure 77). Hence, the storage of the immobilisate for six days at 4 °C has not affected the enzymatic activity.

**Immobilization in phosphate buffer/activity assays in HEPES.** Finally, the enzymatic activity of the immobilisate that was prepared in phosphate buffer (50 mM, pH 7.5) was investigated by performing the activity assays in HEPES (200 mM, pH 7.4). Here again, an increase of the G6PDH activity was observed over an interval of three days; whereas it remained constant in the further course. Prior to the performance of study 2, the immobilisate was stored for six days at 4 °C. Thus, the residual enzymatic activity was affected by extensive time-spreading. The renewed dilution of the original immobilisate by using phosphate buffer (50 mM, pH 7.5) reversed this circumstance in some extent. According to the discussion above, the dilution of the immobilisate increased the ratio of enzyme

molecules to phosphate ions. Hence, three days after dilution, the maximal stabilization of the immobilized G6PDH evened out. The presence of $MgCl_2 \cdot 6\ H_2O$ ($c_{final}$ = 11.5 mM) in the assays resulted in slightly higher activities. However, this effect diminished over time and was negligible after two days.

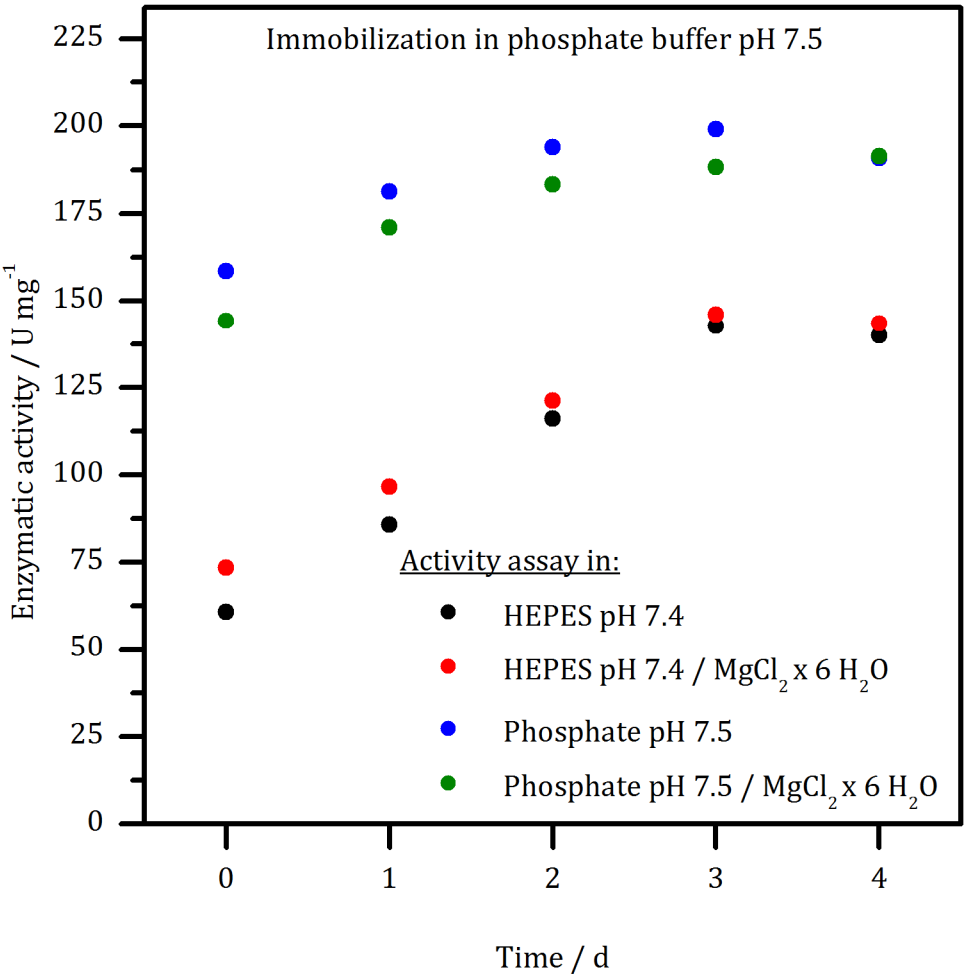


**Figure 79.** Long-term stabilities of G6PDH immobilized onto MCF-$C_3$-$NH_2$ in phosphate buffer (50 mM, pH 7.5) over a period of five days. The dilutions (1:10) of the samples employed for this study were prepared six days after immobilization. Day 0 denotes the day of the dilution. The activity assays were carried out in HEPES (200 mM, pH 7.4) as well as in phosphate buffer solution (50 mM, pH7.5) and performed in the presence or absence of $MgCl_2 \cdot 6\ H_2O$ ($c_{final}$ = 11.5 mM), respectively. The enzymatic activities were extrapolated to the undiluted samples.

**Intermediate summary.** The immobilization of G6PDH onto the surface of MCF-$C_3$-$NH_2$ was carried out in HEPES (200 mM, pH 7.4) and in phosphate buffer solution (50 mM, pH 7.5), respectively. Independent on the buffer system, an enzyme uptake of 100 % was obtained. The residual activity after 24 h of immobilization was almost twice as high when using a phosphate buffer solution instead of HEPES (200 mM, pH 7.4) as medium of the immobilization. The activity

assays were performed in the presence as well as in the absence of $MgCl_2 \cdot 6\ H_2O$. A final $MgCl_2 \cdot 6\ H_2O$ amount of 11.5 mM in the activity assay either stabilizes the immobilized G6PDH when the immobilization and the assay were carried out in HEPES or destabilizes the immobilized enzyme when the immobilization as well as the activity assay were performed in phosphate buffer solution (50 mM, pH 7.5). Furthermore, the influence of the buffer system of the activity assay on the enzymatic activity of the immobilized enzyme was investigated. It turned out that independent on the buffer that was used for the immobilization the enzymatic activity was highest when using a phosphate buffer solution (50 mM, pH 7.5) as a medium for the enzymatic assays. This is a very promising result, as the multienzyme cascade is intended to be operated in phosphate buffer solution (50 mM, pH 7.5) and under exclusion of $MgCl_2 \cdot 6\ H_2O$.

### 4.5.2 Michaelis-Menten kinetics of the immobilized G6PDH

In supplementation of the long-term stabilities of the immobilized G6PDH, it was consequent to investigate the Michaelis-Menten kinetics of the immobilized enzyme. Besides, knowledge concerning the kinetic of the immobilized enzyme was important, as the immobilisate was destined to be incorporated in an enzyme cascade. The immobilization of G6PDH was carried out in HEPES (200 mM, pH 7.4) as well as in phosphate buffer solution (50 mM, pH 7.5). Hence, the kinetic investigations were performed in the respective media employed for immobilization. Furthermore, the kinetic assays of G6PDH immobilized in HEPES (200 mM, pH 7.4) were additionally conducted in phosphate buffer solution (50 mM, pH 7.5). This was accomplished against the background of the utilization of phosphate buffer solution (50 mM, pH 7.5) as a medium of the aspired multienzyme cascade. The kinetic assays were conducted by either varying the G6P concentration or by the variation of the $NADP^+$ concentration at 25 °C, while keeping the concentration of the respective other reaction partner constant (Figure 80). All kinetic measurements were performed by exclusively using the 1:10 diluted immobilisates. With respect to the incorporation of the immobilisates into the enzyme cascade, all measurements were performed in the absence of $MgCl_2 \cdot 6\ H_2O$.

**Immobilization in HEPES (200 mM, pH 7.4).** The immobilization of G6PDH in HEPES (200 mM, pH 7.4), followed by kinetic investigations in the same buffer, resulted in a $K_{m,\,G6P}$ value of 304 µM (Table 25; Eq. 10). Hence, a substrate concentration of 304 µM is necessary to receive a half-maximum reaction rate of

G6PDH. As it was discussed above, $K_m$ is also a measure of the affinity of an enzyme to its substrate or coenzyme. The lower $K_m$, the higher the substrate or coenzyme affinity of the enzyme.[139, 140] When the kinetic assay was performed in phosphate buffer solution a $K_{m, G6P}$ value of 598 µM was calculated. This implies that the substrate affinity of the immobilized G6PDH has been decreased due to the change of the buffer solution employed for the measurement. However, the Michaelis-Menten constant of the coenzyme ($K_{m, NADP^+}$) is quite high (176 µM) when carrying out the kinetic assays in HEPES (200 mM, pH 7.4). Conversely, $K_{m, NADP^+}$ merely amounts to 23.6 µM by conducting the assays in phosphate buffer (50 mM, pH 7.5). Both immobilizations were operated in HEPES (200 mM, pH 7.4). Thus, the divergent $K_m$ values have to be assigned as an effect of the respective buffer that was employed for the kinetic assays, as the orientation and the accessibility of the respective binding sites of the immobilized G6PDH were equal.

**Table 25.** Summary of the kinetic parameters of G6PDH immobilized onto the surface of MCF-$C_3$-$NH_2$. The buffer of the immobilization as well as the buffer of the kinetic assay was varied.

| immobilization in | kinetic assay in | $K_{m, G6P}$ [µM] | $K_{m, NADP^+}$ [µM] | $v_{max}$ [µmol $L^{-1}$ $min^{-1}$] | $k_{cat}$ [$s^{-1}$] | EE [$s^{-1}$ (µmol $L^{-1}$)$^{-1}$] |
|---|---|---|---|---|---|---|
| HEPES | HEPES | 304 | 176 | 10.9 | 111 | $3.66 \cdot 10^{11}$ |
| HEPES | Phos. | 598 | 23.6 | 35.6 | 363 | $6.07 \cdot 10^{11}$ |
| Phos. | Phos. | 512 | 33.0 | 21.5 | 258 | $5.03 \cdot 10^{11}$ |

HEPES: 200 mM, pH 7.4; Phos. = phosphate buffer solution: 50 mM, pH 7.5

Again, the maximum reaction rates ($v_{max}$) were calculated by means of the Lineweaver-Burk plot (Eq. 9; Figure 80). On the basis of the regression line besides $K_m$, $v_{max}$ was calculated. $v_{max}$ accounts 10.9 µmol $L^{-1}$ $min^{-1}$ when carrying out the kinetic assay in HEPES (200 mM, pH 7.4) and 23.6 µmol $L^{-1}$ $min^{-1}$ by using phosphate buffer (50 mM, pH 7.5) for the kinetic assays. Here again, the usage of phosphate buffer as a reaction medium for the G6PDH immobilized in HEPES (200 mM, pH 7.4) turned out to be advantageous. The deviation of the $v_{max}$ values were merely attributed to the different buffer solution within the kinetic assays.

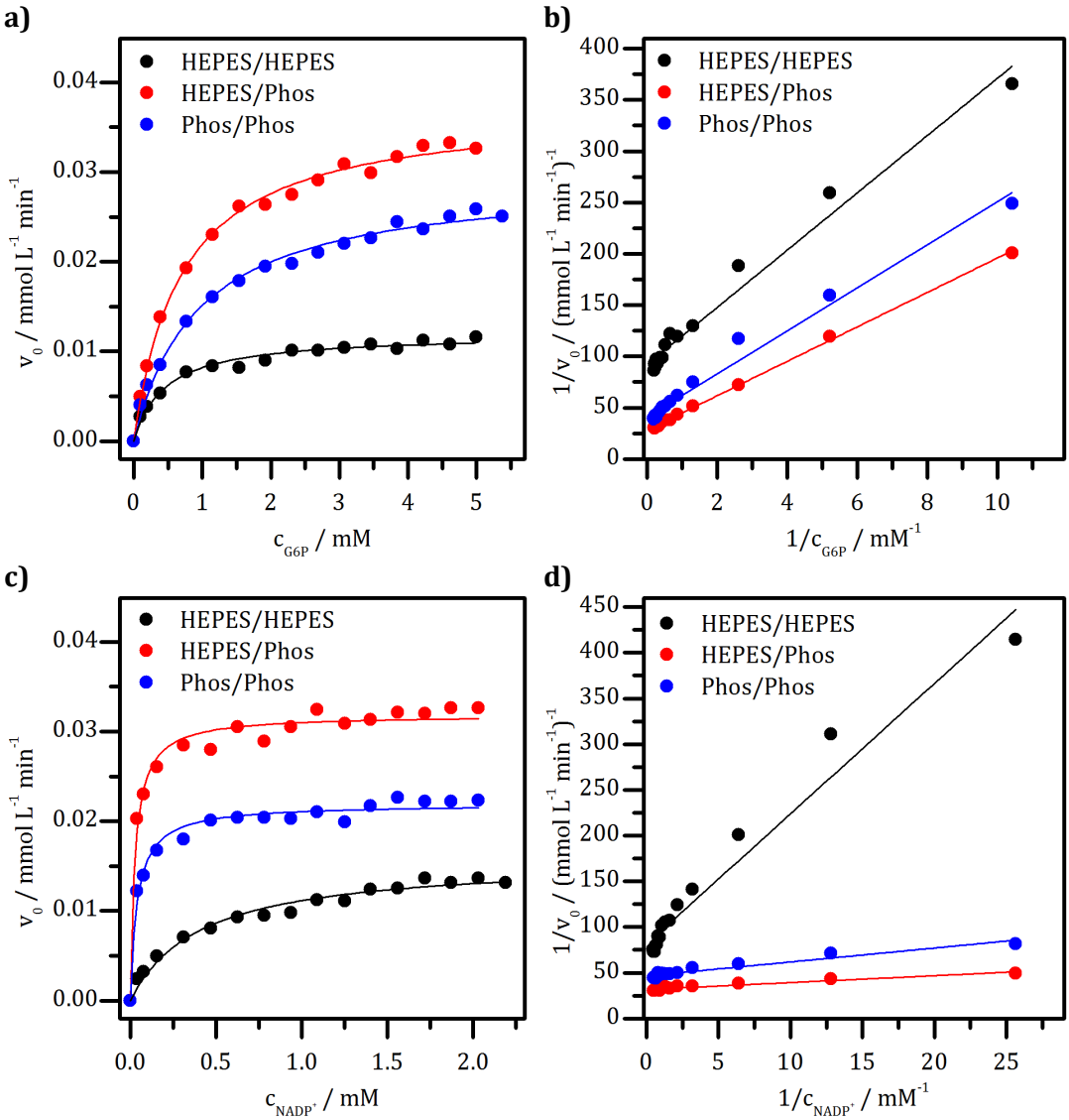


**Figure 80.** Graphical evaluation of the Michaelis-Menten kinetics of G6PDH immobilized onto the surface of MCF-$C_3$-$NH_2$. **a)** Michaelis-Menten diagram for the variation of the G6P concentration; **b)** Lineweaver-Burk diagram for the variation of the G6P concentration; **c)** Michaelis-Menten diagram for the variation of the $NADP^+$ concentration; **d)** Lineweaver Burk diagram for the variation of the $NADP^+$ concentration. Legends: buffer of the immobilization / buffer of the kinetic assay.

$k_{cat}$ is the decomposition constant of the enzyme-substrate complex and is dependent on $K_m$ and $v_{max}$ as well (Eq. 11). To be clearer and more precise, $k_{cat}$ is supposed to be the turnover number of the enzyme. It is quite obvious that $k_{cat}$ is threefold higher when assaying the enzyme in phosphate buffer (363 $s^{-1}$) than in HEPES (111 $s^{-1}$). Thus, in the presence of phosphate buffer, 363 molecules of G6P were converted, whereas in the existence of HEPES solely 111 G6P molecules were oxidized per second and per active site of the immobilized G6PDH. Pursuant to these results, the EE value of the G6PDH assayed in phosphate buffer

($6.07 \cdot 10^{11}$ $s^{-1}$(µmol $L^{-1}$)$^{-1}$) is almost twice as high as the EE value of the immobilized G6PDH that was assayed in HEPES ($3.66 \cdot 10^{11}$ $s^{-1}$(µmol $L^{-1}$)$^{-1}$; Eq. 12).

**Immobilization in phosphate buffer (50 mM, pH 7.5).** The immobilization of G6PDH and the subsequent investigation of the Michaelis-Menten kinetics were additionally carried out in phosphate buffer solution (50 mM, pH 7.5). It is conspicuous that the kinetic parameters are ranging between the respective values calculated for the enzyme immobilized in HEPES and assayed in HEPES as well as the G6PDH immobilized in HEPES and assayed in phosphate buffer solution (Table 25). However, the kinetic parameters tend clearly to the values that were received for the immobilization of G6PDH in HEPES and the subsequent kinetic assay in phosphate buffer solution. Thus, regarding the Michaelis-Menten kinetics, phosphate buffer solution (50 mM, pH 7.5) as a reaction medium of the immobilized G6PDH has unambiguously to be preferred.

**Intermediate summary.** In conclusion, the Michaelis-Menten experiments disclosed that the buffer solution employed for the immobilization has an influence on the kinetic behavior of the immobilized G6PDH. Accordingly, the utilization of HEPES (200 mM, pH 7.4) within the immobilization procedure is preferable. Independent on the buffer of the immobilization, in terms of the enzyme kinetics of the immobilized G6PDH, phosphate buffer solution (50 mM, pH 7.5) turned out to be a benefitting reaction medium, as the highest $v_{max}$ and EE values were obtained by using this buffer in the kinetic assays (Figure 81).

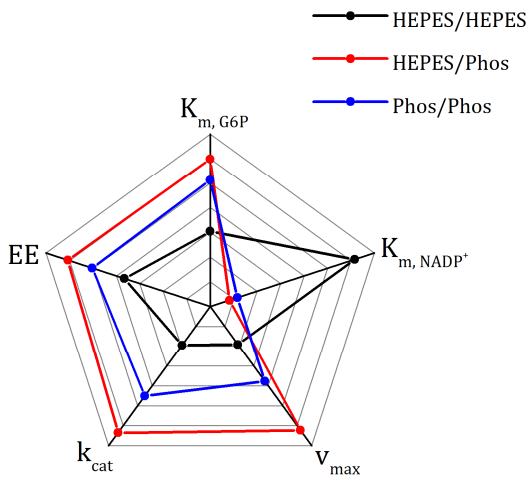


**Figure 81.** Spider chart of the calculated kinetic parameters obtained for the G6PDH that was immobilized onto MCF-$C_3$-$NH_2$ in HEPES (200 mM, pH 7.4) and in phosphate buffer solution (50 mM, pH 7.5), respectively. The kinetic assays were carried out in HEPES as well as in phosphate buffer. Legend: buffer of the immobilization / buffer of the kinetic assay. The respective absolute values of the kinetic parameters can be found in Table 25.

With respect to an incorporation of the immobilized G6PDH into the enzyme cascade, an immobilization in HEPES (200 mM, pH 7.4) and a reaction medium containing phosphate (50 mM, pH 7.5) have to be favored.

### 4.5.3 Immobilization of G6PDH: Summary

The immobilization of G6PDH was electrostatically performed onto the surface of MCF-$C_3$-$NH_2$ by either using HEPES (200 mM, pH 7.5) or phosphate buffer (50 mM, pH 7.5) solution as a medium of the immobilization. First of all, the enzymatic assays were carried out in the buffer of the immobilization, respectively. Furthermore, these assays were conducted in the presence and in the absence of $MgCl_2 \cdot 6\ H_2O$. With respect to the long-term stabilities of the immobilized G6PDH, it was found out that an immobilization in phosphate buffer has to be preferred. The retained activity immediately after 24 h of immobilization was almost twice as high compared to the employment of HEPES as a buffer of the immobilization. When the enzymatic assays were carried out in the same buffer solution, which was used for the immobilization, the presence of $MgCl_2 \cdot 6\ H_2O$ in the assays had an activating (HEPES) or deactivating effect (phosphate buffer) on the immobilized G6PDH. This result was appreciated, as the aimed enzyme cascade was intended to be performed in phosphate buffer solution (50 mM, pH 7.5) without the addition of $MgCl_2 \cdot 6\ H_2O$.

Irrespective of the buffer solution deployed for the immobilization of G6PDH, the enzymatic assays were performed in HEPES or phosphate buffer, respectively. It was found that independent on the buffer used for the immobilization the enzymatic activity was highest by applying phosphate buffer solution (50 mM, pH 7.5) as a medium of the enzymatic assays. Considering the enzyme cascade, this was a promising result.

The kinetic investigations of the immobilized G6PDH revealed a preferential immobilization of G6PDH in HEPES (200 mM, pH 7.4) accompanied by phosphate buffer (50 mM, pH 7.5) as an ideal reaction medium of the immobilisate. The combination of these experimental conditions resulted in the comparatively highest values of $v_{max}$ as well as EE. Hence, this immobilisate is very well suited to be incorporated into the aspired enzyme cascade.

### 4.6 Construction of a modular enzyme cascade

In the prior chapters, the immobilization of G6PDH, 6PGDH as well as ADH onto organically modified MCF has extensively been discussed and the ideal conditions of the immobilizations were identified, respectively. Irrespective of the enzyme, MCF-$C_3$-$NH_2$ figured out to be the most promising support material in each case. In terms of the long-term stability and the Michaelis-Menten kinetics, a distance of three carbon atoms between the respective oxidoreductase and the pore walls turned out to be ideal. The knowledge that was gained concerning the respective immobilization enables to construct a modular enzyme cascade. The main reaction sequence of this cascade is a reaction path of the pentose phosphate pathway. Within living cells it is responsible for the degradation of glucose to ribulose-5-phosphate.[20] In the present approach the reaction sequence is performed outside of a cell with the respective enzymes immobilized onto MCF-$C_3$-$NH_2$. Besides the conversion of G6P to Ru5P, the immobilized G6PDH as well as 6PGDH provide one equivalent $NADP^+$, respectively. The integration of an immobilized ADH into the modular cascade enables the re-oxidation of NADPH to $NADP^+$. Thus, the recycling of the coenzyme is ensured. The $v_{max}$ values of the carrier bound G6PDH as well as 6PGDH are considerable lower than $v_{max}$ of the immobilized ADH. As $v_{max}$ of the 6PGDH attached to the surface of MCF-$C_3$-$NH_2$ is lowest, this reaction step of the enzyme cascade is rate-determining (Figure 82); whereas the ADH-catalyzed oxidation of NADPH to $NADP^+$ is fastest. This is the best prerequisite to ensure a high efficiency of the cofactor recycling system.

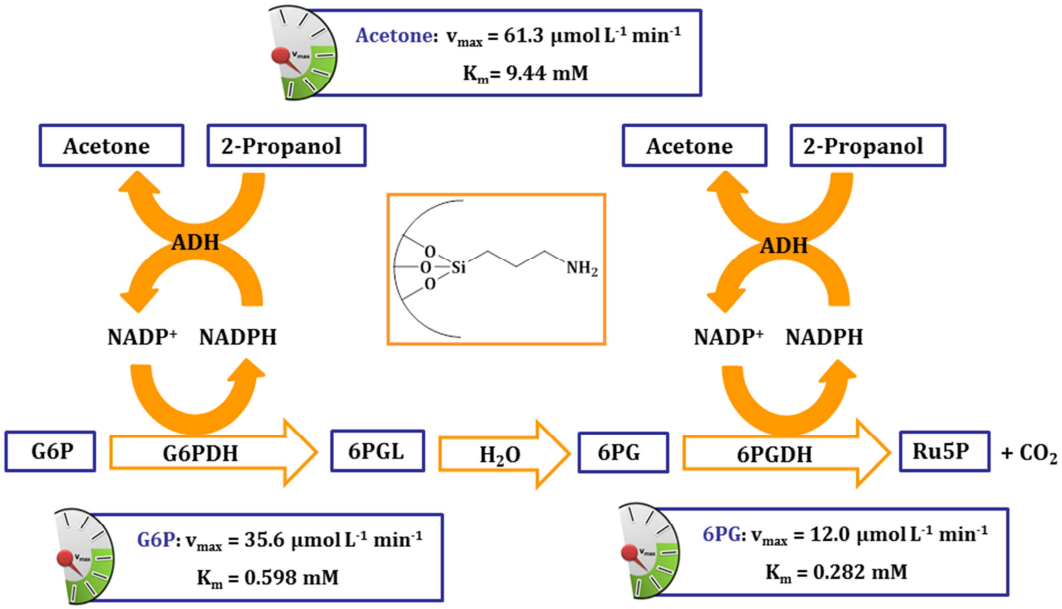


**Figure 82.** Modular enzyme cascade consisting of a reaction sequence of the pentose phosphate pathway, linked to a cofactor recycling system. The immobilizations of the enzymes were carried onto MCF-$C_3$-$NH_2$ (orange box). The blue boxes recap the most prominent kinetic parameters of the immobilized enzymes, respectively. Evidently, $v_{max}$ of the immobilized ADH is highest in comparison to the G6PDH as well as 6PGDH ensuring an efficient recycling of the coenzyme.

The original concept of the enzyme cascade based upon a stationary assembly consisting of three stacked glass columns. Each immobilisate was intended to be deposited onto the filter membrane of one column. However, the implementation of this highly complex system ran into difficulties. After some necessary adjustments, the enzyme cascade was operational. Regarding the initially experienced difficulties, the extended approach of the cascade will be introduced and discussed in this chapter.

### 4.6.1 Cycle stabilities of the immobilized enzymes

Immobilized enzymes have the reputation for frequent recirculation. With regard to an effective catalysis, it had to be proven that the enzyme molecules were tightly bound to the host in order to avoid any leaching. The contamination of the substrate solution by amounts of leached enzyme is unrequired and affects the efficiency of the immobilisate in the further cycles. Furthermore, a long-time use of the immobilisate is requested, as it increases the efficiency of an enzyme-catalytic approach. Thus, cycle stability studies were performed. As described within the former discussion, under certain conditions, no leaching of the immobilized enzymes was detected. However, this result needed to be specified.

In order to guarantee comparability and reproducibility of these tests, with respect to all three immobilized enzymes, it was conducted in centrifugal tubes from *Merck-Millipore* (Figure 83). These tubes own a cylindrical inset with a hydrophilic polytetrafluoroethylene (PFTE) membrane. This membrane possesses a pore size of 0.45 µM avoiding the MCF particles to pass through.

**Figure 83.** Ultrafree®-CL centrifugal devices from *Merck-Millipore* possessing a hydrophilic PFTE membrane with a pore size of 0.45 µm (UFC40LH25). Copyright *Merck-Millipore* 2017.[195] With respect to a high comparability as well as reproducibility, these centrifugal tubes were used for the cycle stability tests of the immobilized enzymes.

Based upon the respective enzymatic activity assays, cycle stability tests were performed. The stability of each immobilisate was tested over 10 cycles. All reactants (substrate, coenzyme and buffer) and the immobilisate were combined in the filter inset of the centrifugal tubes, mixed by inversion and shaken for 3 min at 25 °C and 350 rpm. After this incubation, the substrate/coenzyme solution was separated by centrifugation (2 min, 4000 rpm), whereas the immobilisate remained on the PFTE membrane of the inset. In the further course, to induce the next cycle, the immobilisate was redispersed in a fresh substrate/coenzyme solution. The absorption of the centrifugate was monitored over 1 min ($\lambda$ = 340 nm, 25 °C), respectively. It needs to be emphasized that in order to avoid errors it was irremissible to detect the absorbance of the supernatants over a period of 1 min. If no leaching within the separation step occurred, the absorbance of the centrifugate was assumed to be constant over the measuring time. However, in the case of leaching, the absorbance increases over time. The absorbance of the centrifugate of the first cycle was set to a relative stability of 1.0. The absorbances of the substrate/coenzyme solution of all further cycles were standardized to this value.

[195] *Merck-Millipore*: http://www.merckmillipore.com/DE/de/product/Ultrafree-CL-LH-Centrifugal-Filter,MM_NF-UFC40LH25, **2017**.

The amount of the leached enzyme during ten cycles was calculated by means of the increasing absorbance detected for the respective centrifugate of each cycle. Due to enzyme concentrations below the limit of analytical determination, a determination according to the Bradford assay was unfeasible.

**G6PDH.** According to the pH value of the immobilization (pH 7.4/7.5), the predominant interactions between the surface of G6PDH (pI 4.6) and the surface of MCF-$C_3$-$NH_2$ (pI 8.4) were proposed to be electrostatic.[192] The cycle stability tests were performed for the G6PDH immobilized in HEPES (200 mM, pH 7.4) as well as phosphate buffer (50 mM, pH 7.5). The studies were carried out in HEPES (200 mM, pH 7.4) and phosphate buffer (50 mM, pH 7.5), respectively. Conspicuously, the second cycle was characterized by a distinct loss of the relative stability of the immobilized G6PDH (Figure 84). Dependent on the buffer of the immobilization and the buffer of the cycle stability tests, after the third cycle the enzymatic activity decreased by about 75 – 85 %. With respect to these immobilisates, the relative stability was highest for G6PDH immobilized and assayed in HEPES and lowest for the enzyme immobilized in HEPES and assayed in phosphate buffer solution. The stability of the G6PDH immobilized and assayed in phosphate buffer solution was determined to be in between. In the following cycles, the decrease of the relative stability was considerably lower, whereas the dependency between the buffer of the immobilization and the buffer of the cycle stability tests persists. After ten cycles 52 - 88 % of the immobilized enzyme was leached. This is reflected in the relative stabilities, as the residual amount of immobilized G6PDH becomes reduced from cycle to cycle. Hence, the decrease of the stability can be referenced to leaching of the immobilized enzyme. However, after ten cycles, the remained relative stability did not show a distinctive proportionality to the amounts of leached G6PDH anymore. It was nearly the same for each G6PDH immobilisate. Thus, the decrease of the relative stability of the immobilisates that were minor affected by leaching can be addressed to pronounced denaturation of the immobilized enzyme after ten cycles. Hence, the coexistence of leaching as well as denaturation resulted in a loss of the relative stability of the immobilisates, respectively. However, a correlation of the buffer of the respective immobilization as well as the buffer of the cycle stability test is noteworthy. Leaching was pronounced for G6PDH that was immobilized in HEPES and assayed in HEPES (88 %/10 cycles). By alternatively using phosphate buffer for the stability test, the amount of leached enzyme was reduced to 56 % after ten cycles. This implies a destabilization of the electrostatic bonds between the enzyme and the host by employing HEPES as a

reaction medium. The destabilization of these attractive interactions results in leaching.

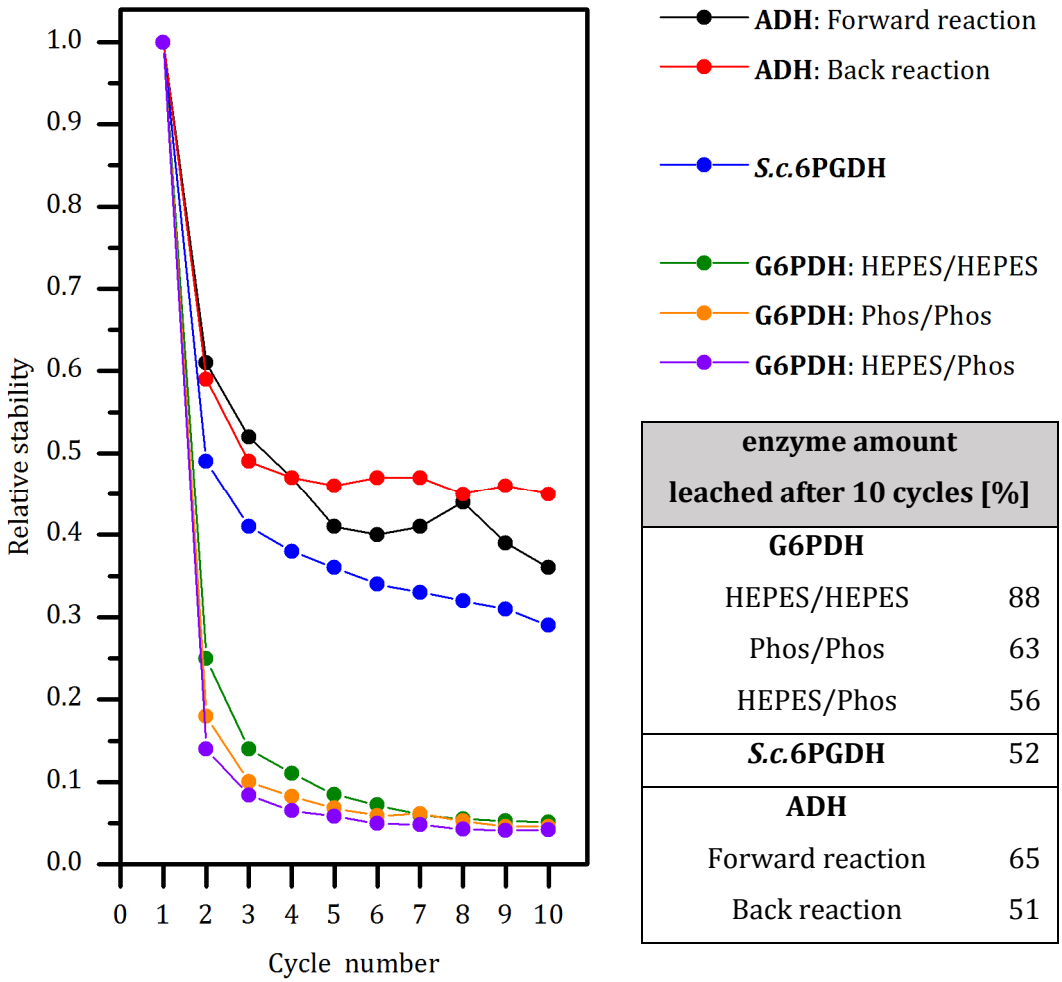


| enzyme amount leached after 10 cycles [%] | |
|---|---|
| **G6PDH** | |
| HEPES/HEPES | 88 |
| Phos/Phos | 63 |
| HEPES/Phos | 56 |
| ***S.c.*6PGDH** | 52 |
| **ADH** | |
| Forward reaction | 65 |
| Back reaction | 51 |

**Figure 84.** Cycle stabilities of the immobilized G6PDH, 6PGDH as well as ADH over 10 reaction cycles. The absorbance of the centrifugate of the first cycle was set to a relative stability of 1.0 and the absorbances of the further cycles were standardized to this value, respectively. The table besides lists the total amounts of enzyme leached after ten cycles.

***S.c.*6PGDH.** The prevailing interactions between 6PGDH and MCF-$C_3$-$NH_2$ were determined to be hydrophobic. After the second cycle, the immobilized 6PGDH suffered a loss of its relative stability of about 50 % (Figure 84). The steep decrease of the stability was followed by a further loss of stability. However, in the further course, it was less distinct. After ten cycles, approximately 30 % of the origin stability of the immobilized 6PGDH remained. The decrease of the stability over ten cycles was accompanied by leaching of 52 % of the originally amount of immobilized 6PGDH. Thus, the decreases of the immobilized enzyme cannot only be attributed to denaturation but rather to a pronounced leaching.

**ADH.** Here, electrostatic interactions between the charged surfaces of ADH (pI 6.1) and MCF-$C_3$-$NH_2$ (pI 8.4) resulted in the immobilization (pH 7.0). The cycle stability studies were performed for the forward as well as the back reaction (Figure 84). Likewise, the second cycle of the forward and the back reaction was associated with a significant loss of relative stability. However, it was lowest in comparison to the immobilized 6PGDH or rather G6PDH, as the relative stability of the immobilized ADH merely decreased by approximately 40 %. After ten reaction cycles in phosphate buffer solution (50 mM, pH 7.5), the stability of the immobilized ADH was reduced by ~65 % concerning the forward reaction and ~55 % regarding the back reaction. The performance of ten cycles was accompanied by leaching of 65 % (forward reaction) as well as 51 % (back reaction) of the originally amount of immobilized enzyme. With respect to the forward reaction, a connection between the amount of leached enzyme and the relative stability can be drawn. The higher amount of leached enzyme after ten cycles resulted in a higher decrease of the relative stability, in comparison to the back reaction. Furthermore, it could have been expected that the relative stability of the immobilized ADH is similar or rather equal for the forward as well as for the back reaction. However, the stabilities differ by 10 %. This indicates an influence of the substrate on the leaching behavior. Apparently, 2-propanol contributes to the leaching of ADH from the support material, whereas acetone prevents the immobilized ADH from leaching in some extend.

Irrespective of the immobilisate used for the cycle stability tests, a more or less distinctive loss of the enzyme stability was observed with increasing number of cycles. These forfeits of the enzymatic activity can mainly be addressed to a pronounced leaching behavior of the immobilized enzyme from the surface of the respective host. Apparently, the leaching occurred during the separation step of the immobilisates (2 min, 4000 rpm). Centrifugal forces arising during centrifugation were proposed to drag along amounts of the immobilized enzyme. This was very distinctive for the second cycle of each immobilized enzyme. Against this background, it can be stated that neither an immobilization by hydrophobic interaction (6PGDH) nor the immobilization due to electrostatic interactions (G6PDH, ADH) are suited to prevent these enzymes from leaching.

The aspired enzyme cascade was intended to be realized by three stacked glass columns with a deposition of one immobilisate onto the membrane of each column. However, as the cycle stability tests came along with extended leaching, a new technique concerning a leaching-free separation of the immobilisates had to be

developed. Countless methods were tested to remove the immobilisates from the substrate/coenzyme solution without the appearance of leaching. First of all, it was evident to stepwise reduce the rpm of the centrifuge to the minimum. However, independent on the rpm, leaching was observed. In the further course a separation of the immobilisates by means of syringe filters, one to five filter papers and much more was tested. None of these separation techniques were qualified to separate the immobilisate from the reaction batch, as leaching appears steadily. Hence, it turned out that not necessarily centrifugal forces initiate leaching of the enzyme from the hosts, as it also occurred when simply using filter papers for separation. On the contrary, apparently, certain amounts of the respective enzyme leach from the host when dispersing the immobilisates in aqueous buffer solution. Correspondingly, the focus of a reliable separation technique was placed onto the re-immobilization of the leached enzyme from the substrate/coenzyme solution by employing an appropriate filter material. Besides less promising approaches using silica gel as well as pristine MCF, it turned out that by using MCF-$C_3$-$NH_2$ as a filter material, no enzyme in the filtrate could be detected. In this credible approach, MCF-$C_3$-$NH_2$ was deposited onto the membrane of the introduced centrifugal tubes and the reaction dispersion containing the immobilisate was completely added. After centrifugation for 2 min at 4000 rpm, no enzyme amounts could be detected in the centrifugate. Hence, the total amount of enzyme leached during the reaction time has been re-immobilized onto the fresh filter MCF-$C_3$-$NH_2$ deposited onto the filter membrane. This effect was ascertained for the three immobilized enzymes. Having regard to this, the modular enzyme cascade was erected.

### 4.6.2 Modular enzyme cascade for cofactor recycling

As discussed in the previous chapters, extensive research has been done concerning the immobilizations of G6PDH, 6PGDH as well as ADH. With respect to its application in a multienzyme cascade, a special focus was placed onto the Michaelis-Menten kinetics and the stabilities of the immobilized enzymes. Now the three immobilisates have to be combined with regard to an efficient regeneration of the coenzyme $NADP^+$. All cascade experiments were carried out in potassium phosphate buffer solution (50 mM, pH 7.5) at 25 °C employing G6PDH, 6PGDH and ADH immobilized onto MCF-$C_3$-$NH_2$, respectively. The immobilizations of these enzymes were carried out in phosphate buffer (50 mM, pH 6.5: 6PGDH; pH 7.0: ADH) as well as HEPES (200 mM, pH 7.4: G6PDH).

A first experiment was intended to demonstrate the necessity of a spatial separation of the immobilisates within the cascade reaction. In this experiment, the G6PDH (50 µL, 1:10 dilution), 6PGDH (50 µL) and ADH (150 µL) immobilisates as well as the required substrates G6P ($c_{final}$ = 50 µM), acetone ($c_{final}$ = 4.0 mM) and the coenzyme $NADP^+$ ($c_{final}$ = 250 µM) were provided simultaneously. The chosen substrate and coenzyme concentrations were kept low in comparison with the common enzymatic assays, whereas the amounts of the immobilisates were high in order to ensure a complete conversion of the substrates in a foreseeable time.

Prior to the photometrical detection of the change of the absorbance ($\lambda_{max\ NADPH}$ = 340 nm) over a period of 30 min, the dispersion was mixed by inversion. No change in the absorbance was expected over time, as the NADPH provided by the immobilized G6PDH and 6PGDH was supposed to be re-oxidized to $NADP^+$ by the immobilized ADH immediately. However, shortly after starting the measurement, a strong decrease of the absorbance was monitored (Figure 85a). The decrease of the absorbance could not be attributed to a re-oxidation of NADPH, as at least, prior to the decrease, a slight increase of the absorbance addressed to the oxidation of $NADP^+$ to NADPH was expected. Hence, this observation demanded further investigations.

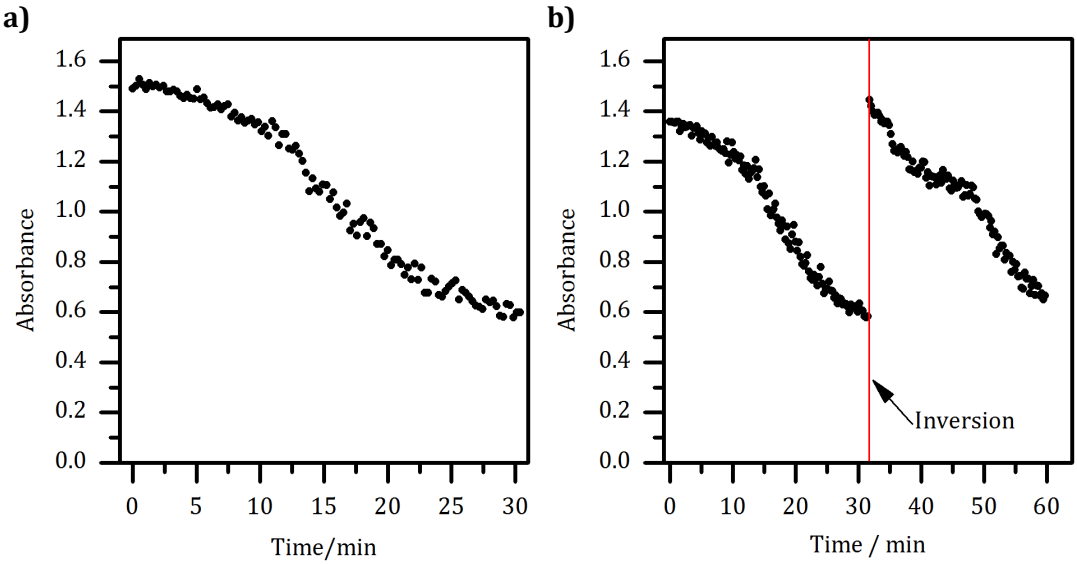


**Figure 85. a)** The simultaneous provision of the immobilized G6PDH, 6PGDH as well as ADH and its substrates and coenzyme resulted in a significant decrease of the absorbance over a period of 30 min. **b)** Likewise, a decrease of the absorbance was observed in the absence of G6PDH and 6PGDH although no enzymatic reaction was possible. The inversion of the dispersion after 30 min resulted in a renew increase of the absorbance but again accompanied by a decrease over the residual measuring time. These observations were addressed to sedimentation of immobilisate particles within the photometric measurements.

The former experiment was repeated over an interval of 60 min (Figure 85b). To prevent an enzymatic reaction in order to simply focus onto the development of the absorbance over time, the test was performed without the addition of the immobilized G6PDH as well as 6PGDH. Merely the ADH immobilisate was present. Thus, no conversion of the substrate and coenzyme was expected. Here again, despite the absence of an enzymatic reaction, the absorbance started to decrease over time. After 30 min, the dispersion was mixed by inversion again. The inversion was accompanied by a renewed increase of the absorbance up to the origin value, followed by a decrease over the next 30 min period again. It turned out that the decrease of the absorbance has to be solely addressed to the sedimentation of immobilisate particles over time. At the first onset, the light beam of the photometer was scattered on the surface of the silica particles, which was implied by the high absorbance detected. The scattered light did not reach the detector. Thus, the light intensity at the detector decreased, which was associated with an increase of the absorbance. Hence, the absorbance was high, shortly after starting the measurement, as the ADH immobilisate was homogeneously dispersed in the buffer solution. The continuous sedimentation of the silica particles over time resulted in a decrease of the scattering, as the intensity of light reaching the detector increased in the same manner. The inversion of the reaction dispersion after 30 min of detection, accompanied by an increase of the absorbance confirmed this assumption. Hence, a high concentration of silica particles within the measurement had to be avoided in order to photometrically follow the conversion of $NADP^+$ NADPH and vice versa. Moreover, the nonobservance of the final particle concentration within the measurement results in a misinterpretation of the measurement results. At this point it is important to emphasize that the particle concentration within the common activity assays of the three immobilized enzymes was considerably lower, respectively. Thus, the former measurements concerning the long-term stabilities of the immobilized enzymes were not negatively affected from particle sedimentation and the calculated enzymatic activities are trustworthy.

Against the background of a rapid regeneration of $NADP^+$, the particle concentration within the cascade reaction was highest for the ADH immobilisate (1 mg $mL^{-1}$). In order to determine the particle concentration that does not affect the absorbance within the measurement, the immobilisate concentration was varied from 938 µg $mL^{-1}$ to 65.4 µg $mL^{-1}$. These tests were conducted by simply dispersing the immobilisate in buffer solution in the absence of any substrates or coenzymes. Hence, the absorbance was not affected by any enzymatic reactions. The absorbance was detected over a period of 30 min (Figure 86).

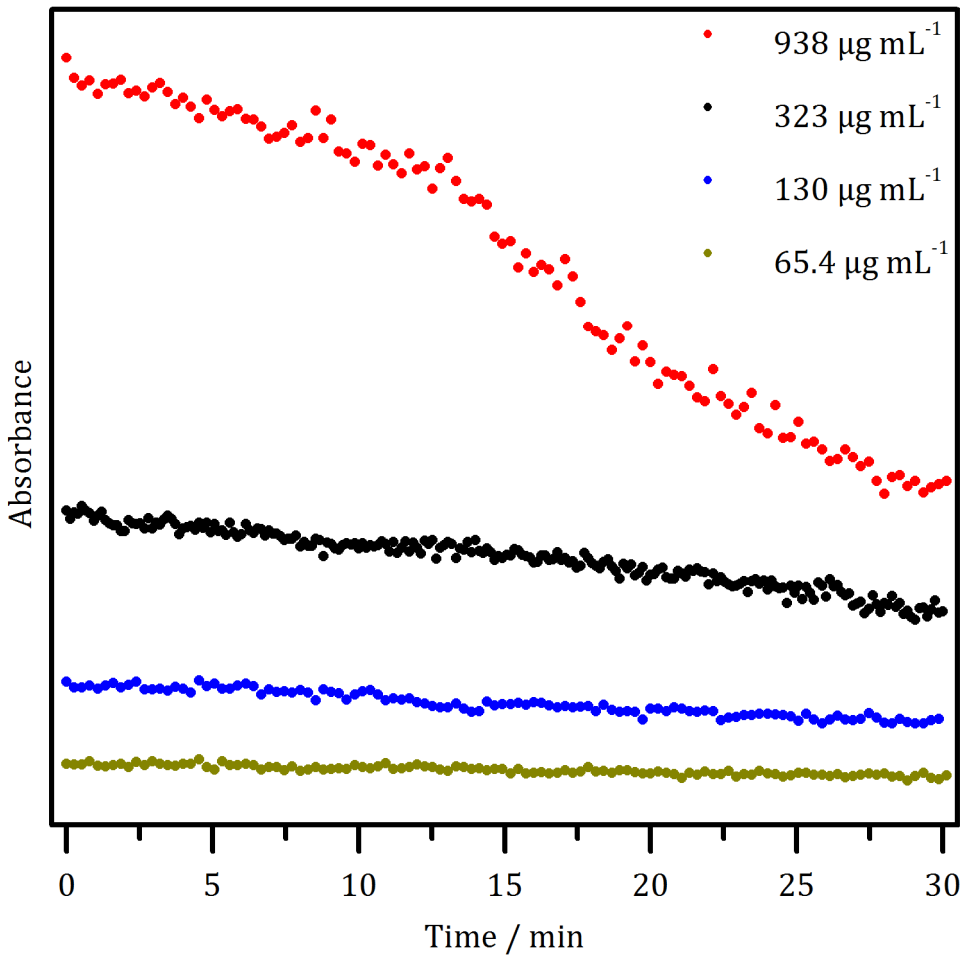


**Figure 86.** Variation of the concentration of immobilisate particles dispersed in phosphate buffer solution (50 mM, pH 7.5) in the absence of any substrates and coenzymes. The absorbance ($\lambda_{max, NADPH}$ = 340 nm) of the dispersions was monitored over an interval of 30 min. Due to continuous sedimentation of the silica particles associated with a decrease of light scattering, the absorbance decreased significantly. The absorbance remained unaffected by applying a particle concentration of 65.4 – 130 µg mL$^{-1}$.

It is obvious that the decrease of the absorbance over time correlates with the concentration of immobilisate particles dispersed in the buffer solution. The decrease of the absorbance can solely be referenced to sedimentation of the particles, as substrate and coenzyme molecules were absent. High concentrations of silica particles led to a strong decrease of the absorbance. The absorbance remained unaffected by employing a particle or rather immobilisate concentration of maximal 130 µg mL$^{-1}$. Hence, the immobilisate concentration in each reaction step of the cascade was requested not to exceed a value of 130 µg mL$^{-1}$.

With respect to the extended leaching behavior of the immobilized enzymes accompanied by the sedimentation of immobilisate particles in the presence of high immobilisate concentrations, the practical implementation of the enzyme cascade

needed to be revised (Figure 87). To bypass these circumvents, filtration over aminopropyl modified MCF after each reaction step was essential. An amount of 20 mg MCF-$C_3$-$NH_2$ (hereinafter labeled as "filter-MCF") turned out to be sufficient to separate the immobilisate and to initiate the re-immobilization of the leached enzyme from the substrate solution, respectively. Thus, it enables the introduction of an enzyme- and particle-free substrate solution into the following step of the enzyme cascade. The separation of the respective immobilisate was carried out by centrifugation (2 min, 4000 rpm) in centrifugal tubes possessing the filter-MCF on its PFTE membrane (Figure 83).

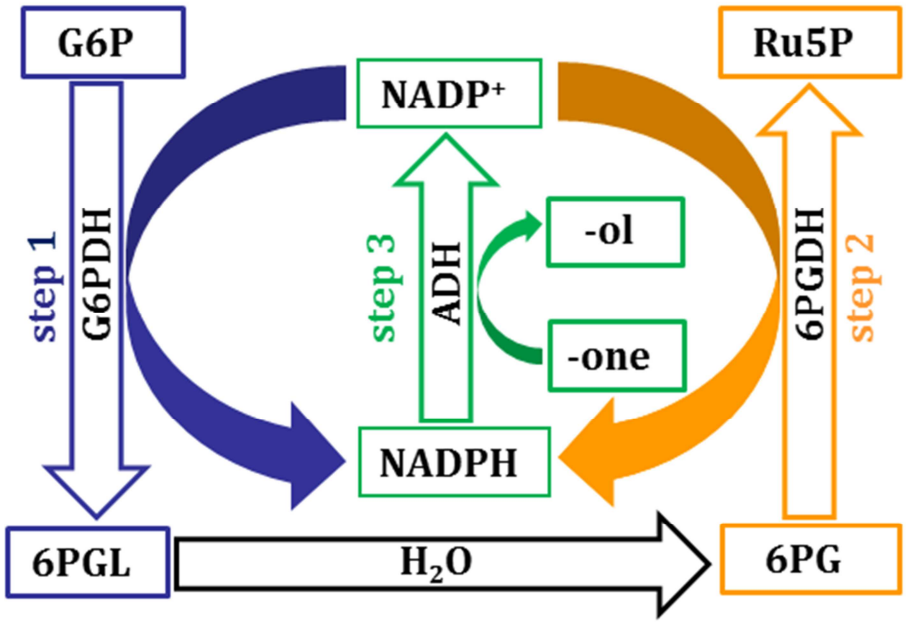


**Figure 87.** Final enzyme cascade: After a full conversion of G6P to Ru5P by the immobilized G6PDH (blue, step 1) as well as 6PGDH (orange, step 2), the total amount of NADPH becomes re-oxidized by the immobilized ADH (green, step 3) with concomitant reduction of acetone to 2-propanol. In accordance to the pronounced leaching behavior of the immobilized enzymes, a separation of the respective immobilisate from the reaction dispersion after each reaction step was indispensable. The separation was carried out by filtration of the dispersion over MCF-$C_3$-$NH_2$.

The enzyme cascade was exemplarily performed over five reaction cycles in order to investigate the stability of the immobilisates within the cascade performance and to examine the efficiency of the cofactor recycling step. In the first cycle (cycle 1) 10 µL G6PDH (1:10 dilution, step 1), 50 µL 6PGDH (step 2) and 10 µL ADH (step 3) immobilisate were provided uniquely. The required substrates, G6P ($c_{final}$ = 50 µM), acetone ($c_{final}$ = 30 mM) and the coenzyme $NADP^+$ ($c_{final}$ = 250 µM), were added freshly to each of the five cascade cycle. To ensure a complete conversion of the respective substrates, a distinct excess of $NADP^+$ was deployed.

Under the assumption of a quantitative conversion of $NADP^+$ to NADPH within the first two steps of the cascade, the concentration of NADPH amounts to 100 µM. With regard to an efficient recycling of $NADP^+$ a 300-fold excess of acetone was provided in step 3 ($c_{final}$ = 30 mM). The considerable excess bases upon the ratio of NADPH and acetone in the common enzymatic assay of the ADH.[199] Furthermore, the investigation of the Michaelis-Menten kinetics of the immobilized ADH revealed that the ADH becomes inhibited by acetone when exceeding a certain acetone concentration ($k_{i,\ acetone}$ = 178 mM). However, an acetone concentration of 30 mM does not affect the enzymatic activity of the ADH (Appendix 7.7).

The first step (step 1) of the cascade was characterized by the G6PDH-catalyzed oxidation of G6P to 6GPGL accompanied by the reduction of $NADP^+$ to NADPH (Figure 87, blue path). In the aqueous buffer solution, 6PGDL hydrolyzes to 6PG immediately. Hence, the back reaction can be excluded. After separation of the G6PDH immobilisate by employing the above mentioned procedure, the 6PGDH immobilisate was added to the centrifugate (step 2). Thus, the oxidation of 6PG to Ru5P and $CO_2$ with concomitant reduction of $NADP^+$ to NADPH was introduced (Figure 87, orange path). Step 2 was likewise followed by the removal of the 6PGDH immobilisate. To initiate the regeneration of $NADP^+$ from NADPH (step 3), the ADH immobilisate as well as acetone were added to the centrifugate of step 2 (Figure 87, green path). After full enzymatic conversion of NADPH, the ADH immobilisate was recovered. All separated immobilisates were stored at 4 °C until introducing them into the next cycle. Cycle 2 was introduced by employing the separated immobilisates of cycle 1 and so forth. The efficiency of the cascade was investigated over 5 cycles.

The first cycle of the cascade was completely photometrically monitored ($\lambda_{max.\ NADPH}$ = 340 nm) over nearly 300 min (Figure 88). In this very first cycle, the absorbance was not affected by the concentration of the immobilisate particles. Due to the separation of the immobilisate after each cascade step by using filter-MCF the particle concentration in the reaction dispersion increased from cycle to cycle. As discussed above, high particle concentrations affect the absorbance. Hence, the further cycles could not be monitored photometrically over the reaction time, respectively. The three steps of the following cycles (cycles 2-5) were carried out by incubation of the immobilisates in the substrate solution at 25 °C followed by a renewed filtration using filter-MCF. The time of incubation was geared to the time that was needed for a complete conversion of the substrate in cycle 1, respectively. After centrifugation over filter-MCF, the absorbance ($\lambda_{max.\ NADPH}$ = 340 nm) of the centrifugate was measured over a period of one minute and the obtained value was

referenced to the respective absorbance received in cycle 1. This allows conclusions concerning the degree of substrate conversion in the respective step. Furthermore, the absorbance of the centrifugates was measured over one minute in order to revise if leaching within the separation step appeared. In the presence of leaching, the absorbance of the centrifugate increases due to the generation of NADPH (step 1: G6PDH; step 2: 6PGDH) or decreases (step 3: ADH) due to the degradation of NADPH over the measuring time.

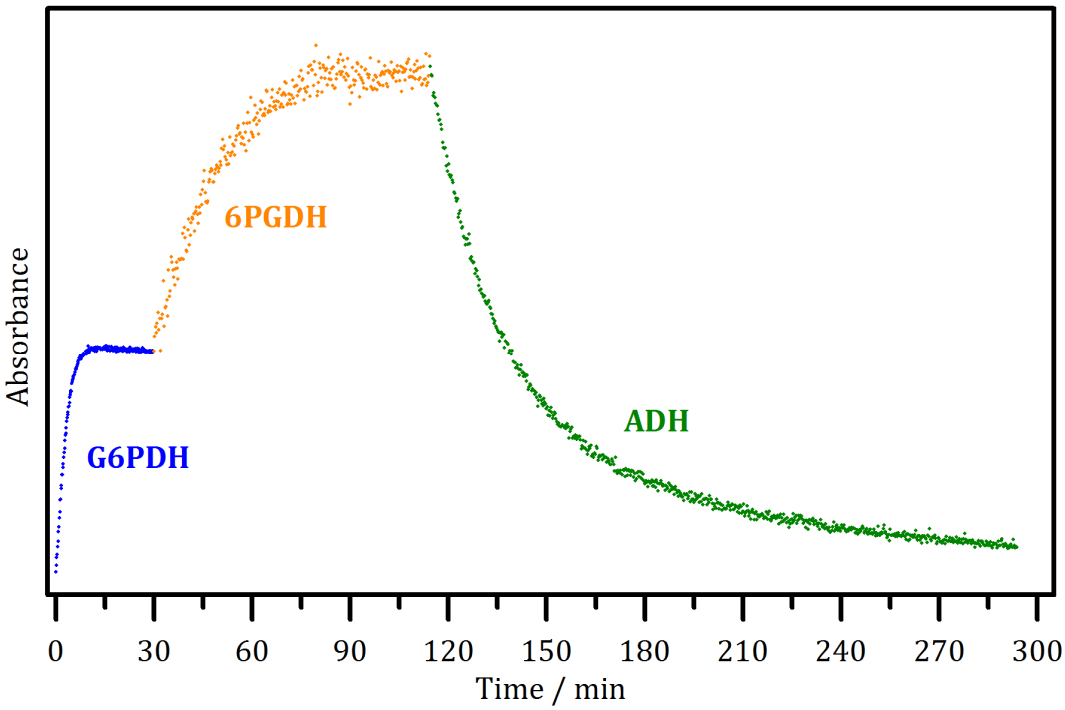


**Figure 88.** Photometrical tracking of the first cycle of the enzyme cascade. The conversion of G6P/$NADP^+$ to 6PG/NADPH by the immobilized G6PDH was completed after approximately 15 min (blue). This reaction step was followed by the conversion of 6PG/$NADP^+$ to Ru5P/$CO_2$/NADPH due to the immobilized 6PGDH (orange). The oxidation of 6PG was completed about 60 min after addition of the 6PGDH immobilisate. In the further course, the total amount of NADPH generated by the G6PDH as well as 6PGDH became fully re-oxidized by the immobilized ADH (green).

**Cycle1.** The first cycle of the enzyme cascade was completely traced photometrically (Figure 88). The conversion of G6P to 6PGDL (→ and further hydrolyzed to 6PG) in step 1 by the immobilized G6PDH proceeded very fast and was completed after approximately 15 min. Within the first 10 min the absorbance increased very steeply. This can be referred to a high initial concentration of the substrate as well as to a high concentration of the immobilisate. The full conversion of G6P was identified by a plateau in the absorbance. With regard to the initial concentration of G6P (50 µM) or rather its quantitative conversion, the concentration of NADPH amounted to 50 µM after the performance of step 1. After

recovery of the G6PDH immobilisate, the immobilized 6PGDH was added to the substrate solution in order to initiate the oxidation of 6PG to Ru5P and $CO_2$. Here again, a sharp increase of the absorbance within the first minutes after addition of the immobilisate was observed. After nearly 90 min the 6PG was oxidized quantitatively. Thus, the NADPH concentration within the cascade amounted to 100 µM at this point. The distinct divergences in the measurement values in comparison to G6PDH as well as ADH can be attributed to the highest concentration of immobilisate particles (85 µg $mL^{-1}$) within this reaction step (G6PDH: 12 µg $mL^{-1}$; ADH: 67 µg $mL^{-1}$). However, sedimentation of the silica particles accompanied by an impairment of the absorbance is not yet pronounced at this concentration. Likewise, the 6PGDH was removed from the reaction dispersion by centrifugation and the addition of the ADH immobilisate to the centrifugate introduced the cofactor recycling step (step 3). The absorbance started to decrease steeply within the first 15-20 min after addition of the immobilized ADH. This was attributed to a rapid re-oxidation of NADPH to $NADP^+$ accompanied by the reduction of acetone to 2-propanol. In the course of time, the concentration of NADPH decreased markedly resulting in a slower decrease of the absorbance. After 295 min almost 100 % of the origin NADPH amount was re-oxidized to $NADP^+$ (Table 27). Prior to initiate the next cycle, the immobilisate was removed by centrifugation and stored at 4 °C.

**Table 26.** Overview of the initial reaction rates ($v_0$) of the immobilized G6PDH, 6PGDH as well as ADH in cycle 1. $v_0$ was examined for the first 10 min of each reaction step, respectively.

| time [min] | $v_0$ (G6PDH) [µmol $L^{-1}$ $min^{-1}$] | $v_0$ (6PGDH) [µmol $L^{-1}$ $min^{-1}$] | $v_0$ (ADH) [µmol $L^{-1}$ $min^{-1}$] |
|---|---|---|---|
| **1** | 9.30 | 1.74 | 2.72 |
| **5** | 6.76 | 0.918 | 1.86 |
| **10** | 4.03 | 0.631 | 1.72 |

The initial reaction rates ($v_0$) of the immobilized enzymes deployed for the cascade reaction were calculated in intervals over 10 min after starting the respective reaction step (Eq. 8). Regarding the first cascade cycle, the highest $v_0$ values were calculated for the immobilized G6PDH (9.30 – 4.03 µmol $L^{-1}$ $min^{-1}$), whereas the lowest values were obtained for the 6PGDH immobilisate (1.74 – 0.631 µmol $L^{-1}$ $min^{-1}$; Table 26, Figure 89). As expected, $v_0$ decreased with passing time, respectively. The reaction rate of an enzyme is highly dependent on the

enzyme concentration as well as on the concentration of the substrate. Hence, the decrease of $v_0$ within the enzyme cascade can be addressed to the reduction of the substrate concentration over time.

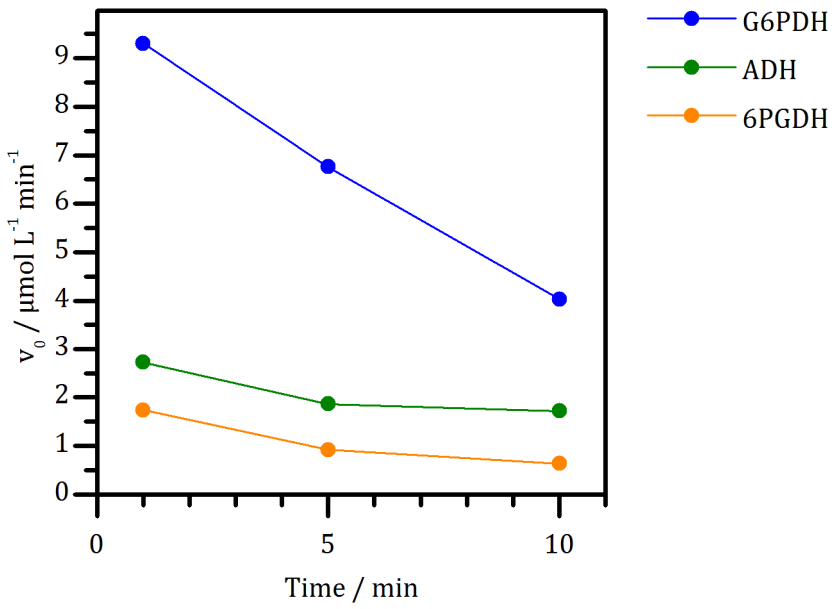


**Figure 89.** Decrease of the initial reaction rate ($v_0$) of the respective immobilized enzyme in cycle 1 within the first 10 min of the respective cascade step. The reduction of the substrate concentration over time resulted in a decrease of $v_0$, respectively.

Apparently, the $v_0$ values correlate with the reaction time needed to receive a full conversion of the respective substrate. The comparatively high $v_0$ value of the immobilized G6PDH is reflected in the rapid conversion of G6P (~15 min), whereas the full oxidation of 6PG to Ru5P and $CO_2$ has taken approximately 60 min. In comparison to the immobilized G6PDH, the re-oxidation of NADPH in step 3 proceeded considerably slower (~180 min). However, it has to be considered that the concentration of NADPH (100 µM) is twice as high as the concentration of G6P (50 µM) in the first step. With respect to the high NADPH concentration and the lower initial reaction rate of the immobilized ADH, the cofactor recycling lasted nearly 180 min.

**Cycle 2-5:** After 30 min of incubation, the immobilized G6PDH has converted 72 % of the origin G6P amount in cycle 2. Thus, the enzymatic activity was reduced by 28 % compared with its activity in the first cycle. In the further cycles, the immobilized G6PDH oxidized 71 – 74 % of the provided G6P (Table 27). Hence, no distinct loss of the enzymatic activity was observed in the further course. It is probable that the separation of the immobilisate in cycle 1 is accompanied by a

partial denaturation of the enzyme. The denaturation can be referred to the re-immobilization of the amounts of leached enzyme. The ratio between the filter-MCF and the leached G6PDH is enormous. Thus, due to the absence of enzyme-enzyme interactions within the re-immobilization onto the filter-MCF and the greater freedom of the enzyme molecules on the surface of the filter-MCF, the G6PDH is affected by pronounced time-spreading that comes along with its denaturation. Apparently, leaching was less pronounced in the further cycles. With respect to the cycle stabilities discussed in chapter 4.6.1, the largest amount of enzyme leached during the first cycle (Figure 84). Hence, the second cycle was characterized by a markedly loss of the relative activity of the immobilized G6PDH. This underpins the assumption concerning the considerable reduction of the enzymatic activity due to re-immobilization of the leached amounts of enzyme coupled with extensive time-spreading of the re-immobilized enzyme. Additionally, as discussed in chapters 4.5.1.2 and 4.5.1.3, the immobilized G6PDH displayed respectable results in terms of its long-term stabilities. Thus, a stable performance of the G6PDH immobilisate leveled off. Even though no full conversion of the substrate after 30 min of incubation was obtained, the enzyme is still able to convert its substrate completely. Merely the reaction time needs to be adjusted. This illustrates a good recyclability of this immobilisate and the major advantage of an immobilized enzyme in a cascade reaction.

**Table 27.** Comparison of the degrees of conversion of the respective substrates over five cascade cycles.

| cycle | G6PDH conversion [%] | 6PGDH conversion [%] | ADH conversion [%] |
|---|---|---|---|
| **1** | 100 | 99 | 96 |
| **2** | 72 | 29 | 46 |
| **3** | 71 | 0 | 43 |
| **4** | 71 | 0 | 44 |
| **5** | 74 | 0 | 54 |

In cycle 2, only 29 % of the provided 6PG amount was converted by the immobilized 6PGDH within 90 min of reaction time (Table 27, Figure 90). In addition, no activity of the 6PGDH was detected in cycles 3-5. Hence, the enzyme was completely denatured. Obviously, this can be traced back to mechanical stress

that arises in the separation step. Despite a promising long-term stability of the immobilized 6PGDH (Chapter 4.3), this immobilisate turned out to be less stable concerning its implementation into the enzyme cascade. Nevertheless, the immobilisate was at least employed twice. Hence, the immobilization of this enzyme was advantageous regardless.

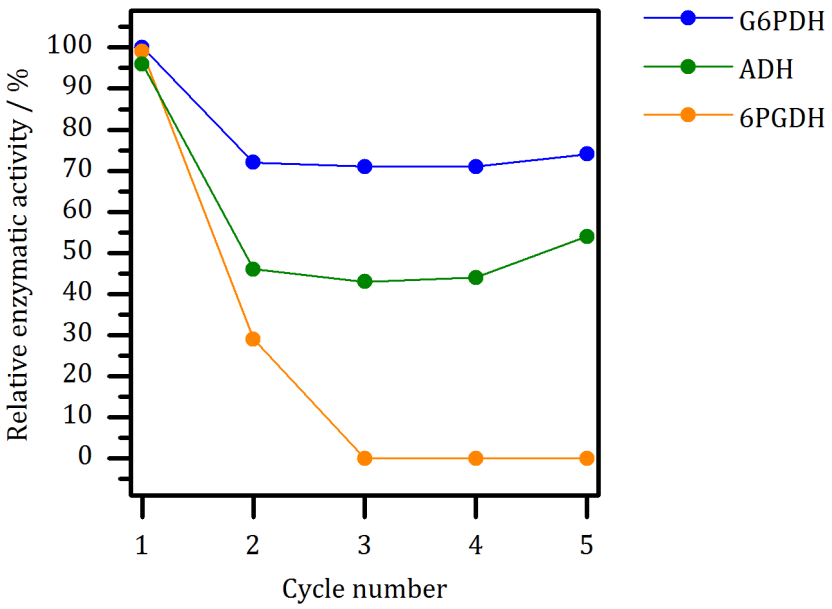


**Figure 90.** Course of the relative activities of the immobilized enzymes within 5 cascade cycles. After the performance of the first cycle, the enzymatic activity dropped, respectively. With respect to the immobilized G6PDH as well as 6PGDH, in the further course the enzymatic activity leveled off at a certain value. However, the immobilized 6PGDH was inactive after the second cascade cycle.

The efficiency of an enzyme cascade has to be measured on the efficiency of the cofactor regeneration step, since a fast and complete recycling of the cofactor is required. In cycle 2, the enzymatic activity of immobilized ADH was diminished by 50 % (Table 27, Figure 90). As discussed for the G6PDH immobilisate, the major drop of the enzymatic activity in cycle 2 can be attributed to a partly denaturation of the ADH due to the re-immobilization of the proportion of leached enzyme onto filter-MCF. With regard to the cycle stability of the ADH immobilisate, the amount of leached enzyme was highest after the performance of the first cycle and came along with a pronounced decrease of the relative activity (Figure 84). The re-immobilization of the leached ADH is accompanied by extensive time-spreading of the freshly immobilized enzyme. However, after a pronounced decrease of the enzymatic activity in cycle 2 of the enzyme cascade, the degree of substrate conversion within the cycles 2-5 varies in the range of 43-54 %. Hence, approximately 50 % of the NADPH amount present in the cascade were oxidized to

$NADP^+$ within 180 min. As the ADH possessed a certain activity, the adjustment of the reaction time ensures a complete re-oxidation of NADPH. Furthermore, the cascade experiment revealed the unproblematic reusability of the ADH immobilisate. This highlights the significant advantage of an immobilized enzyme. The ADH immobilisate displayed an excellent performance concerning its incorporation as a cofactor recycling step in an enzyme cascade. This groundbreaking approach enables the regeneration of the high-grade coenzyme $NADP^+$ by simply deploying the bulk chemical acetone as a substrate for the ADH.

### 4.6.3 Immobilization of ADH onto filter-MCF

After the performance of five complete reaction cycles, the cascade experiment was discontinued. As discussed above, a more or less pronounced leaching behavior of the immobilized enzymes required the application of filter-MCF in order to re-immobilize leached amounts of the respective enzyme after each reaction step. The amount of filter-MCF in each reaction step increased up to 100 mg over five cycles (5 cycles x 20 mg), respectively. However, MCF-$C_3$-$NH_2$ is a high-grade host material for the immobilization of enzymes. Thus, a method concerning its recovery had to be developed. The filter-MCF of each cascade step contains, in comparison to its mass, minor amounts of the enzyme of the respective reaction step. Hence, the filter-MCF is very well suited to likewise operate as a host material. As a proof of concept, the immobilization of ADH was carried out onto the surface of the filter-MCF of the coenzyme recycling step (Figure 91).

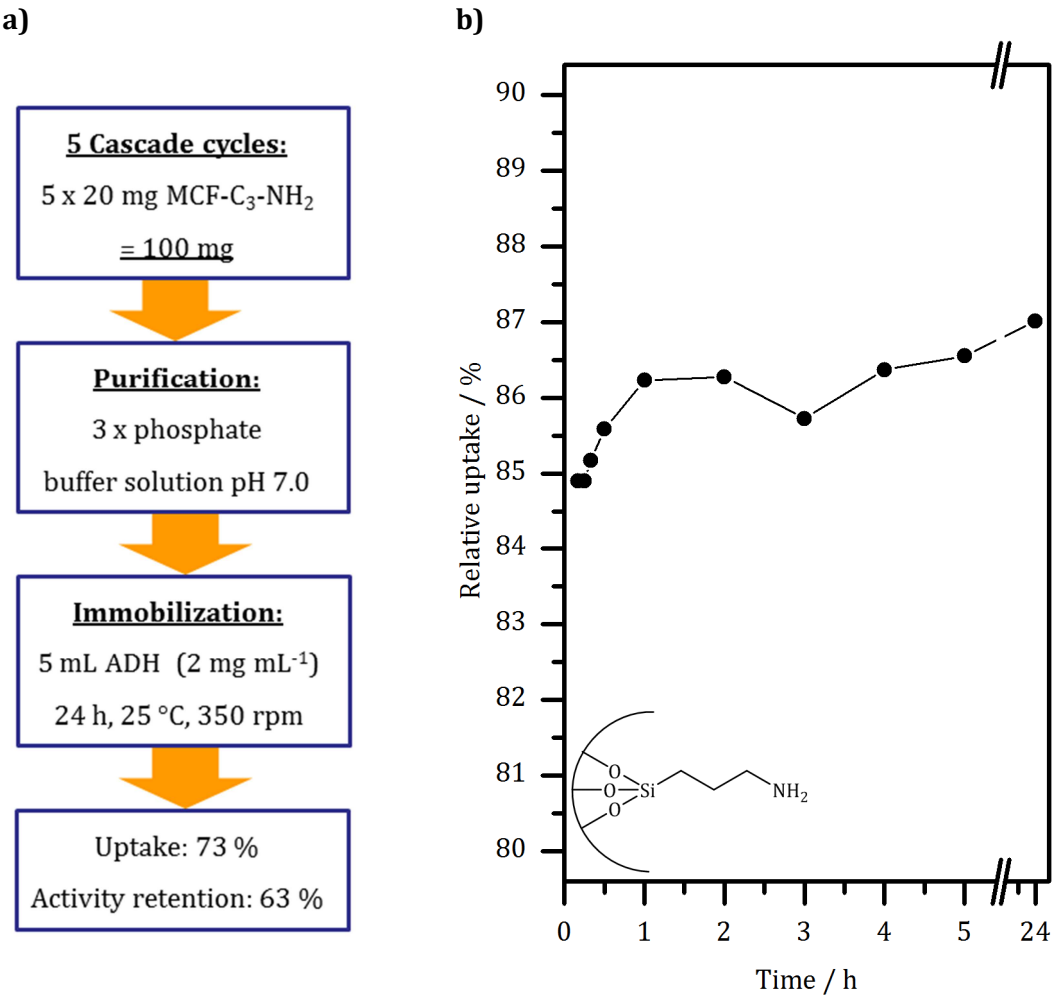


**Figure 91. a)** Proceeding and parameters of the immobilization of fresh ADH onto the filter-MCF (MCF-$C_3$-$NH_2$) of the cofactor regeneration step after the performance of five cascade cycles. **b)** Relative uptake of ADH onto the filter-MCF over 24 h of immobilization. The final relative uptake accounted to 87 %. After purification the absolute uptake was calculated to 73 %.

The immobilization of ADH onto filter-MCF was carried out in phosphate buffer solution (50 mM, pH 7.0). This pH value was identified to be recommendable in terms of the immobilization of ADH (Chapter 4.4). Initially, the filter-MCF was washed with the buffer of the subsequent immobilization in order to remove any residues of the substrate and the coenzyme as well as the cascade buffer (3 x, 2 mL buffer, 2 min, 4000 rpm). In accordance to the actual immobilization of ADH and with respect to the mass of the filter–MCF (100 mg), the immobilization was performed by dispersing the filter-MCF in 5 mL of a buffered ADH solution (2 mg $mL^{-1}$, phosphate: 50 mM, pH 7.0). The mixture was shaken for 24 h at 25 °C and 350 rpm. The relative uptake prior to the purification steps amounted to 87 %, whereas the final absolute uptake was detected to be 73 % (Figure 91). To that effect, the ADH uptake is similar or comparable to the uptakes received for the

immobilization of ADH when using only 20 mg of MCF-$C_3$-$NH_2$ (Chapter 4.4). The retained activity of the immobilized ADH immediately 24 h of immobilization was calculated to 63 % (Figure 91). Likewise, this value is in the same range than obtained for the immobilization of ADH by using only 20 mg MCF-$C_3$-$NH_2$ (Chapter 4.4).

The immobilization of fresh ADH onto the filter-MCF was successfully performed in all aspects. The final results concerning the uptake as well as the activity retention of the immobilized ADH illustrate a completely problem-free upscaling of the immobilization procedure. The freshly prepared immobilisate can be incorporated into further cascade cycles. Hence, the required utilization of filter-MCF within the enzyme cascade is a promising approach, as additionally the recirculation of the filter-MCF is ensured.

### 4.6.4 Construction of a modular enzyme cascade: Summary

Against the background of a stable performance of the multienzyme cascade, cycle stability experiments deploying the immobilized G6PDH, 6PGDH as well as ADH were carried out (Chapter 4.6.1). It turned out that the three immobilisate were subjected to extensive leaching (Figure 84). Correspondingly, the relative activity of the immobilisates decreased significantly over 10 cycles. This was referenced to the decreasing amount of enzyme on the surface of the immobilisates. The best cycle stability was obtained for the ADH immobilized onto MCF-$C_3$-$NH_2$. With regard to the implementation of the three immobilisates into the enzyme cascade, a method to re-immobilize the proportions of leached enzymes was developed. Filtration of the reaction dispersion over filter-MCF (MCF-$C_3$-$NH_2$, 20 mg) turned out to be promising, as the leached enzyme re-immobilizes onto the inner surface of the filter-MCF. Thus, an enzyme- and particle-free substrate solution can be assured.

Initial cascade experiments revealed an essential impact of the concentration of immobilisate particles on the absorbance within photometric measurements (Chapter 4.6.2). To guarantee accurate measurements, a particle concentration of 130 µg $mL^{-1}$ should not be exceeded (Figure 85). With regard to this, only the first of five cascade cycles could be followed photometrically over time. Cycles 2-5 were carried out by simply incubating the respective immobilisates in the substrate solution over a defined period of time. Prior to the measurement of the final absorbance of the substrate solution, the immobilisates were separated by centrifugation over filter-MCF, respectively. The absorbances were referenced to the absorbances obtained for the first cascade cycle. Cycle 1 was characterized by a

quantitative oxidation of G6P as well as 6PG, accompanied by a nearly complete re-oxidation of NADPH to $NADP^+$ (Table 27). In the second cycle the degree of conversion of the immobilized G6PDH as well as ADH within a defined period of time dropped. In the further course (cycles 2-5) it leveled off at a certain value. Despite the decrease of the enzymatic activity in the cycles 2-5, a quantitative conversion was assured. However, the immobilized 6PGDH was inactive after cycle 2. The incorporation of an immobilized ADH into the enzyme cascade illustrates the opportunity to successfully regenerate $NADP^+$ from NADPH. This is the major advantage of this approach, as acetone as a bulk chemical can be employed to recover valuable $NADP^+$ from NADPH. Furthermore, the recyclability of the immobilisates emphasizes the benefit of the utilization of immobilized enzymes instead of native enzyme.

After the performance of five cascade cycles, the recyclability of the filter-MCF was examined (Chapter 4.6.3). The total amount of filter-MCF (5 x 20 mg) after 5 repetitions of the cofactor regeneration step was employed as a host material for the immobilization of fresh ADH. Despite its application as a filter material over 5 cascade cycles, the immobilization of ADH onto this material was comparable to the actual immobilization procedure in terms of the ADH uptake as well as the activity retention after 24 h of immobilization. Thus, this high-grade filter or rather host material can likewise be recycled. This is an additional advantage of the introduced cascade approach.

# 5 GENERAL CONCLUSION AND OUTLOOK

Nowadays, enzyme catalytic approaches are widespread in laboratory scale but also in industrial applications. Enzymes convert its substrate under mild conditions with high selectivity and frequently in the absence of any side-products. Furthermore, the immobilization of an enzyme onto a suited host material ensures its reusability. These benefits place the focus of recent research onto the effective immobilization of the needed enzyme onto an appropriate host material. The requirements imposed on immobilized enzymes are high retained activities matched with optimal kinetics as well as the capability of multiple recycling procedures. However, most enzymes are dependent on a coenzyme or cofactor. Besides the immobilization of an enzyme, the regeneration of coenzymes is a current field of research with respect to an efficient application in industrial scale.

Within this thesis, a modular enzyme cascade was constructed. Special attention was paid on the recycling of the coenzyme $NADP^+$. A sequence of the pentose phosphate pathway deploying the immobilized glucose-6-phosphate dehydrogenase (G6PDH) as well was 6-phosphogluconat dehydrogenase (6PGDH) was coupled to a coenzyme recycling system. The coenzyme recycling step was implemented by an immobilized alcohol dehydrogenase (ADH). The immobilizations of the respective enzyme were carried out onto the inner surface of mesoporous siliceous cellular foams (MCF), as its pore size can be tailored in the range of common enzyme sizes. Mesoporous silicas are mechanically stable and possess a pronounced biocompatibility. Furthermore, the surface of mesoporous silica can be organically modified. Thus, the microenvironment can be tailored according to the preference of the respective enzyme. In this dissertation, the immobilization of 6PGDH and ADH was investigated in detail and the well-known immobilization of G6PDH was optimized. Subsequently, the three immobilisates were effectively merged into a modular model cascade.

6PGDH was adoptively immobilized onto the inner surface of alkyl as well as aminoalkyl modified MCFs. In order to identify the optimal distance between the enzyme molecules and the pore walls of the host, the MCF was grafted using alkyltriethoxysilanes consisting of carbon chain lengths ranging from $-C_3$ to $-C_{11}$, respectively. Frequently, the immobilization of enzymes is performed onto aminoalkyl functionalized materials. Thus, the immobilizations of 6PGDH were additionally carried out onto the surface of aminoalkyl modified MCFs, likewise possessing carbon chain lengths from $-C_3$ to $-C_{11}$. Both material classes were examined and compared concerning its suitability as a carrier for 6PGDH. The

immobilization of 6PGDH onto these materials was initiated due to hydrophobic interactions and the enzyme uptakes amounted to 100 % for nearly each material. The retained enzymatic activity after 24 h of immobilization as well as the long-term stabilities of the immobilized enzyme over a period of 53 days revealed a dependency on the carbon chain length on the surface of the host and the presence of a terminal amino group. After 24 h of immobilization, the retained activity of the immobilized 6PGDH decreased with increasing carbon chain lengths present on the pore walls of the respective host. Thus, the activity retention was highest for the 6PGDH immobilized onto propyl (MCF-$C_3$) as well as onto aminopropyl modified MCF (MCF-$C_3$-$NH_2$). However, the activity was slightly higher for the 6PGDH immobilized onto the aminoalkyl modified MCFs. This was referred to a certain enzyme stabilization by the surface amino groups. The dependency between the carbon chain length and the existence of a terminal amino function on the activity of the immobilized 6PGDH persisted over the total period of the study. Against the background of the incorporation of the 6PGDH immobilisate into the modular enzyme cascade, the Michaelis-Menten kinetics of the immobilized and the native enzyme were elaborated and compared to each other. The immobilization has affected the substrate as well as coenzyme affinities and finally the maximum reaction rates ($v_{max}$) of the immobilized 6PGDH. In this regard, a dependency between the surface functionalization of the MCF and $v_{max}$ was discovered. $v_{max}$ was slightly higher by employing the aminoalkyl modified MCFs as a support material instead of using the alkyl functionalized MCFs. The immobilization of 6PGDH onto the aminopentyl modified MCF (MCF-$C_5$-$NH_2$) resulted in the highest $v_{max}$ value of the study. Hence, under kinetic aspects, an immobilization of 6PGDH onto MCF-$C_5$-$NH_2$ has to be preferred; whereas, under the perspective of a promising long-term stability, an immobilization onto MCF-$C_3$-$NH_2$ has to be considered. On the basis of the appropriate long-term-stability, it was decided to utilize the 6PGDH that was immobilized onto MCF-$C_3$-$NH_2$ for the intended enzyme cascade.

The cofactor recycling step of the enzyme cascade was requested to be realized by an immobilized $NADP^+$/H dependent ADH. In former studies, MCF-$C_3$-$NH_2$ turned out to be an excellent host material for enzymes. Thus, it was implemented for the immobilization of the ADH, too. Besides typical investigations concerning the ADH immobilization, the enzyme to host ratios (1:10/1:20/1:30) within the immobilization procedure as well as the pH values of the immobilization (pH 6.5/7.0/7.5) were varied. Additionally, the forward (2-propanol/$NADP^+$ → acetone/NADPH) and the back reaction (acetone/NADPH → 2-propanol/$NADP^+$) of the ADH were investigated and compared to each other. The driving force of the

immobilization of the ADH (pI 6.1) onto MCF-$C_3$-$NH_2$ (pI 8.4) was identified to be electrostatic interactions, as both reaction partners were oppositely charged at the respective pH value of the immobilization. Regarding the residual activity of the ADH after 24 h of immobilization, an ADH to host ratio of 1:10 figured out to be optimal, as the highest retentions of activity were received by using this ratio. The long-term stability of the immobilized enzyme was monitored over a period of seven days for the forward as well as the back reaction, respectively. Irrespective of whether 2-propanol/$NADP^+$ or acetone/NADPH was provided as a substrate/coenzyme, the activity of the immobilized ADH decreased over this period of time. Moreover, independent on the pH of the immobilization, the activity of the immobilized ADH was lower for higher ADH to host ratios that were present in the former immobilization. However, the enzymatic activity was identified to be considerably higher for the back reaction. Hence, the ADH exhibits a preference for the conversion of acetone/NADPH to 2-propanol/$NADP^+$. Rounding up this approach, the Michaelis-Menten kinetics of the immobilized ADH were elaborated (ADH:MCF-$C_3$-$NH_2$ = 1:10; pH 6.5/7.0/ 7.5). These investigations were conducted for the forward and the back reaction, respectively. The immobilization of the ADH has affected the kinetic behavior in terms of its substrate/coenzyme affinity as well as its $v_{max}$ compared to the native enzyme. A special focus was placed onto the conversion of acetone/NADPH to 2-propanol/$NADP^+$, as the back reaction of the ADH was intended to be used as the coenzyme recycling step within the model cascade. Basically, $v_{max}$ of the back reaction was clearly increased in comparison to the forward reaction. The highest $v_{max}$ was calculated for the ADH immobilized at pH 7.0. Once again, this confirms the preference of the ADH for the back reaction. However, 2-propanol as well as acetone were identified to inhibit the ADH when exceeding a certain concentration. With respect to the forward reaction and the back reaction, an immobilization at pH 6.5 and 7.0 had positively affected the kinetics in terms of the inhibition. In comparison to the free ADH, these immobilisates accept higher substrate concentrations until an inhibition arises. Addressed to the high $v_{max}$ value, the ADH immobilized at pH 7.0 was selected for the cascade experiments.

In addition to the already published research, concerning the immobilization of G6PDH, further research was necessary in order to successful incorporate this immobilisate into the model enzyme cascade. Hence, the electrostatic immobilization of G6PDH (pI 4.6) onto MCF-$C_3$-$NH_2$ (pI 8.4) was carried out in HEPES (pH 7.4) as well as phosphate buffer solution (pH 7.5) and the characteristics of the immobilizations were determined. Initially, the enzymatic assays of the immobilized enzyme were performed in the buffer of the immobilization as well as

in the presence and in the absence of a certain amount of $MgCl_2 \cdot 6\ H_2O$, respectively. In terms of the activity assays that were performed in HEPES, the presence of $MgCl_2 \cdot 6\ H_2O$ resulted in higher enzymatic activities of the immobilized 6PGDH in comparison to the assays that were carried out in the absence of $MgCl_2 \cdot 6\ H_2O$. However, when the activity assays were performed in phosphate buffer solution, the activity of the immobilized G6PDH was slightly higher in the absence of $MgCl_2 \cdot 6\ H_2O$. Furthermore, the immobilization of G6PDH in phosphate buffer solution led to considerable higher activities compared to the immobilization in HEPES. The exchange of the buffer system in relation to the buffer used for the immobilization illustrated that the G6PDH possessed the highest activity when the immobilization was carried in HEPES and the activity assays were conducted in phosphate buffer solution. This is additionally reflected in the $v_{max}$ value of the respective G6PDH immobilisate. This was a promising result, as the enzyme cascade was intended to be performed in phosphate buffer solution (pH 7.5) and in the absence of any side reactants. Thus, this immobilisate was incorporated into the enzyme cascade.

Finally, the three introduced immobilisates were combined to a model cascade. The immobilized G6PDH as well as 6PGDH provide NADPH due to the oxidation of G6P as well as 6PG, whereas the immobilized ADH re-oxidizes the NADPH amounts to $NADP^+$ with concomitant reduction of acetone to 2-propanol. The enzyme cascade was exemplarily performed over five complete cycles. However, initial experiments concerning the cycle stability of the immobilized enzymes revealed an extensive leaching behavior of the enzymes. Hence, a method was developed to re-immobilize the amounts of leached enzyme from the respective substrate solution. The re-immobilization of the enzymes was initiated due to an elegant solution. After the conversion of the respective substrate, the immobilisate was separated from reaction dispersion by filtration over fresh MCF-$C_3$-$NH_2$ (filter-MCF). On this occasion, the amounts of leached enzyme re-immobilized onto the surface of the filter-MCF. The enzyme-free substrate solution was introduced into the following reaction step; whereas the respective filter-MCF was completely re-employed into the next cycle of the cascade.

In the first cycle of the enzyme cascade, the immobilized G6PDH and 6PGDH oxidized the entire provided amount of the substrate. Subsequently, nearly the total NADPH amount that was formed in the first two to steps of the cascade was re-oxidized to $NADP^+$ by the immobilized ADH. The three single steps of the four following cascade cycles were performed over the periods of time that were necessary to obtain a full substrate conversion in the first cycle and the final degrees

of conversion were monitored, respectively. Within the defined periods of time, the degree of conversion of each immobilized enzyme dropped in the second cycle. In the further course of the enzyme cascade, the residual activity of the immobilized enzymes leveled off and a consistent degree of conversion was reached in cycles 2-5. However, the immobilized 6PGDH was already inactive after two cycles. Even though the immobilized 6PGDH was denatured after two cycles, this immobilisate could be used twice, which is a progress in comparison to the alternative utilization of a free enzyme. This model cascade exemplifies the effective reusability of immobilized enzymes. The immobilized G6PDH as well as ADH were employed over five cycles. Even if a definite loss of the activity was observed in cycle 2, the enzymes were still active and a full conversion of the respective substrate was ensured. The regeneration of $NADP^+$ by the immobilized ADH turned out to be very effective, as the low-cost bulk chemical acetone was employed to regenerate a high-grade coenzyme.

The total amount of filter-MCF of the coenzyme regeneration steps after five complete cascade cycles was exemplarily employed for the immobilization of fresh ADH. Through this even the recyclability of the filter material could be ensured, as the results of the immobilization were comparable to the immobilization onto fresh MCF-$C_3$-$NH_2$.

Currently, the immobilization of enzymes is state of the art, as its practical implementation in laboratory scale is acceptable. However, an immobilization requests highly purified enzymes and their immobilization is frequently accompanied by a pronounced loss of their original activity. Additionally, most enzymes are dependent on a coenzyme. Thus, a cofactor regeneration step needs to be considered when intending to realize an enzyme catalytic approach. Out of this, the current trend is the immobilization of entire cells onto (porous) host materials. The benefits of a whole cell immobilization are obvious. The enzymes are located in their natural environment in an intact cell. This assures a high enzymatic activity and the cofactor recycling step is integrated within the cell. However, a lot of research is still imminent to identify suitable host materials. According to cell sizes in the micrometer range, an immobilization onto nanoporous materials is impossible. Furthermore, the cell membrane is mechanically sensitive and leads to pronounced diffusion limitations. Thus, the current trend is no universal panacea and the focus onto the immobilization of single enzymes and its achievements must not be neglected.

# 6 ZUSAMMENFASSUNG

Heutzutage sind enzymkatalytische Verfahren im Labormaßstab, aber auch in der industriellen Anwendung, weit verbreitet. Enzyme setzen ihr Substrat unter milden Reaktionsbedingungen mit einer hohen Selektivität und häufig in der Abwesenheit jeglicher Nebenprodukte um. Zudem gewährleistet die Immobilisierung eines Enzyms auf einem geeigneten Träger seine Wiederverwendbarkeit. Diese Vorteile haben den Fokus der aktuellen Forschung auf die effektive Immobilisierung des benötigten Enzyms auf einem geeigneten Trägermaterial gelenkt. Von immobilisierten Enzymen werden hohe Aktivitätserhalte, im Einklang mit einer optimalen Kinetik, sowie die Möglichkeit einer mehrfachen Wiederverwendbarkeit erwartet. Viele Enzyme sind jedoch von einem Coenzym oder Cofaktor abhängig. Neben der Immobilisierung eines Enzyms, ist, im Hinblick auf eine effiziente Anwendung im Industriemaßstab, die Regenerierung des Coenzyms ein gegenwärtiger Bereich der Forschung.

In dieser Arbeit wurde eine modulare Enzymkaskade konstruiert. Besondere Aufmerksamkeit wurde der Rezyklierung des Coenzyms $NADP^+$ geschenkt. Eine Sequenz aus dem Pentosephosphatweg wurde, unter Einbindung der immobilisierten Glucose-6-phosphatdehydrogenase (G6PDH) sowie 6-Phosphogluconatdehydrogenase (6PGDH), an ein Coenzymrezyklierungssystem gekuppelt. Der Coenzymrezyklierungsschritt wurde mit einer immobilisierten Alkoholdehydrogenase (ADH) realisiert. Die Immobilisierungen des jeweiligen Enzyms wurden auf der Oberfläche von mesoporösem Silicaschaum (MCF) durchgeführt, da seine Porengröße im Bereich üblicher Enzymgrößen maßgeschneidert werden kann. Mesoporöse Silicas sind mechanisch stabil und besitzen eine ausgeprägte Biokompatibilität. Zudem kann die Oberfläche mesoporöser Silicas organisch modifiziert werden. Dementsprechend kann die Mikroumgebung der Präferenz des entsprechenden Enzyms angepasst werden. In dieser Dissertation wurde die Immobilisierung der 6PGDH und ADH detailliert untersucht und die gut verstandene Immobilisierung von G6PDH optimiert. Anschließend wurden alle drei Immobilisate in einer modularen Enzymkaskade effektiv zusammengeführt.

Die 6PGDH wurde adsorptiv auf der Oberfläche von alkyl- sowie aminoalkylmodifiziertem MCF immobilisiert. Um den optimalen Abstand zwischen den Enzymmolekülen und den Porenwänden des Wirtmaterials herauszufinden, wurde das MCF jeweils mit Alkyltriethoxysilanen unterschiedlicher Kohlenstoffkettenlängen mit einer Bandbreite von $-C_3$ bis $-C_{11}$ postsynthetisch modifiziert. Die Immobilisierung von Enzymen wird häufig auf

aminoalkylfunktionalisierten Materialien durchgeführt. Daher wurden die Immobilisierungen der 6PGDH noch zusätzlich auf der Oberfläche amino-alkylmodifizierter MCFs, die ebenfalls Kohlenstoffkettenlängen im Bereich von $-C_3$ bis $-C_{11}$ besaßen, durchgeführt. Beide Materialklassen wurden bezüglich ihrer Eignung als Träger für die 6PGDH untersucht und verglichen. Die Immobilisierung der 6PGDH auf diesen Materialien wurde durch hydrophobe Wechselwirkungen initiiert und die Enzymaufnahmekapazität betrug 100 % für nahezu jedes Material. Die verbleibende Enzymaktivität nach 24-stündiger Immobilisierung sowie die Langzeitstabilität des immobilisierten Enzyms über einen Zeitraum von 53 Tagen offenbarten eine Abhängigkeit von der Kohlenstoffkettenlänge auf der Oberfläche des Trägers und dem Vorhandensein einer terminalen Aminogruppe. Die nach 24-stündiger Immobilisierung beibehaltene Aktivität der 6PGDH nahm mit zunehmender Kohlenstoffkettenlänge auf der Oberfläche des jeweiligen Wirtmaterials ab. Dementsprechend war der Aktivitätserhalt der 6PGDH nach der Immobilisierung auf propyl- (MCF-$C_3$) sowie aminopropylmodifiziertem MCF (MCF-$C_3$-$NH_2$) am höchsten. Jedoch war die Aktivität für die 6PGDH, die auf den aminoalkylmodifizierten MCFs immobilisiert wurde, etwas höher. Dieses wurde auf eine gewisse Enzymstabilisierung durch die Aminogruppen auf der Oberfläche des Wirtmaterials zurückgeführt. Die Abhängigkeit der Aktivität der immobilisierten 6PGDH von der Kohlenstoffkettenlänge und der Existenz einer terminalen Aminofunktion blieb über den gesamten Zeitraum der Studie bestehen. Vor dem Hintergrund der Einbindung der immobilisierten 6PGDH in eine modulare Enzymkaskade, wurden die Michaelis-Menten Kinetik des immobilisierten und des freien Enzyms sorgfältig untersucht und miteinander vergleichen. Die Immobilisierung beeinträchtigte die Substrat- sowie die Coenzymaffinitäten und schließlich die Maximalgeschwindigkeit ($v_{max}$) der immobilisierten 6PGDH. In dieser Hinsicht wurde eine Abhängigkeit zwischen der Oberflächenfunktionalisierung des MCFs und $v_{max}$ entdeckt. $v_{max}$ war bei der Verwendung der aminoalkylmodifizierten MCFs als Wirtmaterial, anstelle der alkylfunktionalisierten MCFs, etwas höher. Die Immobilisierung der 6PGDH auf dem aminopentylmodifiziertem MCF (MCF-$C_5$-$NH_2$) resultierte im höchsten $v_{max}$-Wert der Studie. Dementsprechend ist unter kinetischen Gesichtspunkten eine Immobilisierung auf MCF-$C_5$-$NH_2$ vorzuziehen, wohingegen im Hinblick auf eine vielversprechende Langzeitstabilität eine Immobilisierung auf MCF-$C_3$-$NH_2$ in Betracht gezogen werden muss. Aufgrund der angemessenen Langzeitstabilität wurde entschieden, die auf MCF-$C_3$-$NH_2$ immobilisierte 6PGDH in der vorgesehenen Enzymkaskade einzusetzen.

Es war gefordert, den Coenzymrezyklierungsschritt der Enzymkaskade mithilfe einer $NADP^+$/H-abhängigen ADH zu realisieren. In vorherigen Studien stellte sich MCF-$C_3$-$NH_2$ als exzellentes Wirtmaterial für Enzyme heraus. Dementsprechend wurde es auch für die Immobilisierung der ADH eingesetzt. Neben den üblichen Untersuchungen bezüglich der Immobilisierung der ADH wurden die Enzym-zu-Wirt-Verhältnisse im Immobilisierungsprozess (1:10/1:20/1:30) sowie der pH-Wert der Immobilisierung variiert (pH 6.5/7.0/7.5). Ergänzend wurden die Hinreaktion (2-Propanol/$NADP^+$ → Aceton/NADPH) und die Rückreaktion (Aceton/NADPH → 2-Propanol/$NADP^+$) der ADH untersucht und miteinander verglichen. Es stellte sich heraus, dass elektrostatische Wechselwirkungen die treibende Kraft der Immobilisierung der ADH (pI 6.1) auf MCF-$C_3$-$NH_2$ (pI 8.4) waren, da beide Reaktionspartner bei den pH-Werten der Immobilisierungen entgegengesetzt geladen waren.

Ein ADH-zu-Wirtmaterial-Verhältnis von 1:10 stellte sich als optimal heraus, da bei diesem Verhältnis der höchste Aktivitätserhalt des Enzyms nach 24-stündiger Immobilisierung erhalten wurde. Die Langzeitstabilität des immobilisierten Enzyms bezüglich der Hin- sowie der Rückreaktion wurde jeweils über einen Zeitraum von sieben Tagen überprüft. Unabhängig davon, ob 2-Propanol/$NADP^+$ oder Aceton/NADPH als Substrat/Coenzym eingesetzt wurden, nahm die Aktivität der immobilisierten ADH über diesen Zeitraum ab. Außerdem war die Aktivität der immobilisierten ADH, unabhängig vom pH-Wert der Immobilisierung, geringer, wenn größere ADH-zu-Wirtmaterial-Verhältnisse bei der Immobilisierung eingesetzt wurden. Die Enzymaktivität für die Rückreaktion stellte sich jedoch als deutlich höher heraus. Dementsprechend besitzt die ADH eine Präferenz für die Umsetzung von Aceton/NADPH zu 2-Propanol/$NADP^+$. Um diese Versuche abzurunden, wurde die Michaelis-Menten Kinetik der immobilisierten ADH sorgfältig untersucht (ADH:MCF-$C_3$-$NH_2$ = 1:10; pH 6.5/7.0/ 7.5). Diese Untersuchungen wurden jeweils für die Hin- und die Rückreaktion durchgeführt. Die Immobilisierung der ADH hat die Kinetik hinsichtlich der Substrat-/Coenzymaffinität sowie $v_{max}$ im Vergleich zum freien Enzym beeinträchtigt. Ein besonderer Fokus wurde auf die Umwandlung von Aceton/NADPH zu 2-Propanol/$NADP^+$ gelegt, da die Rückreaktion der ADH als Coenzym-rezyklierungsschritt in der Modellkaskade vorgesehen war. Im wesentlichen war $v_{max}$ der Rückreaktion immer deutlich größer als im Vergleich zur Hinreaktion. Der höchste $v_{max}$-Wert wurde für die ADH, die bei pH 7.0 immobilisiert wurde, gefunden. Dies bestätigt nochmals die Präferenz der ADH für die Rückreaktion. Jedoch wurde auch festgestellt, dass sowohl Aceton als auch 2-Propanol die ADH inhibieren, wenn

eine bestimmte Konzentration überschritten wird. Im Falle der Hin- und Rückreaktion hat die Immobilisierung bei pH 6.5 und pH 7.0 einen positiven Einfluss auf die Kinetik bezüglich der Inhibierung. Im Vergleich zum freien Enzym akzeptiert das immobilisierte Enzym höhere Substratkonzentrationen bis eine Inhibierung einsetzt. Aufgrund des hohen $v_{max}$-Wertes wurde die ADH, die bei pH 7.0 immobilisiert wurde, für die Kaskadenexperimente ausgewählt.

In Ergänzung zur bereits publizierten Forschung bezüglich der Immobilisierung der G6PDH, waren weitere Arbeiten notwendig, um dieses Immobilisat erfolgreich in die Modellkaskade zu integrieren. Dementsprechend wurde die elektrostatische Immobilisierung der G6PDH (pI 4.6) auf MCF-$C_3$-$NH_2$ (pI 8.4) in HEPES (pH 7.4) sowie in Phosphatpufferlösung (pH 7.5) durchgeführt und die Charakteristika der Immobilisierung bestimmt. Zunächst wurden die Aktivitätstests des immobilisierten Enzyms im jeweiligen Immobilisierungspuffer in Anwesenheit und Abwesenheit eines bestimmten Anteils von $MgCl_2 \cdot 6\,H_2O$ durchgeführt. In Bezug auf die Aktivitätstests, die in HEPES durchführt wurden, stellte sich heraus, dass die Anwesenheit von $MgCl_2 \cdot 6\,H_2O$ zu einer höheren Aktivität der immobilisierten G6PDH führt, als im Vergleich zu den Tests, die ohne $MgCl_2 \cdot 6\,H_2O$ durchgeführt wurden. Wurden die Aktivitätstest jedoch in Phosphatpufferlösung durchgeführt, war die Aktivität der immobilisierten G6PDH in Abwesenheit von $MgCl_2 \cdot 6\,H_2O$ leicht höher. Zudem führte die Immobilisierung der G6PDH in Phosphatpufferlösung zu deutlich höheren Enzymaktivitäten als die Immobilisierung in HEPES. Der Wechsel des Puffersystems in Bezug auf den Puffer, der für die Immobilisierung verwendet wurde, zeigte, dass die G6PDH die höchste Aktivität besitzt, wenn die Immobilisierung in HEPES und die Aktivitätstests in Phosphatpufferlösung durchgeführt werden. Dies spiegelt sich auch in den $v_{max}$-Werten der jeweiligen Immobilisate wider. Dies war ein vielversprechendes Ergebnis, da es vorgesehen war, die Enzymkaskade in Phosphatpufferlösung und in der Abwesenheit von jeglichen Nebenreaktanden durchzuführen. Daher wurde dieses Immobilisat in die Enzymkaskade eingebunden.

Im letzten Schritt wurden nun die drei vorgestellten Immobilisate zu einer Modellkaskade vereint. Die immobilisierte G6PDH sowie 6PGDH produzieren über die Oxidation von G6P und 6PG NAPDH, wohingegen die immobilisierte ADH die entstandenen NADPH-Äquivalente, unter gleichzeitiger Reduktion von Aceton zu 2-Propanol, zu $NADP^+$ reoxidiert. Die Enzymkaskade wurde exemplarisch über fünf komplette Zyklen durchgeführt. Einführende Versuche zur Zyklenstabilität der immobilisierten Enzyme offenbarten jedoch ein beträchtliches Auswaschverhalten der Enzyme. Daher wurde eine Methode entwickelt, um heruntergewaschenes

Enzym aus der jeweiligen Substratlösung zu reimmobilisieren. Die Reimmobilisierung wurde durch eine elegante Lösung initiiert. Nach der Umsetzung des jeweiligen Substrats wurde das Immobilisat durch Filtration über frischem MCF-$C_3$-$NH_2$ (Filter-MCF) von der Reaktionsdispersion separiert. Hierbei reimmobilisierten die heruntergewaschenen Enzymmoleküle auf der Oberfläche des Filter-MCF. Die nun enzymfreie Substratlösung wurde dem nächsten Reaktionsschritt zugeführt, wohingegen das jeweilige Filter-MCF vollständig im nächsten Kaskadenzyklus eingesetzt wurde.

Im ersten Zyklus der Enzymkaskade oxidierten die immobilisierte G6PDH und die 6PGDH die gesamte vorgelegte Substratmenge. Anschließend wurde nahezu die gesamte Menge an NADPH, die in den ersten beiden Schritten der Kaskade gebildet wurde, von der immobilisierten ADH zu $NADP^+$ reoxidiert. Die drei Einzelschritte der nachfolgenden Zyklen wurden über den Zeitraum durchgeführt, der im ersten Zyklus notwendig war, um einen kompletten Substratumsatz zu erreichen und der finale Grad der Umsetzung wurde jeweils überprüft. Innerhalb der definierten Zeiträume sank im zweiten Zyklus der Grad der Umsetzung eines jeden Immobilisats. Im weiteren Verlauf der Enzymkaskade pendelte sich die Restaktivität der immobilisierten Enzyme ein und in den Zyklen 2-5 wurde ein gleichbleibender Umsetzungsgrad erzielt. Jedoch war die immobilisierte, durchaus empfindliche, 6PGDH nach zwei Zyklen inaktiv. Auch wenn die immobilisierte 6PGDH nach zwei Zyklen denaturiert war, konnte sie zumindest zweimal verwendet werden, was ein Fortschritt im Vergleich zum alternativen Einsatz eines freien Enzyms ist. Diese Modellkaskade veranschaulicht die effektive Wiederverwendbarkeit immobilisierter Enzyme. Die immobilisierte G6PDH sowie ADH wurden über fünf Zyklen verwendet. Auch wenn ein eindeutiger Aktivitätsverlust im zweiten Zyklus beobachtet wurde, waren diese Enzyme immer noch aktiv und eine vollständige Umsetzung des jeweiligen Substrats konnte sichergestellt werden. Die Regeneration von $NADP^+$ durch die immobilisierte ADH stellte sich als sehr effektiv heraus, da eine preiswerte Chemikalie wie Aceton zur Regenerierung eines hochwertigen Coenzyms verwendet wurde.

Die nach fünf kompletten Kaskadendurchläufen angefallene Gesamtmenge des Filter-MCFs aus dem Coenzymrezyklierungsschritt wurde exemplarisch für die Immobilisierung frischer ADH eingesetzt. Hierdurch konnte auch die Wiederverwendung des Filtermaterials sichergestellt werden, denn die Ergebnisse der Immobilisierung waren vergleichbar zur Immobilisierung auf frischem MCF-$C_3$-$NH_2$.

Gegenwärtig ist die Immobilisierung von Enzymen der Stand der Forschung, da der Aufwand für eine praktische Umsetzung im Labormaßstab vertretbar ist. Jedoch erfordert eine Immobilisierung hochreine Enzyme und ihre Immobilisierung geht häufig mit einem ausgeprägten Verlust ihrer ursprünglichen Aktivität einher. Zudem sind viele Enzyme abhängig von einem Coenzym. Daher muss bei der Realisierung eines enzymkatalytischen Verfahrens ein Coenzymregenerierungsschritt berücksichtig werden. Hieraus ergibt sich der aktuelle Trend zur Immobilisierung ganzer Zellen auf (porösen) Wirtmaterialien. Die Vorteile der Immobilisierung ganzer Zellen ist offensichtlich. Die Enzyme sind befinden sich in einer intakten Zelle in ihrer natürlichen Umgebung. Dies gewährleistet hohe Enzymaktivitäten und der Cofaktorrezyklierungsschritt ist in der Zelle integriert. Jedoch diesbezüglich immer noch viel Forschungsarbeit erforderlich, um geeignete Wirtmaterialien zu finden. Aufgrund der Größe von Zellen im Mikrometerbereich, ist eine Immobilisierung auf nanoporösen Materialien unmöglich. Zudem ist die Zellmembran mechanisch empfindlich und führt zu ausgeprägten Diffusionsbeschränkungen. Daher ist der aktuelle Trend auch kein Allheilmittel und die Fokussierung auf die Immobilisierung einzelner Enzyme mit all ihren Errungenschaften sollte nicht vernachlässigt werden.

# 7 APPENDIX

## 7.1 Experimental Section

### 7.1.1 Instrumental details of the characterization techniques

**Zeta potential titrations**

Zeta potential titrations were conducted on a *Zetasizer Nano ZS* (He-Ne laser, λ = 633 nm, detection angle 13°) in combination with a *MPT-2* autotitrator from *Malvern Instruments Ltd.* (Works, United Kingdom). The respective functionalized MCF (15 mg) was dispersed in distilled water (10 mL) and sonicated for 15 min at rt. The titration was performed at 25 °C from the current pH to pH 2 by using 0.1 mol $L^{-1}$ hydrochloric acid as well as from pH 2 to pH 10 by employing 0.1 mol $L^{-1}$ sodium hydroxide solution. The zeta potential values were measured in pH steps of 0.5 (± 0.2) and the evaluation was carried out according to the Smucholski approximation.

**Nitrogen physisorption**

Nitrogen physisorption measurements were conducted on an *Autosorb® 6* from *Quantachrome Instruments* (Boynton Beach, Florida, USA) in a relative pressure range from $p/p_0$ = 0.02-0.99 at 77 K. The samples were degassed at 120 °C for 20 h in vacuum. The specific surface areas $S_{BET}$ were calculated by means of the BET method in a relative pressure range from $p/p_0$ = 0.05-0.3.[165] The nonlocal density functional theory (NLDFT) was employed to calculate the pore size distributions from the adsorption branch of the respective isotherms (kernel: silica, cylindrical pores, adsorption); whereas the average pores size was determined from the mean of the FWHM. The total pore volume was calculated at a relative pressure of $p/p_0$ = 0.99.

**Thermal analysis (TG/DTA/MS)**

Thermogravimetry and differential thermal analysis with simultaneous mass spectroscopy were performed on a *STA 449®F3* coupled to a *QMS 403 C Aëolos Quadrupol mass spectrometer* from *Netzsch Proteus* (Selb, Germany). 20 mg of the respective sample were weighed in an $Al_2O_3$ crucible and heated from rt to 900 °C (heating rate: 5 K $min^{-1}$). The measurements were carried out in an argon/oxygen atmosphere (8:2) with a gas flow of 20 mL $min^{-1}$.

**UV-Vis spectroscopy**

All enzymatic assays were performed by using the *BioSpectrometer® kinetic* from Eppendorf (Hamburg, Germany).

**Infrared spectroscopy (IR)**

All IR spectra were recorded on a *1720 Fourier Transform Infrared Spectrometer* from PERKIN-ELMER (Norwalk, Connecticut, USA). The measurements were performed with a KBr pellet in the wavenumber range from 450 – 4000 $cm^{-1}$ at 25 °C.

**NMR spectroscopy**

All NMR spectra were recorded on an *AVANCE 400* from Bruker (Billerica, Massachusetts, USA).

### 7.1.2 Synthesis and functionalization of MCF

#### 7.1.2.1 Synthesis of MCF

In a typical synthesis Pluronic® P123 (9.6 g) was dissolved in hydrochloric acid (361 mL, 1.50 mol $L^{-1}$) at room temperature and TMB (16.7 mL, 120 mmol) as well as ammonium fluoride (111 mg, 3.00 mmol) were added. The solution was stirred for 60 min at 40 °C. After dropwise addition of TEOS (22.7 mL, 102 mmol), the solution was stirred further for 20 h at 40 °C followed by a hydrothermal treatment at 120 °C for 20 h. The obtained precipitate was separated, washed with distilled water and ethanol (96 %) and dried at 60 °C. Calcination was carried out in air for 5 h at 550 °C (5 K $min^{-1}$).[126]

#### 7.1.2.2 Syntheses of the alkyltriethoxysilanes and (5-bromopentyl)triethoxy–silane

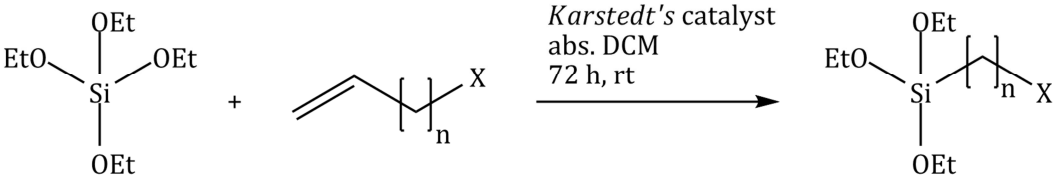


X = Br, H
n = 3, 5, 9

Heptyl-, undecyl- and (5-bromopentyl)triethoxysilane were prepared as described elsewhere.[196] Under a nitrogen atmosphere, triethoxysilane (30 mmol), 1-undecene, 1-heptene or 5-brom-1-pentene (30 mmol) as well as *Karstedt's* catalyst (35 mg) and absolute dichloromethane (1.2 mL) were mixed and stirred for 72 h at room temperature. After removal of the solvents under reduced pressure, the crude product was dissolved in absolute ethanol and filtered over neutral aluminium oxide. Ethanol was removed in vacuum to obtain heptyl-, undecyl- and (5-bromopentyl)triethoxysilane as colorless liquids.

[196] S.-T. Wener, Examensarbeit **2013**, Universität Tübingen, 60.

**(Heptyl)triethoxysilane**

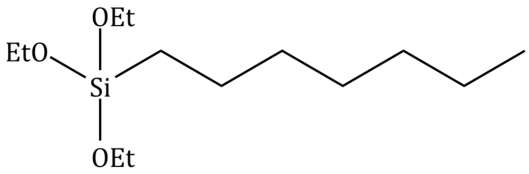


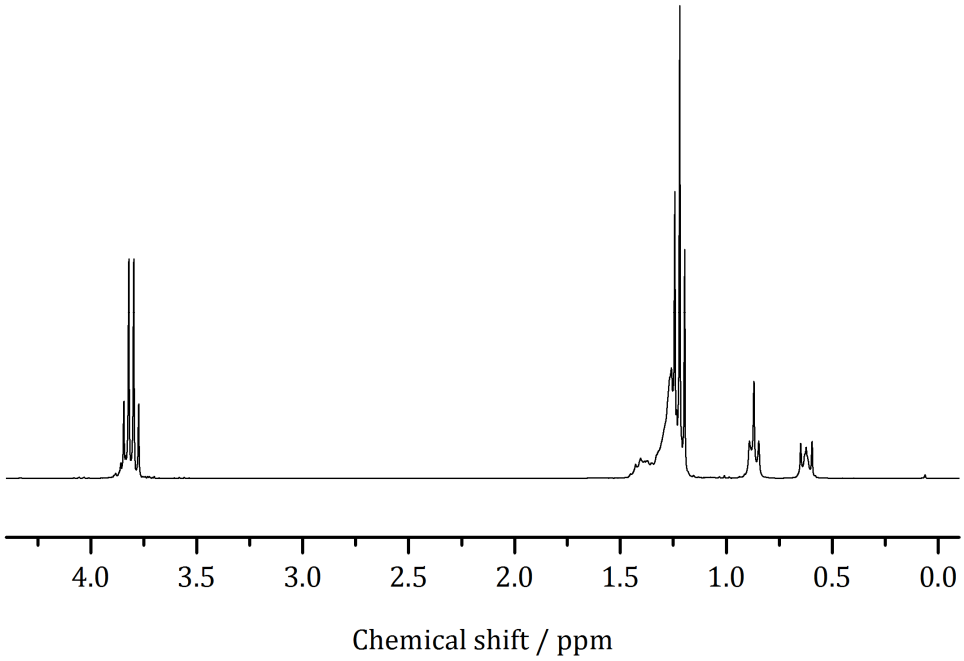


$^{1}$H-NMR (300 MHz, rt, $CDCl_3$): $\delta$ [ppm]: 3.84-3.77 (q,$^{3}J$=7.0 Hz, 6H, $OCH_2$), 1.45-1.20 (m, 19H, $CH_3$, $CH_2$) 0.89-0.85 (m, 3H, $CH_3$), 0.65-0.60 (m, 2H, $SiCH_2$).

MS (EI): 262 [$M^{\cdot+}$].

**(Undecyl)triethoxysilane**

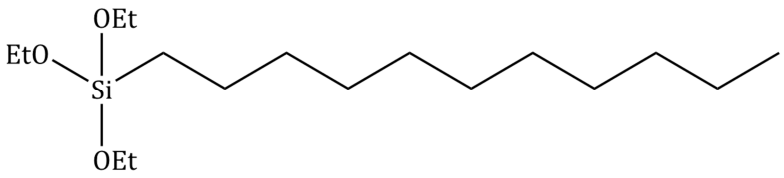


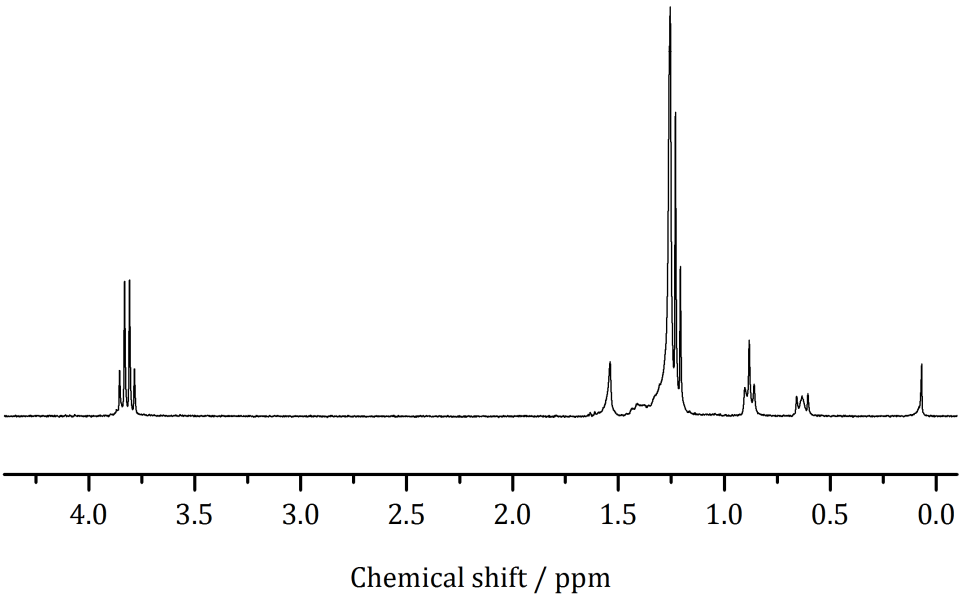


$^{1}$H-NMR (300 MHz, rt, $CDCl_3$): $\delta$ [ppm]: 3.85-3.78 (q,$^{3}J$=7.0 Hz, 6H, $OCH_2$),1.44-1.21 (m, 27H, $CH_3$, $CH_2$), 0.90-0.86 (m, 3H, $CH_3$), 0.66-0.61 (m, 2H, $SiCH_2$).

MS (EI): 318 [$M^{\cdot+}$].

**(5-Bromopentyl)triethoxysilane**

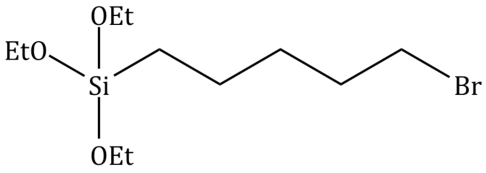


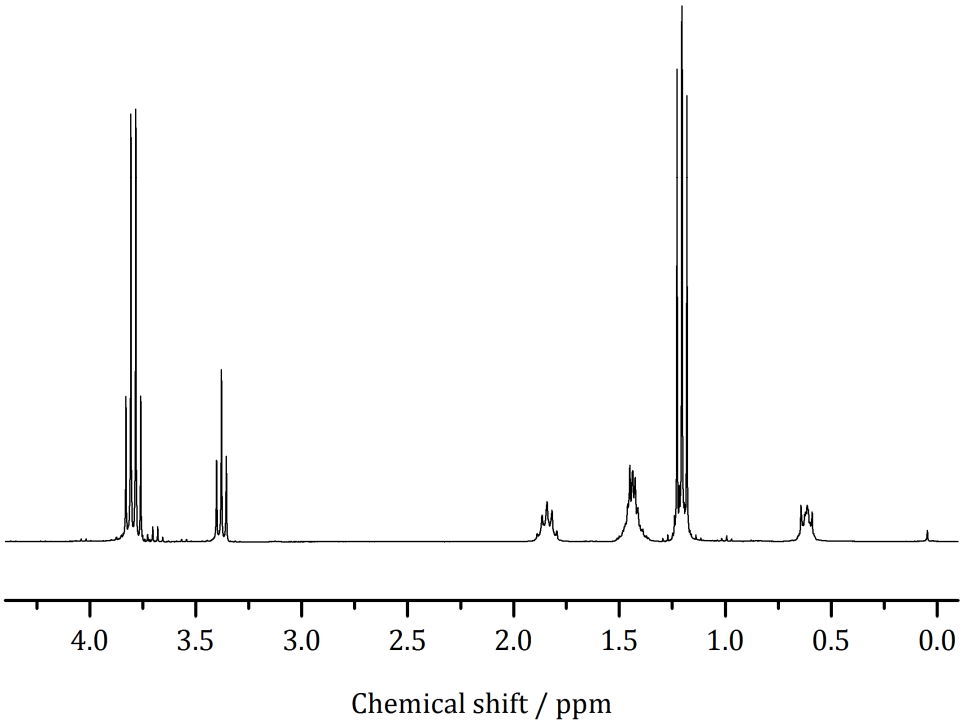


$^{1}$H-NMR (300 MHz, rt, $CDCl_3$): $\delta$ [ppm]: 3.83-3.76 (q,$^{3}J$=7.0 Hz, 6H, $OCH_2$), 3.40-3.36 (t, $^{3}J$=6.9 Hz, 2H, $CH_2Br$), 1.89-1.79 (m, 2H, $CH_2$), 1.46-1.41 (m, 4H, $CH_2$), 1.23-1.18 (t, $^{3}J$=7.0 Hz, 9H, $CH_3$), 0.64-0.59 (m, 2H, $SiCH_2$).

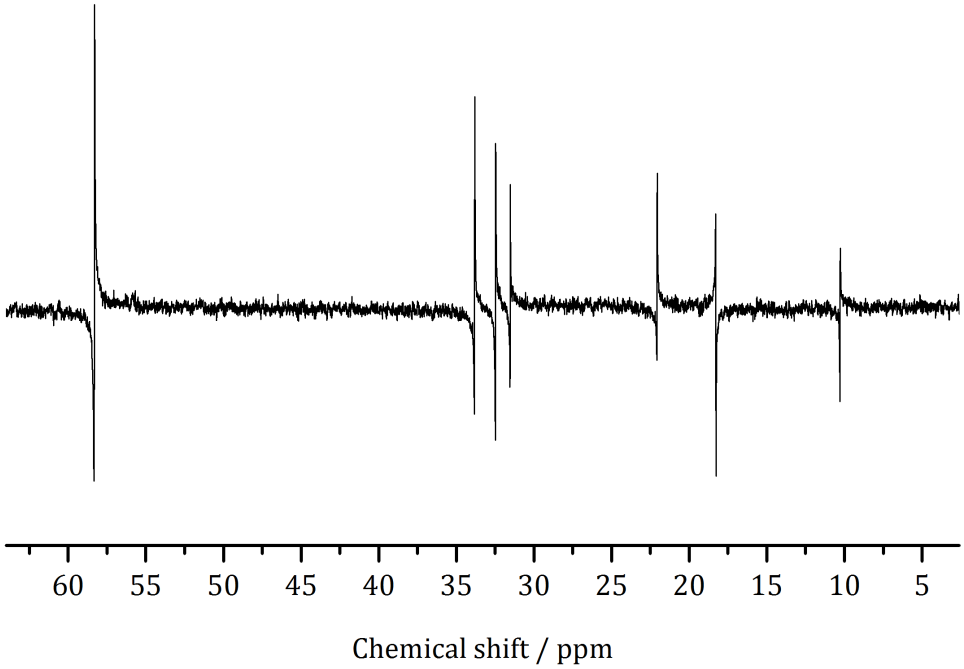


$^{13}$C-NMR (100 MHz, rt, $CDCl_3$): $\delta$ [ppm]: 58.3 ($OCH_2$), 33.8 ($CH_2Br$), 32.5 ($CH_2$), 31.6 ($CH_2$), 21.9 ($CH_2$), 18.2 ($CH_3$), 10.3 ($SiCH_2$).

### 7.1.2.3 Syntheses of the aminoalkyltriethoxysilanes

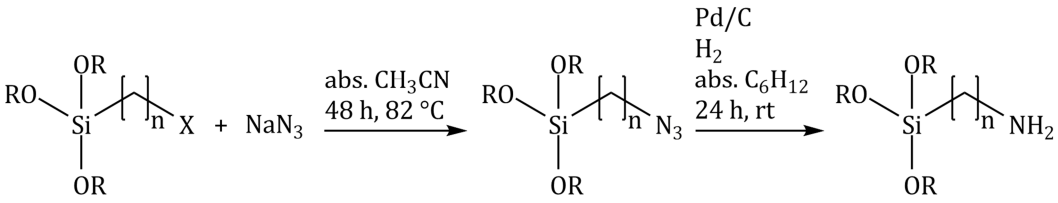


R = Et, Me
n = 5, 7, 11
X = Br

The aminoalkyl silanes (5-aminopentyl)-, (7-aminoheptyl)- and (11-amino-undecyl)tri(m)ethoxysilane were synthesized according to the literature.[197] Under a nitrogen atmosphere the respective (bromoalkyl)tri(m)ethoxysilane (11 mmol) was dissolved in absolute acetonitrile (60 mL). After addition of sodium azide (39 mmol), the mixture was refluxed for 48 h. The solvent was removed under

[197] B.P. Pichon, C. Wong Chi Man, J.J.E. Moreau, *J. Organomet. Chem.* **2006**, *691*, 1126-1130.

reduced pressure prior to addition of absolute cyclohexane (120-350 mL). The occurring precipitate was separated from the liquid by filtration. Pd/C (1.0-2.6 g) was added to the solution that was stirred under hydrogen atmosphere for 24 h at room temperature. After filtration and solvent removal, the product was obtained as a colorless liquid.

**(5-Azidopentyl)triethoxysilane**

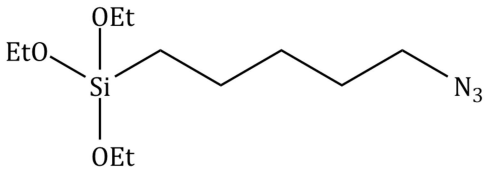


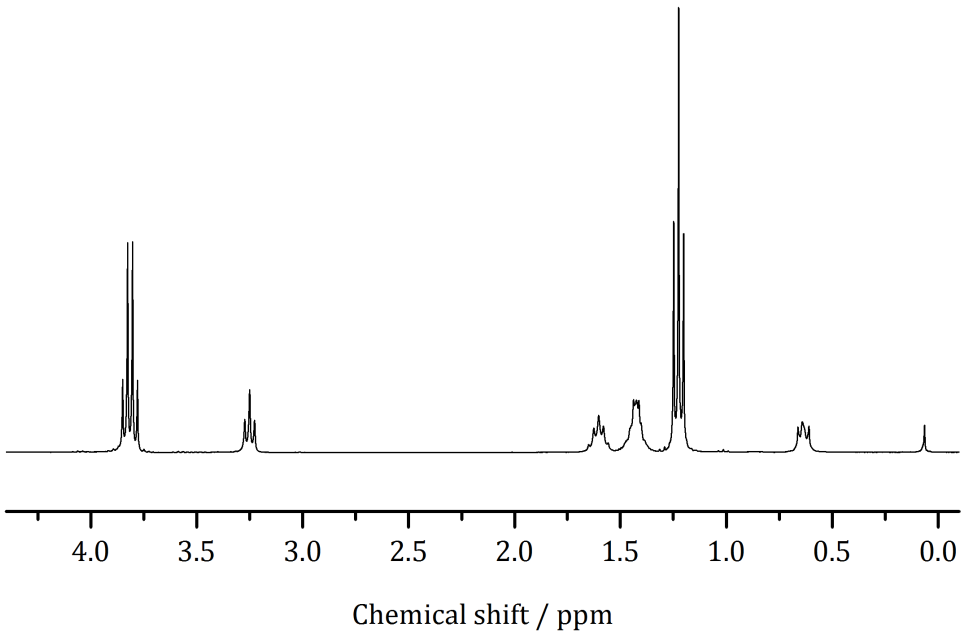


$^{1}$H-NMR (300 MHz, rt, $CDCl_3$): $\delta$ [ppm]: 3.85-3.78 (q, $^{3}J$=7.0 Hz, 6H, $OCH_2$), 3.27-3.23 (t, $^{3}J$=6.9 Hz, 2H, $CH_2N_3$), 1.65-1.56 (m, 2H, $CH_2$), 1.45-1.39 (m, 4H, $CH_2$), 1.25-1.20 (t, $^{3}J$=7.0 Hz, 9H, $CH_3$), 0.66-0.61 (m, 2H, $SiCH_2$).

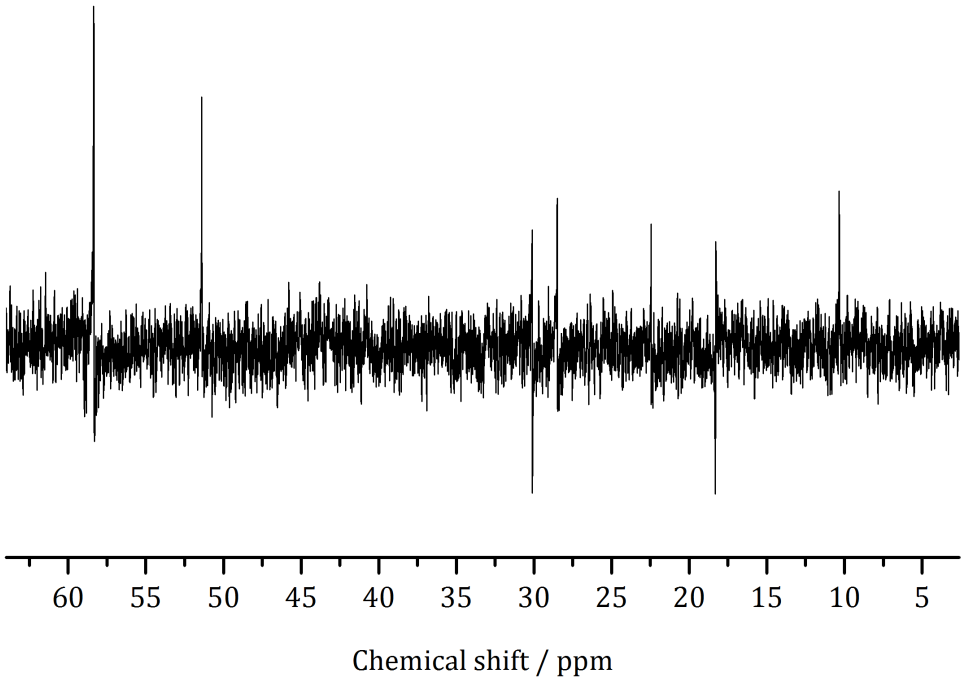


$^{13}$C-NMR (100 MHz, rt, $CDCl_3$): $\delta$ [ppm]: 58.4 ($OCH_2$), 51.5 ($CH_2N_3$), 30.1 ($CH_2$), 28.5 ($CH_2$), 22.4 ($CH_2$), 18.3 ($CH_3$), 10.3 ($SiCH_2$).

**(5-Aminopentyl)triethoxysilane**

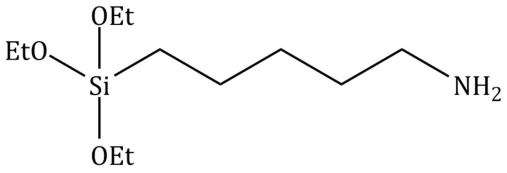


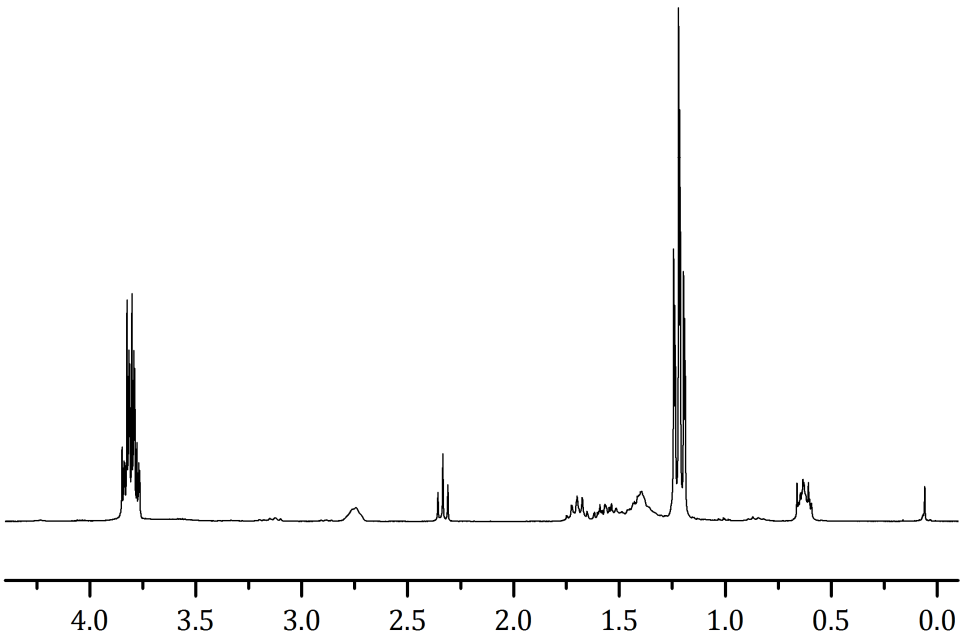


$^{1}$H-NMR (300 MHz, rt, $CDCl_3$): $\delta$ [ppm]: 3.85-3.76 (m, 6H, $OCH_2$), 2.74 (m, 1H, $CH_2N$), 2.36-2.31 (t, $^{3}J$=7.0 Hz, 1H, $CH_2N$), 1.75-1.36 (m, 6H, $CH_2$), 1.24-1.19 (m, 9H, $CH_3$), 0.66-0.59 (m, 2H, $SiCH_2$).

MS (EI): 249 [$M^{\cdot+}$].

**(7-Azidoheptyl)trimethoxysilane**

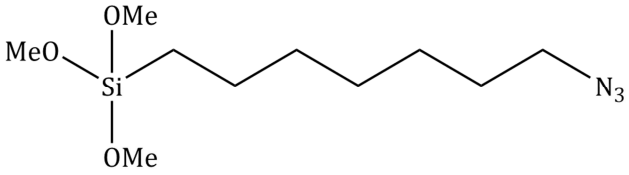


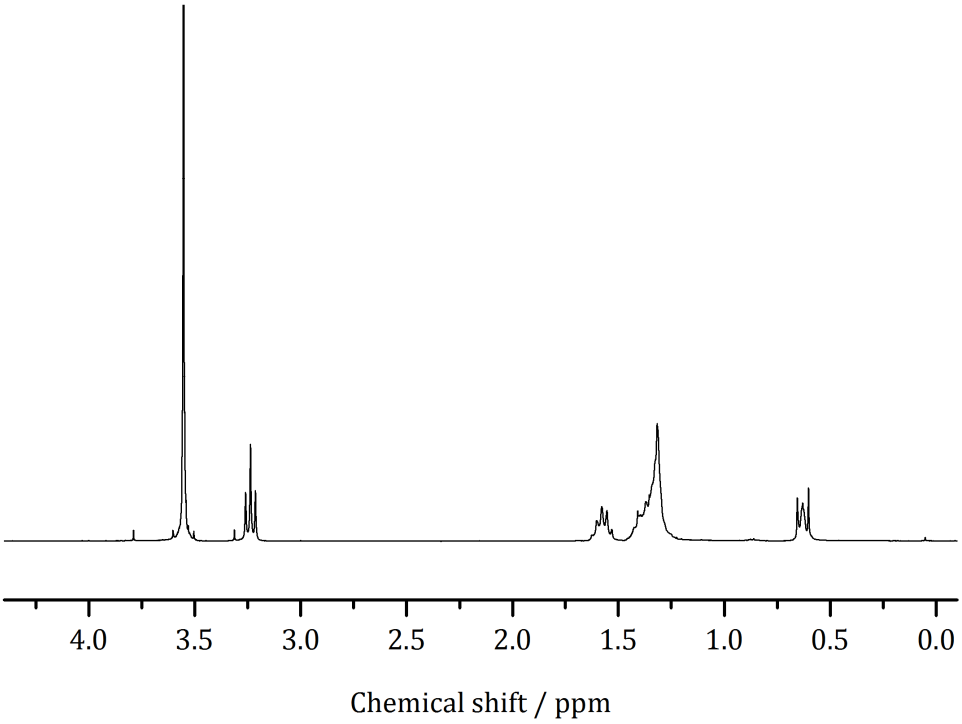


$^{1}$H-NMR (300 MHz, rt, $CDCl_3$): $\delta$ [ppm]: 3.55 (s, 9H, $OCH_3$), 3.26-3.21 (t, $^{3}J$=6.9 Hz, 2H, $CH_2N_3$), 1.62-1.53 (m, 2H, $CH_2$), 1.43-1.32 (m, 8H, $CH_2$), 0.66-0.60 (m, 2H, $SiCH_2$).

**(7-Aminoheptyl)trimethoxysilane**

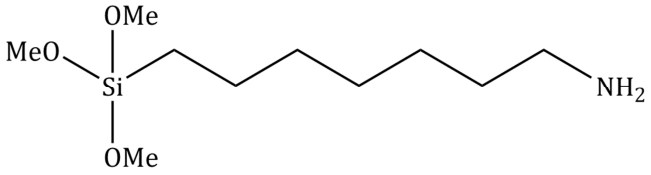


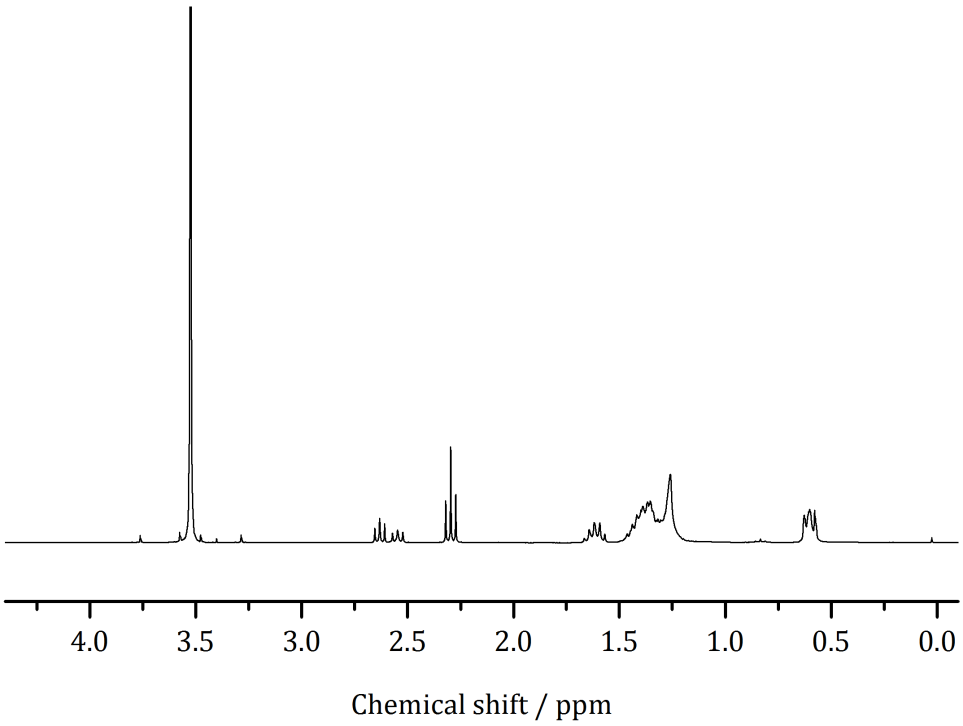


$^{1}$H-NMR (300 MHz, rt, $CDCl_3$): $\delta$ [ppm]: 3.52 (m, 9H, $OCH_3$), 2.65-2.52 (m, 1H, $CH_2N$), 2.32-2.27 (t, $^{3}J$=7.1 Hz, 1H, $CH_2N$), 1.66-1.57 (m, 1H, $CH_2$), 1.46-1.26 (m, 9H, $CH_2$), 0.63-0.58 (m, 2H, $SiCH_2$).

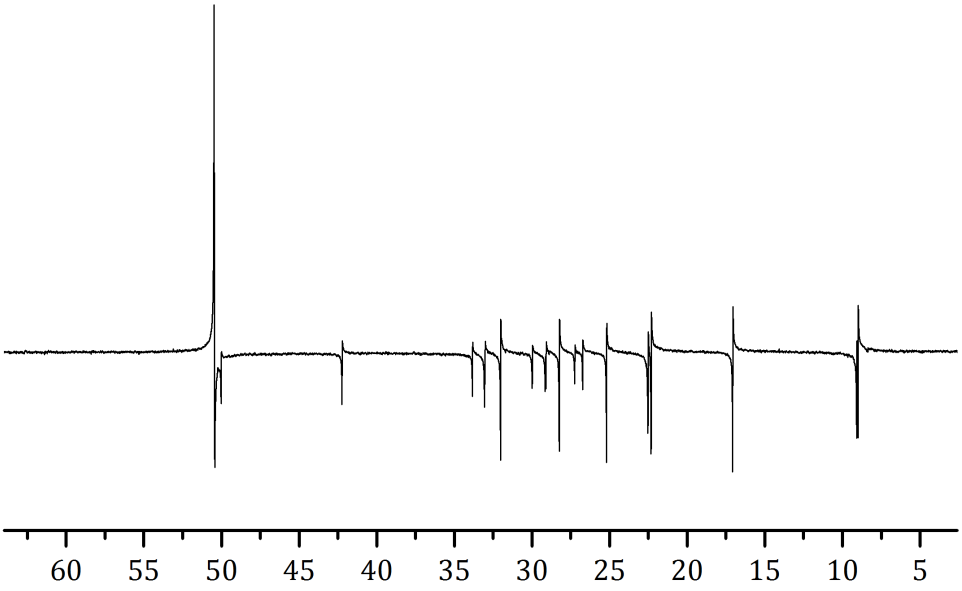


$^{13}$C-NMR (100 MHz, rt, $CDCl_3$): $\delta$ [ppm]: 50.4 ($OCH_3$), 42.2 $CH_2NH_2$, 33.9 ($CH_2$), 33.1, 32.0 ($CH_2$), 30.0 ($CH_2$), 28.2 ($CH_2$), 25.2 ($CH_2$), 17.1($CH_2$), 9.0 ($SiCH_2$).

MS (EI): 235 [$M^{\cdot+}$].

**(11-Azidoundecyl)trimethoxysilane**

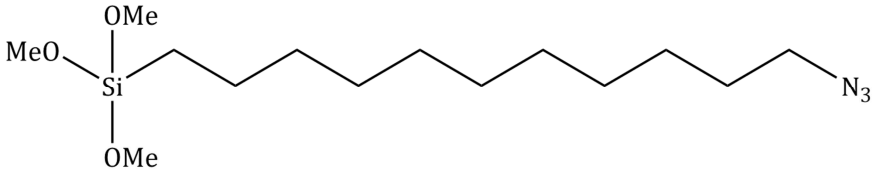


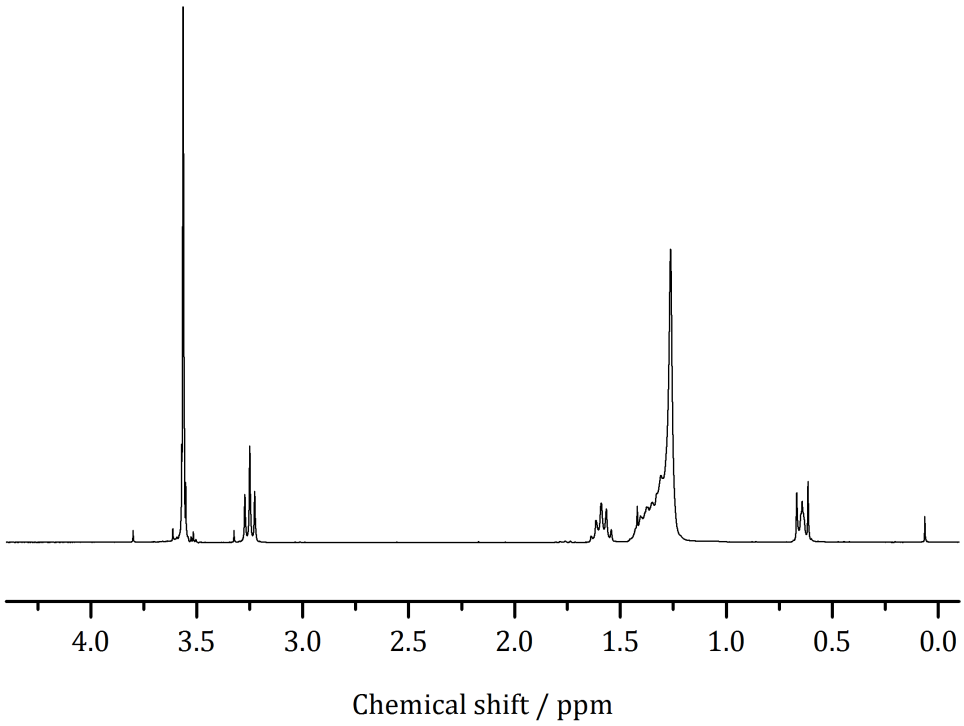


$^{1}$H-NMR (300 MHz, rt, $CDCl_3$): $\delta$ [ppm]: 3.56 (s, 9H, $OCH_3$), 3.27-3.23 (t, $^{3}J$=7.0 Hz, 2H, $CH_2N_3$), 1.64-1.54 (m, 2H, $CH_2$), 1.48-1.26 (m, 16H, $CH_2$), 0.67-0.61 (m, 2H, $SiCH_2$).

**(11-Aminoundecyl)trimethoxysilane**

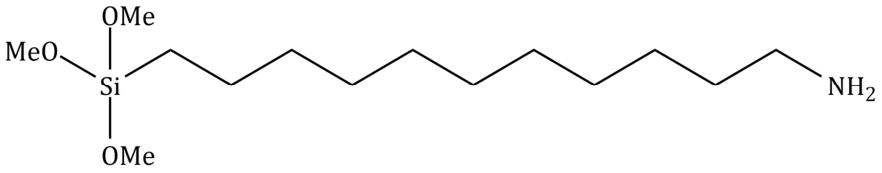


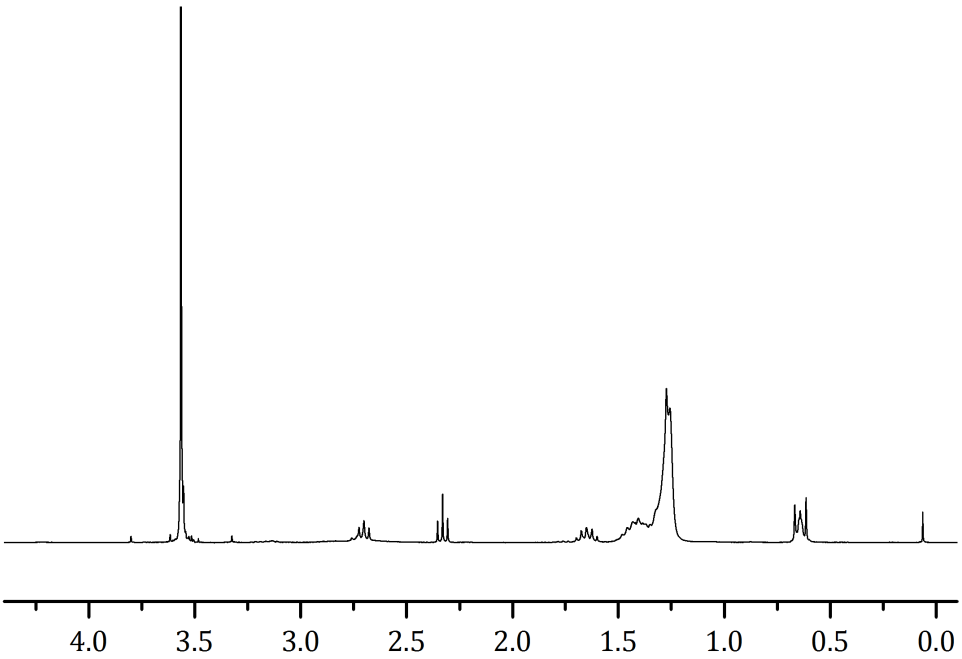


$^{1}$H-NMR (300 MHz, rt, $CDCl_3$): $\delta$ [ppm]: 3.56 (s, 9H, $OCH_3$), 2.72-2.68 (t, $^{3}J$=7.0 Hz, 1H, $CH_2N$), 2.35-2.31 (t, $^{3}J$=7.1 Hz, 1H, $CH_2N$), 1.64-1.54 (m, 2H, $CH_2$), 1.42-1.26 (m, 16H, $CH_2$), 0.67-0.61 (m, 2H, $SiCH_2$).

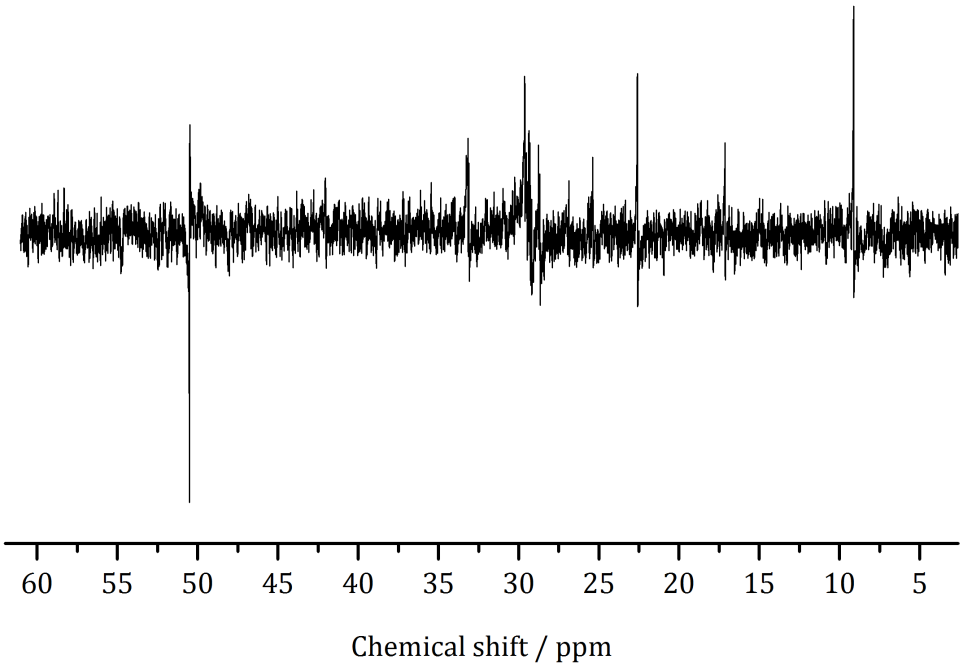


$^{13}$C-NMR (100 MHz, rt, $CDCl_3$): $\delta$ [ppm]: 50.8 ($OCH_3$), 42.1 ($CH_2NH_2$), 33.2 ($CH_2$), 33.1 ($CH_2$), 29.6 ($CH_2$), 29.4 ($CH_2$), 29.30 ($CH_2$), 29.26 ($CH_2$), 28.8 ($CH_2$), 28.7 ($CH_2$), 25.4 ($CH_2$), 22.6 ($CH_2$), 17.2 ($CH_2$), 9.1 ($SiCH_2$).

MS (EI): 291 [$M^{\cdot+}$].

### 7.1.2.4 Functionalization of MCF

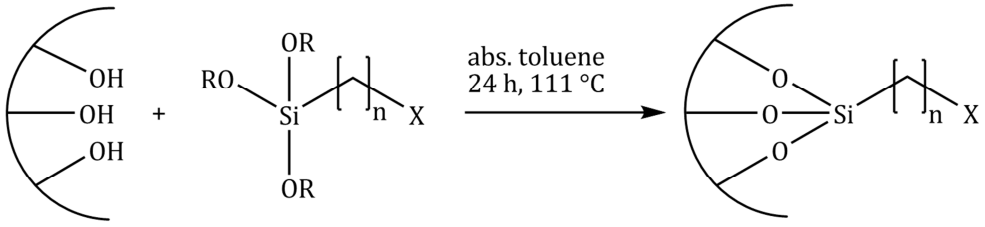


R = Et, Me
n = 3, 5, 7, 11
X = $NH_2$, H

To organically modify the surface of the host material, MCF (200 mg) was dispersed in dry toluene (15 mL) and the respective organosilane (1.5 mmol) was added. The mixture was heated to reflux for 24 h prior to filtration of the solid. The modified silica was rinsed off with water as well as ethanol and dried at 60 °C.[193]

### 7.1.3 Immobilization and enzymatic assays of 6PGDH

#### 7.1.3.1 Immobilization of 6PGDH

The respective modified MCF (5 mg) was dispersed in potassium phosphate buffer solution (1.000 mL, 50 mmol $L^{-1}$) containing 6PGDH (ca. 0.5 mg $mL^{-1}$). The reaction mixture was shaken for 24 h at 25 °C and 350 rpm. After 5, 10, 15, 30 min as well as 1, 2, 3, 4, 5 and 24 h of immobilization, aliquots (60 µL) of the reaction mixture were removed and centrifuged for 2 min at 4000 rpm. Hereof aliquots (50 µL) were sampled and kept for the determination of the enzyme concentration in order to follow the progress of the immobilization. To remove non-immobilized and loosely attached enzyme molecules, the MCF was re-suspended in potassium phosphate buffer (1.000 mL, 50 mmol $L^{-1}$, pH 6.5) and recovered by centrifugation three times. The supernatants of all purification steps were kept in order to calculate the total amount of immobilized enzyme. All immobilisates were stored at 4 °C in potassium phosphate buffer (1.000 mL, 50 mmol $L^{-1}$, pH 6.5).

#### 7.1.3.2 Activity assay of 6PGDH

In a common activity assay, potassium phosphate buffer (2750 µL, 50 mmol $L^{-1}$, pH 7.5), 6PG solution (50 µL , 100 mmol $L^{-1}$) , $NADP^+$ solution (100 µL, 60 mmol $L^{-1}$) and the respective enzyme sample (20 µL, 0.5 mg $mL^{-1}$, free or immobilized) were combined, mixed by inversion and incubated for 1 min at 25 °C. The increase of the absorbance (Δabs) at λ = 340 nm was monitored for 5 min at 25 °C under stirring to monitor the conversion of $NADP^+$ to NADPH (threefold determination). The enzymatic activity [U $mg^{-1}$] was calculated as follows with the millimolar extinction coefficient (6.22 L $cm^{-1}$ $mmol^{-1}$) of NADPH and the 6PGDH concentration ($c_{enzyme}$) of the reaction mix in mg per mL.[198]

$$U \cdot mg^{-1} = \frac{\Delta abs \cdot min^{-1}}{6.22\ L \cdot cm^{-1} \cdot mmol^{-1} \cdot c_{enzyme}} \qquad \textbf{Eq.19}$$

#### 7.1.3.3 Long-term stability of the (immobilized) 6PGDH

After immobilization, the immobilisates were stored at 4 °C in phosphate buffer solution (50 mmol $L^{-1}$, pH 6.5). For a daily investigation of the remained activity of the immobilized 6PGDH, the immobilisates were allowed to warm to

[198] Sigma-Aldrich: Enzymatic assay of 6-phosphogluconic dehydrogenase (EC1.1.1.44): https://www.sigmaaldrich.com/content/dam/sigma-aldrich/docs/Sigma/Enzyme_Assay/6phosphogluc dehydrog75.pdf, **2017**.

room temperature. This was followed by re-dispersion of the immobilisates in the supernatant buffer solution and the performance of the activity assay that was described above. After performing the activity assay, the immobilisates were again stored at 4 °C for further 24 h until the next activity assay was required. The long-term stability of the native 6PGDH was investigated in an analogous manner.

#### 7.1.3.4 Kinetic activity assay

Kinetic measurements were performed with varied 6PG concentrations in the range of 0.034 – 3.4 mmol $L^{-1}$ and final concentrations of $NADP^+$ from 0.01 – 2.0 mmol $L^{-1}$. After combining all components the reaction mixture was gently mixed by inversion and the increase of the absorbance was monitored for 1 min at 25 °C.

#### 7.1.3.5 Leaching experiments

The supernatant buffer solution of the respective immobilisate was removed by centrifugation (2 min, 4000 rpm). The sample was redispersed in phosphate buffer (1.000 mL, pH 6.5, 50 mmol $L^{-1}$) and shaken for 24 h at 25 °C and 350 rpm. Once again the supernatant buffer was removed, the sample redispersed in buffer and the leaching test repeated. The protein concentrations of the supernatants were detected according to the Bradford method.

#### 7.1.3.6 Bradford assay

The enzyme concentration was detected using the Bradford assay.[169] A calibration curve was established by deploying bovine serum albumin (BSA) as a protein standard in the range between 0 mg $mL^{-1}$ and 1.400 mg $mL^{-1}$ protein. The Bradford reagent (1.500 mL, *Sigma-Aldrich*) was added to an aliquot of each sample (50 µL) and incubated for 10 min at room temperature. Subsequently the absorbance of each sample was measured at $\lambda$ = 595 nm.

### 7.1.4 Immobilization and enzymatic assays of *E.c.*ADH

#### 7.1.4.1 Immobilization of *E.c.*ADH

MCF-$C_3$-$NH_2$ (6.7 mg, 10 mg, or 20 mg) was dispersed in potassium phosphate buffer solution (1.000 mL, 50 mmol $L^{-1}$, pH 6.5, 7.0 or 7.5) containing ADH (ca. 2.0 mg $L^{-1}$). The immobilization mixture was shaken for 24 h at 350 rpm and 25 °C. After 5, 10, 15 and 30 min as well as 1, 2, 3, 4, 5 and 24 h, aliquots (40 µL) were removed and centrifuged for 2 min at 4000 rpm to separate any solid phase. Thereof aliquots (30 µL) were sampled to determine the respective remained ADH concentration in the supernatants. After 24 h of immobilization, the buffer solution was centrifuged (5 min, 4000 rpm) and the immobilisates were re-dispersed four times in the respective potassium phosphate buffer solution (1.000 mL, 50 mmol $L^{-1}$, pH 6.5, 7.0 or 7.5) to remove any non-immobilized enzyme. All supernatants of the purification steps were kept in order to calculate the total amount of immobilized ADH. The immobilisate was stored in phosphate buffer solution (1.000 mL, 50 mmol $L^{-1}$, pH 6.5, 7.0 or 7.5) at 4 °C.

#### 7.1.4.2 Activity assay of ADH

The enzymatic activity assay was performed according to a modification of the common ADH assay.[199] The respective ADH sample (20 µL immobilized or free enzyme), $NADP^+$ or NADPH solution (100 µL, 15 mmol $L^{-1}$) in potassium phosphate buffer (50 mmol $L^{-1}$, pH 7.5) and 2-propanol or acetone solution (300 µL, 1.5 mol $L^{-1}$) in potassium phosphate buffer (50 mmol $L^{-1}$, pH 7.5) were added to potassium phosphate buffer solution (2580 µL, 50 mmol $L^{-1}$, pH 7.5). The assay mixture was gently mixed by inversion and incubated for 1 min at 25 °C followed by the detection of an increase ($NADP^+$/2-propanol) or decrease (NADPH/acetone) of the absorbance at $\lambda$ =340 nm for 3 min at 25 °C (threefold determination). The enzymatic activity [U $mg^{-1}$] of the free and immobilized ADH was calculated by using Eq. 19.

The long-term stabilities of the immobilized as well as the free ADH were determined according to the procedure described in section 7.1.3.3 employing the respective substrates and coenzymes.

[199] Sigma-Aldrich: Enzymatic assay of alcohol dehydrogenase, $NADP^+$ dependent (EC.1.1.1.2): https://www.sigmaaldrich.com/content/dam/sigma-aldrich/docs/Sigma/Enzyme_Assay/a8435enz.pdf, **2017**.

#### 7.1.4.3 Kinetic activity assay

To perform the kinetic activity assay, the ADH sample (20 µL, free or immobilized enzyme) was pipetted into a mixture consisting of $NADP^+$ or NADPH (0-1.0 mmol $L^{-1}$) and 2-propanol or acetone (0-200 mmol $L^{-1}$) in a total volume of 2980 µL potassium phosphate buffer solution (50 mmol $L^{-1}$, pH 7.5). Prior to the photometric detection of the increase ($NADP^+$/2-propanol) or decrease (NADPH/acetone) of the absorbance at $\lambda$ = 340 nm for one minute at 25 °C, the reaction mixture was shortly mixed by inversion.

#### 7.1.4.4 Leaching experiments

In a typical leaching experiment, the immobilisate (300 µL) was dispersed in potassium phosphate buffer solution (700 µL, 50 mmol $L^{-1}$, pH 6.5, 7.0 or 7.5) followed by centrifugation at 4000 rpm for 5 min. After removal of the supernatant, the immobilisate was re-dispersed in buffer solution (1000 µL) and shaken for 24 h at 25 °C and 350 rpm. Repeatedly, the immobilisate was separated by centrifugation (5 min, 4000 rpm) and immediately re-dispersed in fresh buffer solution. The leaching experiment was repeated for further 24 h and the buffer solutions were kept to determine the concentration of the free enzyme present in the supernatants by employing the Bradford method.

#### 7.1.4.5 Bradford assay

To determine the ADH concentrations of the stock solutions as well all supernatants, the typical Bradford assay was applied. A calibration curve in the range between 0 mg $mL^{-1}$ and 2.000 mg $mL^{-1}$ was erected by using BSA as a standard. An aliquot (30 µL) of each protein sample was mixed with Bradford reagent (1500 µL, *Thermo Scientific*) and incubated for 10 min at room temperature followed by the detection of the absorbance at $\lambda$ = 595 nm.

### 7.1.5 Immobilization and enzymatic assays of *L.m.*G6PDH

#### 7.1.5.1 Immobilization of *L.m.*G6PDH onto MCF-$C_3$-$NH_2$

The immobilization of G6PDH was carried out in HEPES (200 mmol $L^{-1}$, pH 7.4) as well as in phosphate buffer solution (50 mmol $L^{-1}$, pH 7.5), respectively. MCF-$C_3$-$NH_2$ (14 mg) was suspended in the respective buffer solution (2.000 mL) containing G6PDH (0.5 mg $mL^{-1}$). The immobilization mixture was shaken for 24 h at 25 °C and 350 rpm. After 5, 10, 15, 30 min as well as 1, 2, 3, 4, 5 and 24 h of immobilization, aliquots (60 µL) of the reaction mixture were removed and centrifuged for 2 min at 4000 rpm. Hereof aliquots (50 µL) were sampled and kept for the determination of the enzyme concentration in order to follow the progress of immobilization. To remove non-immobilized and loosely attached enzyme molecules MCF-$C_3$-$NH_2$ was re-suspended in buffer (2.000 mL) and recovered by centrifugation three times. The supernatants of all purification steps were kept in order to calculate the total amount of immobilized G6PDH. All immobilisates were stored at 4 °C in the respective immobilization buffer (2.000 mL).

#### 7.1.5.2 Activity assay of G6PDH

The enzymatic activity assay was performed according to a modification of the common G6PDH assay.[200, 201] The immobilisates and the stock solutions were diluted by 1:10 in the respective immobilization buffer in order to assure that all measurements are carried out within the operational range of the photometer. The activity assays were either performed in HEPES (200 mmol $L^{-1}$, pH 7.4) or potassium phosphate buffer solution (50 mmol $L^{-1}$, pH 7.5). Thus, the required substrate and coenzyme solutions were prepared by utilizing the respective assay buffer.

To the diluted G6PDH sample (10 µL, immobilized or free enzyme), G6P solution (100 µL, 57.7 mmol $L^{-1}$), $NADP^+$ solution (100 µL, 23.4 mmol $L^{-1}$), optional $MgCl_2 \cdot 6\,H_2O$ solution (100 µL, 345 mmol $L^{-1}$) and the respective buffer solution were added to give a total assay volume of 3000 µL. The assay mixture was gently mixed by inversion and incubated for 1 min at 25 °C followed by a detection of the increase of the absorbance at $\lambda$ =340 nm for 5 min at 25 °C (threefold determination). The enzymatic activity [U $mg^{-1}$] of the free and immobilized G6PDH was calculated by applying Eq. 19.

[200] Sigma-Aldrich: Enzymatic Assay of Glucose-6-Phosphate Dehydrogenase (EC 1.1.1.49): http://www.sigmaaldrich.com/technical-documents/protocols/biology/enzymatic-assay-of- glucose-6-phosphate-dehydrogenase.html, **2017**.
[201] E.A. Noltmann, C.J. Gubler, S.A. Kuby, *J. Biol. Chem.* **1961**, *236*, 1225-1230.

The long-term stabilities of the immobilized as well as the free G6PDH were determined according to the description in section 7.1.3.3 employing the respective substrate and coenzyme.

#### 7.1.5.3 Kinetic activity assay of G6PDH

The kinetic investigations of the immobilized G6PDH were carried out in HEPES (200 mmol $L^{-1}$, pH 7.4) and phosphate buffer solution (50 mmol $L^{-1}$, pH 7.5), respectively, with varied G6P concentrations in the range of 0.096 – 5.0 mmol $L^{-1}$ and final concentrations of $NADP^+$ from 0.039 – 2.0 mmol $L^{-1}$. After combining all components the reaction mixture was gently mixed by inversion and the increase of the absorbance was monitored for 1 min at 25 °C.

#### 7.1.5.4 BCA protein assay

The enzyme concentration was detected according to the bicinchoninic acid (BCA) assay.[170, 178] A calibration curve was established using BSA as protein standard in the range between 0 mg $mL^{-1}$ and 2.000 mg $mL^{-1}$ protein. The BCA reagent (1.000 mL, *Millipore*) was added to an aliquot of each sample (50 µL) and incubated for 30 min at 37 °C. Subsequently, the absorbance of each sample was measured at $\lambda$ = 562 nm.

### 7.1.6 Enzyme cascade

#### 7.1.6.1 Enzyme cascade: Performance cycles 1-5

The enzyme cascade was carried out in phosphate buffer solution (50 mmol $L^{-1}$, pH 7.5) at 25 °C. Correspondingly all substrate and coenzyme solutions were prepared in phosphate buffer solution (50 mmol $L^{-1}$, pH 7.5).

**Cycle 1**

Step 1: G6PDH

The G6PDH immobilisate (50 µL of a 1:10 dilution) was dispersed in a reaction mixture consisting of G6P (2.6 µL, 57.7 mmol $L^{-1}$) and $NADP^+$ (32.1 µL, 23.4 mmol $L^{-1}$) as well as phosphate buffer solution (2915.3 µL). Subsequently, the conversion of $NADP^+$ to NADPH was photometrically detected (25 °C, λ = 340 nm). After a full substrate conversion was reached, the reaction mixture was filtered over fresh MCF-$C_3$-$NH_2$ (20 mg) to remove the immobilisate and to re-immobilize any amounts of leached enzyme from the reaction mixture (2 min, 4000 rpm). The filter-MCF-$C_3$-$NH_2$ was kept for the next cycle and stored at 4 °C. Prior to the introduction of the filtrate in step 2, its absorbance (25 °C, λ = 340 nm) was detected for 1 min.

Step 2: 6PGDH

The 6PGDH immobilisate (50 µL) was dispersed in the filtrate of step 1 and the oxidation of $NADP^+$ to NADPH was photometrically monitored (25 °C, λ = 340 nm). After a full substrate conversion was detected, the reaction mixture was filtered over fresh MCF-$C_3$-$NH_2$ (20 mg, 2 min, 4000 rpm). The filter-MCF-$C_3$-$NH_2$ was kept for the next cycle and stored at 4 °C. Prior to the introduction of the filtrate in step 2, the absorbance (25 °C, λ = 340 nm) was detected for 1 min.

Step 3: ADH

In order to initiate the re-oxidation of NADPH to $NADP^+$ the ADH immobilisate (10 µL) was dispersed in the filtrate of step 2 and a sufficient amount of acetone (6.61 µL, 90.0 µmol) was added. After a complete conversion of NADPH was photometrically detected, the reaction mixture was filtered over fresh MCF-$C_3$-$NH_2$ (20 mg). The filter-MCF-$C_3$-$NH_2$ was kept for the next cycle and stored at 4 °C. Concluding, the absorbance of the filtrate was detected for 1 min (25 °C, λ = 340 nm).

**Cycles 2-5**

Step 1: G6PDH

The filter-MCF-$C_3$-$NH_2$ of the preceding cycle containing the immobilized G6PDH was again redispersed in a fresh G6P/$NADP^+$ solution (cf. cycle1 step 1). The dispersion was incubated for 30 min at 25 °C followed by filtration over fresh MCF-$C_3$-$NH_2$ (20 mg). The filter-MCF-$C_3$-$NH_2$ was kept for the next cycle and stored at 4 °C. Prior to the introduction of the filtrate in step 2, the absorbance (25 °C, λ = 340 nm) was detected for 1 min in order to detect the degree of conversion.

Step 2: 6PGDH

The filter-MCF-$C_3$-$NH_2$ of the preceding cycle containing the immobilized 6PGDH was again redispersed in the filtrate of step 1. The dispersion was incubated for 90 min at 25 °C followed by filtration over fresh MCF-$C_3$-$NH_2$ (20 mg). The filter-MCF-$C_3$-$NH_2$ was kept for the next cycle and stored at 4 °C. Prior to the introduction of the filtrate in step 3, the absorbance (25 °C, λ = 340 nm) was detected for 1 min in order to detect the degree of conversion.

Step 3: ADH

The filter-MCF-$C_3$-$NH_2$ of the preceding cycle containing the immobilized ADH was redispersed in the filtrate of step 2 and 6.61 µL (90.0 µmol) acetone was added. The dispersion was incubated for 180 min at 25 °C followed by filtration over fresh MCF-$C_3$-$NH_2$ (20 mg). The filter-MCF-$C_3$-$NH_2$ was kept for the next cycle and stored at 4 °C. The absorbance of the filtrate was detected for 1 min (25 °C, λ = 340 nm) in order to detect the degree of conversion.

### 7.1.6.2 Immobilization of *E.c.*ADH onto filter MCF-$C_3$-$NH_2$

The collected filter-MCF-$C_3$-$NH_2$ (5 x 20 mg = 100 mg) of the five cofactor recycling steps was triply redispersed in phosphate buffer solution (2.000 mL, 50 mmol $L^{-1}$, pH 7.0) and centrifuged for 2 min at 4000 rpm in order to remove any substrate, coenzyme or buffer residues of the cascade cycles. Subsequently, the purified filter-MCF-$C_3$-$NH_2$ was dispersed in an ADH stock solution (potassium phosphate, 5.000 mL, 50 mmol $L^{-1}$, pH 7.0) containing ADH (ca. 2 mg $mL^{-1}$) and shaken for 24 h at 350 rpm and 25 °C. After 10, 15, 20 and 30 min as well as 1, 2, 3, 4, 5 and 24 h, aliquots (40 µL) were removed and centrifuged for 2 min at 4000 rpm to separate any solid phase. Thereof aliquots (30 µL) were sampled to determine the respective remained ADH concentrations in the supernatant. After 24 h of

immobilization, the buffer solution was centrifuged (5 min, 4000 rpm) and the immobilisate was redispersed six times in potassium phosphate buffer solution (5.000 mL, 50 mmol $L^{-1}$, pH 7.0) to remove any non-immobilized enzyme. All supernatants of the purification steps were kept in order to calculate the total amount of immobilized ADH. The immobilisate was stored in potassium phosphate buffer solution (5.000 mL, 50 mmol $L^{-1}$, pH 7.0) at 4 °C.

The activity assay as well as the Bradford assay was performed as can be found in chapters 7.1.4.2 and 7.1.4.5.

## 7.2 Thermal analyses (TA/DTA/MS) of the functionalized MCFs

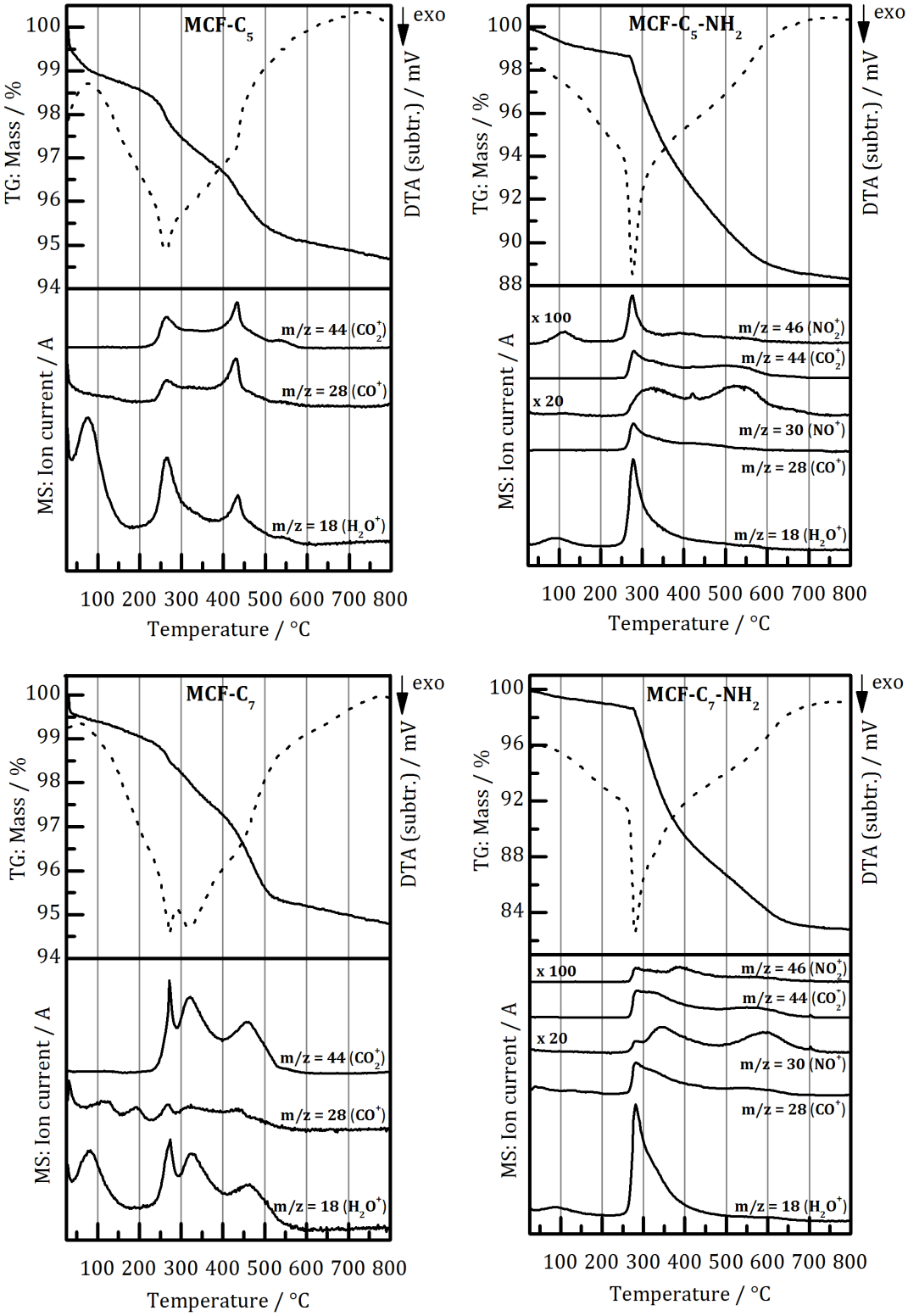


**Figure 92.** TG-DTA-MS of MCF-$C_5$/MCF-$C_5$-$NH_2$ as well as MCF-$C_7$/MCF-$C_7$-$NH_2$ in an Ar/$O_2$ atmosphere (8:2). The upper spectra show the TG (solid line) and the DTA (dashed line) curves, whereas the ion currents detected by a mass spectrometer are depicted at the bottom at each diagram.

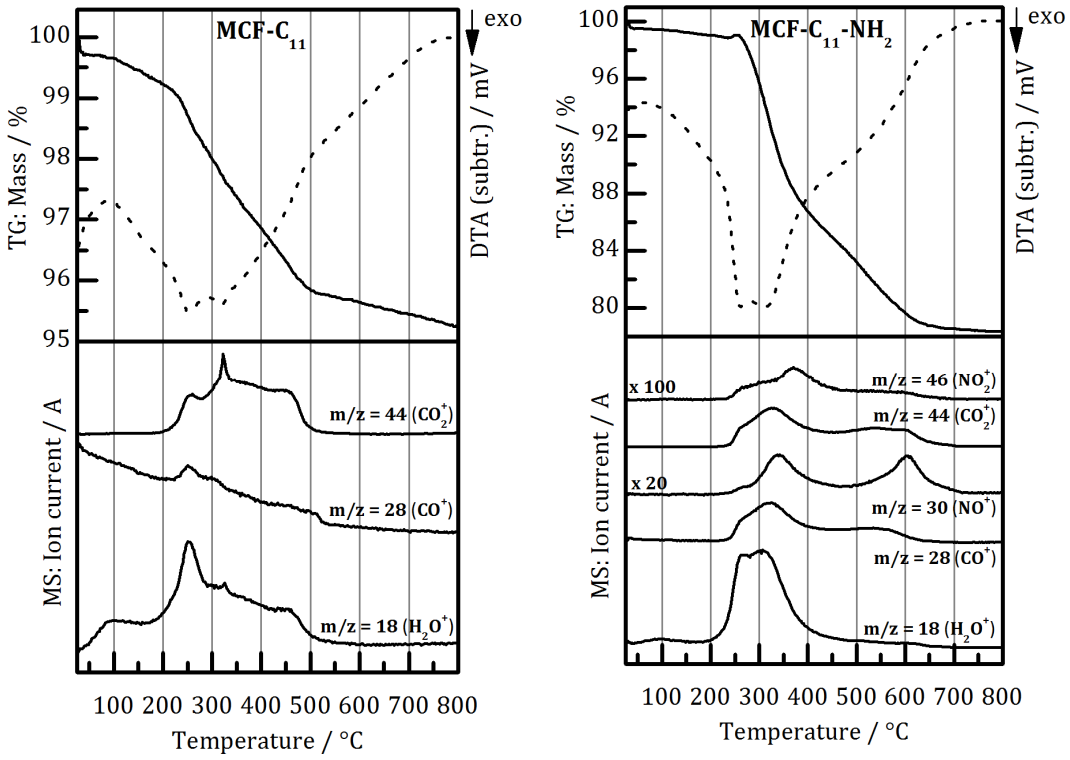


**Figure 93.** TG-DTA-MS of MCF-$C_{11}$ as well as MCF-$C_{11}$-$NH_2$ in an $Ar/O_2$ atmosphere (8:2). The upper spectra show the TG (solid line) and the DTA (dashed line) curves, whereas the ion currents detected by a mass spectrometer are depicted at the bottom at each diagram.

### 7.2.1 Calculation of the functionalization density of the functionalized MCFs

- Calculation in mol per g functionalized MCF:[193]

$$\frac{m_{\text{amount of organic residues per g MCF}}}{M_{\text{organic residue}}} = \delta_F\ [\text{mol}] \qquad \textbf{(Eq. 20)}$$

- Calculation in mg per g functionalized MCF:[193]

$$1000\ \text{mg} \cdot (100\ \% - \text{massloss}\ [\%]) = \delta_F\ [\text{mg}] \qquad \textbf{(Eq. 21)}$$

## 7.3 Zeta potential titration curves of the functionalized MCFs

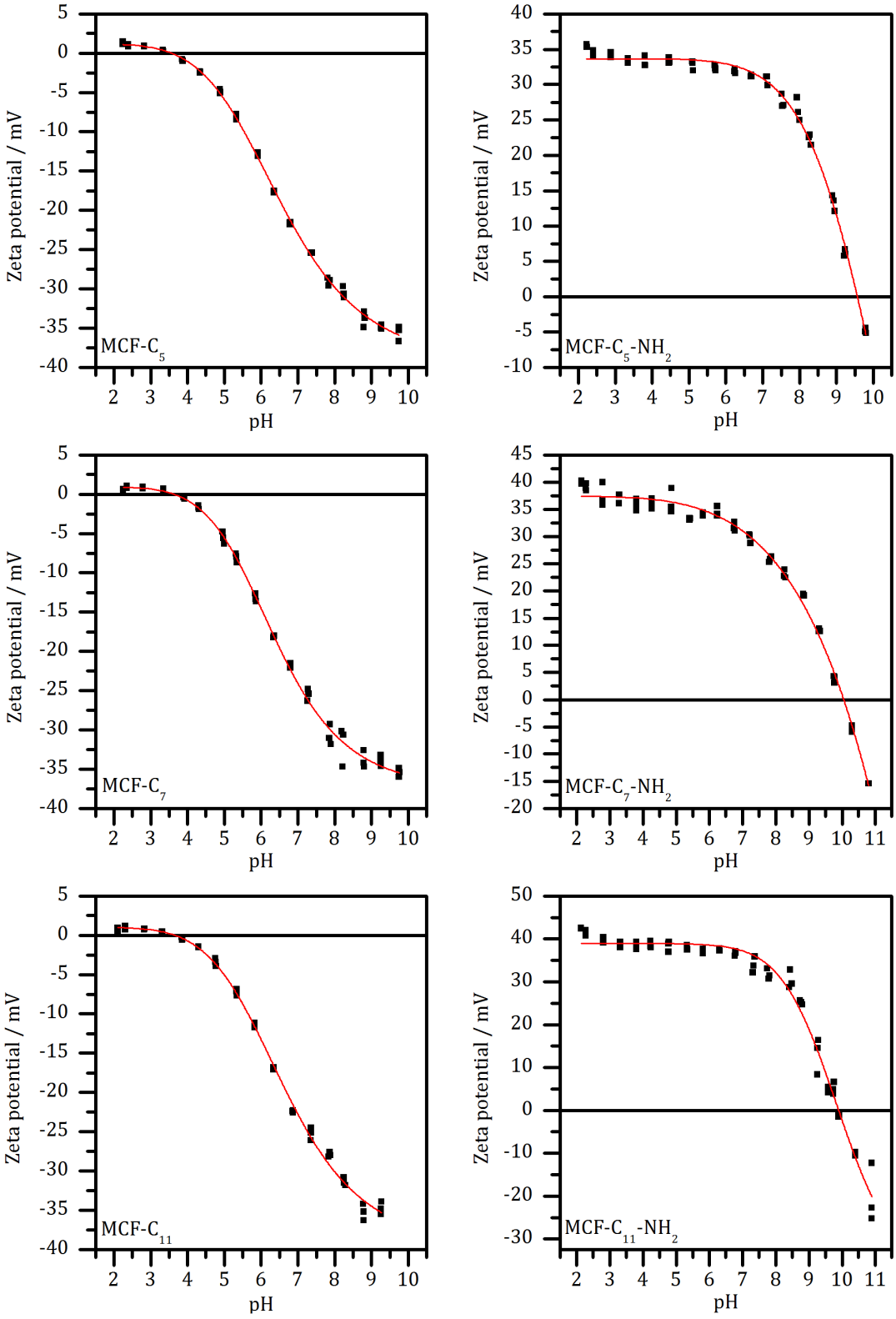


**Figure 94.** Zeta potential titration curves of the alkyl as well as the aminoalkyl modified MCFs.

## 7.4 Uptake diagrams: Immobilization of *G.s.*6PGDH

### 7.4.1 Immobilization G.s.6PGDH onto pristine MCF

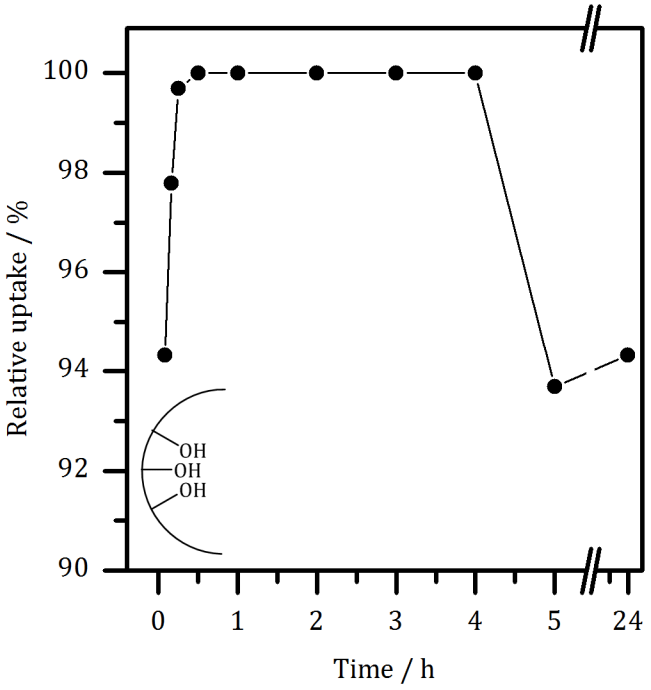


**Figure 95.** Relative uptake of *G.s.*6PGDH immobilized onto pristine MCF.

### 7.4.2 Variation of the ionic strength of the buffer solution within the immobilization of *G.s.*6PGDH

**a)** **b)**

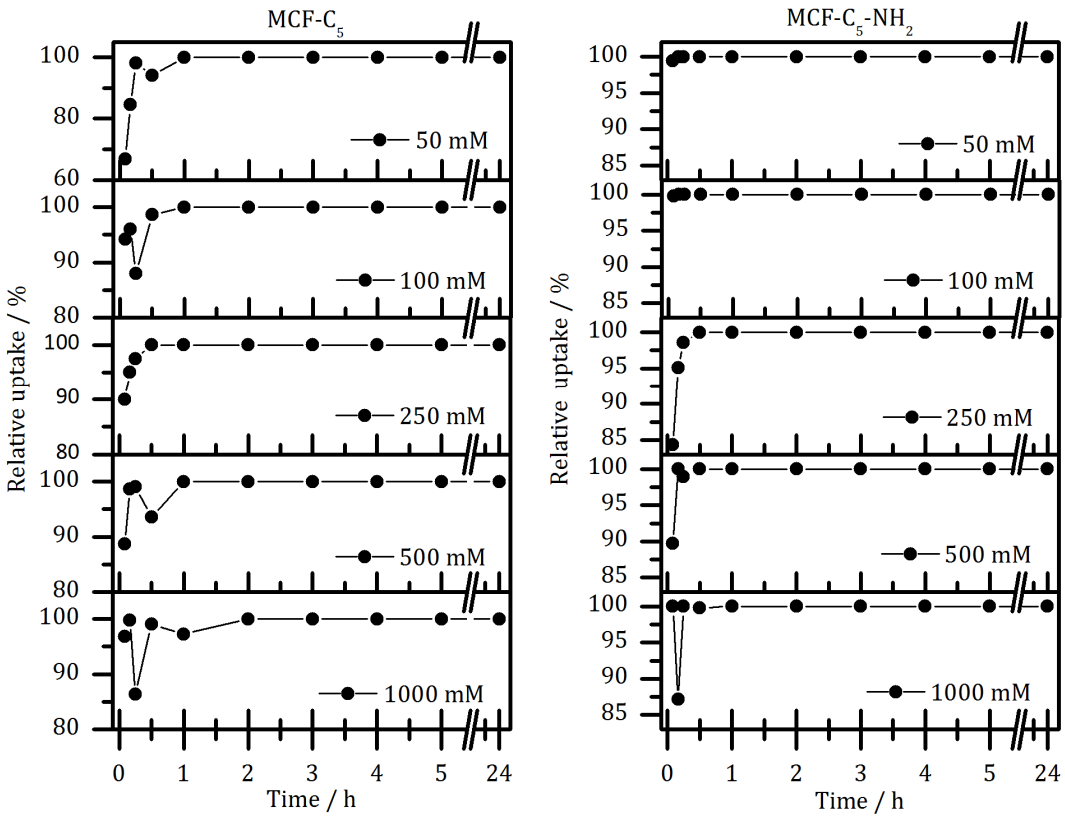


**Figure 96.** Relative uptakes of *G.s.*6PGDH immobilized onto **a)** MCF-$C_5$ and **b)** MCF-$C_5$-$NH_2$. The ionic strength of the buffer solution employed for the immobilization was varied from 50 mM to 1000 mM, respectively.

### 7.4.3 Variation of the initial concentration of *G.s.*6PGDH employed for immobilization

**a)** **b)**

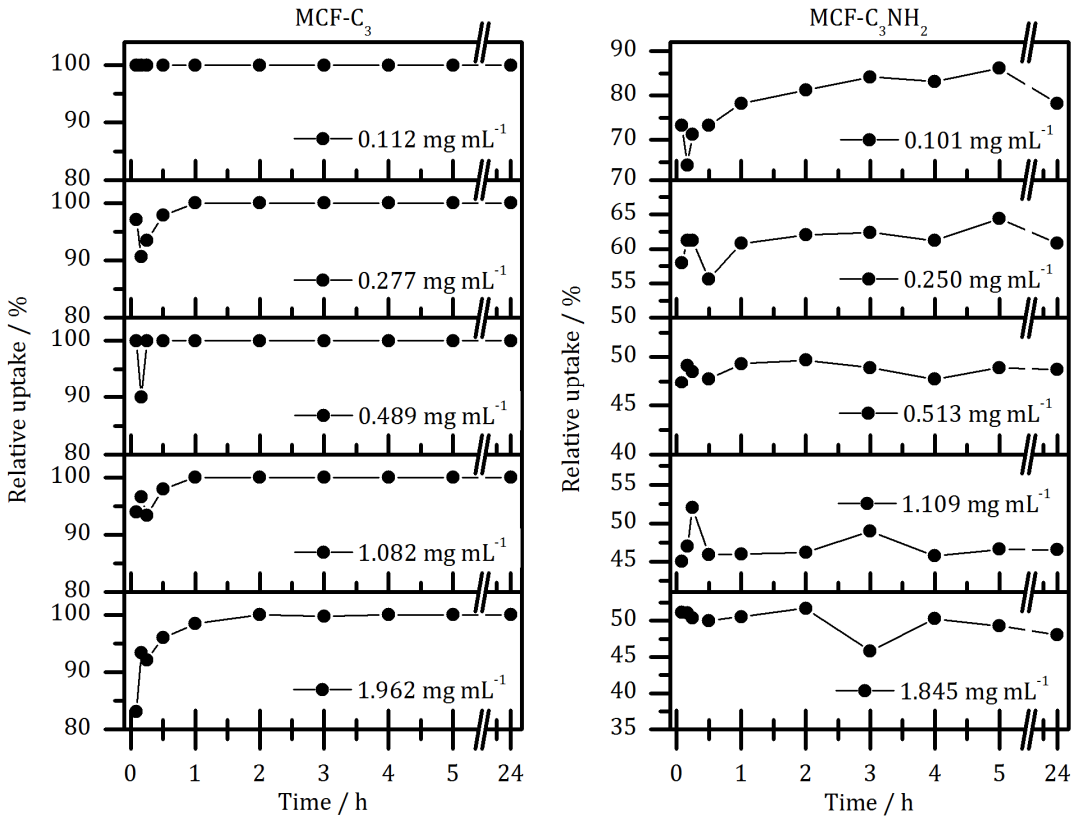


**Figure 97.** Relative uptakes of *G.s.*6PGDH immobilized onto **a)** MCF-$C_3$ as well as **b)** MCF-$C_3$-$NH_2$. The concentration of *G.s.*6PGDH was varied from 0.112 mg $mL^{-1}$ to 1.962 mg $mL^{-1}$ (MCF-$C_3$) and 0.101 mg $mL^{-1}$ to 1.845 mg $mL^{-1}$ (MCF-$C_3$-$NH_2$).

## 7.5 Michaelis-Menten and Lineweaver-Burk plots of the free and the immobilized *G.s.*6PGDH

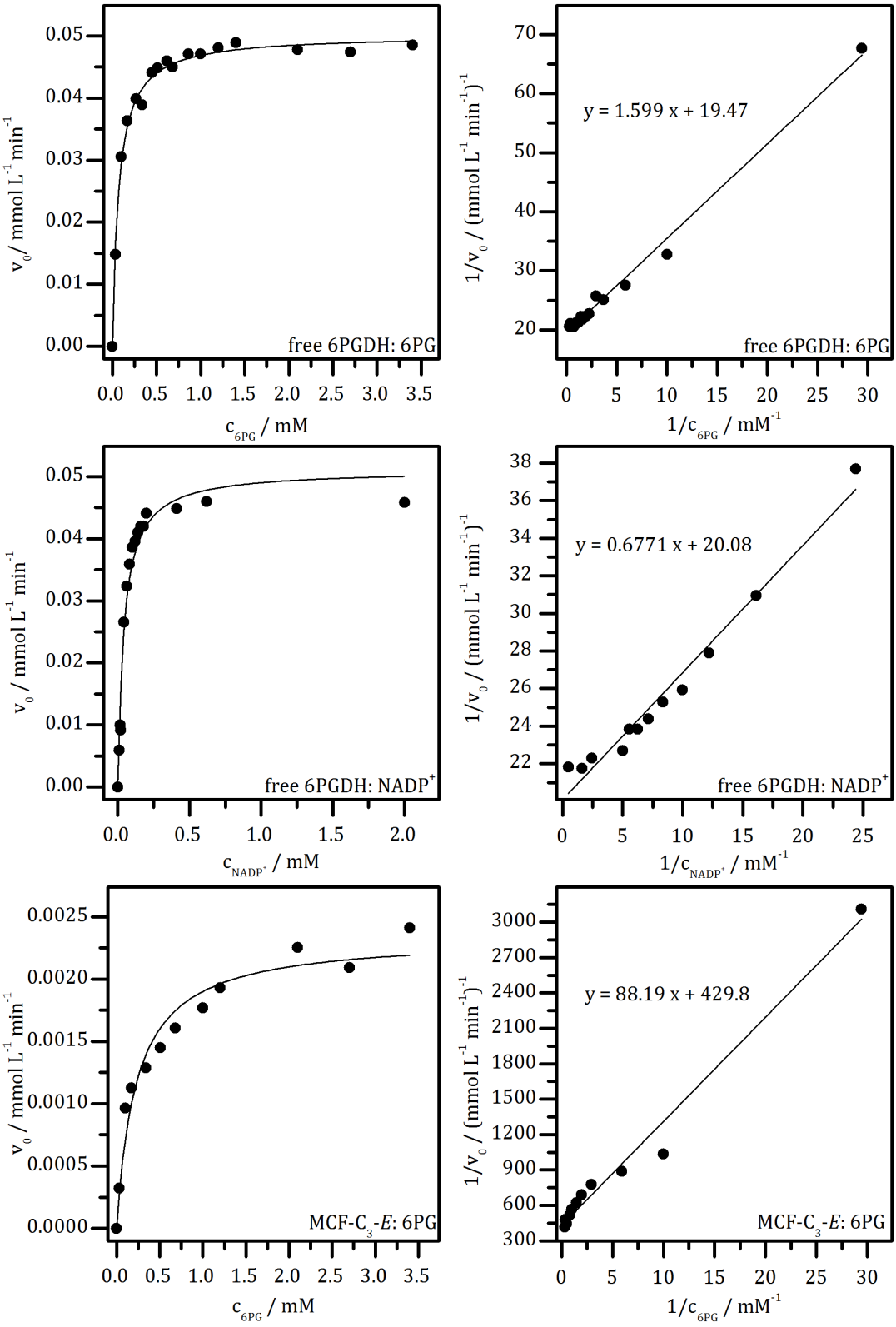


**Figure 98.** Michaelis-Menten and Lineweaver-Burk plots of the free and the immobilized *G.s.*6PGDH with varied concentrations of 6PG or $NADP^+$ at 25 °C.

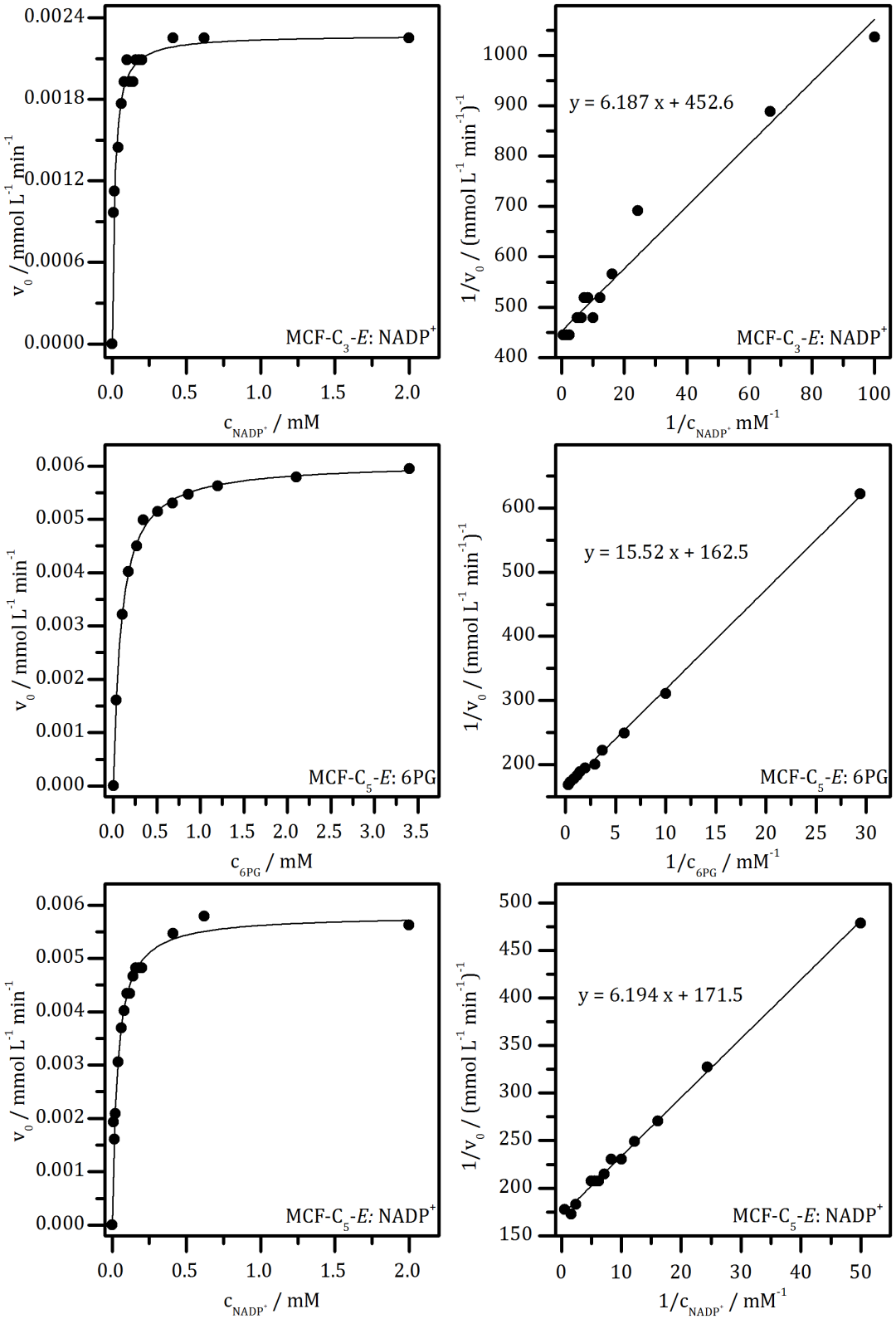


**Figure 99.** Michaelis-Menten and Lineweaver-Burk plots of the free and the immobilized *G.s.*6PGDH with varied concentrations of 6PG or $NADP^+$ at 25 °C.

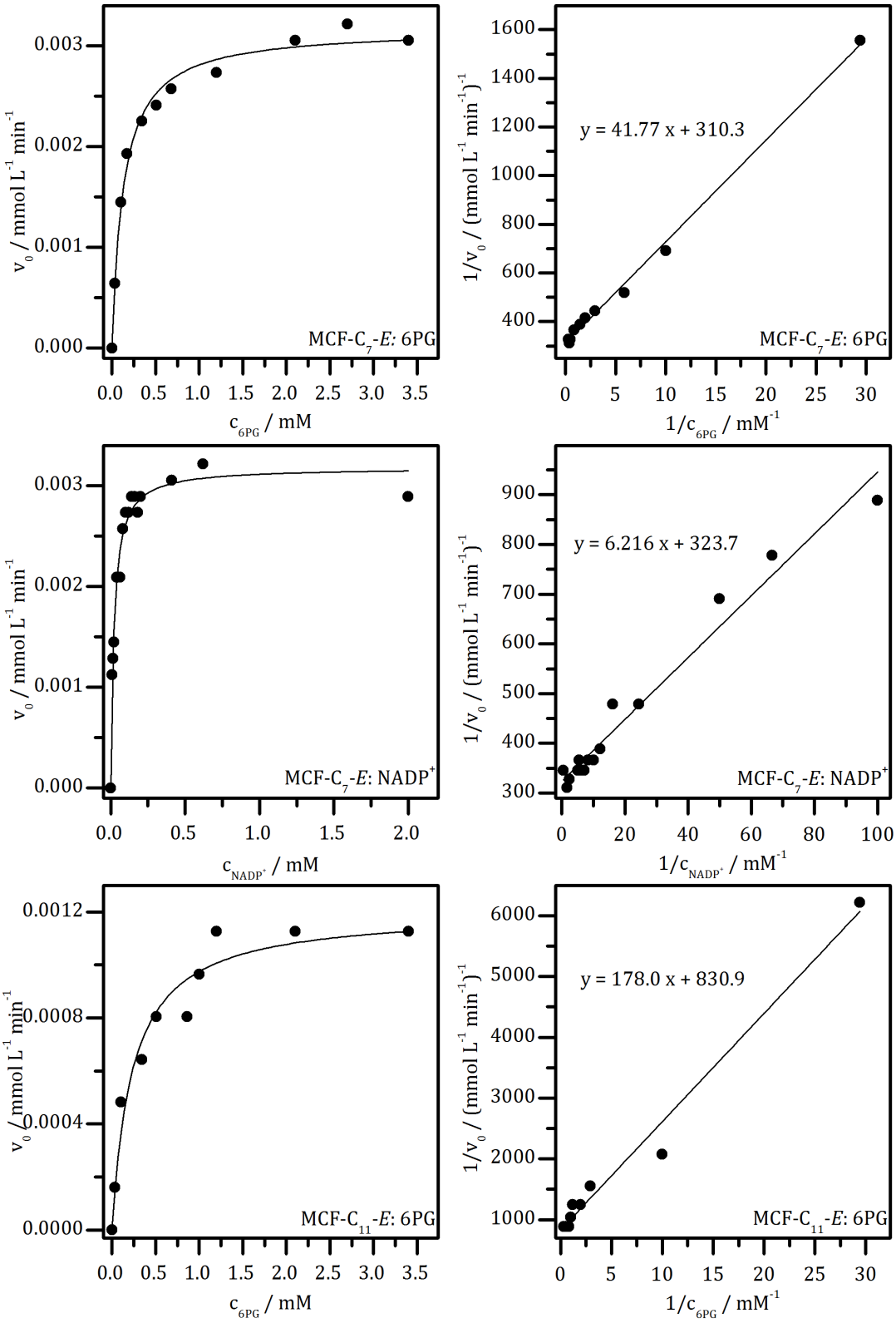


**Figure 100.** Michaelis-Menten and Lineweaver-Burk plots of the free and the immobilized *G.s.*6PGDH with varied concentrations of 6PG or $NADP^+$ at 25 °C.

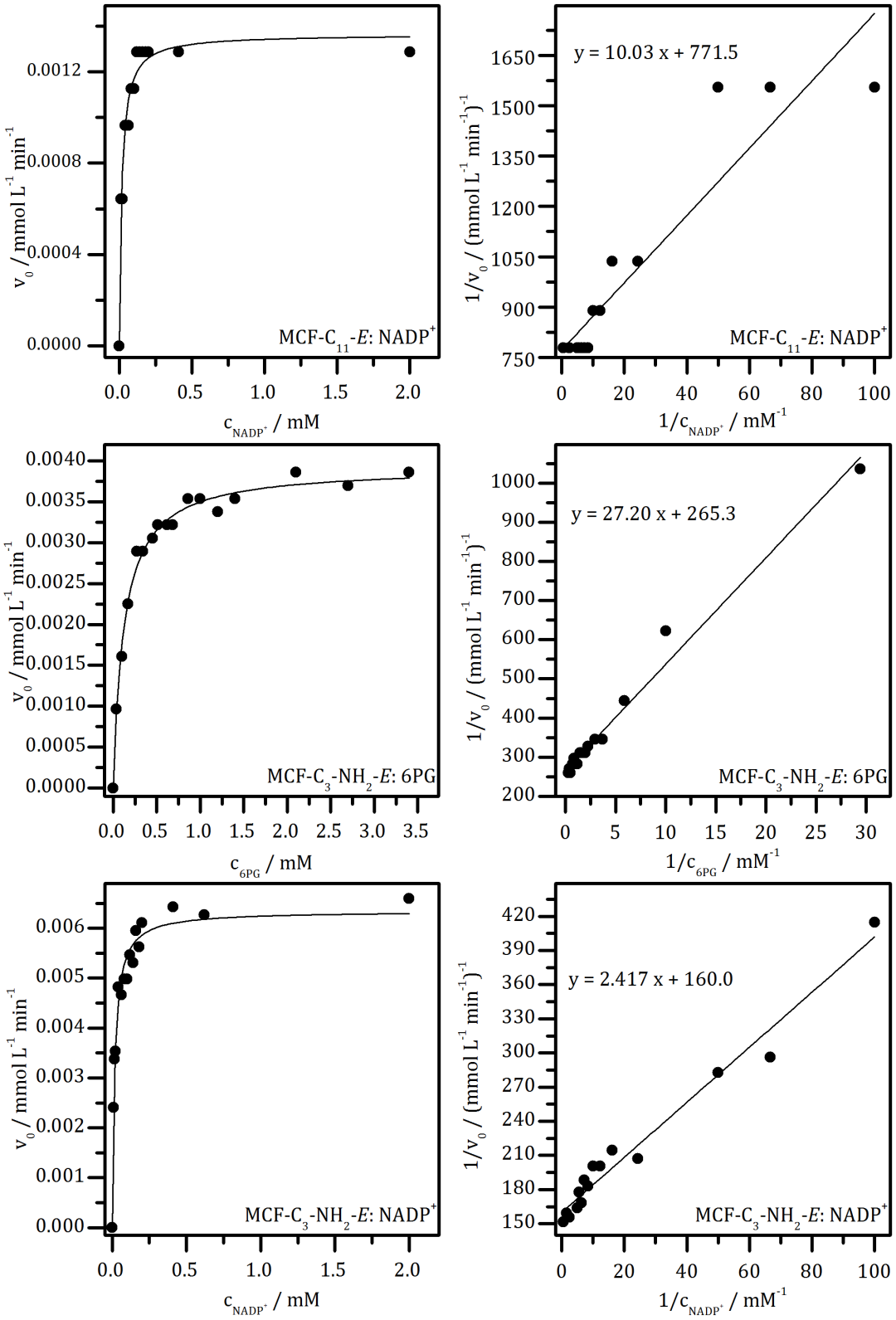


**Figure 101.** Michaelis-Menten and Lineweaver-Burk plots of the free and the immobilized *G.s.*6PGDH with varied concentrations of 6PG or $NADP^+$ at 25 °C.

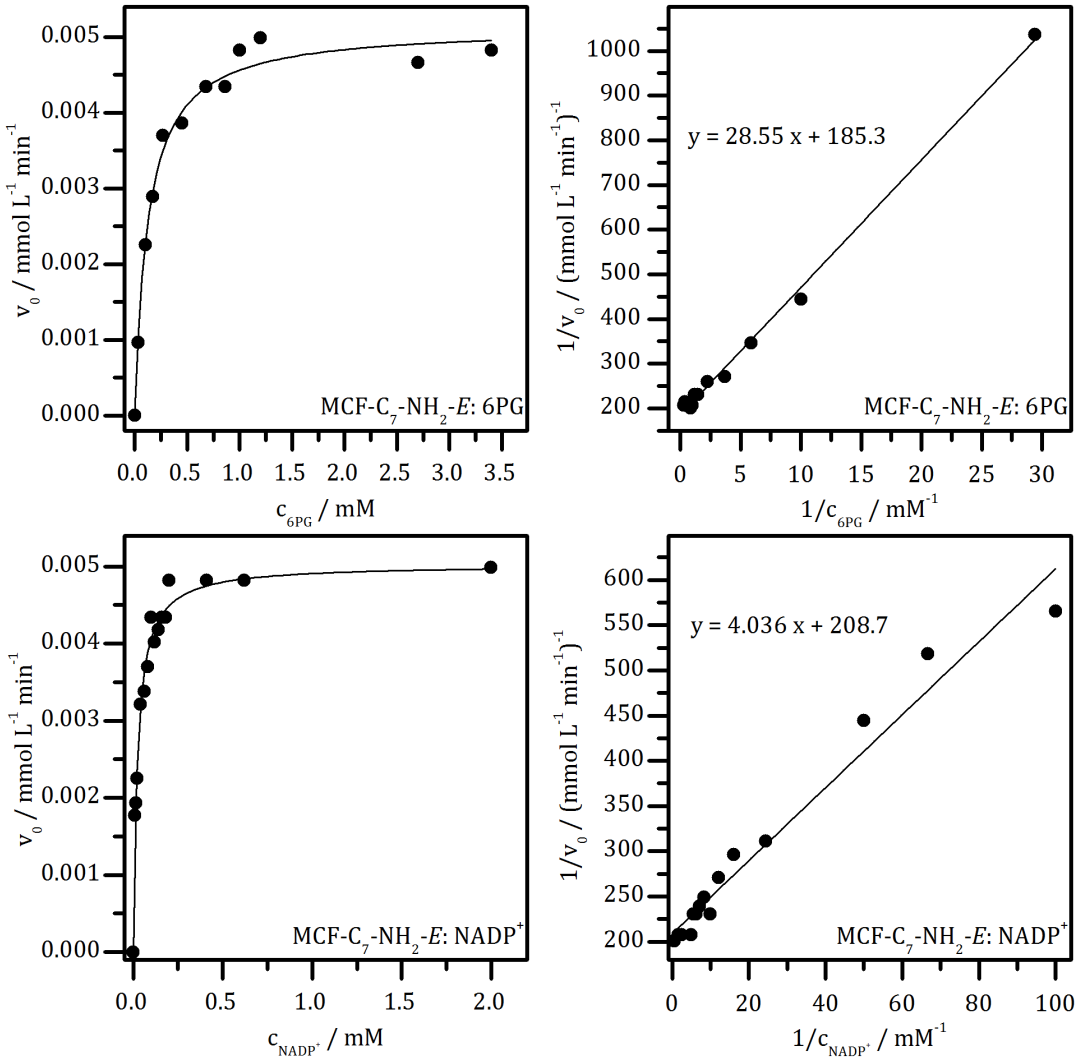


**Figure 102.** Michaelis-Menten and Lineweaver-Burk plots of the free and the immobilized *G.s.*6PGDH with varied concentrations of 6PG or $NADP^+$ at 25 °C.

## 7.6 Michaelis-Menten and Lineweaver-Burk plots of the free and the immobilized *S.c.*6PGDH

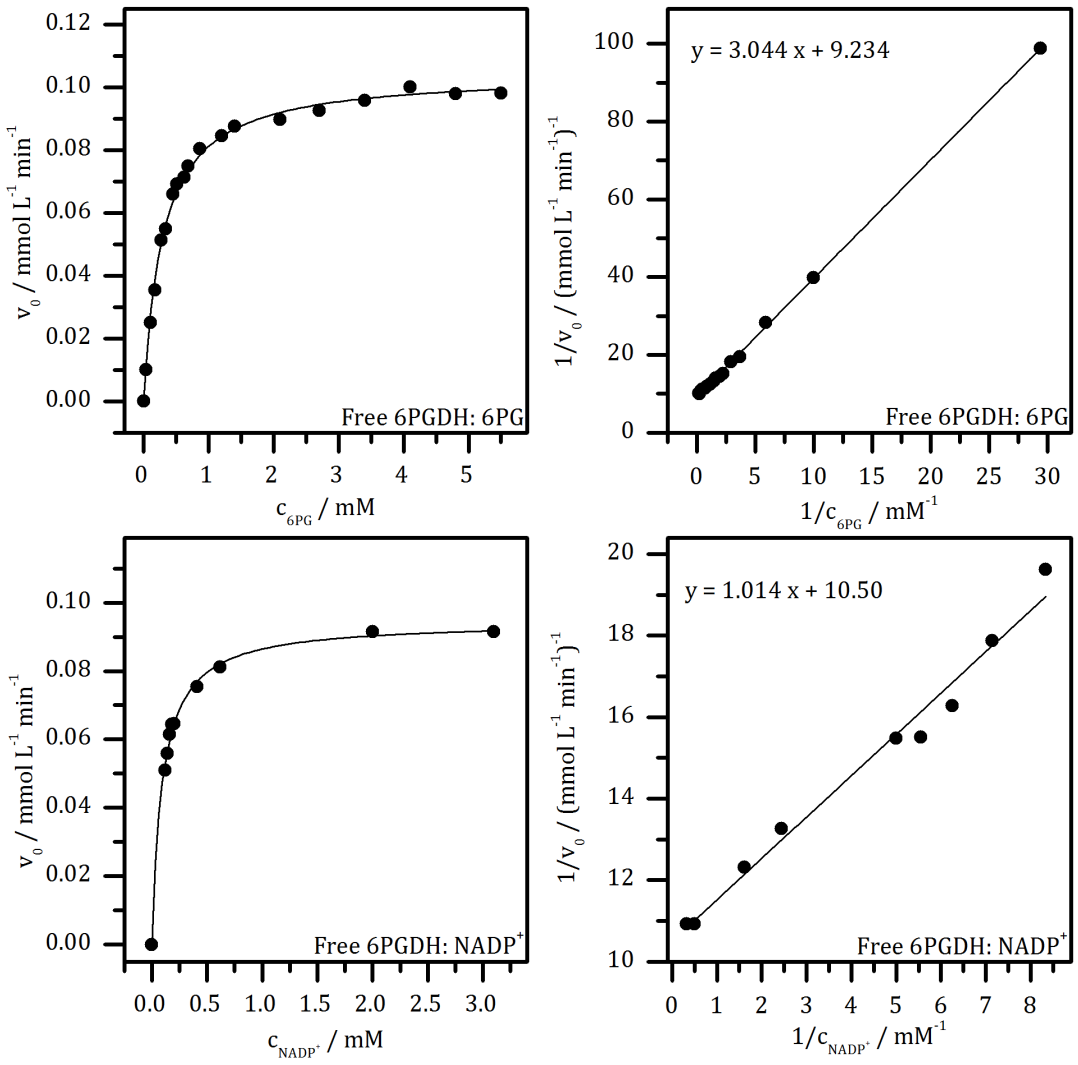


**Figure 103.** Michaelis-Menten and Lineweaver-Burk plots of the free *S.c.*6PGDH, stored in pH 6.5 buffer, with varied concentrations of 6PG or $NADP^+$ at 25 °C.

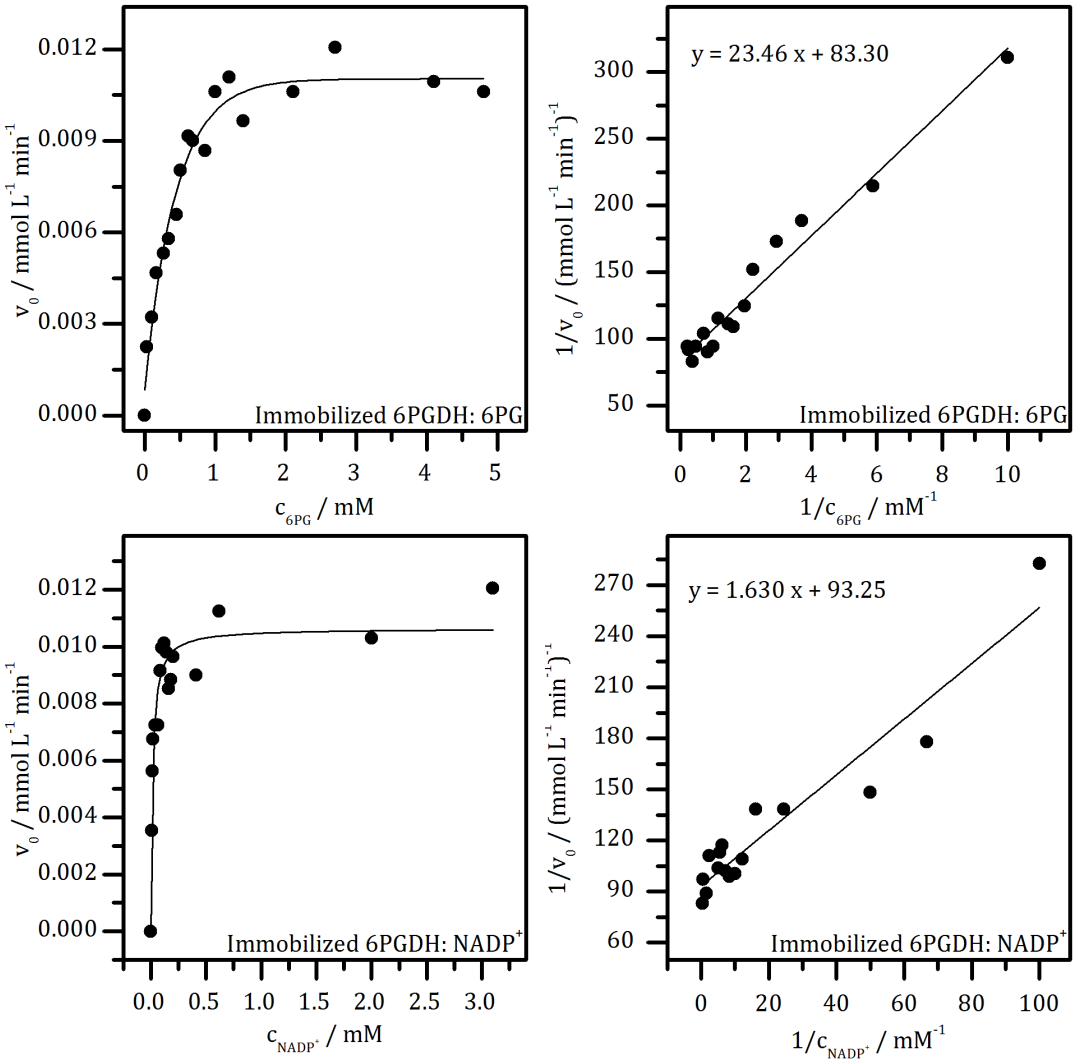


**Figure 104.** Michaelis-Menten and Lineweaver-Burk plots of the *S.c.*6PGDH, immobilized at pH 6.5, with varied concentrations of 6PG or $NADP^+$ at 25 °C.

## 7.7 Michaelis-Menten, Lineweaver-Burk and Dixon plots of the free and the immobilized *E.c.*ADH

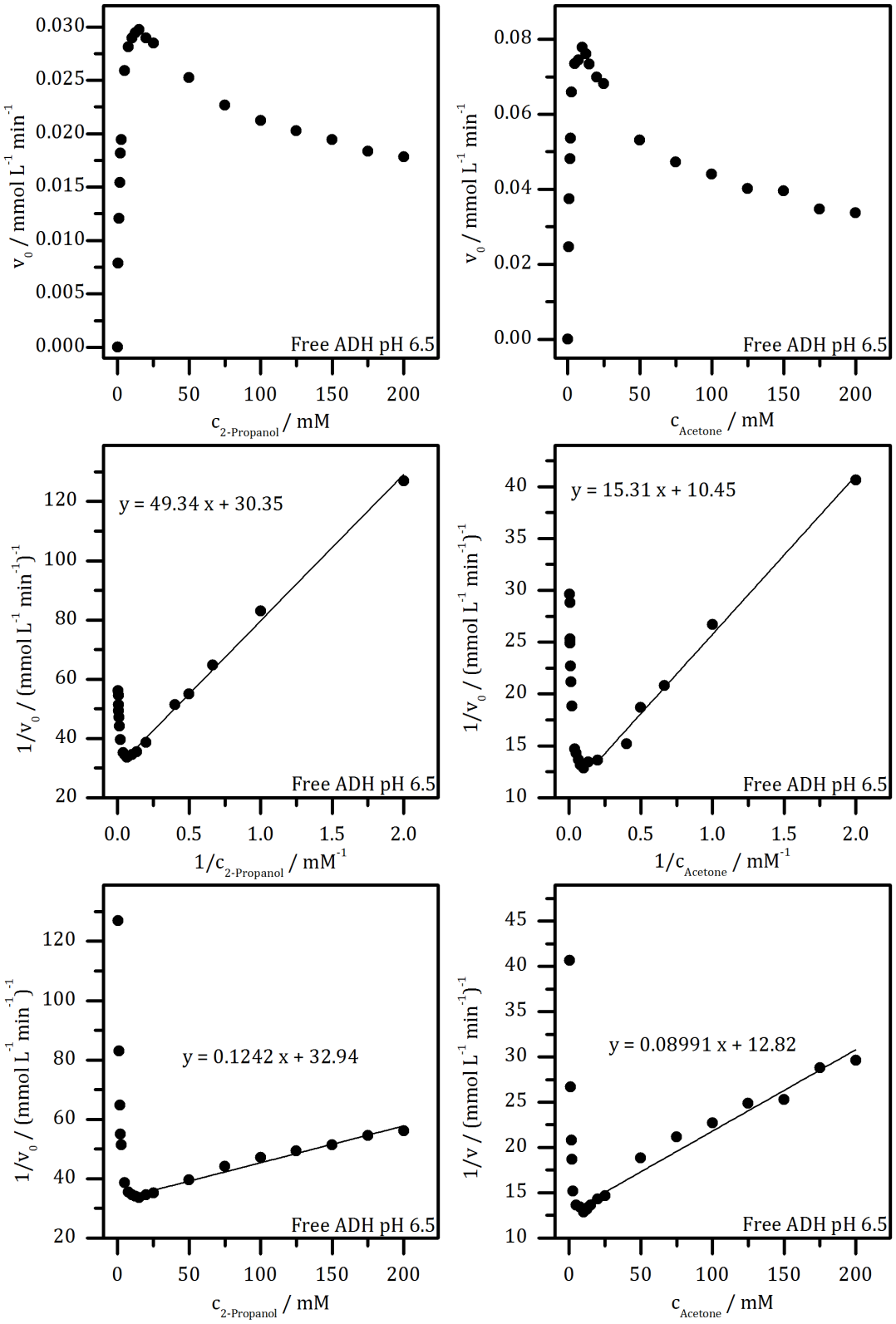


**Figure 105.** Michaelis-Menten, Lineweaver-Burk and Dixon plots of the free ADH, stored in pH 6.5 buffer, with varied concentrations of 2-propanol or acetone at 25 °C.

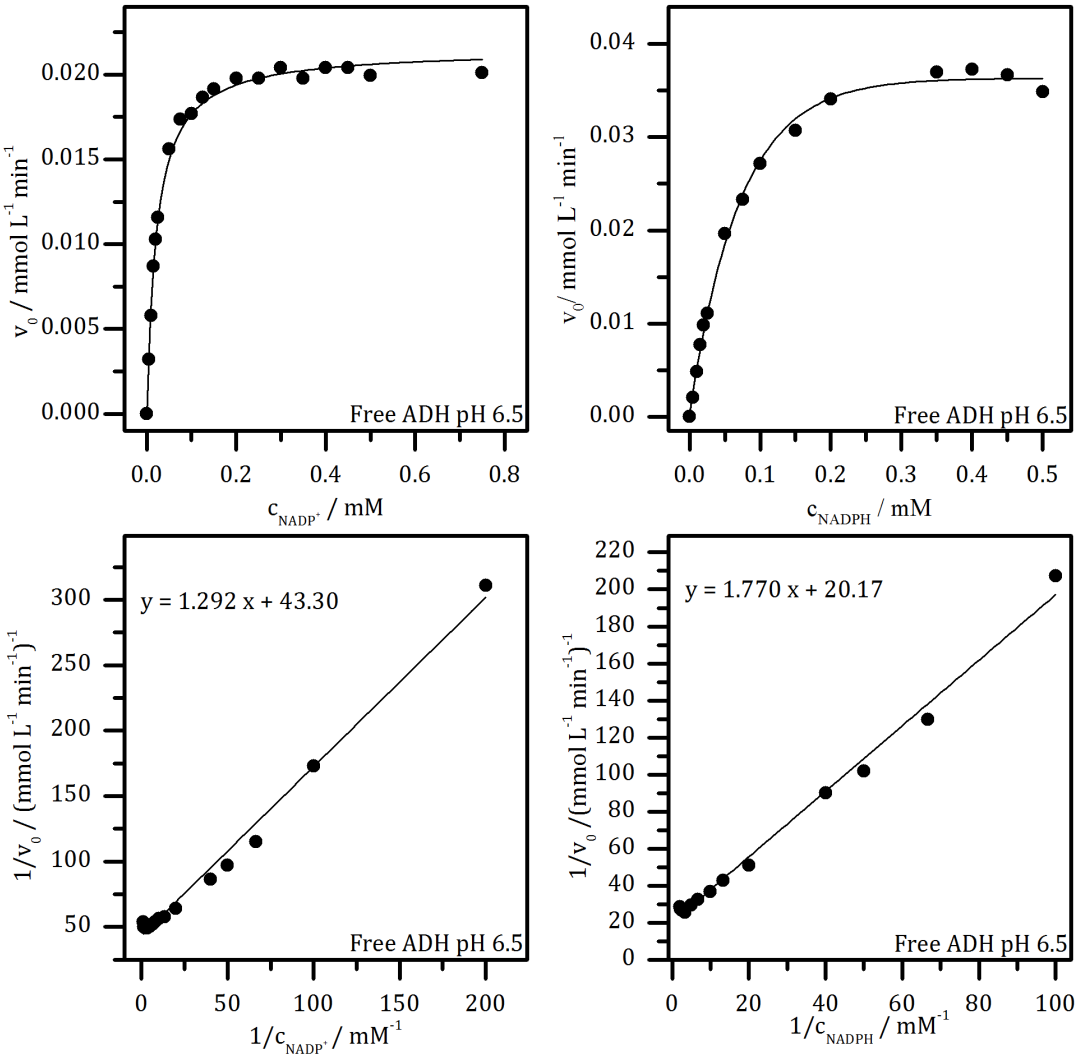


**Figure 106.** Michaelis-Menten and Lineweaver-Burk plots of the free ADH, stored in pH 6.5 buffer, with varied concentrations of $NADP^+$ or NADPH at 25 °C.

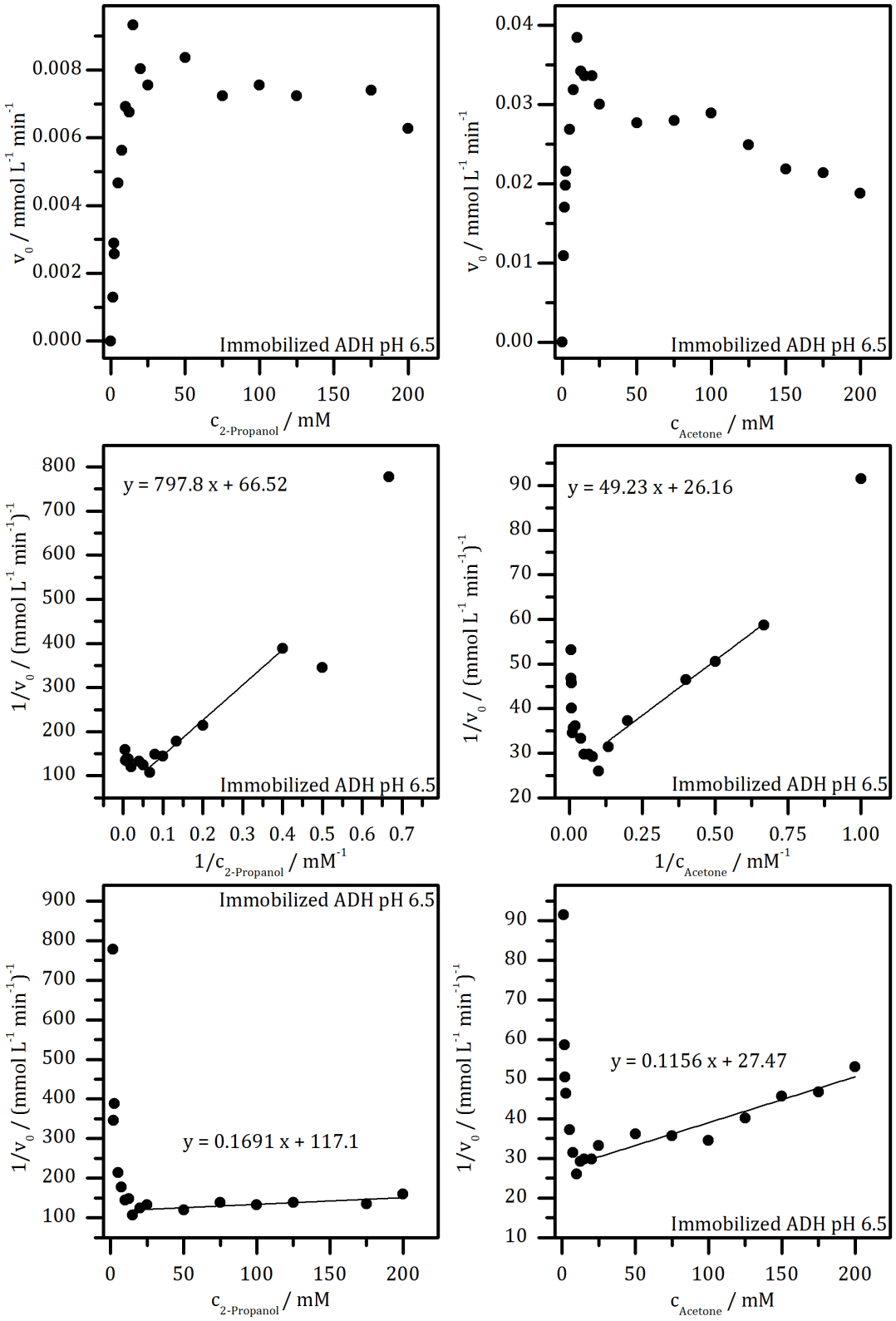


**Figure 107.** Michaelis-Menten, Lineweaver-Burk and Dixon plots of the ADH, immobilized at pH 6.5, with varied concentrations of 2-propanol or acetone at 25 °C.

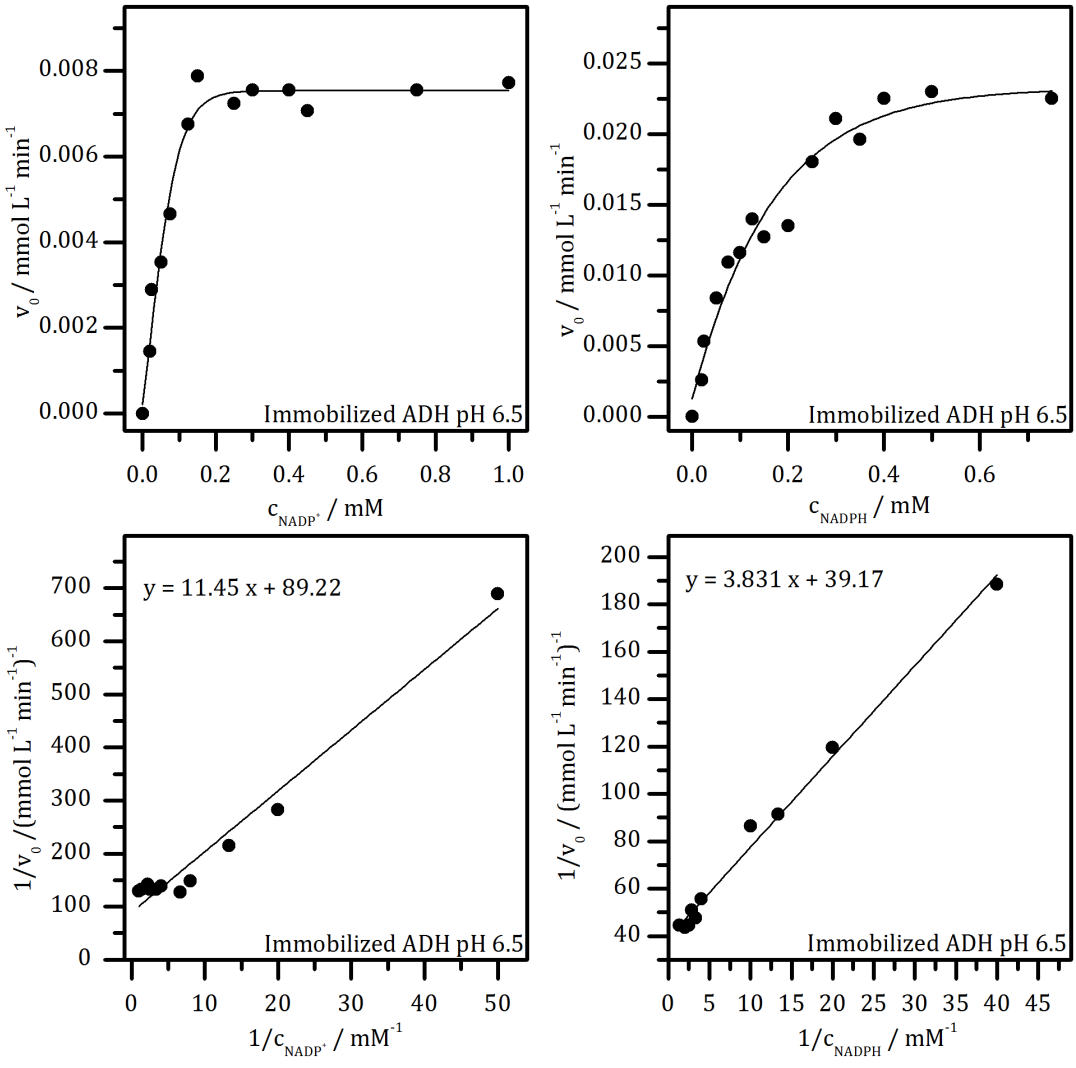


**Figure 108.** Michaelis-Menten and Lineweaver-Burk plots of the ADH, immobilized at pH 6.5, with varied concentrations of $NADP^+$ or NADPH at 25 °C.

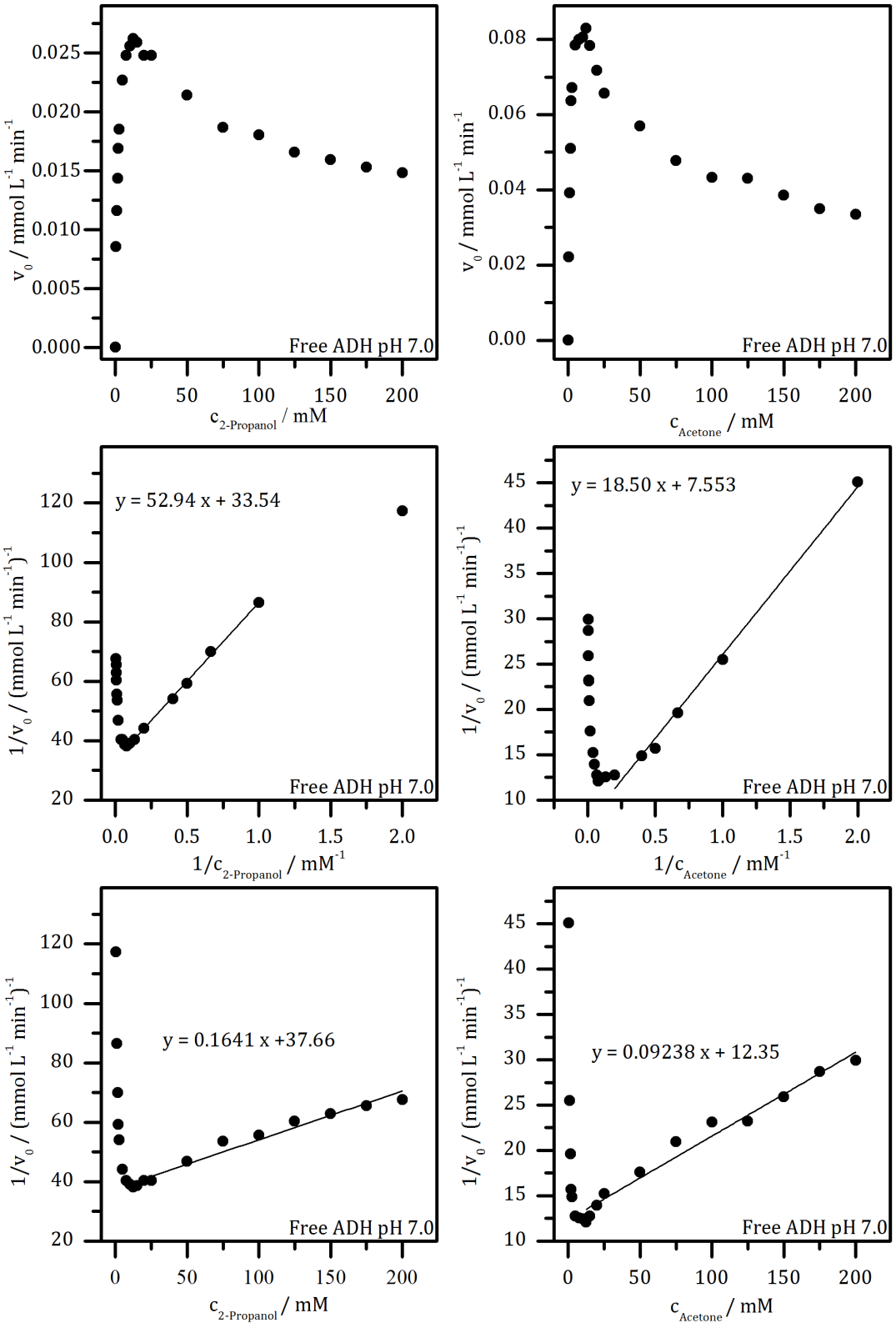


**Figure 109.** Michaelis-Menten, Lineweaver-Burk and Dixon plots of the free ADH, stored in pH 7.0 buffer, with varied concentrations of 2-propanol or acetone at 25 °C.

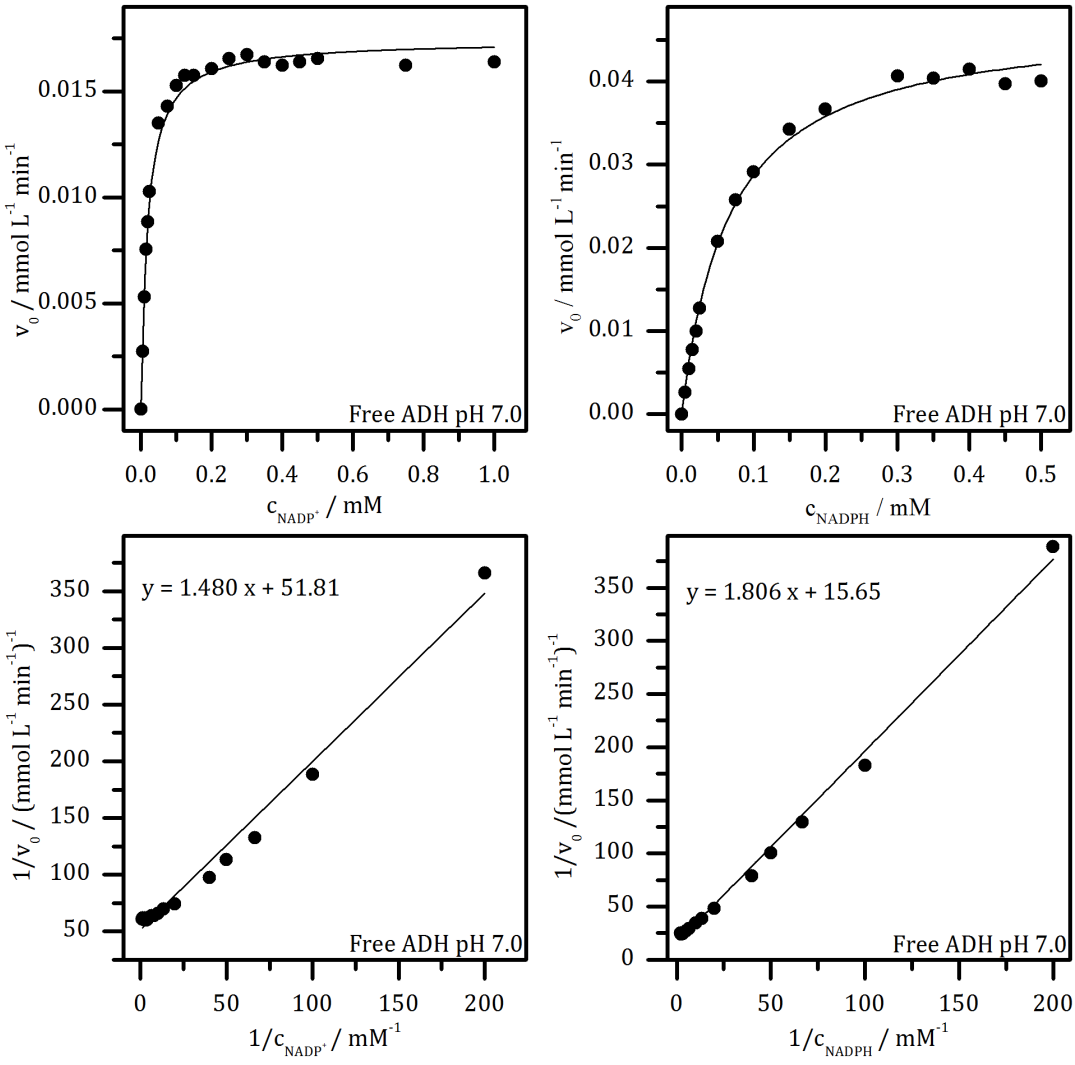


**Figure 110.** Michaelis-Menten and Lineweaver-Burk plots of the free ADH, stored in pH 7.0 buffer, with varied concentrations of $NADP^+$ or NADPH at 25 °C.

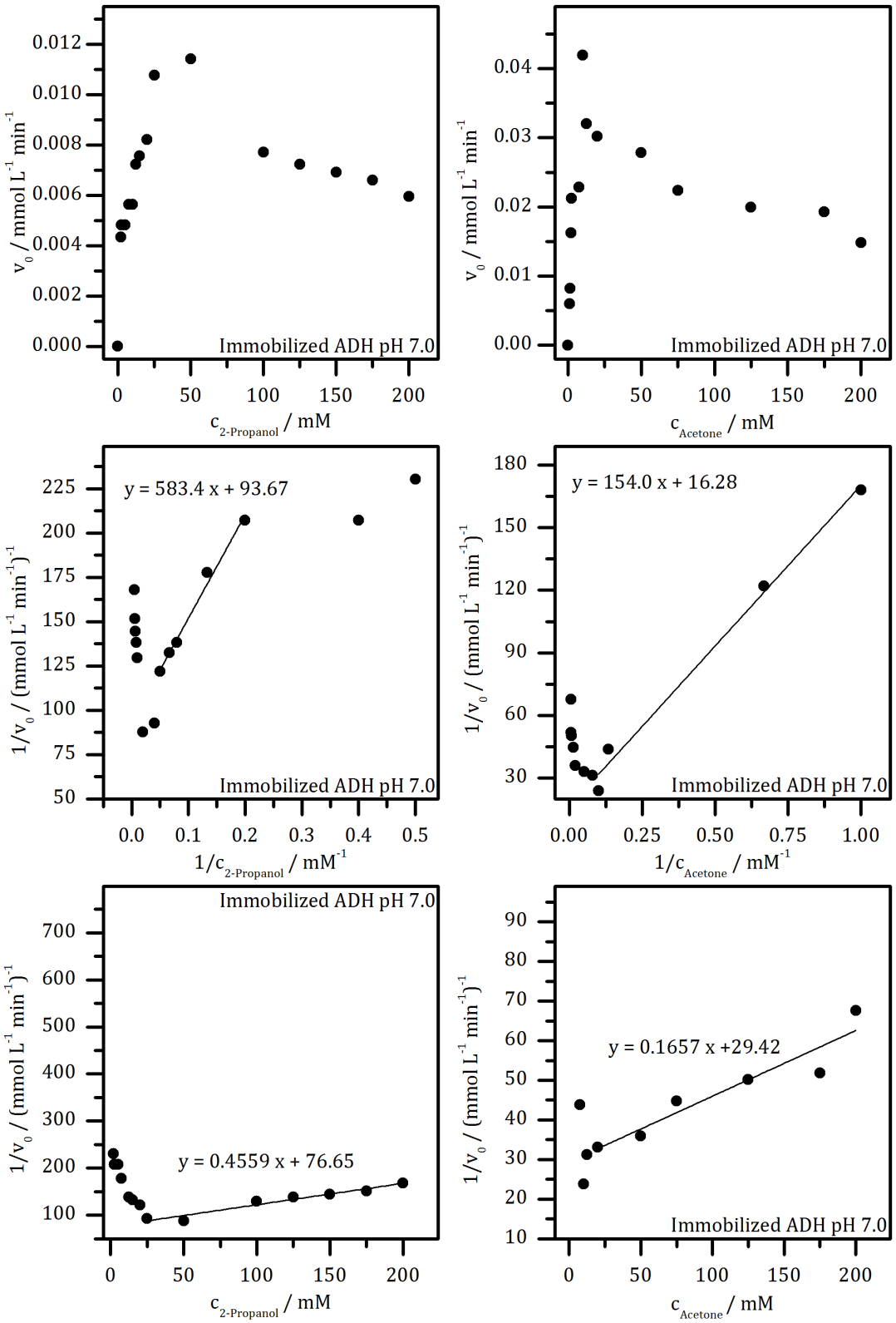


**Figure 111.** Michaelis-Menten, Lineweaver-Burk and Dixon plots of the ADH, immobilized at pH 7.0, with varied concentrations of 2-propanol or acetone at 25 °C.

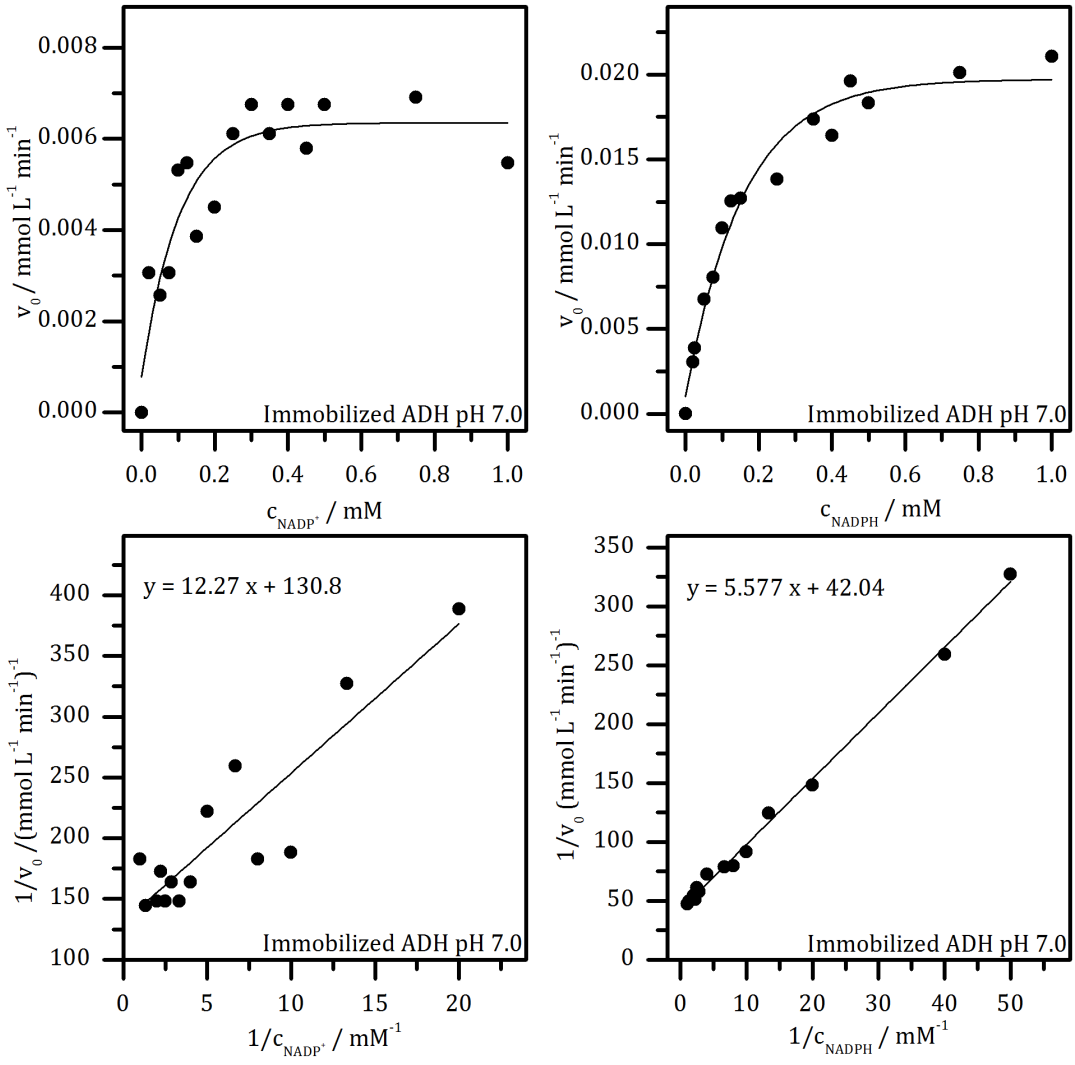


**Figure 112.** Michaelis-Menten and Lineweaver-Burk plots of the ADH, immobilized at pH 7.0, with varied concentrations of $NADP^+$ or NADPH at 25 °C.

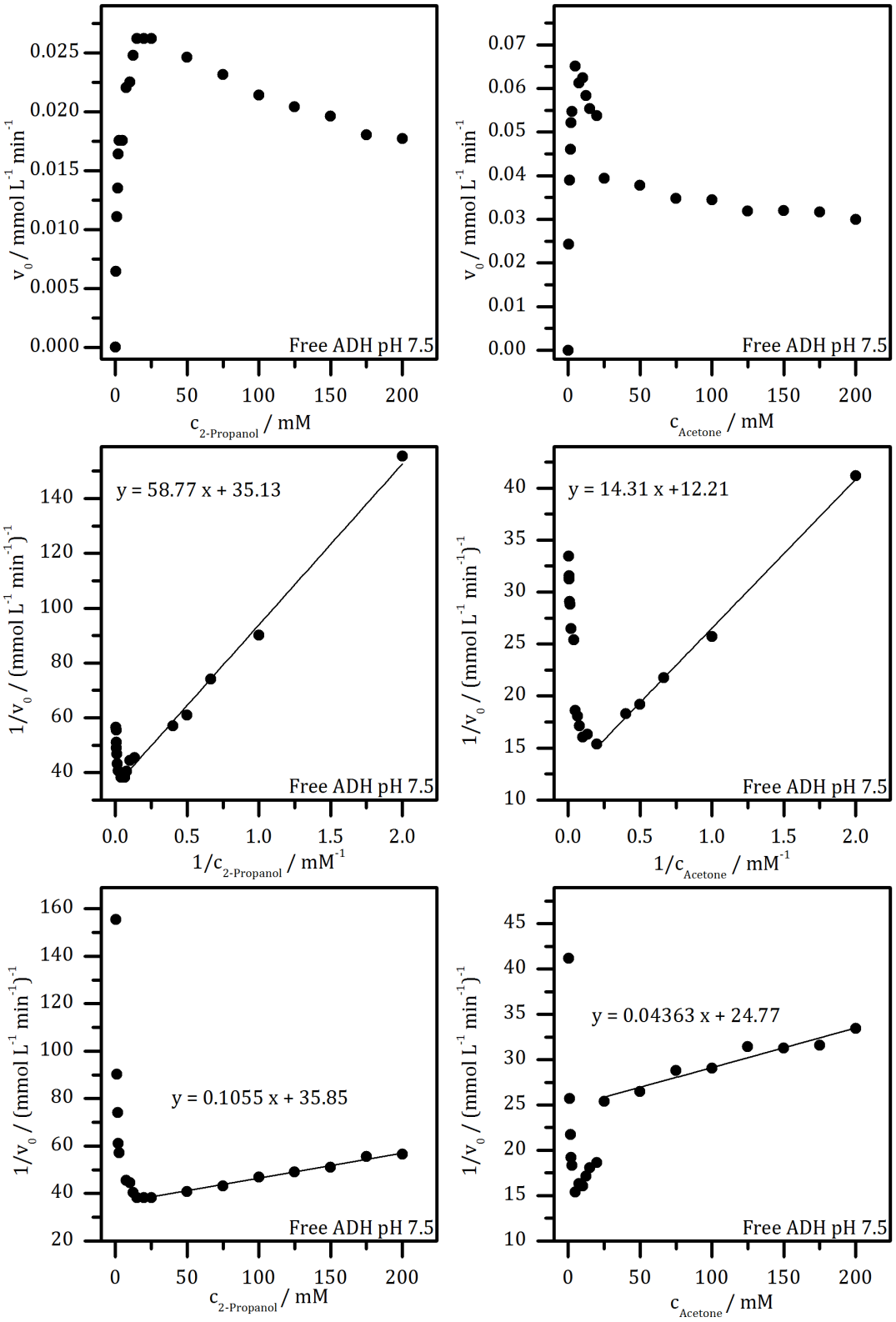


**Figure 113.** Michaelis-Menten, Lineweaver-Burk and Dixon plots of the free ADH, stored in pH 7.5 buffer, with varied concentrations of 2-propanol or acetone at 25 °C.

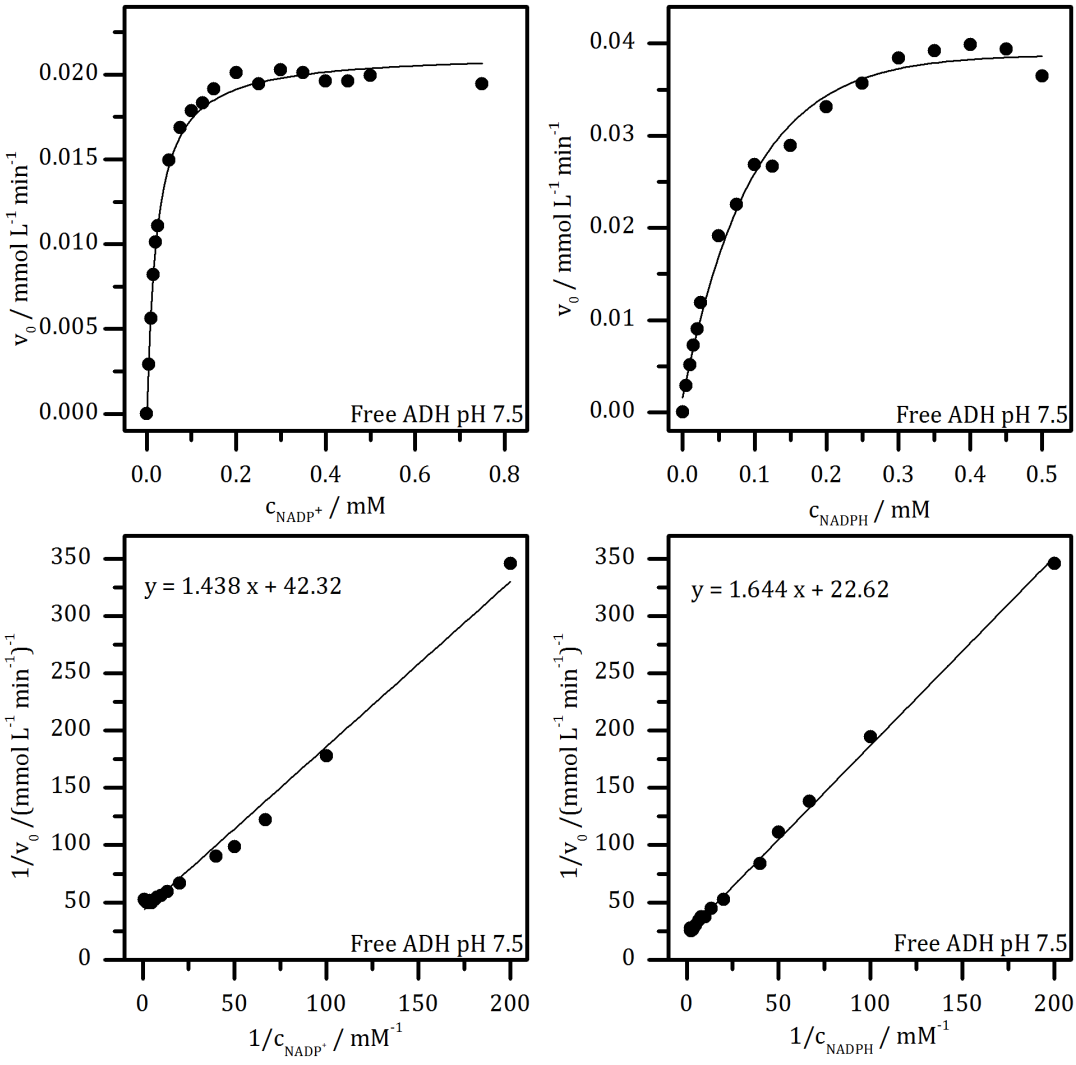


**Figure 114.** Michaelis-Menten and Lineweaver-Burk plots of the free ADH, stored in pH 7.5 buffer, with varied concentrations of $NADP^+$ or NADPH at 25 °C.

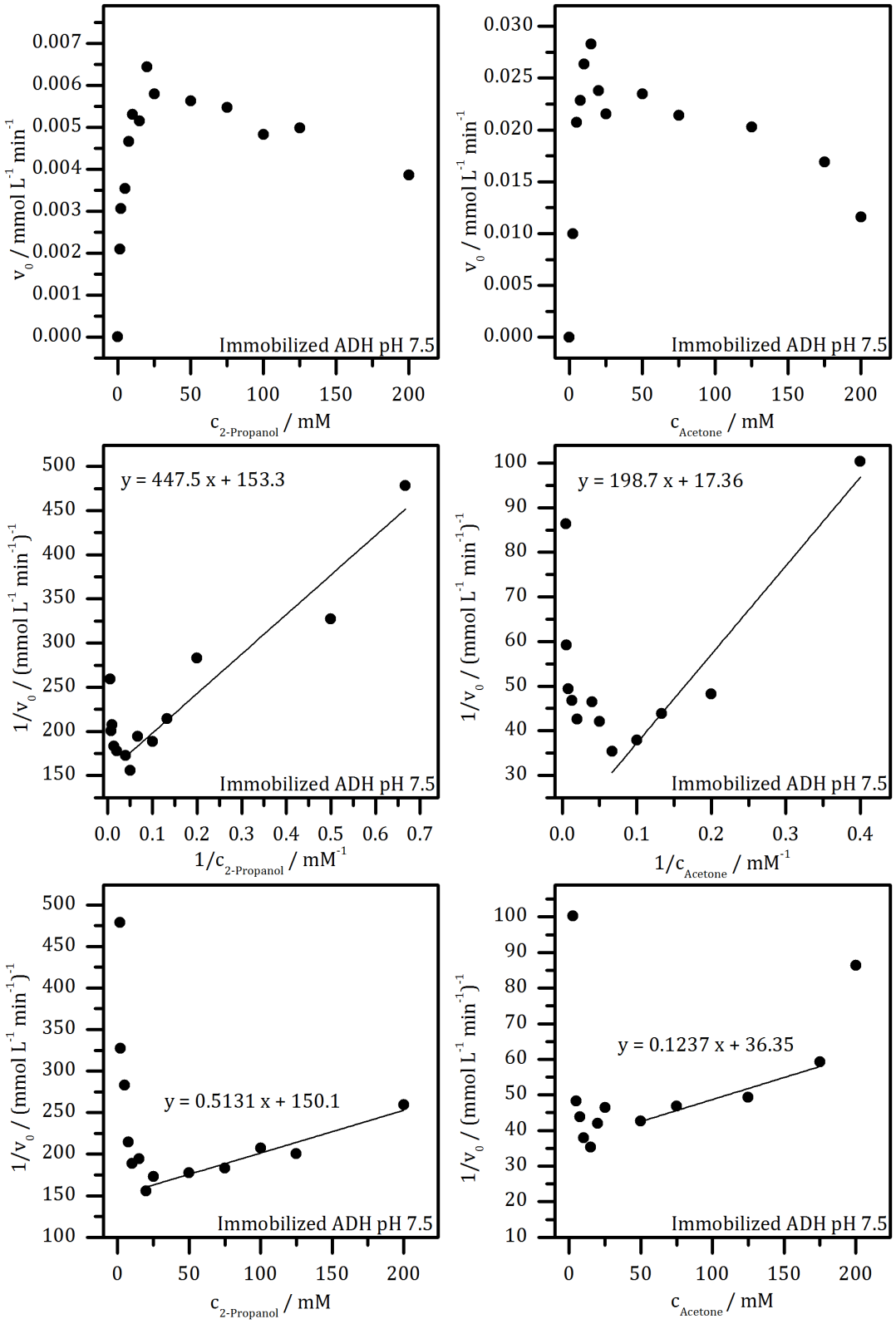


**Figure 115.** Michaelis-Menten, Lineweaver-Burk and Dixon plots of the ADH, immobilized at pH 7.5, with varied concentrations of 2-propanol or acetone at 25 °C.

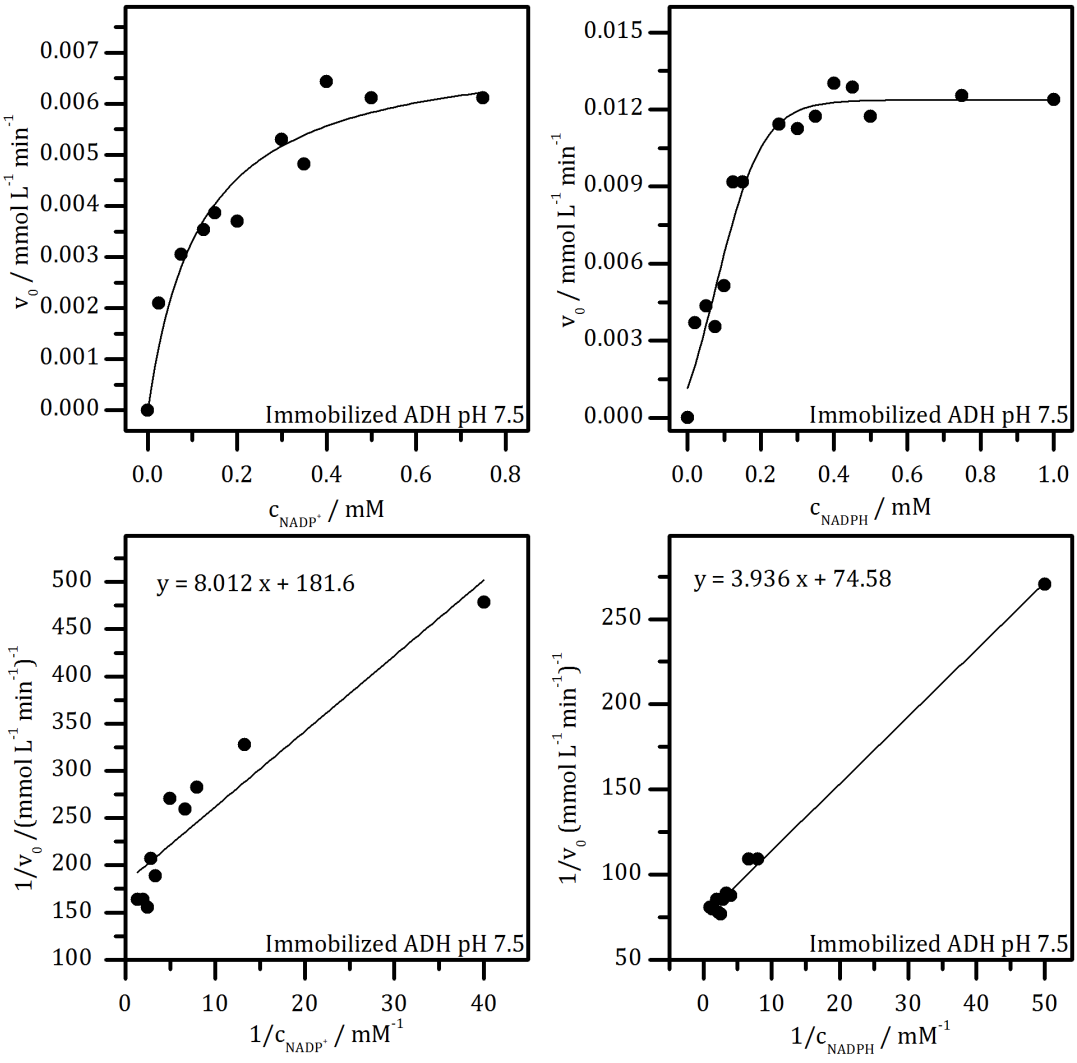


**Figure 116.** Michaelis-Menten and Lineweaver-Burk plots of the ADH, immobilized at pH 7.5, with varied concentrations of $NADP^+$ or NADPH at 25 °C.

# 8 PUBLICATIONS AND PRESENTATIONS

## Publications

M. DREIFKE, F.J. BRIELER, M. FRÖBA
Immobilization of Alcohol Dehydrogenase from *E. coli* onto Mesoporous Silica for Application as a Cofactor Recycling System
*ChemCatChem* **2017**, *9*, 1148-1163.

M. DREIFKE, M. FRÖBA
Immobilisierung von Enzymen: Spielerei oder biotechnologischer Fortschritt?
*BIOspektrum* **2017**, *23*, 95-97.

M. DREIFKE, D.I. FRIED, F.J. BRIELER, M. FRÖBA
Kinetic investigations of 6-phosphogluconic dehydrogenase confined in mesoporous silica
*J. Mol. Catal. B: Enzymatic* **2016**, *132*, 5-15.

M. DREIFKE, M. ARMBRECHT, M. FRÖBA
Eppendorf BioSpectrometer® kinetic: activity measurements of enzymes immobilized on a mesoporous silica matrix
*Eppendorf Application Note No. 370* **2016**.

D.I. FRIED, D. BEDNARSKI, M. DREIFKE, F.J. BRIELER, M. THOMMES, M. FRÖBA
Influence of the hydrophilic-hydrophobic contrast of porous surfaces on the enzymatic performance
*J. Mater. Chem. B* **2015**, *3*, 2341-2349.

## Oral presentation

M. DREIFKE, D.I. FRIED, F.J. BRIELER, M. FRÖBA
Designing Enzyme Cascades for Cofactor Recycling
International Mesostructured Symposium (IMMS) **2015**, Brisbane, Queensland, Australia.

**Poster Presentations**

M. DREIFKE, F.J. BRIELER, M. FRÖBA
A Modular Enzyme Cascade for Cofactor Regeneration
29. Deutsche Zeolith-Tagung **2017**, Frankfurt am Main.

M. DREIFKE, D.I. FRIED, M. FRÖBA
Designing Enzyme Cascades for Cofactor Recycling
Thermal Analysis and Calorimetry in Industry and Research
- 40 Years of GEFTA **2014**, Berlin.

M. DREIFKE, D.I. FRIED, M. FRÖBA
Designing Enzyme Cascades for Cofactor Recycling
Summer School Biotransformation **2014**, Bad Herrenalb.

M. DREIFKE, D.I. FRIED, M. FRÖBA
Designing Enzyme Cascades for Cofactor Recycling
7th International Congress on Biocatalysis **2014**, Hamburg.

M. DREIFKE, D.I. FRIED, M. FRÖBA
Immobilization of 6-Phosphogluconate dehydrogenase onto Mesoporous Silica Hosts
25. Deutsche Zeolith-Tagung **2013**, Hamburg.

# 9 CHEMICALS CATEGORIZED ACCORDING TO GHS

**Table 28.** Chemicals used within the PhD study.[202, 203, 204, 205]

| Substance | H statements | P statements | Hazard pictograms |
|---|---|---|---|
| Acetone | H225-H319-H336 | P210-P261-P305+P351+P338 | GHS02, GHS07, danger |
| Acetonitril | H225-H302+H312+H332-H319 | P210-P261-P280-P305+P351+P338-P370+P378-P403+P235 | GHS02, GHS07 danger |
| Alcohol dehydrogenase (ADH) | --- | --- | --- |
| Aluminum oxide 90 active neutral | --- | P260 | --- |
| (3-Aminopropyl)triethoxysilane, 97 % | H302-H314 | P280-P270-P264-P304-P340-P310-P301-P330-P331-P303-P361-P353-P363-P305-P351-P338-P337-P313-P405-P501 | GHS05, GHS07 |
| Ammonium fluoride | H301+H311+H331-H318 | P280-P301+P330+P331+P310-P302+P352+P312-P304+P340+P311-P305+P351+P338+P310 | GHS05, GHS06, danger |
| Bicinchoninic acid (BCA) assay kit | H410 | P273-P391-P501 | GHS09, warning |
| Bradford reagent | H290-H315-H319-H371 | P260-P305+P351+P338-P308+P311 | GHS05, GHS08, warning |
| 5-Bromo-1-pentene | H226-H315-H319-H335 | P261-P305+P351+P338 | GHS02, GHS07, warning |
| (7-Bromoheptyl)trimethoxysilane, 95% | H315-H319-H335 | P280-P271-P261-P264-P304-P340-P312-P302-P352-P362-2-P363-P332-P313-P305-P351-P338-P337-P405-P501 | GHS07 |

[202] Sigma-Aldrich: http://www.sigmaaldrich.com/germany.html, **04.2017.**
[203] ABCR: https://www.abcr.de/startseite/, **04.2017.**
[204] AppliChem: https://www.applichem.com/home/, **04.2017.**
[205] Carl Roth: https://www.carlroth.com/de/de, **04.2017.**

| Substance | H statements | P statements | Hazard pictograms |
|---|---|---|---|
| (11-Bromoundecyl)trimethoxysilane, 95 % | H302-H312-H315-H319-H332-H335 | P280-P271-P261-P270-P264-P304-P340-P312-P301-P330-P302-P352-P362-2- P363-P332-P313-P305- P351-P338-P337-P405- P501 | GHS07 |
| Bovine serum albumin (BSA), 2 mg $mL^{-1}$ | --- | --- | --- |
| Cyclohexane, abs. | H225-H304-H315-H336-H410 | P210-P261-P273-P301+P310-P331-P501 | GHS02, GHS07, GHS08, GHS09, danger |
| Dichloromethane, abs. | H315-H319-H335-H336-H351-H373 | P260-P280-P305+P351+P338 | GHS07, GHS08 warning |
| Ethanol, abs. | H225-H319 | P210-P280-P305+P351+P338-P337+P313-P403+P235 | GHS02, GHS07, danger |
| Glucose-6-phosphate dehydrogenase (G6PDH) | --- | --- | --- |
| Glucose-6-phosphate disodium salt dihydrate (G6P) | --- | --- | --- |
| 1-Heptene, 98 % | H225-H304 | P210-P301+P310-P331-P370+P378-P403+P235 | GHS02, GHS08, danger |
| Hydrochloric acid, 37 % | H290-H314-H335 | P261-P280-P305+P351+P338-P310 | GHS05, GHS07 danger |
| Hydrogen | H220-H280 | P210-P377-P381-P410+403 | GHS02, GHS04, danger |
| 4-(2-Hydroxyethyl)piperazine-1-ethanesulfonic acid (HEPES) | --- | --- | --- |
| Karstedt's catalyst in xylene, 2.1-2.4 % Pt | H226-H304-H312+H332, H315-H319-H335-H373 | P210-P260-P280-P301+P310-P305+P351+P338-P370+P378 | GHS02, GHS07, GHS08, danger |
| Magnesium chloride hexahydrate | --- | --- | --- |
| Methanol, abs. | H225-H301+H311+H331-H370 | P210-P260-P280-P301+P316-P311 | GHS02, GHS06, GHS08, danger |
| β-Nicotinamide adenine dinucleotide phosphate disodium salt ($NADP^+$) | --- | --- | --- |
| β-Nicotinamide adenine dinucleotide phosphate tetrasodium salt (NADPH) | --- | --- | --- |
| 6-Phosphogluconate dehydrogenase (6PGDH) | --- | --- | --- |

9 Chemicals categorized according to ghs

| Substance | H statements | P statements | Hazard pictograms |
|---|---|---|---|
| 6-Phosphogluconic acid trisodium salt (6PG) | --- | --- | --- |
| Palladium on activated carbon, 10 wt.-% loading | H228 | P210 | GHS02, warning |
| (Pentyl)triethoxysilane, 97 % | H315-H319-H335 | P280-P271-P261-P264-P304-P340-P312-P302-P352-P362-2-P363-P332-P313-P305-P351-P338-P337-P405-P501 | GHS07 |
| *Pluronic*® P123 | --- | --- | --- |
| Potassium phosphate monobasic | --- | --- | --- |
| 2-Propanol | H225-H319-H336 | P210-P261-P305+P351+P338 | GHS02, GHS07, danger |
| (n-Propyl)trimethoxysilane, 97 % | H226-H332 | P280-P210-P241-P242-P243-P233-P271-P261-P304-P340-P312-P303-P361-P353-P403-P235-P501 | GHS02, GHS07 |
| Sodium azide | H300+H310-H373-H410, EUH032 | P273-P280-P301+P310+P330-P302+P352+P310+P391+P501 | GHS06, GHS08, GHS09 danger |
| Tetraethyl orthosilicate (TEOS) | H226-H319-H332-H335 | P210-P261-P280-P304+P340+P312-P337+P313-P403+P235 | GHS02, GHS07, warning |
| Toluene, abs. | H225-H304-H315-H336-H361d-H373 | P210-P260-P280-P301+P310-P370+P378-P403+P235 | GHS02, GHS07 GHS08 danger |
| Triethoxysilane, 95 % | H226-H314-H330 | P260-P280-P284-P305+P351+P338-P310 | GHS02, GHS05, GHS06 |
| 1, 3, 5-Trimethylbezene (TMB) | H226-H315-H335-H411 | P261-P273 | GHS02, GHS07, GHS09, warning |
| 1-Undecene, 97 % | --- | H302-H315-H319-H332-H335-H411 | GHS07, GHS09 |

**Hazard pictograms**


**Figure 117.** Hazard pictogram according to GHS.